USE OF DRILLING PARAMETERS TO PREDICT IN-SITU ROCK STRESS BOUNDS

By

GEIR HARELAND

Bachelor of Mechanical Engineering
University of Minnesota
Minneapolis, Minnesota
1981

Master of Science in Engineering
University of Tulsa
Tulsa, Oklahoma
1985

Submitted to the Faculty of the
Graduate College of the
Oklahoma State University
in partial fulfillment of
the requirements for
the Degree of
DOCTOR OF PHILOSOPHY
December, 1991

USE OF DRILLING PARAMETERS TO PREDICT

IN-SITU ROCK STRESS BOUNDS

Thesis Approved:

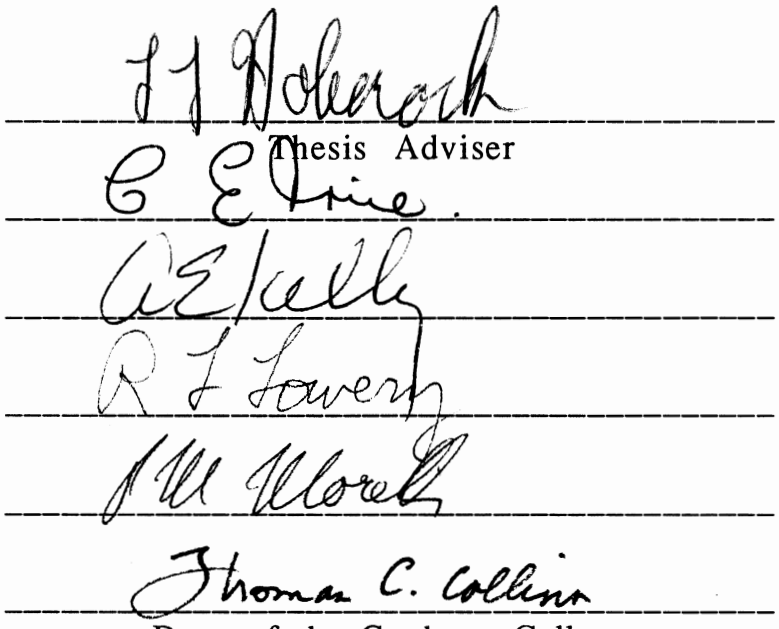

Thesis Adviser

Dean of the Graduate College

ACKNOWLEDGEMENT

I wish to express sincere appreciation to my advisor Dr. L. L. Hoberock for his guidance and strong support throughout my graduate program. Many thanks also go to Dr. R. L. Lowery, Dr. C. E. Price, Dr. A. E. Kelly and Dr. P. M. Moretti for serving on my graduate committee. Their suggestions and support were very helpful throughout the study.

To Ercil Hunt of Ercil Hunt and Associates who participated in the study, I extend sincere thanks, both for his counsel and advice, and for the financial support that made this study possible. Dr. Ralph Veatch, Zissis Moschovides and Gil Feather of Amoco Production Company Research Center in Tulsa, OK, were most helpful for their support and for arranging for the use of Amoco's computational facilities and laboratory drilling data base. The financial support of the Gas Research Institute arranged through Ercil Hunt and Associates is gratefully acknowledged.

Finally, I would like to offer my sincere thanks to my family in Norway, Arne Petter and Solveig Hareland for their support throughout my college career.

TABLE OF CONTENTS

Chapter Page

LIST OF TABLES

LIST OF FIGURES

Figure Page

Figure Page

Figure Page

Figure Page

Figure Page

Figure Page

Figure Page

Figure Page

CHAPTER I

INTRODUCTION

The research reported herein is to determine the feasibility of using data collected during typical drilling operations to predict an upper bound on the minimum principal in-situ stress of rock. These predictions are desired in order that hydraulic fracturability of reservoir rock can be better determined and fracturing programs designed without the need for expensive fracturing stress tests, guesswork, or empiricism. The work uses data available from four wells already drilled, namely the GRI (Gas Research Institute) Staged Field Experiment Wells (SFE # 1, 2, 3 & 4), which were drilled mainly with conventional tri-cone roller bits in east Texas and western Wyoming. A high-fidelity drilling model is used in an "inverted" mode to predict in-situ ultimate rock strength. This strength is a function of effective confining pressure available from published laboratory data for various rock types. The ultimate rock strength at a given depth is then used to estimate bounds on the in-situ minimum principal rock stress, or "formation closure stress". This is accomplished by employing principles of elastic and plastic deformation theory together with principles of soil mechanics. The results from this approach are compared with good agreement to available hydraulic fracturing stress test data from the four SFE

wells. This approach can provide an inexpensive means to assist with the design of hydraulic fracturing treatments.

CHAPTER II

LITERATURE REVIEW AND TECHNICAL DISCUSSION

Drilling Models

The concept of using drilling data to predict drilling rock strength has developed over a number of years as drilling models for various types of bits have steadily improved. Although models have been proposed for full-hole polycrystalline diamond compact bits (PDC bits) [1], natural diamond bits [2], and core bits [3], the more traditional tricone roller bit has received the most attention [4-13] because of its widespread use. Consequently, this model is the most highly-developed, and a recent article by Winters, et al [13] has demonstrated very high fidelity in predicting penetration rates.

In this model, penetration rate of the drill bit is calculated as a function of known operating conditions, bit design constants, mud properties and hydraulics, and ultimate compressive rock strength and ductility. The relationship given in [13] is:

$$\frac{1}{R} = \frac{SD^2}{NW}\left(\frac{aSDe}{W} + \frac{d}{e}\right) + \frac{b}{ND} + \frac{c\rho\mu D}{I_m} \qquad (1)$$

where R is the bit penetration rate (ft/hr), and:

a,b = Bit design constants (hr*rpm*in/ft)

c = Bit design constant (hr*lbf*gal/ft*lb*cp*in)

D = Bit diameter (inches)

e = Rock ductility or strain at rock failure (dimensionless)

d = Cone offset coefficient (in^{-1})

I_m = Modified jet impact force (lbf)

N = Rotary Speed (rpm)

W = Weight-on-bit (lb)

S = Compressive strength of rock at failure (psi)

ρ = Drilling fluid (mud) density (lb/gal)

μ = Plastic viscosity (Bingham Plastic Model) of drilling fluid (mud)(cp)

By using known laboratory and field data together with experimentally determined bit coefficients in the right side of (1) Winters, et al [13] claim that penetration rate can be predicted with a mean-square error (compared to measured penetration) of 2.0% or less. Such accuracy has led several authors [13, 14, 15] to propose using this model in an "inverted" mode to predict rock strength S if the penetration rate and other parameters are known. Rearranging (1) such that S is expressed as a function of the other variables produces this "inversion" [13]:

$$S = \frac{W}{D\sqrt{a\,e}}\left(\frac{N}{RD} - \frac{b}{D^2} - \frac{cN\rho\mu}{I_m} + \frac{d^2}{4ae^3}\right)^{0.5} - \left(\frac{dW}{2ae^2D}\right) \qquad (2)$$

Usually, in the absence of direct measurements made from core samples, ductility values in (2) must be estimated to calculate S.

Reasonable estimates can be made based on published literature values [13] for various lithologies, provided these lithologies are known. If cutting samples are collected by a "mud logger" during drilling, and a lithology log is plotted, lithologies can be identified. Otherwise, offset-well lithology data must be used.

Winters' [13] model development is a continuation of Warren's [12] work. The drilling model proposed by Warren [12] is given by;

$$\frac{1}{R} = \frac{aS^2D^3}{W^2N} + \frac{b}{ND} + \frac{cD\rho\mu}{I_m} \qquad (3)$$

where the variables are defined as in (1).

Winters continued development of (3) because predictions for R were low in drilling soft shales and in situations where underbalanced drilling was performed. By introducing the fourth bit coefficient, "d", and the rock ductility, "e", or strain at failure, it was believed that penetration rates in the softer formations could be modeled better. The "d" coefficient is defined as the drill bit cone offset and has units of 1/length. This is a very difficult parameter to measure and was assigned numerical values to give the best fit of the model to laboratory data. The ductility e also involves some sources of error. Values for strain at failure, or ductility, were determined from laboratory triaxial tests performed on different rock cores. Values for strain at failure, defined as a function of differential pressure by Winters [13], were all developed at room temperature and with a single strain rate. Values for strain at failure for a rock selected from a stress-strain rock failure curve, are

extremely subjective and would be a strong function of whoever made the selection. Also, it is believed that the strain at failure is a strong function of strain rate and temperature [16] which were not considered in Winters' work. A proper model for ductility should include both rotary speed and formation temperature.

Because the ductility and cone offset model (1) is suspect, in this study it was decided to begin with the model presented by Warren [12] in equation (3). Inverting this for rock strength gives:

$$S = \left[\frac{NW^2}{aRD^3} - \frac{bW^2}{aD^4} - \frac{c\rho\mu NW^2}{aI_mD^2}\right]^{.5} \qquad (4)$$

Neither Winters [13] nor Warren [12] addressed "chip hold down effects" on penetration rate modeling, but it is known [17, 18] that this effect is important.

The effective differential pressure is the primary contributor to the "chip hold-down effect" [17] for a given lithology. The chip hold-down effect arises because the actual pressure difference across a drilled chip under the bit must be overcome before the chip can be removed by the flowing mud and bit teeth. Figure 1 illustrates this effect. The effective differential pressure is the difference between the pressures at top and the bottom of a "formed", but not "free", chip. High chip hold-down causes the formation to appear harder to drill. The chip hold-down effect is a complicated and poorly understood phenomenon, and is believed to be a function of the aforementioned pressures; the penetration rate; chip thickness; chip permeability; mud type and viscosity; mud fluid mechanics at

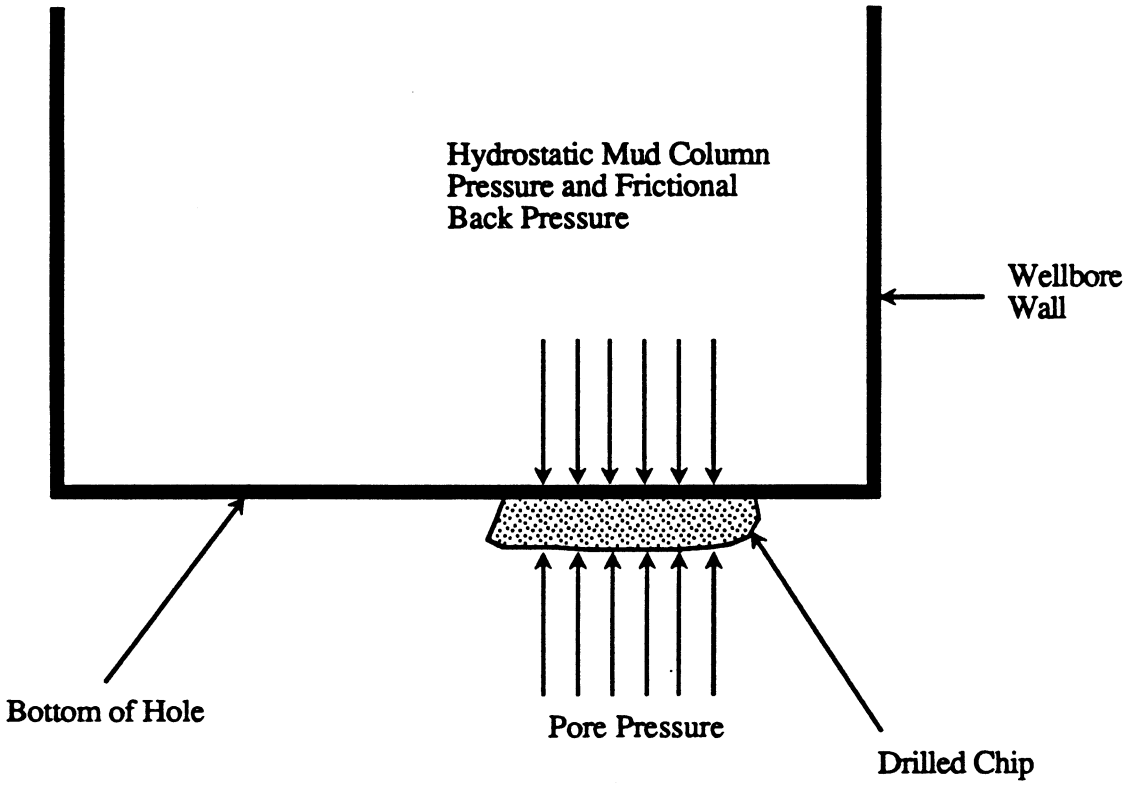

Figure 1. Chip Hold-Down Illustration

bottom-hole; and mud solids size, type and quantity. Several investigators [17, 18] have examined this problem, with no clear physical model emerging. As a first step in the study herein, we propose to include this effect with a purely empirical relationship.

In (3) and (4) the bit coefficients must be obtained after a suitable "chip hold down" modification has been included. The initial task was to determine the most appropriate form for this modification, or "chip hold-down function". Increasing differential pressure acts to reduce rate of penetration by two primary mechanisms. First, increasing differential pressure increases rock strength, discussed later in equation (8); second, the "chip hold down" effect increases with differential pressure, further reducing penetration rate. It is also lithology dependent.

Three different approaches were used in an attempt to describe the chip hold-down effect. These were;

A. Multiply the third term (the "hydraulic effect" term) on the R.H.S of (3) by a suitable function of differential pressure. This approach assumes that chip hold down is totally coupled to the effect of hydraulic jets cleaning bottom hole.

B. Multiply the first term (the "crushing effect" term) on the R.H.S. of (3) by a suitable differential pressure term. This approach assumes that the chip hold-down effect increases the strength of the rock indirectly, such that when the chip is not removed, and thus "reground", the rock appears stronger.

C. Multiply the first two terms (the "crushing effect" and the "effect of more than one tooth penetrating the rock") on the R.H.S. of (3) by a suitable differential pressure term. This approach assumes the same effect as in B, but includes the effect of more than one tooth in contact with the rock.

To establish the best relationship for chip hold-down, data from laboratory full scale drilling tests was used in which bottom hole pressure varied and other conditions remained constant. A reasonably complete set of laboratory drilling data from Amoco Production Company in Tulsa, OK, was available for an IADC 537 bit, 8.5 inches, in diameter, in which the bottom hole pressure was varied from 120 to 1200 psi. (An IADC bit code indicates the hardness of the formation the bit is designed to drill, together with certain features of the bit's tooth cutting structure and other special features). Such data was available for drilling both Catoosa Shale and Carthage Limestone, which yielded the most complete data set for determination of chip hold down effects. Because data was somewhat limited, it was decided to determine values for the bit coefficients a, b and c in (3) for the IADC 537 bit at one effective confining pressure (1200 psi) with different operating conditions and lithologies. The values of a, b and c that gave the best match of results from (3) with this data were obtained using SAS [19] and a mean-square fit routine.

The values of a, b and c obtained at 1200 psi differential pressure were held constant while various chip hold-down functions were tried, using the three approaches listed above. Drilling data at

other differential pressures was then employed to produce a chip hold-down function that gave the best fit of equation (3), modified as in the three approaches above. Results from the chip hold down functions obtained in Catoosa Shale and Carthage Limestone for the three cases discussed above are shown in Figures 2-4. When evaluating the chip hold down functions for approaches A, B and C it was observed that approach C yielded the most reasonable model of the chip hold down effect because it alone yielded positive values of the chip hold-down function for all differential pressures. The results in Figure 4 for both Catoosa Shale and Carthage Limestone were used, and a reasonable fit to this data is given in (5), with the coefficients a_c, b_c and c_c for Catoosa Shale and Carthage Limestone given in Table 1:

$$f_c(P_e) = c_c + a_c(P_e\text{-}120)^{b_c} \qquad (5)$$

where $f_c(P_e)$ is defined as the differential pressure or the "chip hold down function", and

P_e = Effective confining pressure (psi)

a_c b_c c_c = Chip hold down coefficients (lithology dependent) Units on a_c, b_c and c_c chosen such that $f_c(P_e)$ is dimensionless.

The equations (3) and (4) are now modified to include a chip hold-down effect, and the final version of the 3-term model is given as:

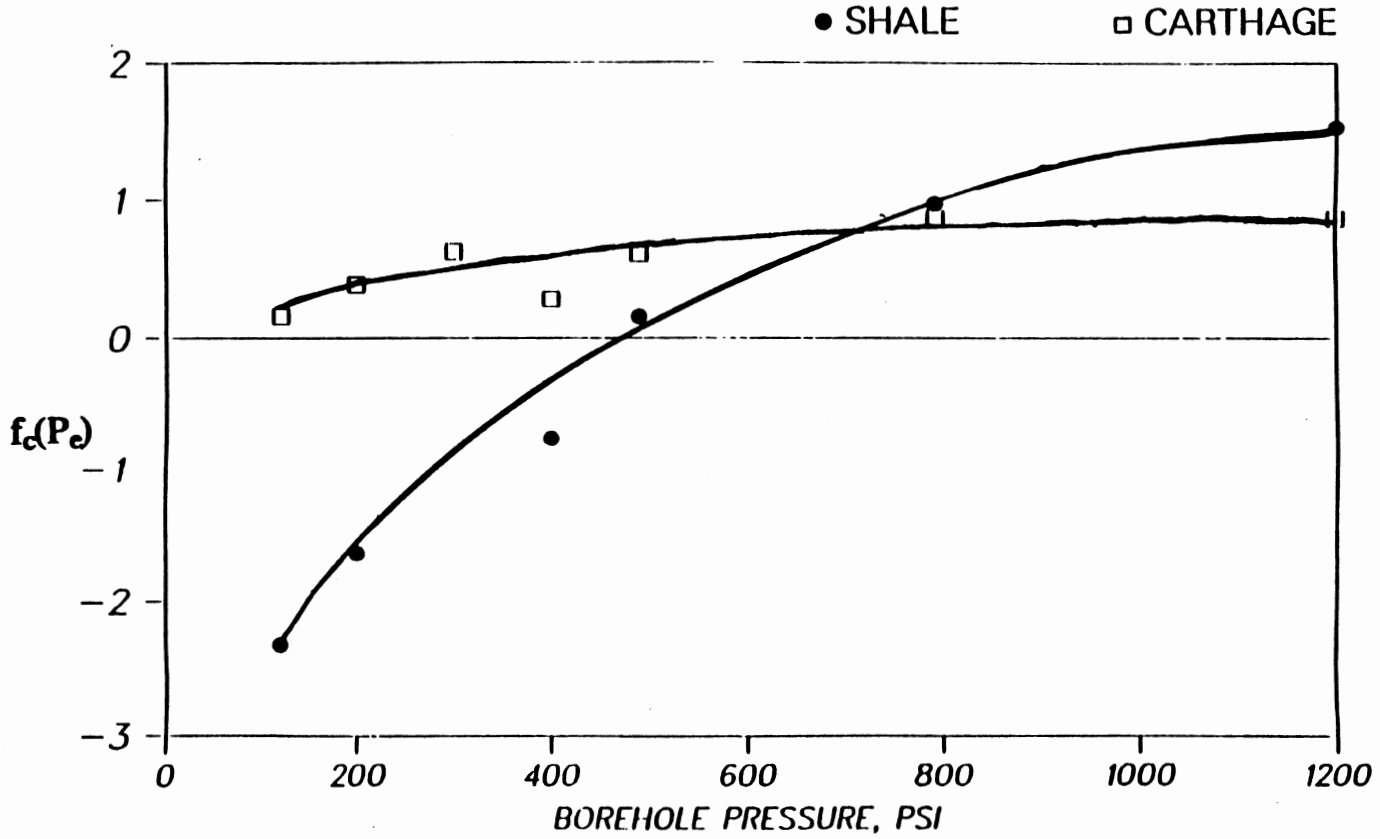

Figure 2. Chip Hold-Down Evaluation Function - Approach A

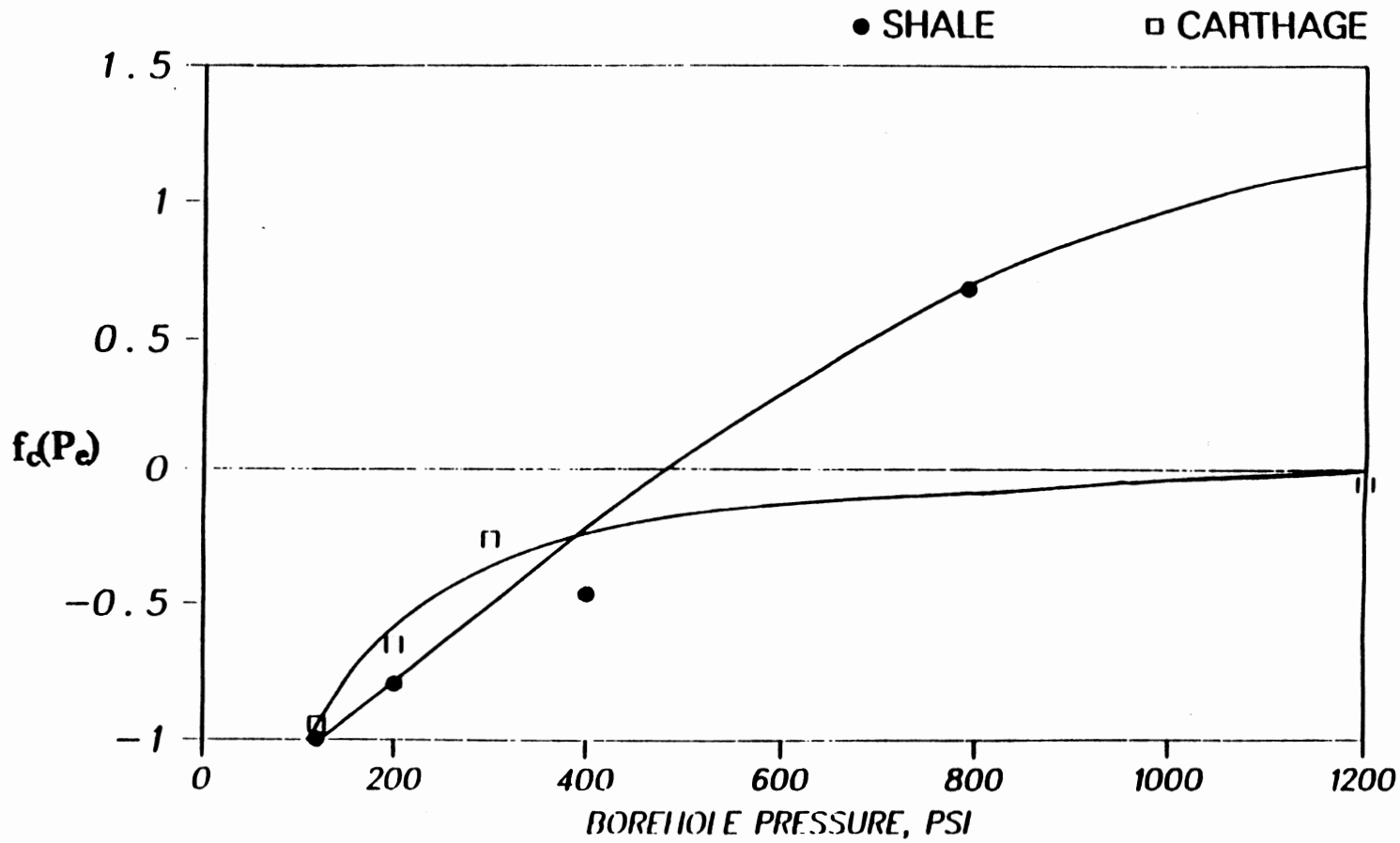

Figure 3. Chip Hold-Down Evaluation Function - Approach B

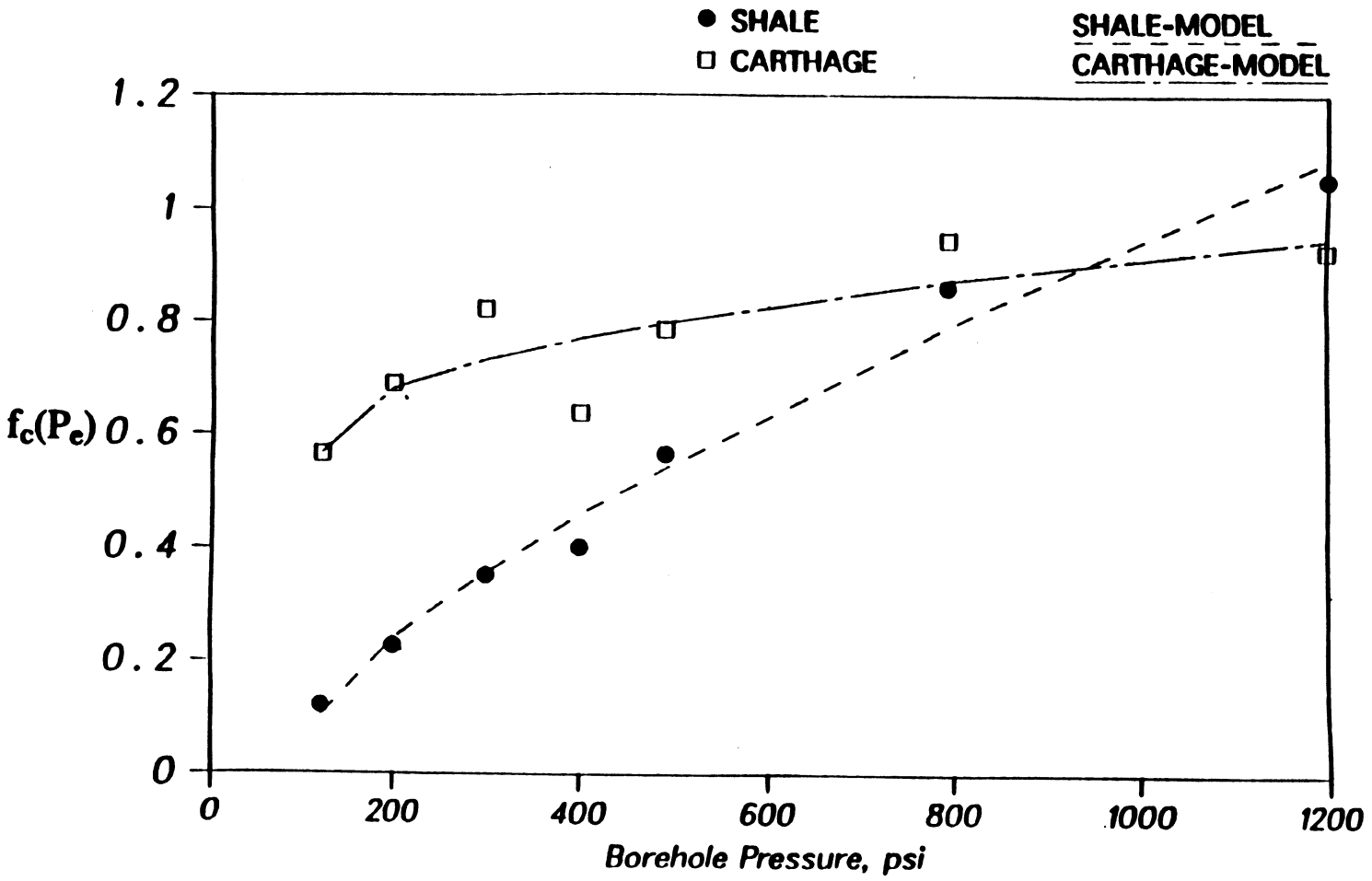

Figure 4. Chip Hold-Down Evaluation Function - Approach C

TABLE I

CHIP HOLD DOWN FUNCTION
LITHOLOGY COEFFICIENTS

Lithology	a_c*	b_c*	c_c*
Catoosa Shale	.004966	.75721	.10254
Carthage Limestone	.014132	.47016	.56948

* Units on a_c, b_c and c_c chosen such that $f_c(P_e)$ is dimensionless.

$$\frac{1}{R} = f_c(P_e)\left[\frac{aS^2D^3}{W^2N} + \frac{b}{ND}\right] + \frac{cD\rho\mu}{I_m} \qquad (6)$$

Then, solving for rock strength gives:

$$S = \left[\frac{NW^2}{af_c(P_e)RD^3} - \frac{bW^2}{aD^4} - \frac{c\rho\mu NW^2}{af_c(P_e)I_mD^2}\right]^{.5} \qquad (7)$$

For bits used in the SFE wells for which no published laboratory drilling data is available, laboratory drilling data was obtained from a bit manufacturing company and from Amoco Production Company Research Center, Tulsa, OK.

To verify the utility of (1), three "sharp" 8.5 inch bits with IADC codes of 4-3-7, 5-3-7, and 6-2-7 were used by Winters [13] in a shallow field test in Oklahoma over a 3000 foot interval. Values of S were calculated foot-by-foot from (2), and the results were compared with results from 18 selected core samples from a nearby well. These cores were tested in a triaxial load cell with appropriate confining pressure to determine mechanical properties. A close match was obtained between measured triaxial rock strengths and computed rock strengths from (2). The computed bottomhole rock strengths varied from 3,000 to 30,000 psi.

Equation (3) was verified in [12] with good penetration rate predictions, but the laboratory tests used limited differential pressure variability. Equation (4) was not verified for rock strength with field triaxial core tests. However, because the penetration rate predictions of (3) are comparable to those of (1) for most drilling

situations, we believe rock strength calculations will be of comparable accuracy.

A problem arises in using equations (1), (2), (3) and (4) when the bit is dull, either because of tooth wear or missing teeth. No published models are available to predict penetration rates with dull bits, and we expect such situations will arise. The simplest approach would be to use drilling data only over the footage interval of the bit run where confidence exists that the bit remained sharp. However, this would ignore as much as 50% of the data, if we discarded say the bottom half of each bit interval. A second approach would be to linearly degrade the bit sharpness from beginning to end of the bit interval. This assumes, of course, that accurate dull-bit grading is available from the bit records. Then using an unpublished procedure communicated by Warren [20], the penetration rate R in (1) or (3) can be adjusted as a function of the tooth dullness. This is done by multiplying the inverse of the R.H.S. of (1), (3) or (6) with a reduction factor that linearly decreases with bit tooth wear. Unfortunately, this procedure holds some promise only for worn teeth, not for broken teeth. If the bit was pulled with large numbers of insert teeth missing, only the initial footage for the sharp bit could be used. It should be empathized that during conversations with the drilling engineer on the four SFE wells, it was learned that no bits had severe tooth damage and that almost all bits were pulled green (with little or no wear). Accordingly, in the work reported herein, all bits were assumed to have insignificant wear.

Relation Between the Ultimate Rock Strength and the Minimum Principal Fracturing Stress

The value of S determined from Equation (2) has been shown [13] to be the ultimate compressive strength of the rock under the confining pressures determined by the annular friction backpressure and hydrostatic pressure of the drilling fluid, or "mud" and the rock pore pressure. However it should be noted that Winters [13] verified the ultimate compressive rock strength at no deeper than 1500 feet, such that the chip hold down effect would be negligible, and would not have to be modeled. On the other hand, rock strength and ductility in (2) were modeled in [13] as a function of confining pressure.

In order to use this "confined" ultimate rock strength for stress calculations, the "unconfined" rock strength must be determined, which will be lithology dependent. The required lithology information can be obtained from [13], [21] and [22]. The major problem in this project is to relate the unconfined ultimate rock strength to the in-situ fracturing stress. A physical correlation between the ultimate rock strength and the minimum principle failure stress is difficult, because there are two different criteria of failure. The ultimate rock strength from the drilling model is determined by failure in compression, while the minimum in-situ fracturing stress is determined by tensile failure after overcoming the appropriate in-situ stresses. It is known that the tensile strength of rock is very small compared to the compressive strength [16, 23]. Also, during a fracturing test, the tensile strength of the rock is

overcome only during the initial fracturing. After the initial fracture, only the minimum principal in-situ stress must be overcome to maintain an open fracture. This stress is called the formation closure stress. It is believed that the tensile strength is also small compared with the minimum principal in-situ stress [16].

The compressive rock strength is a function of effective differential pressure for various rock types, and can be normalized as shown by Winters et al [13] and others [21, 22], with sample results, given in Figures 5 and 6. The effective differential pressure is initially defined as: (1) for permeable formations, the difference between the hydrostatic mud column pressure and the rock pore fluid pressure and (2), for impermeable formations, only the mud pressure. This is over-simplified, but perhaps reasonable, because when the formation is permeable, a "mud cake" at bottom hole serves as a barrier to higher-pressure mud attempting to equalize with the pore fluid beneath an "incident" chip. Accordingly, in this simplified treatment, the net "differential" pressure acting on an "incident" chip is the bottom hole pressure minus the pore pressure. For impermeable formations, we assume that substantially reduced pressure (from overburden pressure) on rock at bottom-hole causes sufficient increase in rock volume to reduce pore fluid pressure to zero. Because the rock is impermeable, far-field pore pressure cannot equalize with the near-chip "zero" pore pressure. Accordingly, the net differential pressure acting on an incident chip is simply the bottom-hole mud pressure. Empirical expressions for rock strength as a function of effective differential pressure for given

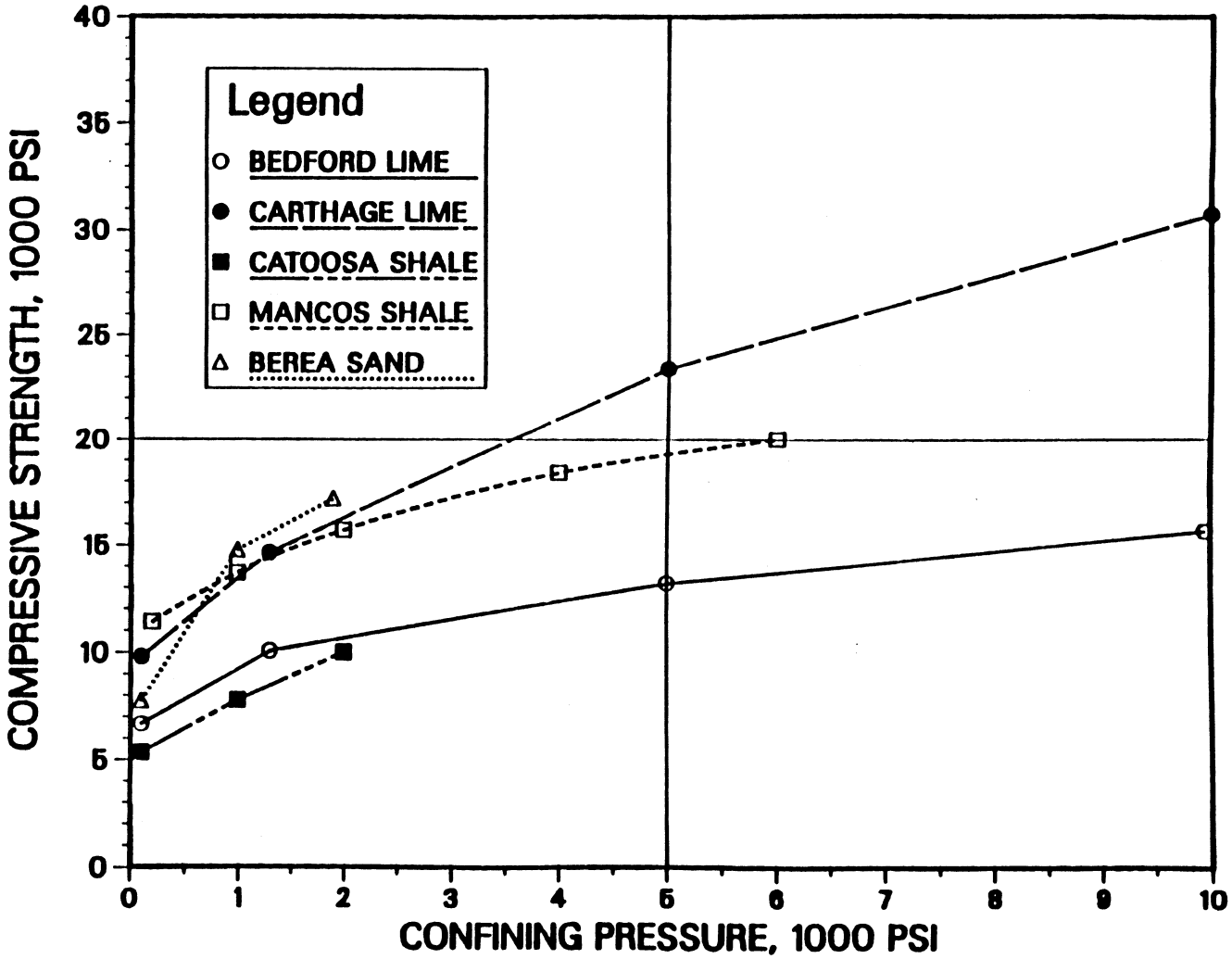

Figure 5. The Effect of Confining Pressure on Rock Strength

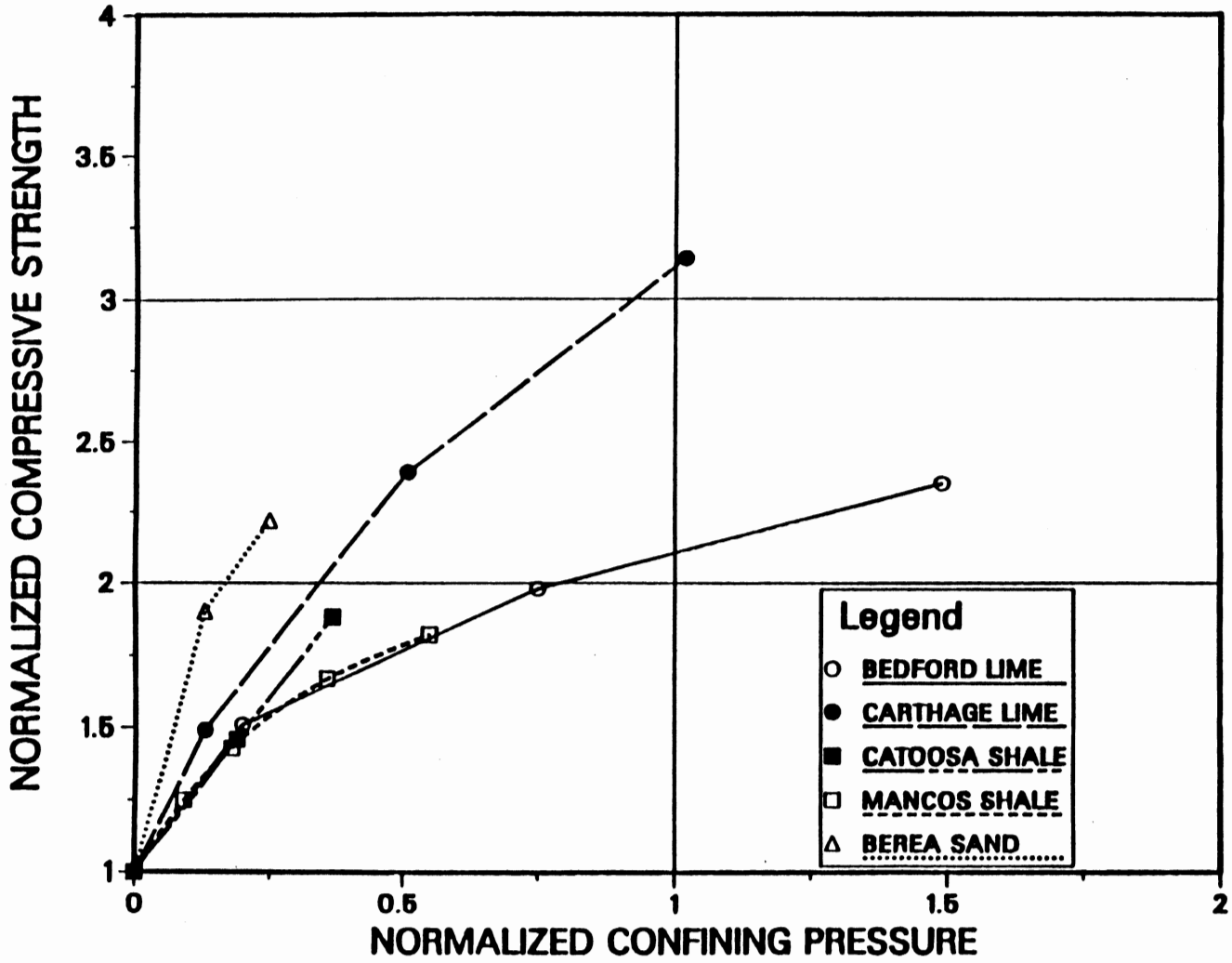

Figure 6. The Effect of Confining Pressure on Normalized Rock Strength

lithologies can be obtained by fitting data from [13, 24] with equations given by:

$$\frac{S}{S_0} = \left(1 + a_s P_e^{b_s}\right) \tag{8a}$$

where

S = Compressive strength at rock failure (confined)(psi)

S_0 = Compressive strength at rock failure(unconfined)(psi)

P_e = Effective confining pressure(psi)

a_s, b_s = Lithology coefficients (dimensions chosen such that $a_s P_e^{b_s}$ is dimensionless)

For each lithology a set of coefficients a_s and b_s can be determined by using a mean square fit routine in SAS [19] (SAS is a suite of commercially available computer programs for statistical analysis of data). For a given lithology the unconfined rock strength, S_0, will typically change with well depth due to rock hardening caused by cementation, grain size changes, compaction, and other burial factors. Table 2 lists the unconfined rock strength values for the lithologies given in Figures 5 and 6.

Now consider calculating the unconfined rock strength, S_0 from (8a), in which the lithology composition is known and the confined rock strength S has been determined from (7). Equation (8a) can be re-arranged to solve for S_0, which yields:

$$S_0 = \frac{S}{\left(1 + a_s P_e^{b_s}\right)} \tag{8b}$$

TABLE II

UNCONFINED ROCK STRENGTH FOR
THE LITHOLOGIES SHOWN
IN FIGURES 5 AND 6

Lithology	Unconfined Rock Strength (psi)
Bedford Limestone	6500
Carthage Limestone	9800
Catoosa Shale	5000
Mancos Shale	10800
Berea Sandstone	7100

Now with S known, S_0 varies inversely with effective confining pressure, P_e. It can be seen that if the rock is assumed "impermeable", S_0, will be small because P_e will equal the large bottom hole mud pressure. On the other hand if the rock is assumed "permeable", S_0 will be larger because P_e will equal the "smaller" difference between bottom-hole mud pressure and pore pressure. In effect, this means that determination of unconfined rock strength depends upon knowledge of rock permeability and pore pressure in addition to knowledge of confined rock strength S and lithology. (It is shown in Appendix A that the impermeable case gives an upper bound on in-situ stress). An estimate of permeability can be obtained from the Self Potential (SP) electric log of the wellbore after the well is drilled. Pore pressure is more difficult to obtain, but can be estimated if data from offset wells in the area is available. In this study we will calculate unconfined rock strength and in-situ stress separately for both assumptions, namely, permeable and impermeable rock, and compare the results with field stress test and lithology data to determine under what conditions, if any, these assumptions might hold.

Assume that S_0 has been determined for the two permeability assumptions. Then from (8a) we have:

$$S_p = S_{0p}(1 + a_s P_e^{b_s}) \tag{9a}$$

$$S_i = S_{0i}(1 + a_s P_e^{b_s}) \tag{9b}$$

where p and i denote the permeable and impermeable assumptions, respectively.

Now with lithology coefficients known, Mohr circles for the stress state of the rock [16] can be drawn for any effective confining pressure, as suggested by Cheatham [25], and shown in Figure 7. One of the Mohr circles in Figure 7 is obtained by solving equation (9a) or (9b) with an effective confining pressure P_{e1}, which gives a value S_1 for rock strength. The unconfined rock strength S_{01} and the lithology coefficients a_s and b_s are known values. The Mohr circle is constructed by using a radius of the maximum stress divided by 2.0 which is:

$$\text{radius} = \frac{S_1}{2.0}$$

and the center of the Mohr circle is at compressive and shear stress values of, respectively:

$$\left(P_{e1} + \frac{S_1}{2.0}, 0 \right)$$

By generating a large number of Mohr circles from (9a) or (9b) at different confining pressures, a Mohr failure envelope can be constructed from tangents, as shown in Figure 8. The failure envelope can then be used to determine whether a rock sample under any stress loading condition will fail. Failure will occur if the Mohr circle for that given stress state intercepts the failure envelope. Otherwise, the rock will not fail.

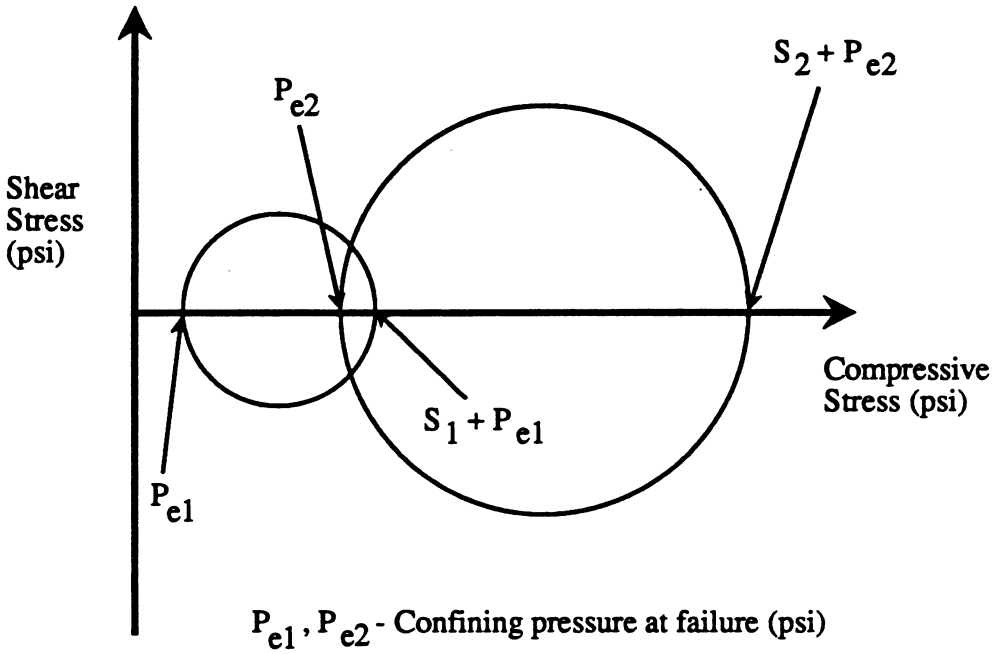

P_{e1}, P_{e2} - Confining pressure at failure (psi)

S_1, S_2 - Confined Rock Strength at Failure (psi)

Figure 7. Mohr Circles for Two Confining Pressures

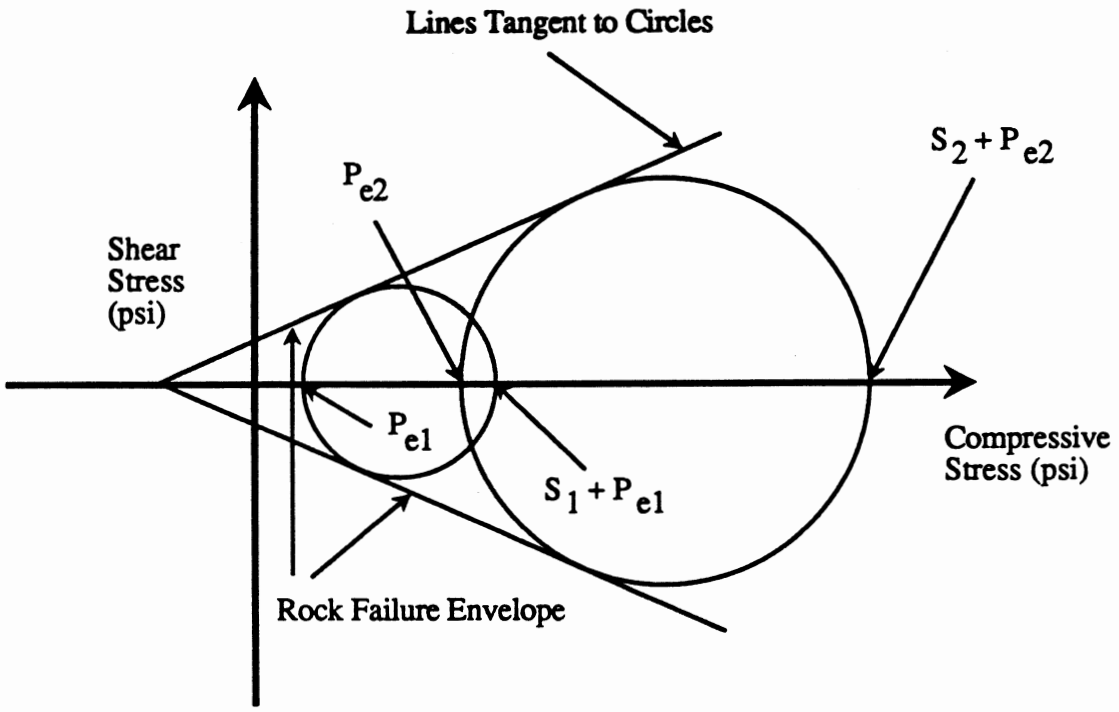

P_{e1}, P_{e2} - Confining pressure at failure (psi)

S_1, S_2 - Confined Rock Strength at Failure (psi)

Figure 8. Sample Mohr Failure Envelope

It has been observed from triaxial rock stress tests on cores from the SFE #1 well that there is a difference in the shape of the failure envelope for different lithologies, as shown in Figures 9 and 10 [24]. The sandstone failure envelope is approximated by almost straight lines, while the shale failure envelope has more of a concave shape. Other investigators [25] have concluded that sandstone tends to fail according to the elastic Coulomb failure criteria, while shale fails plastically. It can also be observed from Figures 9 and 10 that the tensile strength is small compared to the compressive strength.

A sample set of "permeable" and "impermeable" failure envelopes are shown in Figure 11. The failure envelope for a given rock describes compressive failure as a function of confining pressure. Because the failure envelope gives the maximum possible stress state of the rock, it can be used as an upper bound on the minimum in-situ principal rock stress. From this envelope, a new quantity called the "failure angle of internal friction", β, [16] can be determined for all values of P_e.

The "failure angle of internal friction" can be defined from soil mechanics tests [26-30] where the defining experiment employs a horizontally divided box filled with sand and placed under a vertical load, illustrated in Figure 12. The shearing force necessary to displace the upper box is measured for various values of vertical load [30]. In this way it is found that the shearing stress for failure is directly proportional to the normal stress, such that

$$\frac{\tau}{\sigma} = \tan \beta \qquad (10)$$

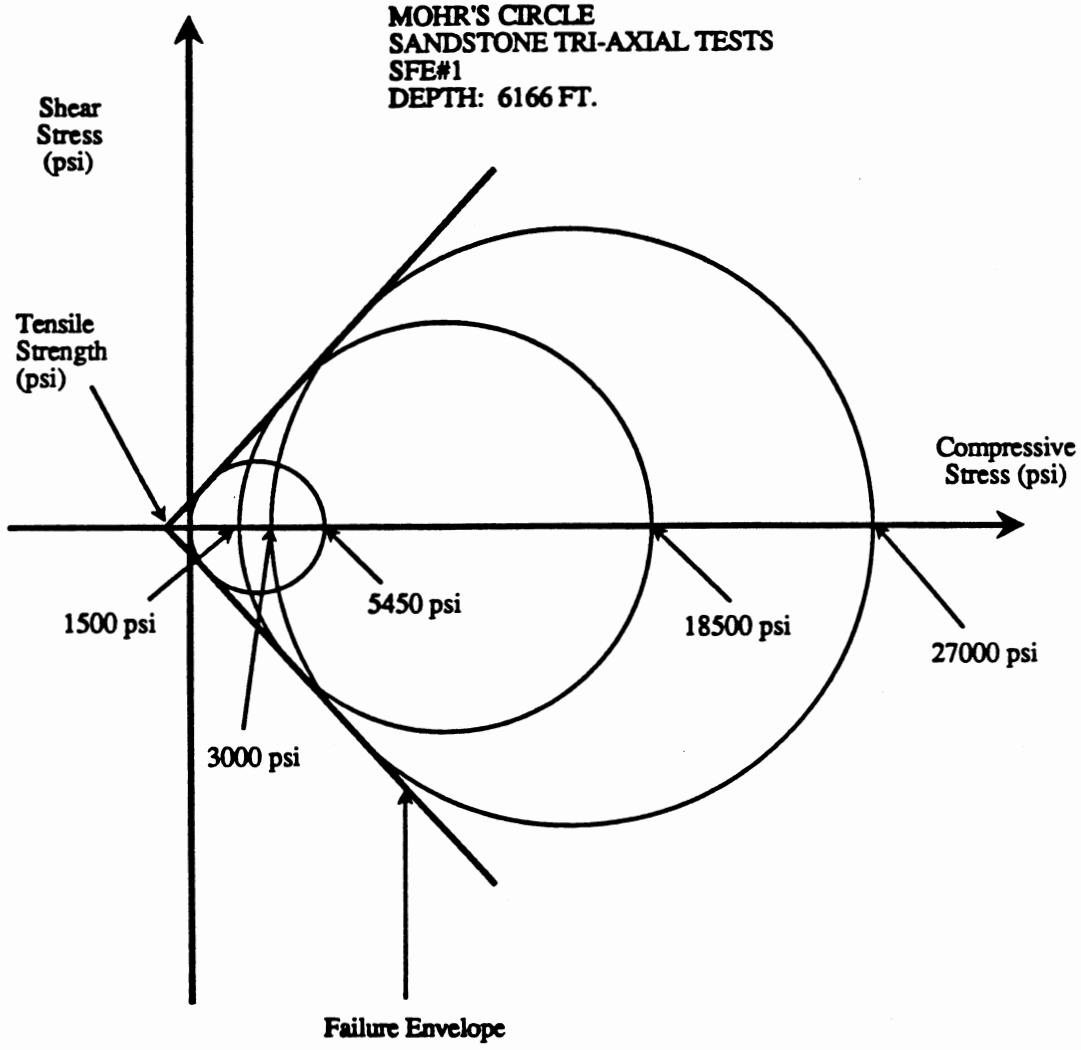

Figure 9. Sandstone Failure Envelope from SFE #1

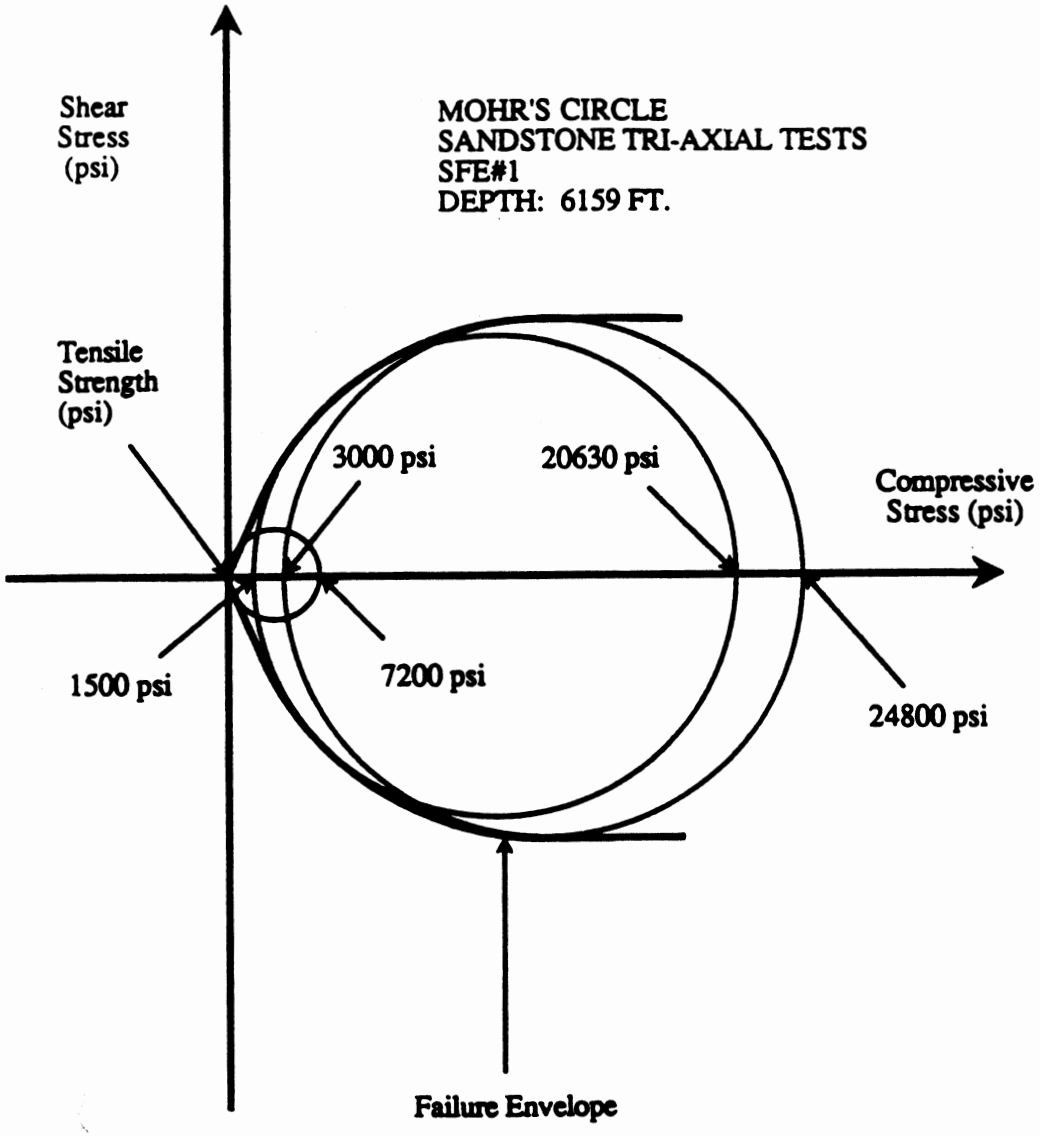

Figure 10. Shale Failure Envelope from SFE #1

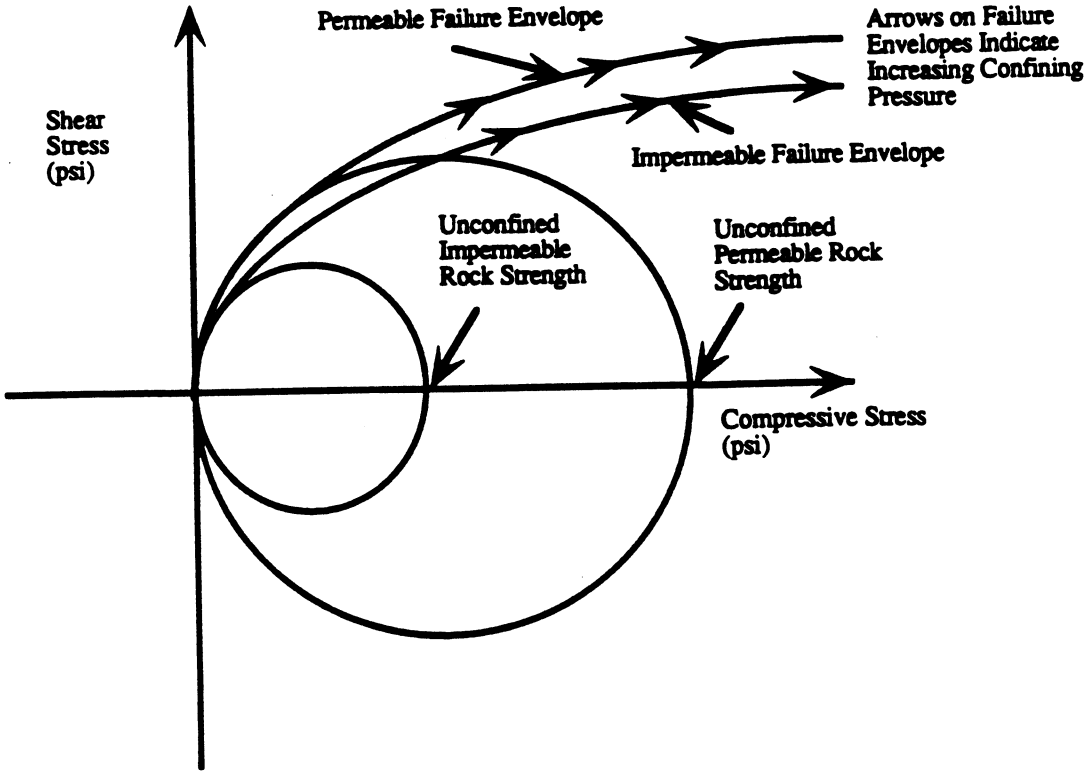

Figure 11. Sample Failure Envelope for the Permeable and Impermeable Cases

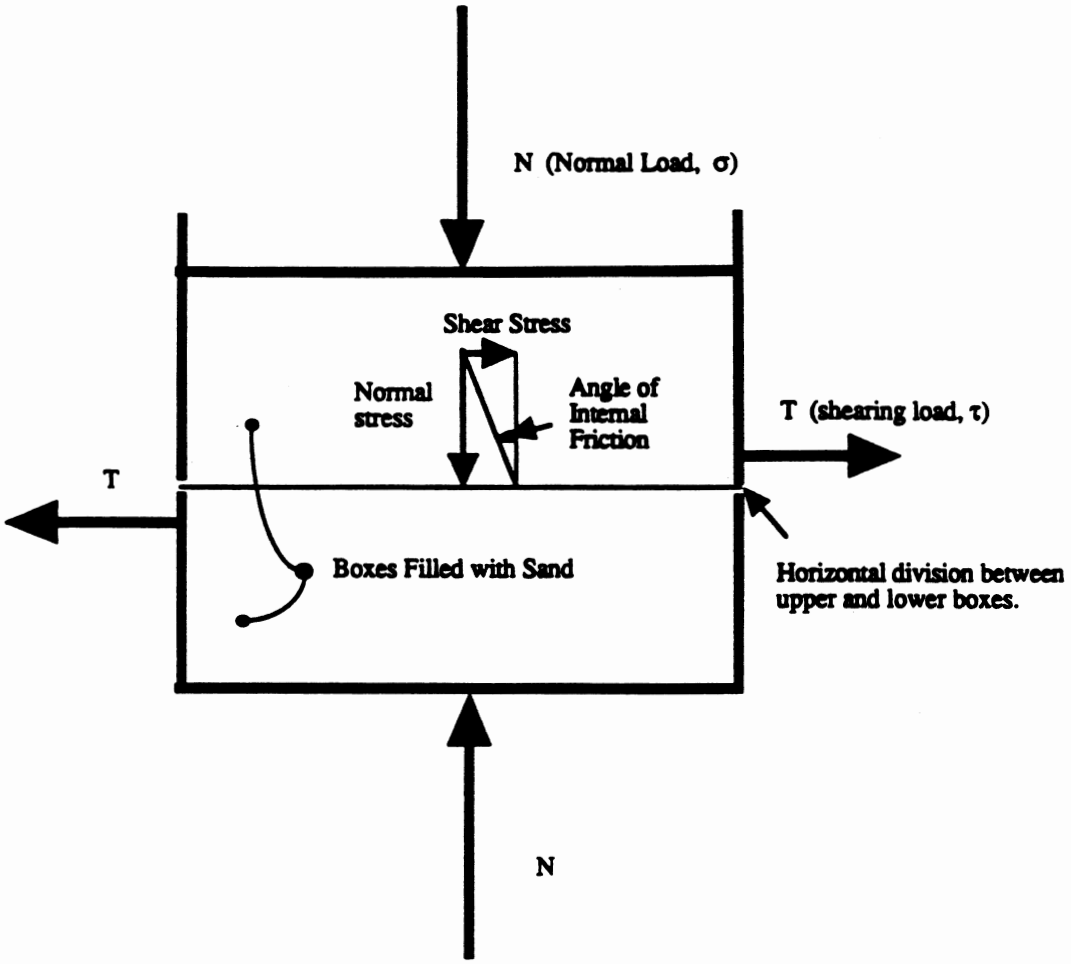

Figure 12. Soil Mechanics Test For Determination of Angle of Internal Friction

where

τ = shear stress at box movement (psi)

σ = normal stress at box movement (psi)

β = angle of internal friction (degrees)

Figure 13 illustrates how the angle of internal friction, β, is found on a Mohr failure envelope. The angle of internal friction is the angle between axis of normal stress and the tangent to the Mohr failure envelope at a point representing a given failure stress condition. The internal friction is considered to be due to the interlocking of the soil or rock grains and resistance to sliding between the grains. The "failure angle", α, is illustrated in Figure 13. If shear failure takes place according to Mohr's hypothesis, the plane of failure should run at an angle, α, relative to the normal stress axis of the specimen [16].

The derivation of an expression for β, from (9a) and (9b) is given in Appendix B, and the result is;

$$\beta = \arcsin\left[\frac{1.0}{1.0 + \left(\frac{4\Delta}{S_0 a_s (P_{e+\Delta}^{\,b_s} - P_{e-\Delta}^{\,b_s})}\right)}\right] \qquad (11)$$

where

β = Failure angle of internal friction (degrees)

Δ = Arbitrarily small pressure (psi) - 50 psi used in this study

S_0 = Unconfined rock strength (psi)

$P_{e+\Delta}$ = Effectine confining pressure plus the arbitrarily small pressure (psi)

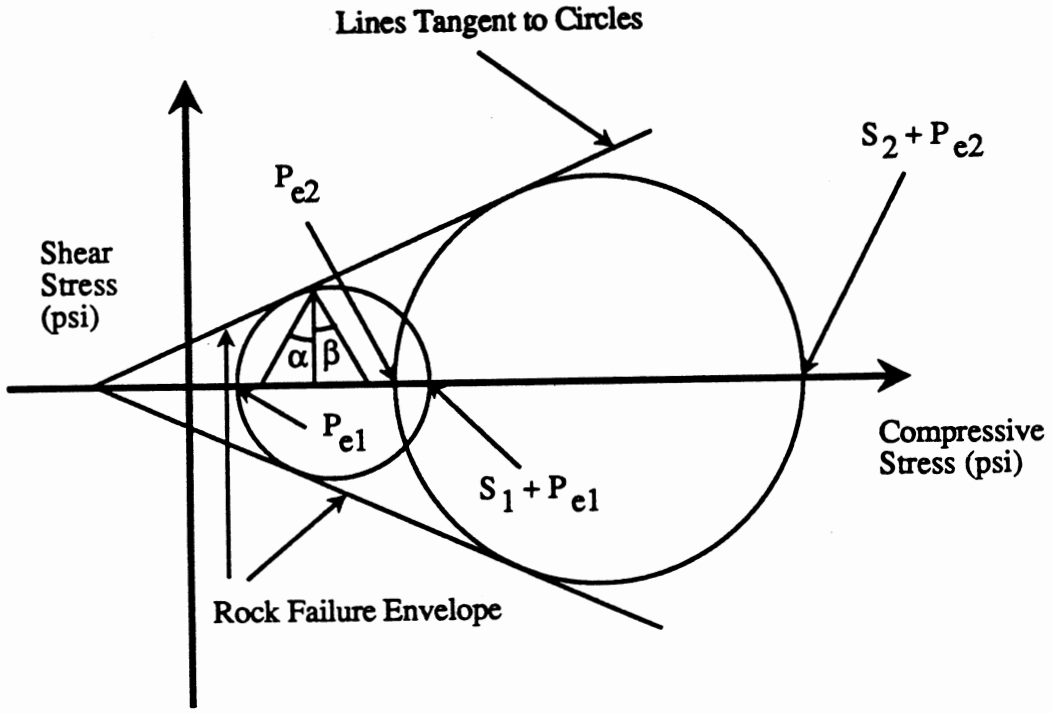

P_{e1}, P_{e2} - Confining pressure at failure (psi)

S_1, S_2 - Confined Rock Strength at Failure (psi)

β - Angle of interal friction

α - Failure angle

Figure 13. Failure Envelope Showing Angle of Internal Friction

$P_{e-\Delta}$ = Effectine confining pressure minus the arbitrarily small pressure (psi)

This failure angle is the primary mechanism to relate rock strength to in-situ stress. The in-situ rock effective confining pressure used in (11) is given by the difference between the in-situ horizontal stress and in-situ pore pressure;

$$P_{e\text{-}is}=S_h-P_p \tag{12}$$

where

P_{e-is} = Effective in-situ pressure (psi)

P_p = In-situ pore pressure (psi)

S_h = In-situ horizontal stress (psi)

Note that this in-situ confining pressure in (12) is not the same as the drilled rock confining pressure, discussed earlier in the paragraph preceding (8a) (and given explicitly by (25) in the next section). Unfortunately, the in-situ horizontal stress S_h needed in (12) is the principal unknown in our problem. Accordingly, we will use an iterative procedure (in conjunction with (20), to converge to the correct angle of internal friction, to be discussed below following (21)).

Now, let us examine the calculation of in-situ stress. Early investigators encountering this problem were civil engineers, who needed information on horizontal stresses in the ground to design structures. Literature studies reveal that "a coefficient of earth at

rest", K_0, has been used by various investigators [26-30], in a relationship given by

$$S_h = K_0 S_{ob} \tag{13}$$

where

S_{ob} = Overburden pressure or vertical stress (psi)

S_h = Horizontal or lateral stress (psi)

K_0 = Coefficient for earth pressure at rest (dimensionless)

Relationships for K_0, determined for rock at failure, were obtained experimentally by different investigators as follows:

$$K_0 = 1 - \sin(\beta) \quad [27] \tag{14}$$

$$K_0 = 0.9(1 - \sin(\beta)) \quad [28] \tag{15}$$

$$K_0 = 1 + (2/3)\sin(\beta) \quad [29] \tag{16}$$

$$K_0 = 0.95 - \sin(\beta) \quad [30] \tag{17}$$

where

β = angle of internal friction (degrees)

The foregoing theory from soil mechanics is applicable to solid rocks provided the Mohr failure envelopes have been determined [31]. These will have been determined from the "inverted" penetration rate model (7) and the rock strength pressure relationship (9a) and (9b).

Equations (13) - (17) were developed for situations in which the pressure in the pores of the rock was zero. Alkpan [32] compared the results from (14) - (17), shown in Figure 14. It can be seen that differences are small. Brooker and Ireland [30] found that results from (14) matched data from sand and that data from shales and clays matched predictions from (15) - (17) quite well. This approach, modified to account for non-zero pore pressure, will be applied to data from the four SFE wells, where the angle of internal friction β can be determined from (11) for every foot drilled.

A similar concept has been used in several investigations [33, 34] by relating horizontal to vertical earth stresses through Poisson's Ratio. The approach from the hydraulic fracturing literature assumes non-zero pore pressure and has been used with varying degrees of success. It is given by:

$$S_h = S_{he} + P_p$$

$$S_{he} = \frac{\nu}{1-\nu} S_{ve} \qquad (18)$$

$$S_{ve} = S_{ob} - P_p$$

where

S_{he} = Net effective horizontal stress (psi)

S_{ve} = Net effective vertical stress (psi)

ν = Poisson's Ratio

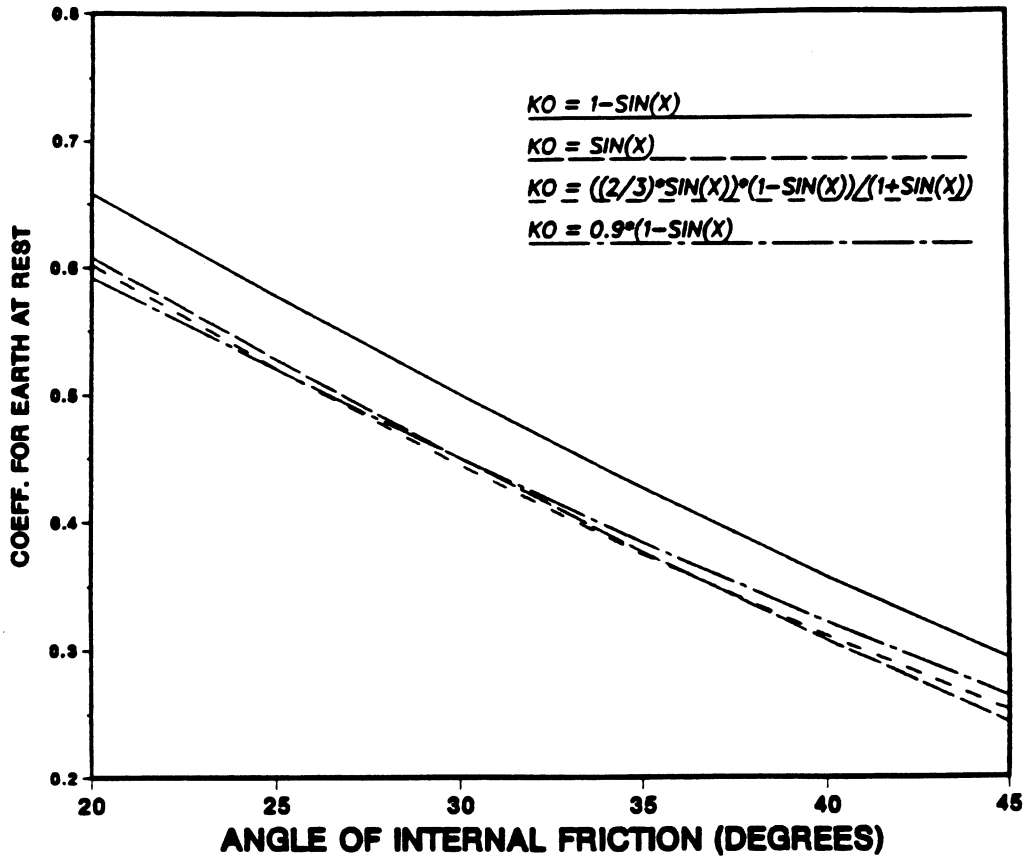

Figure 14. Comparisons of Different Calculations of K_0

From [24], the in-situ closure stress, or horizontal stress S_h, is obtained by combining the relations in (18) to obtain:

$$S_h = \frac{\nu}{1 - \nu}(S_{ob} - P_p) + P_p \qquad (19)$$

Now, assuming the overburden and the pore pressure are known, the fracture closure pressure could be predicted for given values of Poisson's Ratio. In fact (19) has been applied to data from the SFE #1-3 wells, with good results, where Poisson's Ratio was obtained from electric log data [24]. The equation was also applied to data from Gulf of Mexico wells [35] with mixed results, assuming a constant value, $\nu = 0.25$, for sandstone. Now by comparing (19) with (13), we propose a more general relationship, given by:

$$S_h = K_0(S_{ob} - P_p) + P_p \qquad (20)$$

in which, as a special case for (20):

$$K_0 = \frac{\nu}{1-\nu} \qquad (21)$$

In fact, if (21) holds, we would have a method of determining Poisson's Ratio from the internal angle of friction used to calculate K_0. This calculation for ν from SFE well data could then be checked against values of ν determined from electric logs to determine if, in fact, (21) is valid.

Equation (20) shows that the minimum in-situ stress occurs when K_0 equals zero, such that a minimum value of in-situ horizontal stress is the the pore pressure. This lower bound on horizontal in-situ stress would be expected to occur in an unconsolidated sand.

Determination of S_h in (20) requires knowledge of β to find K_0. In turn, calculation of β in (11) requires knowledge of S_h in (12). Accordingly, we will use an iterative procedure by first assuming a first guess for S_h in (12), calculate β in (11) with the guess to give K_0 in (14) - (17), and then S_h in (20). This value of S_h is put back into (12) and the process repeated until values of S_h on successive trials differ by only a small amount.

The utilization of Poisson's Ratio to obtain the in-situ stress is discussed by various investigators [31, 34], who conclude that it is not always applicable. In a personal communication [36], J. B. Cheatham emphasized that various investigators in hydraulic fracturing have questioned the general applicability of (18) and (19). Hubbert and Willis [31] also demonstrate, that (18) and (19) may lead to incorrect results. They state that the general state of stress underground is that in which the three principal stresses are unequal. Consider a normal fault, which is a vertical or near-vertical break in the continuity of a rock formation caused by shifting or dislodging of the earth's crust, in which adjacent surfaces are differentially displaced parallel to the plane of fracture. For techtonically relaxed areas characterized by normal faulting, the least principal stress should be horizontal and the fractures produced should be vertical. The injection pressure required for fracturing would be less than that of the overburden. In areas of active

tectonic compression, the least principal stress should be vertical and equal to the pressure of the overburden. For these more rare situations, the fractures should be horizontal, with injection pressures equal to or greater than the pressure of the overburden. Horizontal fractures cannot be produced by hydraulic fracturing pressures less than the total pressure of the the overburden. Another important conclusion was that regardless of whether the fracturing fluid was of the rock penetrating or non-penetrating type, the fractures should be approximately perpendicular to the axis of least stress. The assumption that the three principal stresses should in general, be equal, was due to the fact that over long periods of geologic time, the earth has exhibited a high degree of mobility wherein the rocks have been repeatedly deformed to the limits of failure by faulting and folding. In order for this to have occurred, substantial differences between the principal stresses would have been required. With experiments involving a gelatin model, Hubbert [37] demonstrated that for sand having an angle of internal friction of 30 degrees, failure will occur in both normal faults, as well as thrust faults, when the largest principal stress reaches a value which is about three times the least principal stress. A thrust fault is a fault whose plane has a small angle of inclination with the horizontal. Furthermore, the failure will occur along a plane making an angle of about 60 degrees with the direction of the least principal stress. Also, for a fixed vertical stress, the horizontal stress may have any value between the limits of one-third to three times the minimum vertical stress.

The presence of a wellbore distorts the pre-existing stress field in the rock. An approximate calculation of this distortion may be made by assuming that the rock is elastic, the borehole smooth and cylindrical, and the borehole axis vertical and parallel to one of the preexisting regional principal stresses. The stresses to be calculated should all be viewed as the effective stresses carried by the rock in addition to fluid pressures, which exist within the wellbore as well as in the rock. The calculation employs elastic theory for the stresses in an infinite plate containing a circular hole, with its axis perpendicular to the plate. This was first done by Kirsch [38] and Timoshenko [39]. In the study herein, the distortion in near-wellbore rock stresses caused by the presence of the wellbore can be neglected. This is because the drilled compressive rock strength (used in the penetration rate model) is a function only of the differential pressure across the undrilled rock. Moreover, the formation closure stress, for which we seek bounds, is determined mainly by stresses away from the wellbore in fractures that can extend at least 100 feet. Stress distortions would typically occur only within inches of the wellbore. While these distortions might affect the pressure required to initially fracture the well, they would not be expected to significantly affect the closure stress.

The calculation of the minimum principal in-situ stress as a function of Poisson's Ratio is complicated by the fact that the rock has been under high pressure during millions of years and has likely undergone chemical reactions, including bonding and cementing. The problem of developing a stress history for a sedimentary basin has been considered by various investigators. Voight [40] considered

effects due to the overburden pressure, pore pressure and thermal stresses, including a superposed tectonic stress, for the elastic case. He pointed out the importance of using the correct material properties at deposition and initial burial, compared to properties at later events when the rock is cemented. The effects of thermal stresses are handled assuming "locked in" stresses, which are a result of the changing material properties, and require that the analysis be performed in time steps by calculating stress changes at each step. These stress changes are accumulated to arrive at a stress state at any time. Later, Prats [41] used elastic and viscoelastic analysis to calculate the stress difference expected in different rocks at depth. He concluded that the effects of overburden, pore pressure, temperature, tectonic strains, and variable material properties were all important. His analyses show that with creep, soft materials, such as shales, will have considerably larger stresses than harder rocks, such as sandstones. Prats also reported that "the least horizontal stresses may be different in a sandstone reservoir than in an adjacent shale and that the measured stress does not correlate with measured ambient formation properties. Reported compressive stresses in shales exceed those in sandstones. In some cases the difference in the stresses appears to contain growth of hydraulically induced vertical fractures.

Warpiniski [42] uses a combination of the time-history approach and a new proposed viscoelastic model. He proposed that the minimum horizontal stress be given by

$$S_h = \frac{\nu}{1-\nu}(S_{ob} - \gamma P) + \gamma P + S_t \qquad (22)$$

where

γ = Biot's modulus, which is a coefficient of linear expansion of the formation and may be a function of overburden, temperature and horizontal strain (dimensionless)

S_t = A generalized term that accounts for tectonic imbalance in horizontal stresses (psi)

In a later paper, Warpinsky and Teufel [43] apply this approach to field data on three MWX (Multi-Well Experiments) wells, where they actually measure the quantities needed for prediction of horizontal stresses. The results agree well with the stress tests performed on these wells. The approach has merit, but there is a problem with obtaining lateral strain of a formation during drilling operations.

In [44], Warpinsky discusses the difficulty of obtaining data needed for evaluation of the horizontal stresses in Prats's work [41]. He states that in general, none of the needed parameters are known, so the calculation is currently more of academic than of practical interest. The equation proposed by Prats [41] shows that the differential horizontal effective stress induced by changes in depth, temperature, strain or pressure could be written as

$$\Delta S_h = \frac{\nu}{1-\nu}\Delta(S_{ob} - P) + \left(\frac{E\alpha_t}{1-\nu}\right)\Delta T + \frac{E\Delta e_i}{(1-\nu^2)} + \frac{\nu E\Delta e_i}{(1-\nu^2)} \qquad (23)$$

where

Δ = differential

T = temperature (degrees Fahrenheit)

e_i, e_j = tectonic strains (dimensionless)

α_t = thermal coefficient of expansion (1/degrees Fahrenheit)

E = Young's modulus (psi)

ν = Poisson's Ratio (dimensionless)

It is obvious that some account of geology and depositional history is needed in the final modeling, but this should be done in great detail and might not be directly available from data collected during drilling operations. However, this could possibly be applied in post analysis of well data when the complete depositional history is known for the formation drilled.

All previous efforts for predicting in-situ horizontal stresses requires either extensive logging or stress testing. Also, some approaches [41, 42] require guessing and estimation of parameters that are almost impossible to verify. The use of electric logs to obtain Poisson's ratio for closure stress predictions has shown to be unreliable [30, 34, 36] and expensive. The approach proposed herein is believed to be the least expensive, since the only field requirement is instrumentation for collection of drilling data. Such instrumentation is becoming more and more routine with most drilling operations, and will therefore add little extra cost.

CHAPTER III

RESULTS AND TECHNICAL DISCUSSION

In what follows, an approach is given to obtain rock strength from drilling data and to use it to estimate in-situ closure stress bounds for four SFE (Staged Field Experiment) wells.

Rock Strength Lithology Coefficients

The lithology coefficients a_s and b_s in (8) for each lithology were determined from triaxial stress test performed on cores at different confining pressures. The triaxial test data were obtained from [13] and [24], and coefficients obtained using the statistical analysis computer program SAS [19] are shown in Table 3. Results from (8a) for sandstone and shale are shown plotted versus the measured triaxial rock strengths at different confining pressures in Figures 15 and 16 with the corresponding data points listed in Table 4 and 5.

Penetration Rate Model: Coefficients and Chip Hold Down Function

The modified 3-term tricone drilling model developed by Warren [12] will be used to predict drilling rock strength, as given in

TABLE III

CONFINED ROCK STRENGTH
LITHOLOGY COEFFICIENTS

Lithology	a_s	b_s
Shale (general) (See Table 4)	.0043188	.74191
Sandstone (general) (See Table 5)	.01331	.57106
Mancos Shale	.0033110	.649783
Carthage Limestone	.0041415	.678632
Catoosa Shale	.0029602	.969626

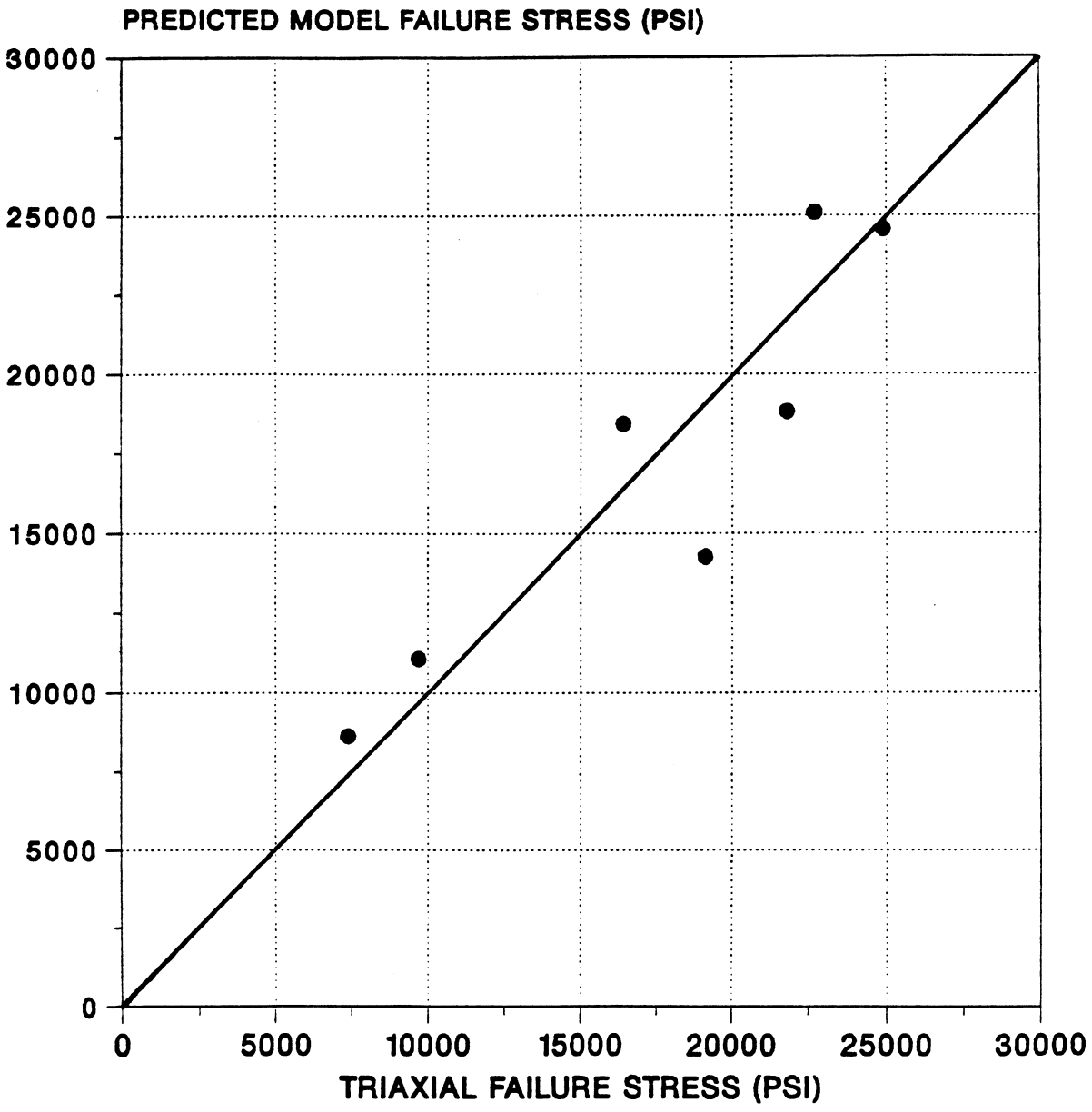

Figure 15. Rock Strength Model Prediction for Shale Versus Triaxial Rock Strength Tests

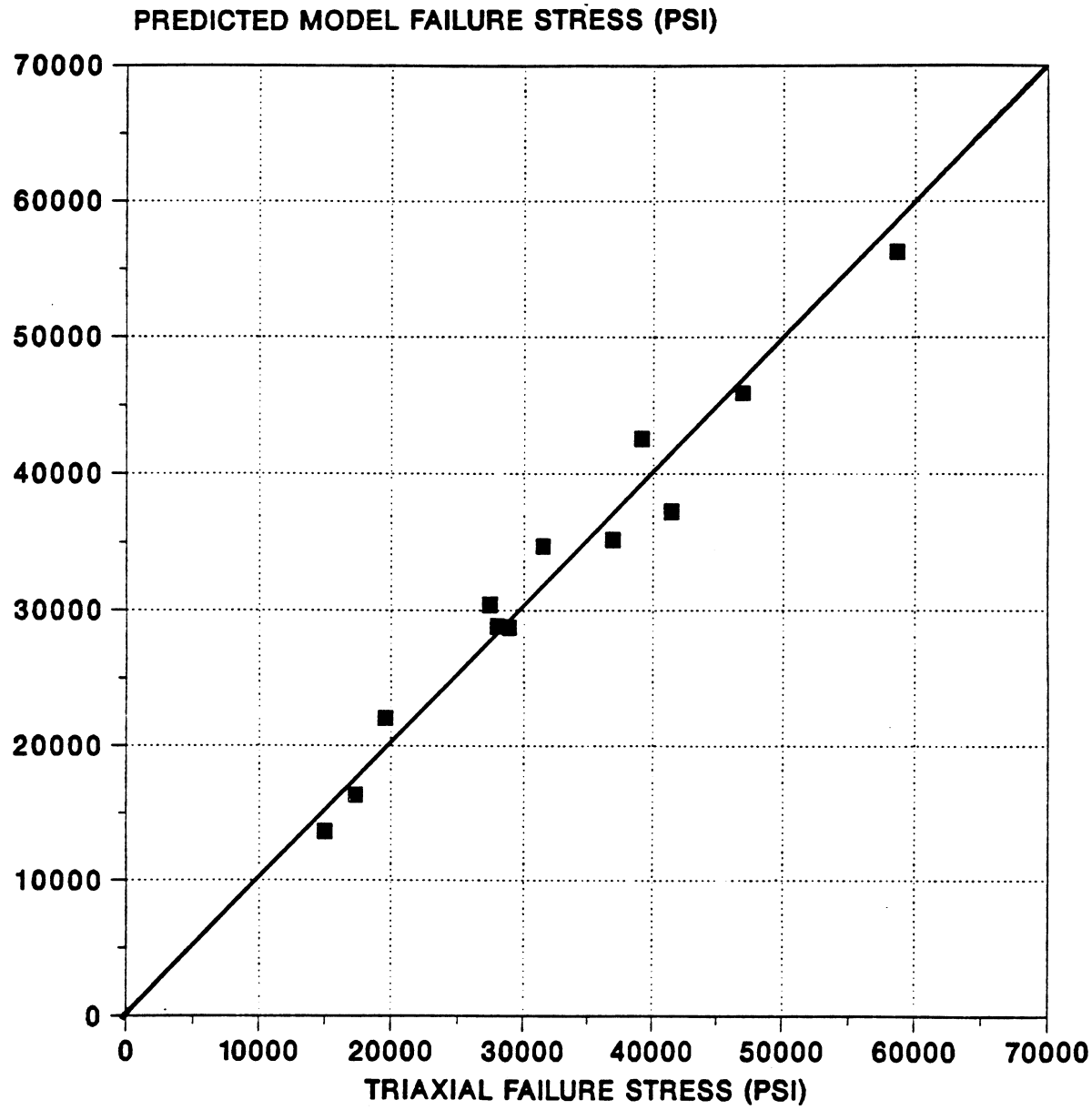

Figure 16. Rock Strength Model Prediction for Sand Versus Triaxial Rock Strength Tests

TABLE IV

SHALE TRIAXIAL TEST AND
MODEL PREDICTIONS

Confining Pressure (psi)	Triaxial Failure Stress (psi)	Model Failure Stress (psi)	Unconfined Failure Stress (psi)	Reference
1000	7400	8631	5000	[13]
2000	9700	11073	5000	[13]
1500	19130	14264	7200	[24]
3000	21800	19014	7200	[24]
1500	18400	18821	8700	[24]
3000	22700	25088	8700	[24]
1500	16400	18425	9300	[24]
3000	24900	24560	9300	[24]

TABLE V

SANDSTONE TRIAXIAL TEST AND
MODEL PREDICTIONS

Confining Pressure (psi)	Triaxial Failure Stress (psi)	Model Failure Stress (psi)	Unconfined Failure Stress (psi)	Reference
1000	15000	13671	8100	[22]
2000	17300	16377	8100	[22]
5000	19600	22068	8100	[22]
10000	28000	28851	8100	[22]
1500	31500	34728	18600	[24]
3000	39100	42560	18600	[24]
1500	28900	28753	15400	[24]
3000	36900	35238	15400	[24]
1500	27400	30433	16300	[24]
3000	41400	37297	16300	[24]
1500	46900	45930	24600	[24]
3000	58600	56289	24600	[24]

(7). In this model, both the bit coefficients and the "chip hold down" coefficients in (5) most be determined from laboratory drilling data. The task of determining the bit coefficients for various bit types involved collection, evaluation and editing of this data. Sample input laboratory drilling data is listed in Table 6. The initial task was to determine the most appropriate form for the chip hold-down function. As discussed earlier increasing differential pressure reduces rate of penetration by two primary mechanisms: Rock strength increases and chip hold-down increases.

In our earlier section "Literature Review and Technical Discussion", we described the procedure for modeling the chip hold-down effect, using a "chip hold-down function" given by (5), with appropriate coefficients listed in Table 1 for two lithologies, Catoosa Shale and Carthage Limestone. Because the chip hold-down function is independent of the drilling bit used, it could be applied, along with the rock strength function in (8a), to obtain the bit coefficients for the other IADC bit types drilling both Catoosa Shale and Carthage Limestone. Table 7 presents the results, and Appendix C lists the SAS program. The predicted ROP's using equations (5), (6), and (8a) are plotted versus laboratory drilling ROP's in Figures 17-23. From these Figures, it can be concluded that the modified 3-term drilling model (6) predicts laboratory penetration rates with acceptable accuracy. We therefore believe these models (5), (6), and (8a) can be applied with good accuracy in the field. However, this will require a method to handle inhomogeneous, or "mixed" lithologies, because rocks encountered in field drilling will rarely be homogeneous, as in laboratory drilling.

TABLE VI
SAMPLE LABORATORY DRILLING DATA

Lithology Type	Borehole Pressure (psi)	N (rpm)	Bit Torque (ft-lb)	W (lbs)	R (ft/hr)
1*	1161	62	256	6.96	3.84
1	1202	62	575	13.7	7.03
1	1202	62	952	20.7	10.90
1	1199	61	1304	27.64	14.87
1	1202	60	1685	34.63	19.57
1	1205	61	2066	41.38	24.34
1	1200	60	2559	47.52	31.66
1	1201	122	238	7.14	5.01
1	1198	122	513	14.13	10.34
1	1198	122	823	21.08	17.34
1	1201	121	1178	28.00	26.01
1	1198	121	1587	34.90	30.15
1	1197	121	1966	41.53	42.06
1	1200	120	2413	47.53	48.69

* 1= Catoosa Shale

TABLE VII*

DRILLING MODEL BIT COEFFICIENTS
FOR DIFFERENT IADC CODES

Bit Make	Bit Type	Size (in)	IADC	a $\left(\frac{hr \cdot rpm \cdot in}{ft}\right)$	b $\left(\frac{hr \cdot rpm \cdot in}{ft}\right)$	c $\left(\frac{hr \cdot lbf \cdot gal}{ft \cdot lb \cdot cp \cdot in}\right)$
Security	S33CF	8.75	116	.020641	2.69531	.001892
Security	S82F	8.75	437	.018172	3.07096	.002094
Security	S84F	8.75	517	.025865	4.21486	.003350
Smith	F3	8.50	537	.013830	9.77070	.002231
Security	M84F	8.50	617	.019020	13.45270	.003256
Hughes	J55R	8.50	627	.047020	13.47211	.003306
Security	H87F	8.50	737	.016841	9.31402	.003350

* Reducing to three significant digits for the coefficients a, b, and c yields less than 0.5 percent possible error in in-situ stress bound calculation as discussed in Appendix K. While Table VII shows more than three significant digits, the accuracy of the data used to compute values for a, b, and c probably does not justify more than three.

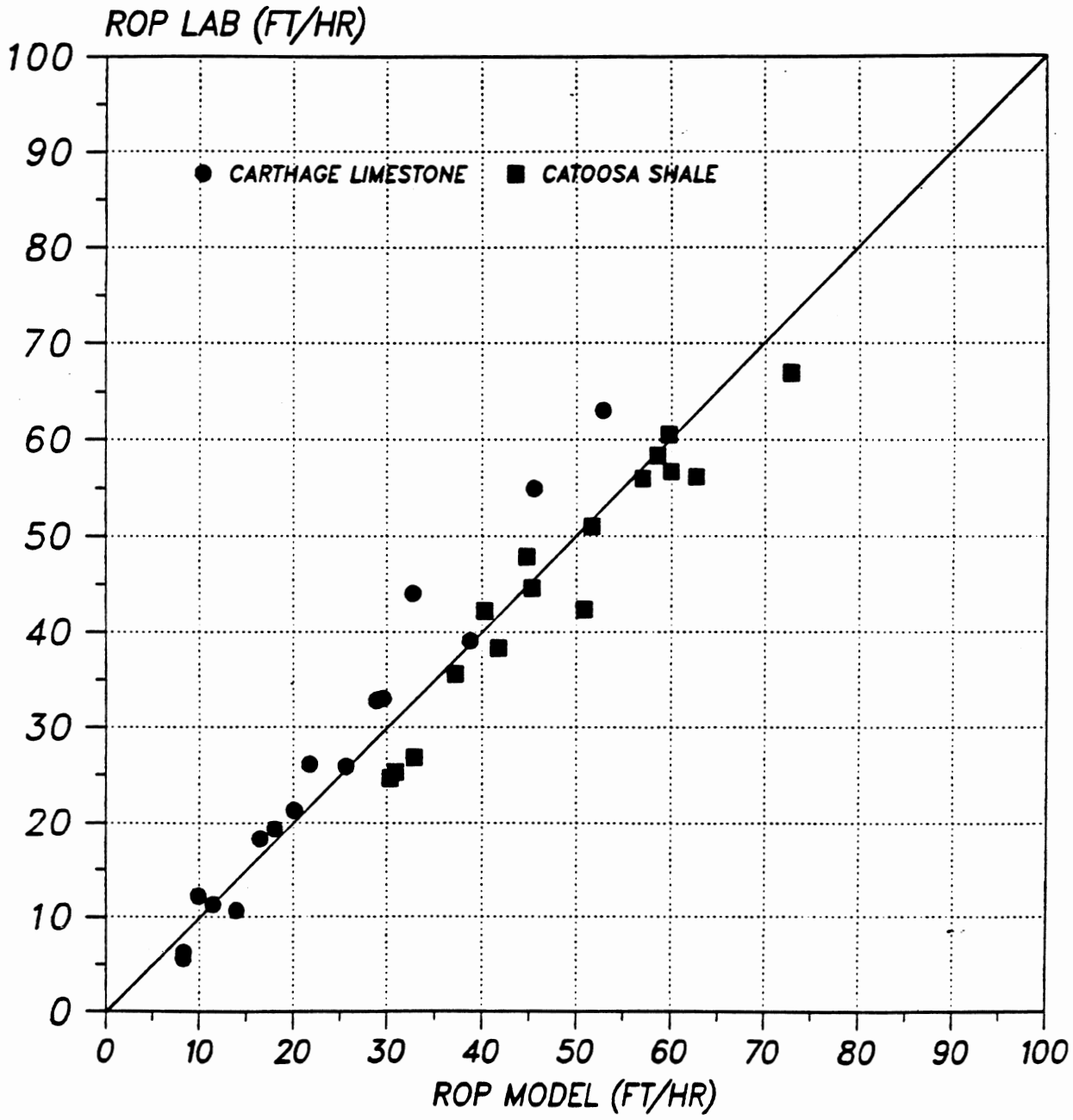

Figure 17. 3-Term Model Prediction Versus Laboratory Drilling Data for 116 IADC Bit

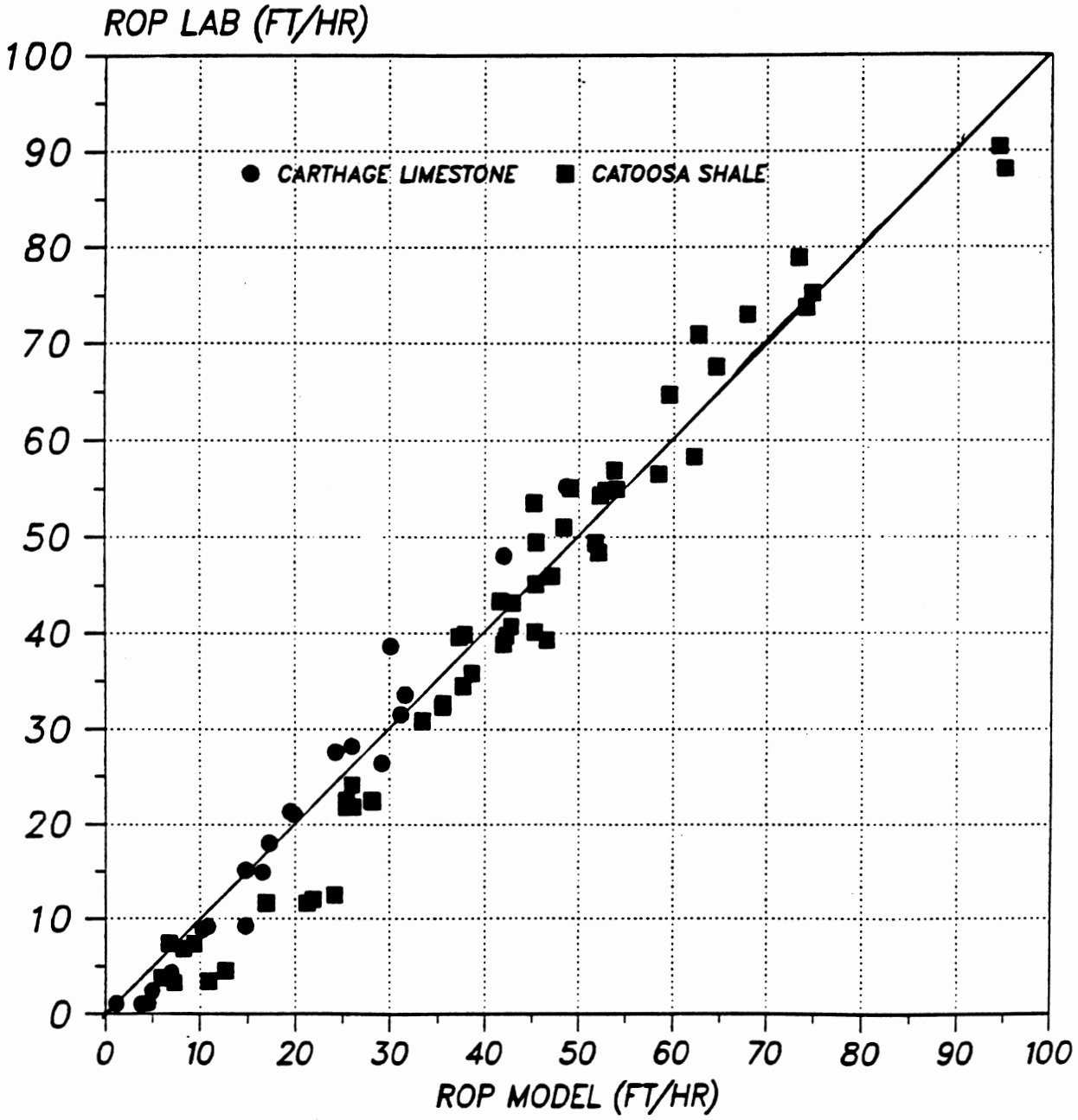

Figure 18. 3-Term Model Prediction Versus Laboratory Drilling Data for 437 IADC Bit

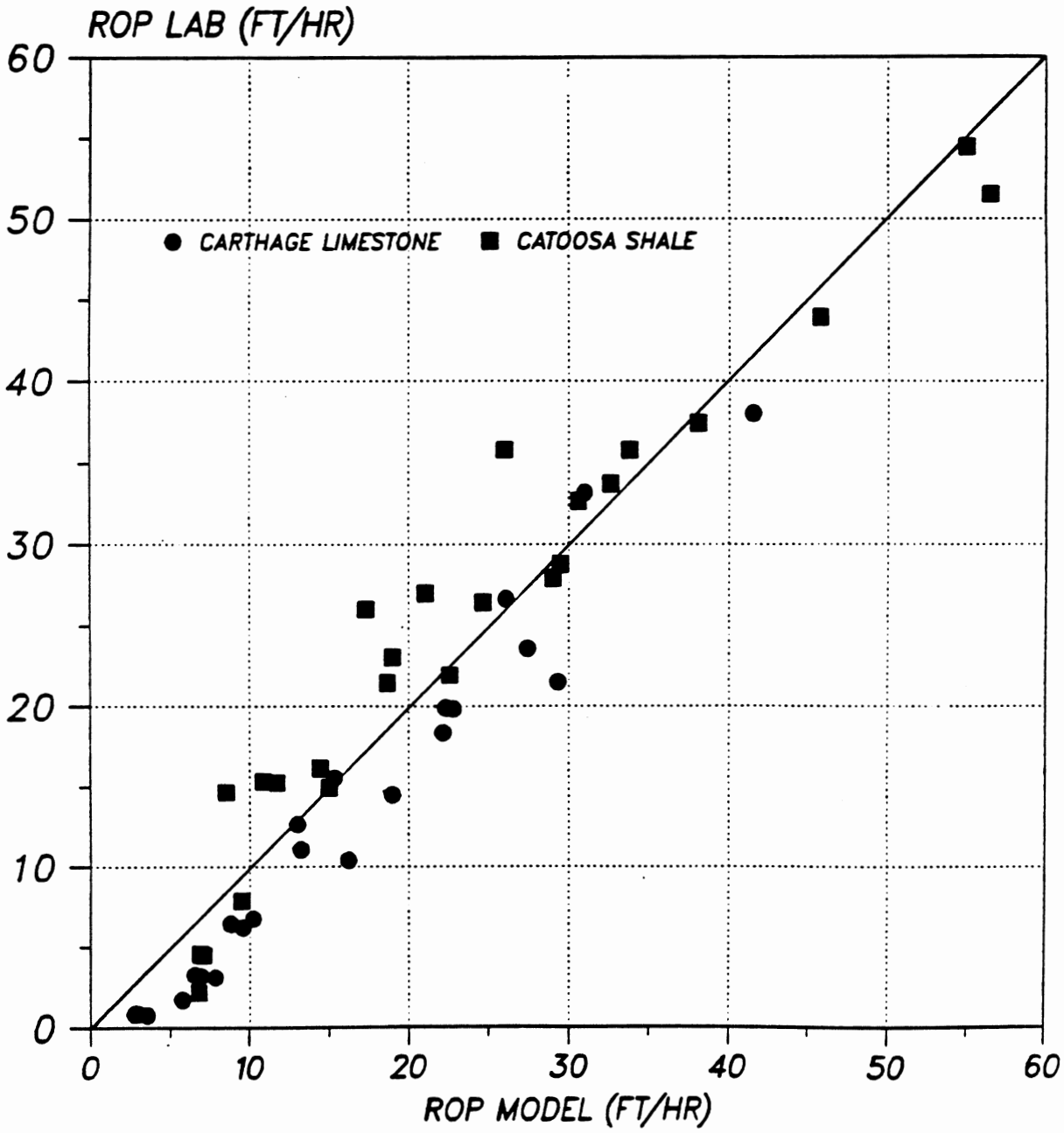

Figure 19. 3-Term Model Prediction Versus Laboratory Drilling Data for 517 IADC Bit

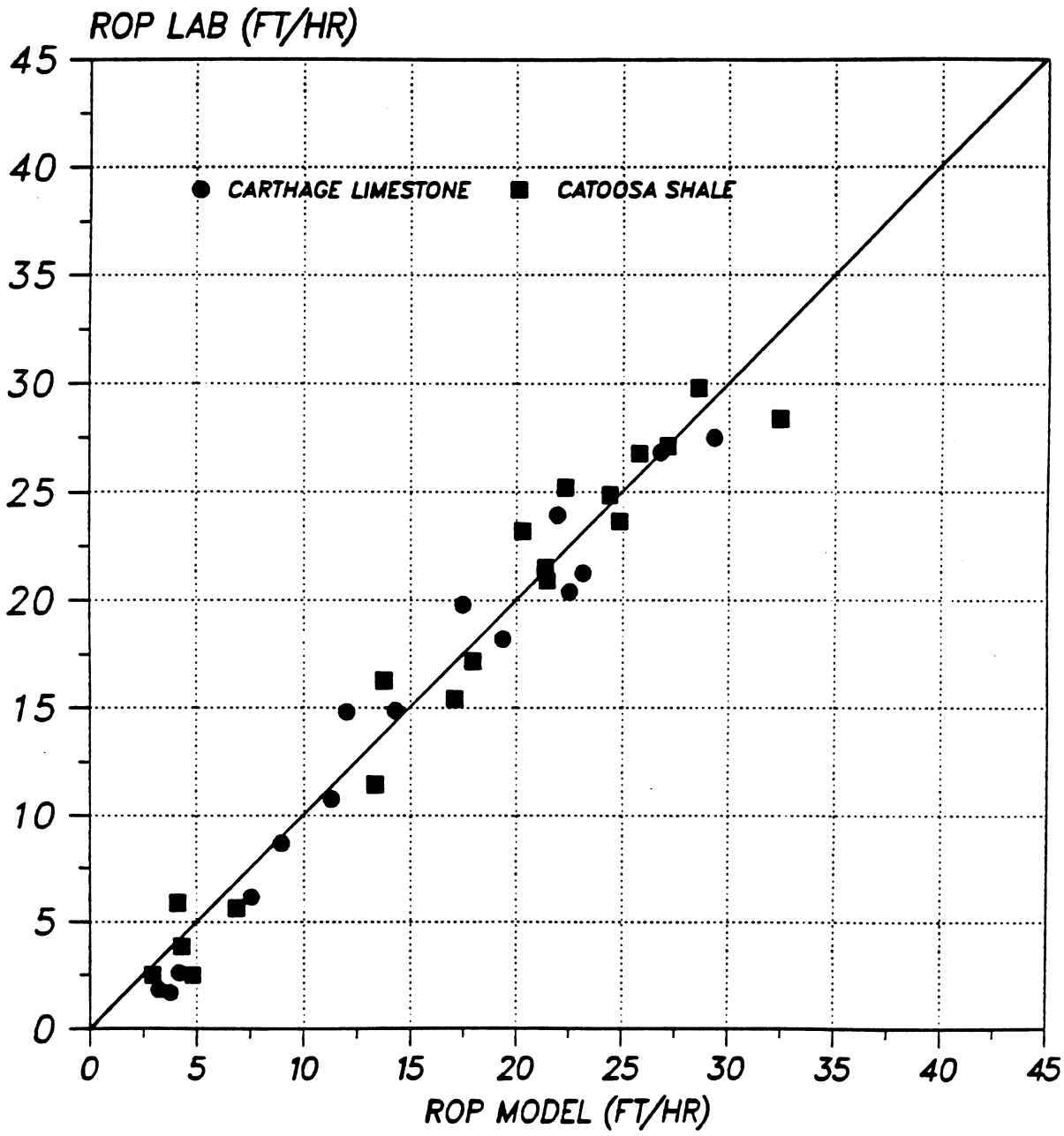

Figure 20. 3-Term Model Prediction Versus Laboratory Drilling Data for 537 IADC Bit

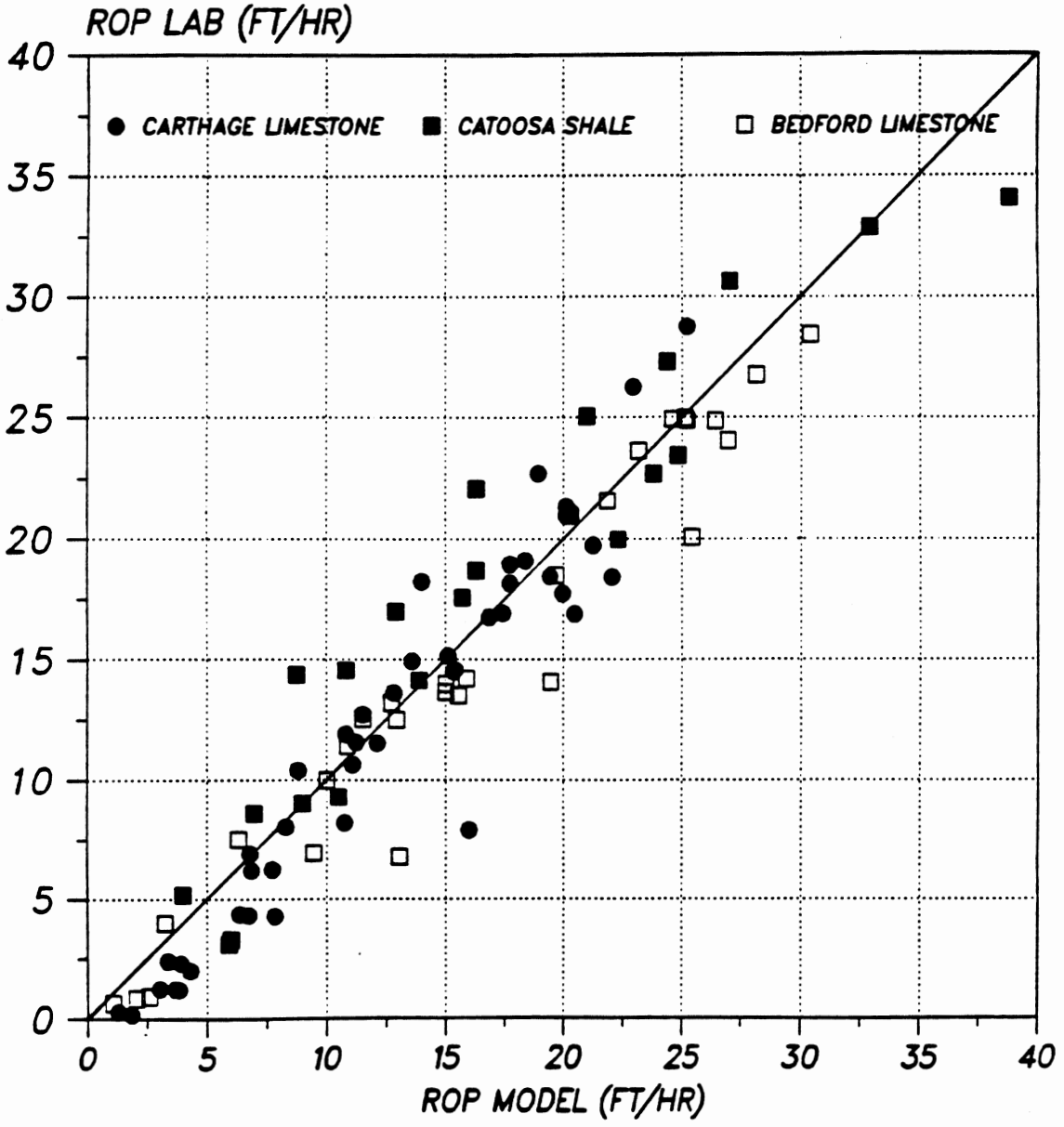

Figure 21. 3-Term Model Prediction Versus Laboratory Drilling Data for 617 IADC Bit

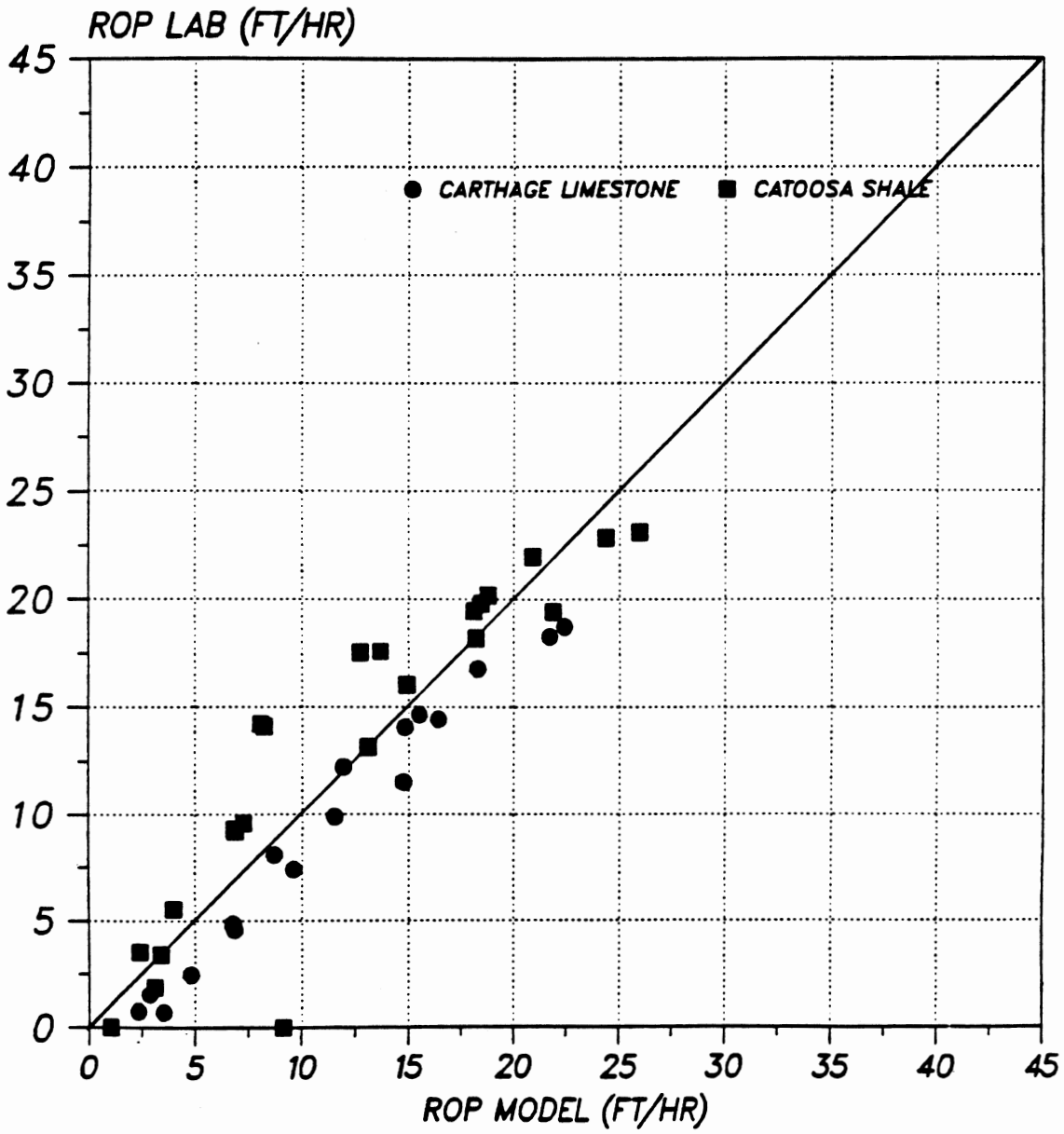

Figure 22. 3-Term Model Prediction Versus Laboratory Drilling Data for 627 IADC Bit

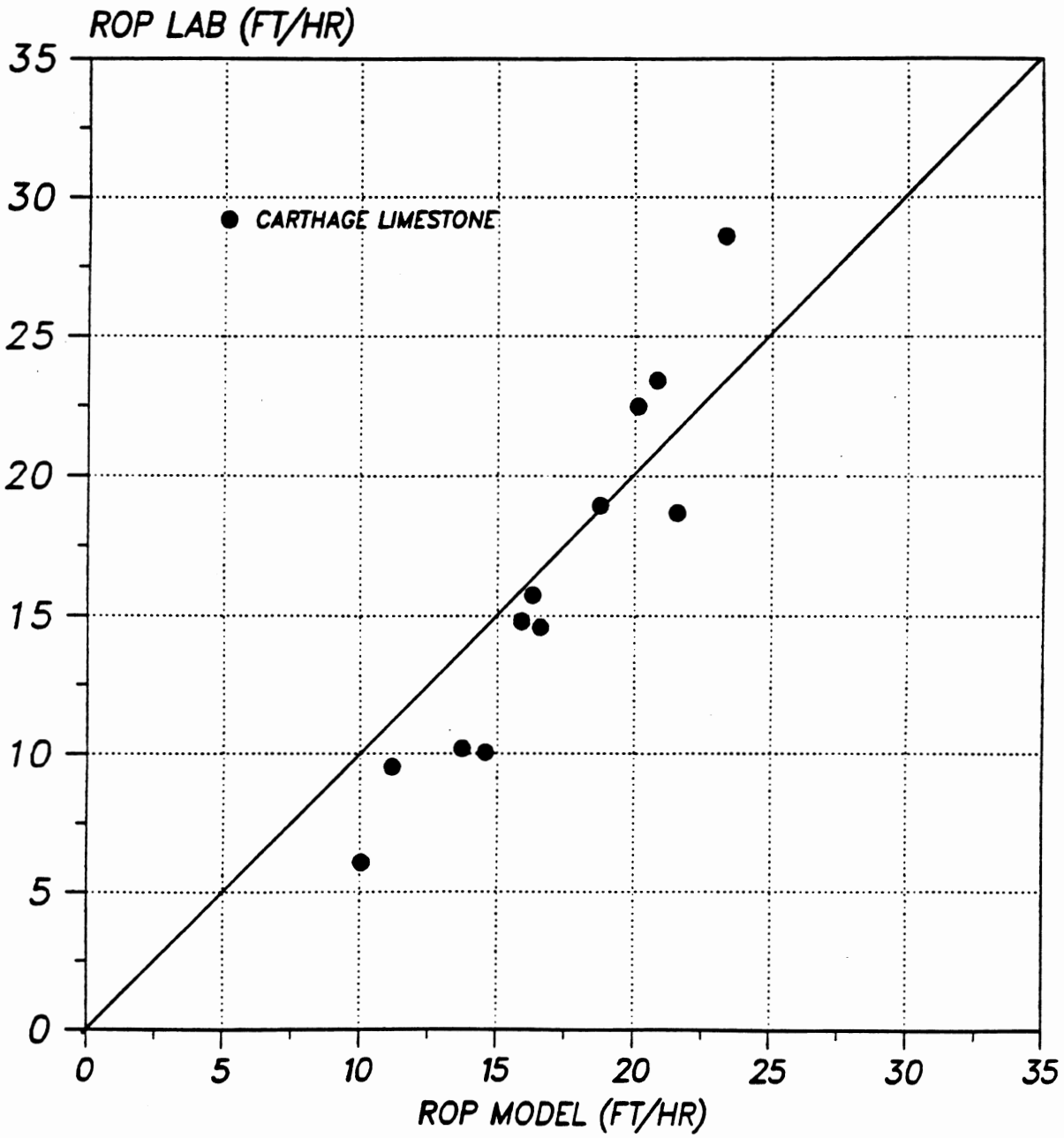

Figure 23. 3-Term Model Prediction Versus Laboratory Drilling Data for 737 IADC Bit

Mixed Lithology Treatment

When data is gathered from drilled formations with mixed or "non-pure" lithological components (ie, sand and shale mixed together), a combined effect of the mix should be reflected in the model. This means that the two independent effects, the chip hold down function (5) and the function correlating unconfined and confined rock strength (8) discussed in the preceding paragraphs must be related to the percent and type of each lithology present to obtain the combined effect. Again, this is an extremely complicated problem, and no useful studies are available from the literature. All available data and physical modeling is for pure lithological components. We propose to handle mixed lithologies with an empirical approach by weighting each of the two effects by the volumetric percentage of the lithological component present and averaging the effect over all components in the mix. The resulting expressions from (5) and (8a) become:

$$f_c = \sum_{i=1}^{n} \theta_i \, (c_{ci} + a_{ci} P_e^{b_{ci}}) \tag{24a}$$

$$S = S_{0c} \sum_{i=1}^{n} \theta_i (1 + a_{si} P_e^{b_{si}}) \tag{24b}$$

where

θ_i = Volume fraction of lithology "i" present at given depth

n = Number of different lithologies present at a given depth

S_{0c} = Compressive strength of mixed lithologies at rock failure (unconfined) (psi)

S = Compressive strength of mixed lithology rock at failure (confined) (psi)

a_{ci}, b_{ci}, c_{ci}, a_{si}, b_{si} = Coefficients for lithology i

P_e = Effective confining pressure

f_c = Chip hold-down function for mixed lithologies

We note that values for θ_i for every foot drilled are obtained from "mud logger" data. This data is collected during the drilling of the well by microscopic examination of drilled chips collected from the drilling mud return line. Together with (7), these equations were applied to the collected drilling data for every foot of drilled depth for prediction of drilling rock strength. The procedure is straight forward, but computationally intense. By substituting the right side of 24(a) into (7) we obtain one equation with one unknown, S. The value of S_{0p} and S_{0i} can be found from (9). For the four SFE wells we assume that the pore pressure, P_p, is known. We observed in the discussion following (4) that the effective confining pressure, P_e, or effective differential pressure, for drilled rock is a complicated and poorly understood phenomenon. A thorough understanding and mathematical modeling of this effect is beyond the scope of this work. In our calculations, we propose a much simplified approximation of this effect using the relationship:

$$P_e = P_h - P_p + P_a \qquad (25)$$

where P_e is effective confining pressure and P_p is the pore pressure. Mud column hydrostatic pressure at bottom hole, P_h, is calculated from:

$$P_h = .052*\rho*\text{Depth} \tag{26}$$

where

P_h = Hydrostatic bottom-hole pressure (psi)

ρ = Mud Weight (ppg)

Depth = Well Depth (feet)

Circulating pressure in the wellbore annulus, P_a, is calculated from a suitable hydraulics model knowing the drilling fluid flow rate, annulus geometry, and drilling fluid rheology. In the work herein, we used the non-Newtonian Power Law model [46] which is described in detail in Appendix D.

For impermeable formations (ie, shale), P_p is assumed zero in (25) such that the effective confining pressure equals the bottom hole pressure. The unconfined rock strength, computed for every foot of depth, is the intermediate quantity sought.

SFE Well Data Gathering

The initial task for the SFE wells was to collect and organize the data necessary for predicting drilling rock strength. The required data includes the IADC bit codes, together with bit and nozzle sizes

used on the wells. Tables 8-11 summarize this data for the 4 SFE wells. The conditions under which these bit were operated are needed as input to the rock strength model (7) and include weight on bit (W), rotary speed (N), fluid flowrate (Q) and rate of penetration (R), all recorded versus depth. Table 12 shows a sample input drilling file. The formation and core data must be collected such that the best description of the formation at a given depth is obtained. This will include primary, secondary and tertiary lithology descriptions, together with percentages present, as shown in Table 13. Primary lithology refers to the lithology present from the mudlogger that has the highest percent by volume at a given depth. The secondary and tertiary lithologies are those with the second and third highest lithology percentages by volume, respectively, from the mudlogger information. The determination of these percentages is usually done by a geologist, who analyzes drilled chips under a microscope at wellsite. Pore pressure (See Table 14) and overburden pressure (See Table 15) are also required input. To be able to edit and interpret this data, and to obtain supplementary information such as mud properties, the daily drilling reports from the SFE wells were collected.(See Appendix E for sample daily drilling wire) From the daily drilling wire, drilling fluid properties were collected and organized as shown in Table 16.

Questionable or useless drilling data was culled out. This data editing employed knowledge of drilling operations and common sense. For example, data taken during drilling with poor hydraulics, bit balling, cone locking or abnormal bit wear must be eliminated. In

TABLE VIII

SFE #1 BIT SUMMARY

Bit No.	Depth in (ft)	Depth out (ft)	Size (in)	Type	IADC CODE	Jets (32nd's of an in.)		
1	55	1480	17.50	S3Sj	111	20	20	20
2	1480	3060	12.25	S33SF	116	15	15	16
3	3060	5830	12.25	S84F	517	16	16	15
2	5830	5846	12.25	S33SF	116	12	15	15
4	5846	5950	8.75	F5	627	10	10	11
5	5950	6012	8.75	CORE	----		OPEN	
6	6012	6060	8.75	CORE	----		OPEN	
4	6060	6181	8.75	F5	627	10	10	11
7	6181	6211	8.75	CORE	----		OPEN	
4	6211	7271	8.75	F5	627	10	10	11
8	7271	7395	8.75	M89TF	627	11	11	0
7	7395	7470	8.75	CORE	----		OPEN	
9	7470	7531	8.75	CORE	----		OPEN	
7	7531	7556	8.75	CORE	----		OPEN	
8	7556	7900	8.75	M89TF	627	11	11	0

TABLE IX

SFE #2 BIT SUMMARY

Bit No.	Depth in (ft)	Depth out (ft)	Size (in)	Type	IADC CODE	Jets (32nd's of an in.)		
1	0	2865	12.25	S33S	116	18	18	18
2	2865	3945	12.25	S3SJ	111	16	16	16
3	3945	5660	8.75	S82F	437	11	11	11
4	5660	6811	8.75	S84F	517	10	10	10
5	6811	8116	8.75	F2	527	10	10	10
6	8116	8230	8.75	S86CF	537	11	11	11
7	8230	8260	8.75	CORE	----		OPEN	
6	8260	8265	8.75	S86CF	537	11	11	11
7	8265	8360	8.75	CORE	----		OPEN	
8	8360	8678	8.75	H87F	737	11	11	11
7	8678	8709	8.75	CORE	----		OPEN	
9	8709	8739	8.75	CORE	----		OPEN	
10	8739	9206	8.75	H87F	737	11	11	11
11	9206	9480	8.75	H87F	737	11	11	11
9	9480	9572	8.75	CORE	----		OPEN	
12	9572	9806	8.75	H87F	737	11	11	11
13	9806	9821	8.75	CORE	----		OPEN	
14	9821	9835	8.75	CORE	----		OPEN	
12	9835	9846	8.75	CORE	----		OPEN	
15	9846	9887	8.75	CORE	----		OPEN	
16	9887	9942	8.75	CORE	----		OPEN	
17	9942	10163	8.75	H87F	737	12	12	12

TABLE X

SFE #3 BIT SUMMARY

Bit No.	Depth in (ft)	Depth out (ft)	Size (in)	Type	IADC CODE	Jets (32nd's of an in.)		
1	68	1480	17.50	S3SJ	111	16	15	15
2	1480	3256	12.25	S33SF	116	14	14	14
3	3256	4547	12.25	WM52F	-	14	14	13
4	4547	6298	12.25	S84F	517	14	14	13
2	6298	6315	12.25	S33SF	116	14	14	14
5	6315	6365	8.75	S84F	517	10	10	10
6	6365	6811	8.75	S86F	537	10	10	10
7	6811	7351	8.75	CORE	-		OPEN	
8	7351	7411	8.75	CORE	-		OPEN	
9	7411	7868	8.75	CORE	647	10	10	10
8	7868	7916	8.75	CORE	-		OPEN	
10	7916	7945	8.75	CORE	-		OPEN	
11	7945	8079	8.75	CORE	-		OPEN	
12	8079	9017	8.75	M90F	647	10	10	10
10	9017	9046	8.75	CORE	-		OPEN	
13	9046	9199	8.75	M85F	617	11	11	11
10	9199	9229	8.75	CORE	-		OPEN	
14	9229	9294	8.75	CORE	-		OPEN	
15	9294	9367	8.75	CORE	-		OPEN	
13	9367	9449	8.75	M85F	617	11	11	11
15	9449	9502	8.75	CORE	-		OPEN	
13	9502	9600	8.75	M85F	617	11	11	11
12	9600	9700	8.75	CORE	-		OPEN	

TABLE XI

SFE #4 BIT SUMMARY

Bit No.	Depth in (ft)	Depth out (ft)	Size (in)	Type	IADC CODE	Jets (32nd's of an in.)		
1	17.50	40	980	HP11	111	14	14	14
2	12.25	980	2460	S33SF	116	14	14	14
3	12.25	2460	3071	ATJ-11	437	12	12	12
4	12.25	3071	4158	S82F	437	13	13	13
5	12.25	4158	5041	ATJ11	437	13	13	13
6	12.25	5041	5740	S82F	437	16	16	16
5RR	12.25	5740	6023	ATJ11	437	16	16	16
6RR	12.25	6023	6146	S82F	437	18	18	18
7	12.25	6146	6352	S33SF	437	16	16	16
5RR	12.25	6352	6777	ATJ11	437	15	15	15
8	8.50	6777	6805	CORE				
9	12.25	6805	7117	HP43A	437	16	16	16
10	8.50	7117	7217	HP11J	116	12	12	12
11	8.50	7217	7310	ATJ11	437	13	13	13
12	8.50	7310	7317	CORE				
13	8.50	7317	7388	CORE				
14	8.50	7388	7493	CORE				
11RR	8.50	7493	7753	ATJ11	437	13	13	0
14RR	8.50	7753	7782	CORE				
11RR	8.50	7782	7963	ATJ11	437	13	13	0
8RR	8.50	7963	8004	CORE				
11RR	8.50	8004	8093	ATJ!!	437	13	13	0

TABLE XII

SECTION OF DRILLING DATA FOR SFE #2

Depth (ft)	W (Kips)	N (RPM)	R (FT/HR)	Q (GPM)
8000	40.021	65.981	8.625	321
8001	40.017	65.968	9.064	321
8002	39.825	65.704	8.965	321
8003	40.176	65.647	8.038	321
8004	39.356	65.704	13.117	321
8005	39.148	65.357	12.651	321
8006	39.253	65.625	13.583	321
8007	39.202	65.713	12.005	321

TABLE XIII

SECTION OF LITHOLOGY DATA FOR SFE #2

Depth (ft)	% Sandstone	% Limestone	%Shale
8000	30	30	40
8001	50	40	10
8002	50	30	20
8003	50	30	20
8004	60	30	10
8005	60	30	10
8006	30	50	20
8007	60	30	10

TABLE XIV

PORE PRESSURE GRADIENT SUMMARY FOR THE SFE WELLS

Item	Depth (ft)			Pore Pressure Gradient (psi/ft)
SFE #1 from [24]	7000	to	7209	.44
	7209	to	7279	.43
	7279	to	7307	.40
	7307	to	7465	.434
	7465	to	7487	.295
	7487	to	7503	.48
	7503	to	7560	.44
	7560	to	7575	.46
	7575	to	7784	.51
	7784	to	TD*	.52
SFE #2 from [45]	0	to	8000	.46
	8000	to	8800	.46 + .04*(Depth-8000)/1000
	8800	to	8900	.44
	8900	to	9000	.46 + .04*(Depth-8000)/1000
	9000	to	TD*	.50
SFE #3 from [45]	0	to	TD*	.515
SFE #4 from [45]	0	to	TD*	.520

* TD indicates total well depth

TABLE XV

OVERBURDEN PRESSURE GRADIENT SUMMARY
FOR THE SFE WELLS

Well	S_{ob}
SFE #1 [45]	1.015 psi/ft
SFE #2 [45]	1.040 psi/ft
SFE #3 [45]	1.040 psi/ft
SFE #4 [45]	1.100 psi/ft

TABLE XVI

DRILLING FLUID INPUT FOR THE SFE WELLS

Item	Depth (ft)	Mud Weight (ppg)	Plastic Viscosity (cp)
SFE #1	7000-7384	9.4	9
	7384-7474	9.4	7
	7474-7692	9.4	7
	7692-TD	9.4	9
SFE #2	0-8082	9.9	9
	8082-8183	10.0	9
	8183-8251	10.1	8
	8251-8457	10.0	6
	8457-8591	10.0	5
	8591-8709	9.9	6
	8709-8770	10.0	6
	8770-8949	9.9	6
	8949-9122	10.0	8
	9122-9377	10.0	6
	9377-9481	10.0	6
	9481-9640	10.0	7
	9640-9780	9.9	9
	9780-9942	9.8	8
	9842-TD	9.9	14
SFE #3	9500-9600	10.7	15
SFE #4	6500-6713	9.7	11
	6713-6799	9.7	12
	6799-7039	10.0	9
	7039-7117	10.0	14
	7117-7310	10.3	15
	7310-7331	10.3	16
	7331-7388	10.4	16
	7388-7439	10.4	20
	7439-7607	10.3	19
	7607-7651	10.3	19
	7651-7782	10.3	24
	7782-7963	10.2	20
	7963-8097	10.3	19

addition, the drilling and lithology data had to be "depth shifted" to match the electric log data and the stress test data. This is needed because depths measured during drilling are not calibrated against depths measured during logging. Depth shifting is done by overlaying foot-by foot the rock strengths calculated from (7) with simular electric log plots, namely, Gamma Ray, Self Potential and Compressional Wave Travel Time logs. The rock strength depths are then shifted the number of feet needed to match lithology and formation changes with drilling rock strength changes. This depth shifting allows stress test data, where electric logs are used for depth, to be correlated with drilling data. A summary of the depth shifts for the SFE wells 1-4 is listed in Table 17. Finally, data from all hole sections that appear to have complete and sufficiently high-quality data must be organized for further analysis.

Rock Strength Calculations

The calculation of rock strength, confined and unconfined, for both the permeable and impermeable cases, is accomplished in a SAS routine (See Appendix F) which draws upon both lithology and drilling input files. The rock strength is calculated from (7), and the mixed lithologies are treated as described by (24a) and (24b). The rock strength coefficients from Table 3 used in this study were the general sandstone coefficients for sandstone and conglomerate and the general shale coefficients for all other lithologies. The permeable and impermeable rock strengths are calculated using effective differential pressures, as discussed earlier. A problem arises,

TABLE XVII

DEPTH SHIFTS FOR THE SFE WELLS

Item	Drilling Interval (ft)	Depth Shift* (ft)
SFE #1	NONE	
SFE #2	7900-8230	-10
	8320-8734	+7
	8734-8855	+0
	8855-9480	+4
	9480-9806	+2
	9806-10163	+4
SFE #3	9000-9700	+6
SFE #4	NONE	

* Depth Shift indicates the footage the rock strength had to be adjusted to match the electric log and stress test data.

however, with the chip hold-down function used in (7). Data is presently available to calculate the coefficients a_c, b_c and c_c for the function in (5) for only two lithologies, namely Catoosa Shale and Carthage Limestone. Obtaining data for other lithologies is an expensive and time consuming process, and is beyond the scope of the work reported here. Accordingly, we will assume for this work, that the coefficients for Catoosa Shale can be used for impermeable lithologies (mainly shales), and that the coefficients for Carthage Limestone can be used for all other lithologies. This is admittedly an unsupported hypothesis, but appears to be the only mechanism at hand to test the proposed approach. A sample output from the rock strength SAS program is shown in Appendix G, and a sample plot of permeable and impermeable confined rock strength versus depth for the SFE #2 well is given in Figure 24. Appendix H contains rock strength plots from all four wells. For "impermeable" rock strength, pore pressure was assumed zero in (25), while for "permeable" rock strength, pore pressures given in Table 14 were used. These two rock strength calculations in Figure 24 and Appendix H show the significant effect that confining pressure has on in-situ rock strength. Moreover, these figures illustrate that knowledge of in-situ permeability or impermeability is necessary in order to calculate rock strengths, and by implication, in-situ stress bounds.

Upper In-Situ Stress Bounds Calculation

The rock strength calculation is used to calculate a "permeable" and an "impermeable" upper bound on stress (See Appendix F for

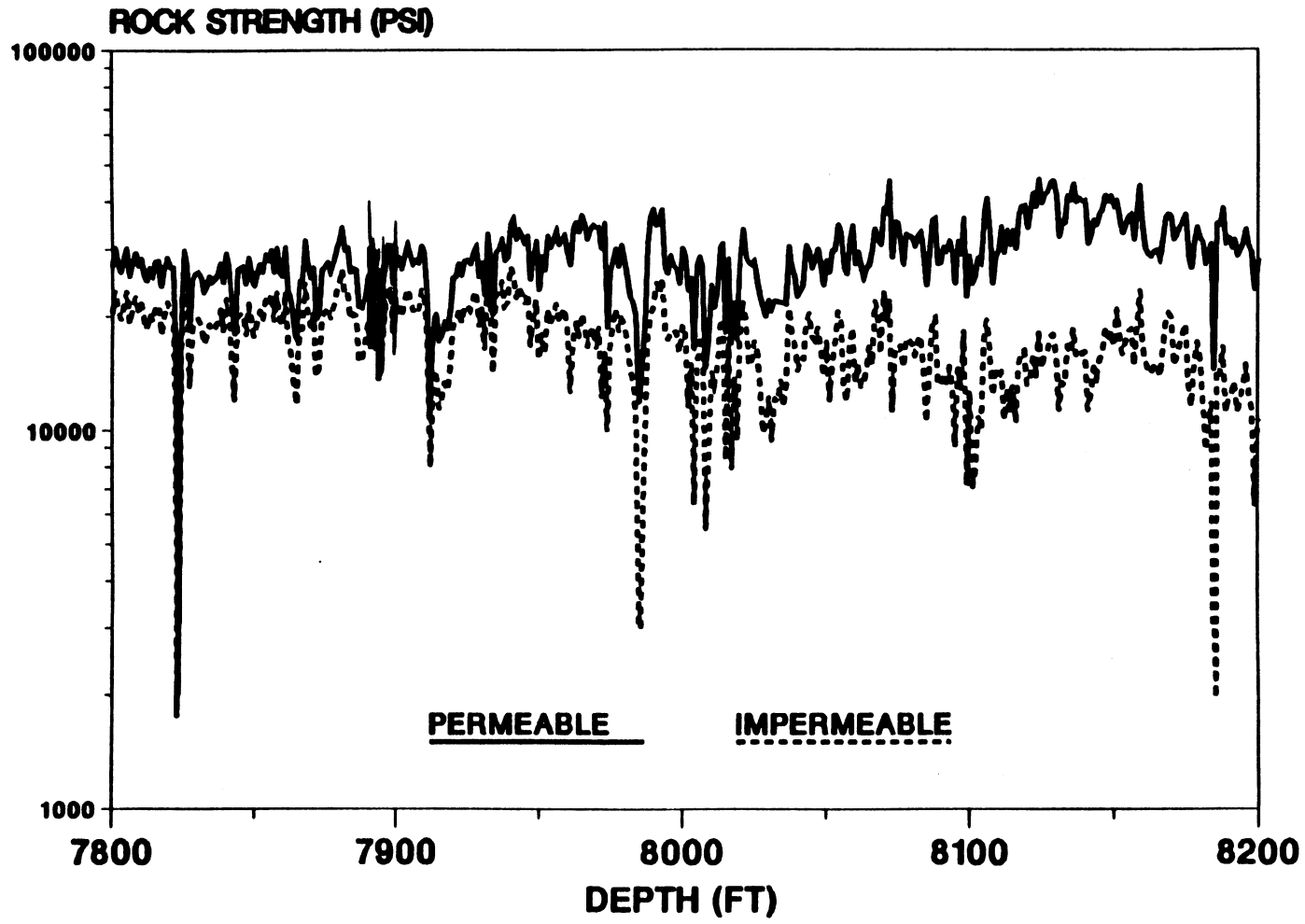

Figure 24. Section of Permeable and Impermeable Rock Strength for SFE #2 (7800-8200 Feet)

program). The first step is to calculate the unconfined rock strength for both the permeable and the impermeable cases. Then equations (9a) and (9b) can be applied, using the in-situ effective pressure given by (12) and mixed lithologies treated as in equations (24a) and (24b). An initial guess of 0.65 psi/ft is used for S_h in (12). The resulting effective pressure is used in (11) for both the permeable and impermeable cases to calculate an angle of internal friction. Now by using equations (14) (for the permeable case) and (15) for the impermeable case as suggested by [30], a coefficient for earth at rest, K_0, can be calculated. The value of K_0 for both the permeable and impermeable cases is employed in (20) for calculation of S_h. These values for S_h are then used in (12) and the procedure is repeated. This procedure is iterated four times, which was found to yield less than a 1 psi change in S_h between the two last iterations. A sample output from this routine is shown in Appendix G, and Figure 25 present values of K_0 plotted versus depth for a section of SFE # 2, for both the permeable and impermeable assumptions. Appendix I contains coefficients for earth at rest from all four wells. Similar plots of β are given in Figure 26 and Appendix J.

Comparison of the Calculated Upper Bounds on In-Situ Stress to Results from Field In-Situ Stress Tests

The field stress tests performed on SFE wells #1-4 are summarized in Tables 18-21. The stress test is typically performed over a two foot interval in the wellbore. This test is performed by

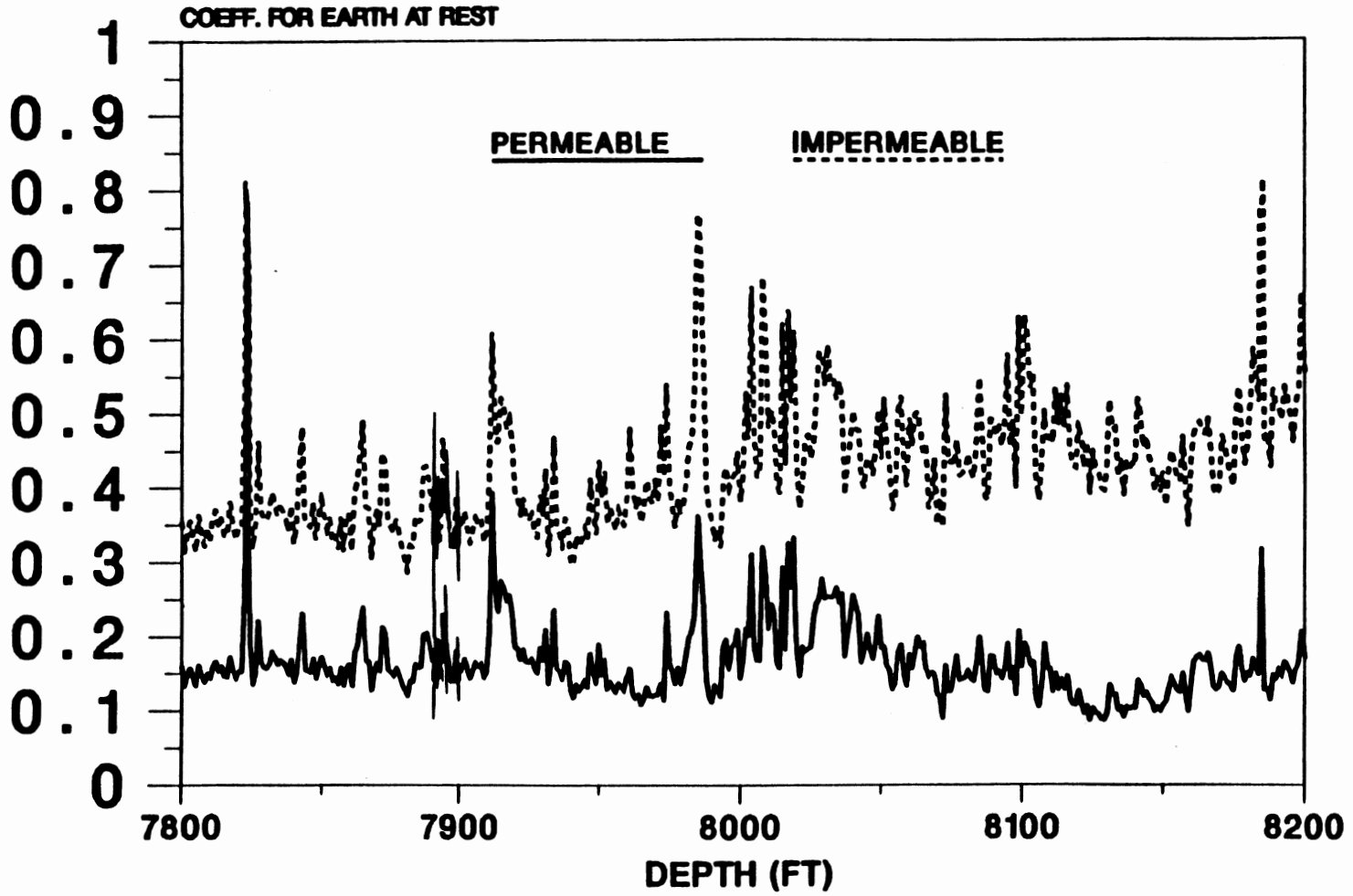

Figure 25. Section of Permeable and Impermeable Coefficient of Earth at Rest for SFE #2 (7800-8200 Feet)

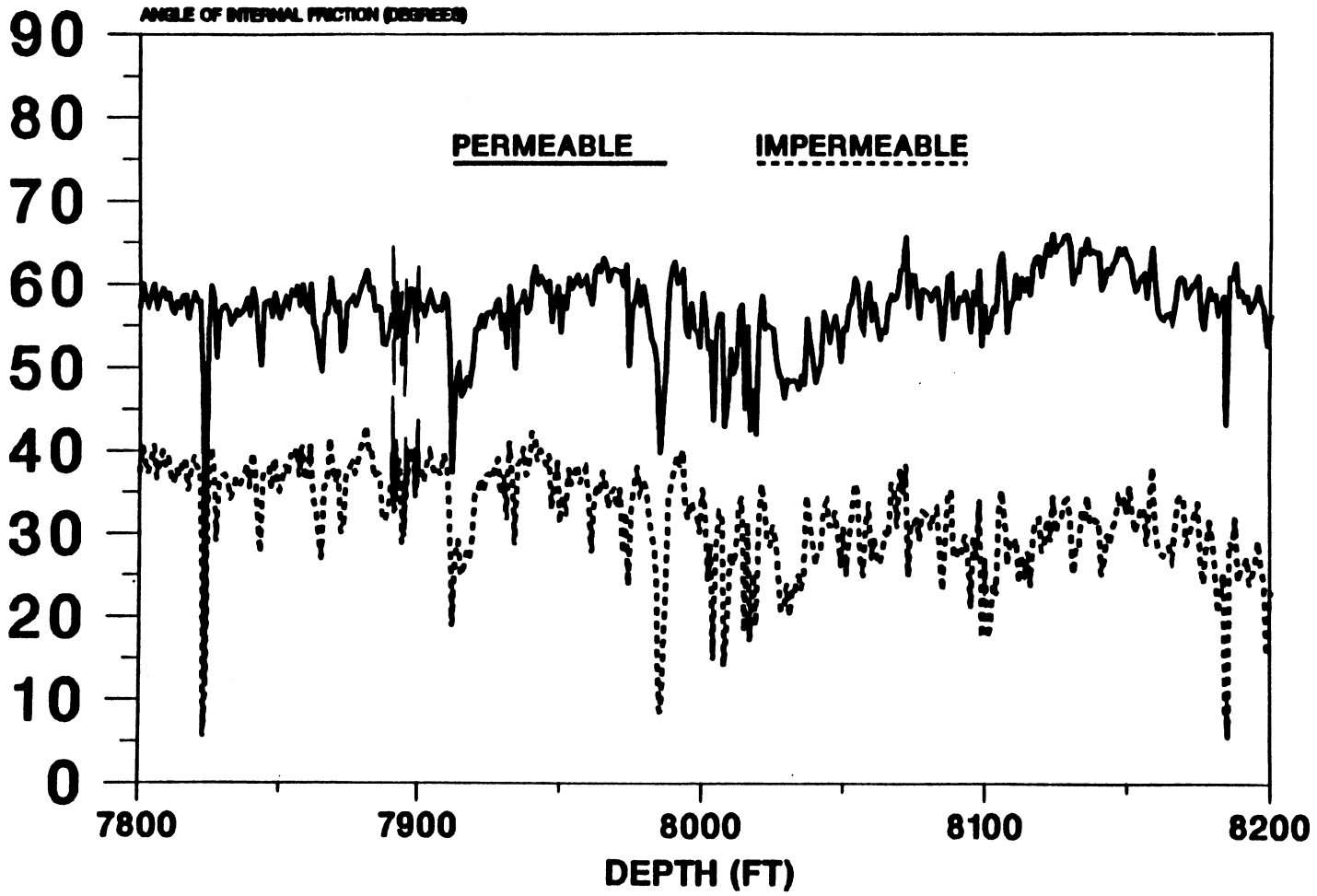

Figure 26. Section of Permeable and Impermeable Angle of Internal Friction for SFE #2 (7800-8200 Feet)

TABLE XVIII

STRESS TEST DATA FOR SFE #1

Depth of Stress Tests (ft)	Closure Stress (psi)	Lithology
7209-11	4145	Sand
7279-81	4760	Sand
7307-09	4164	Sand
7560-62	5216	Shale
7575-77	5196	Shale
7724-26	5329	Shale
7784-86	4896	Shale

TABLE XX

STRESS TEST DATA FOR SFE #3

Depth of Stress Tests (ft)	Closure Stress (psi)	Lithology
9227-29	5400	Sand
9266-68	5275	Sand
9324-26	5800	Shale/Sand
9554-56	7950	Shale
9600-02	7950	Shale
9630-32	8200	Shale

TABLE XXI

STRESS TEST DATA FOR SFE #4

Depth of Stress Tests (ft)	Closure Stress (psi)	Lithology
6780-82*	6540	Shale
7044-46*	6695	Shale
7328-30*	6980	Shale
7328-30**	6741	Shale
7411-13*	6220	Sand
7411-13**	6003	Sand
7801-03*	6730	Shale
7801-03**	6630	Shale
7881-83*	6785	Shale
7881-83**	6611	Shale
7931-33*	7690	Shale
7931-33**	7455	Shale

* Indicates Analysis of Stress Test Performed by S. Holditch And Associates.

** Indicates Analysis of Stress Test Performed by Res Tech.

isolating with "packers" a two-foot section of wellbore and slowly increasing the fluid pressure in this section by pumping in more test fluid. During this procedure the pressure and the volume pumped into the isolated section are monitored. Figure 27 illustrates the results. When the formation breaks down the test fluid flows into the formation, and a decrease in pressure may be observed on the pressure versus volume curve. As more fluid is pumped, the pressure versus volume curve levels out. The pressure at which this leveling occurs is taken as the formation closure pressure. This is, however a subjective determination, and is dependent upon the person making the judgement.

The data from stress tests performed on these wells are plotted with the calculated in-situ stress bounds in Figures 28-40. In Figures 28-40, PP indicates the pore pressure, SH the horizontal permeable upper stress bound and SHI the horizontal impermeable upper stress bound. For SFE #1 and SFE #3 the results from the stress tests are plotted as one point, referred to as either PERMEABLE or IMPERMEABLE which describes the permeability in which the stress tests were performed. For SFE #2 there is given an upper and a lower limit from the stress test analysis. Also, for SFE #2 the stress tests performed in permeable formations are separated from impermeable formations by different symbols. It can be observed from SFE #1-3 that all the stress tests yield fracture closure pressures between or on the impermeable upper bound and the lower bound of pore pressure. It is also observed from SFE #1-3 that the closure pressures from stress test performed in impermeable formations lie on or close to the calculated impermeable upper in-

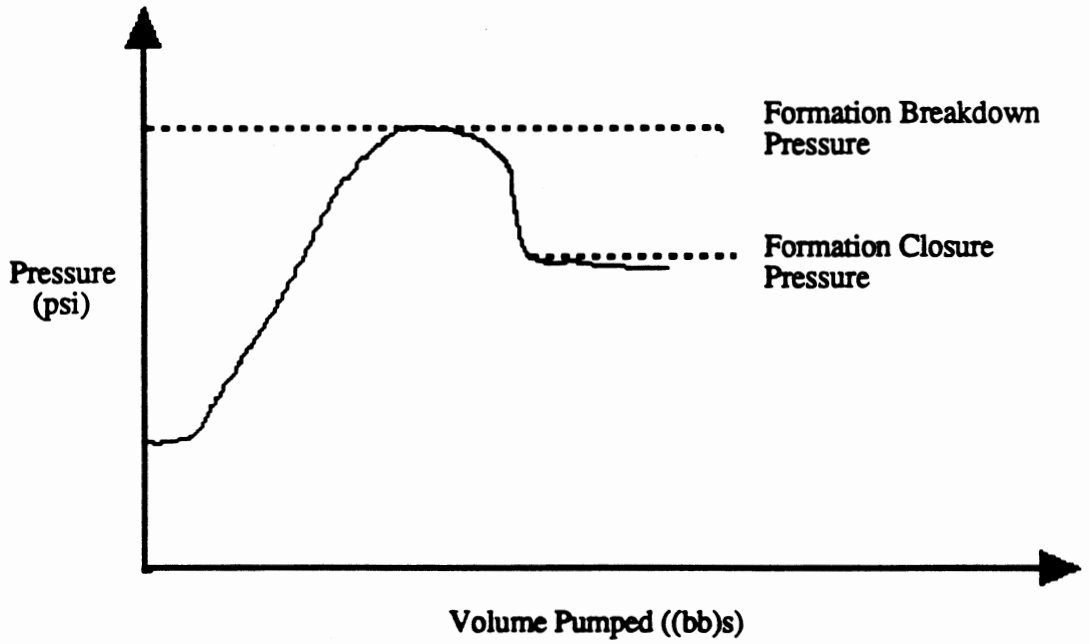

Figure 27. Pressure Versus Volume for Typical Stress Test

TABLE XIX

STRESS TEST DATA FOR SFE #2

Depth of Stress Tests (ft)	Closure Stress (psi)	Lithology
7973-75	5700 +/- 50	Lime
7997-99	5620 +/- 50	Sand/Lime
8054-56	5450 +/- 100	Shaley Sand
8111-13	5350 +/- 100	Sand
8161-63	5950 +/- 100	Shale
8233-35	5600 +50/-100	Shale
8265-67	5350 +/-50	Sand
8304-06	5750 +/-50	Shale
8329-31	4840 +/-50	Sand
8416-18	5390 +50/-100	Sand
8516-18	5400 +/-100	Shale
8702-04	5270 +/-50	Sand
8844-46	6050 +/-150	Shaley Sand
8962-64	5750 +/-25	Shaley Sand
9065-67	6200 +/-100	Shale
9425-27	6200 +50/-200	Shaley Sand
9508-10	5900 +/-100	Sand
9590-92	7100 +/-500	Shale
9676-78	6600 +/-500	Shale
9754-56	6400 +/-200	Siltstone
9823-25	6160 +/-150	Sand
9887-89	6080 +/-100	Sand
9944-46	6100 +/-50	Sand
9985-87	6935 +50/-300	Shale
10025-27	6580 +/-150	Shaley Sand
10102-04	7160 +/-150	Lime

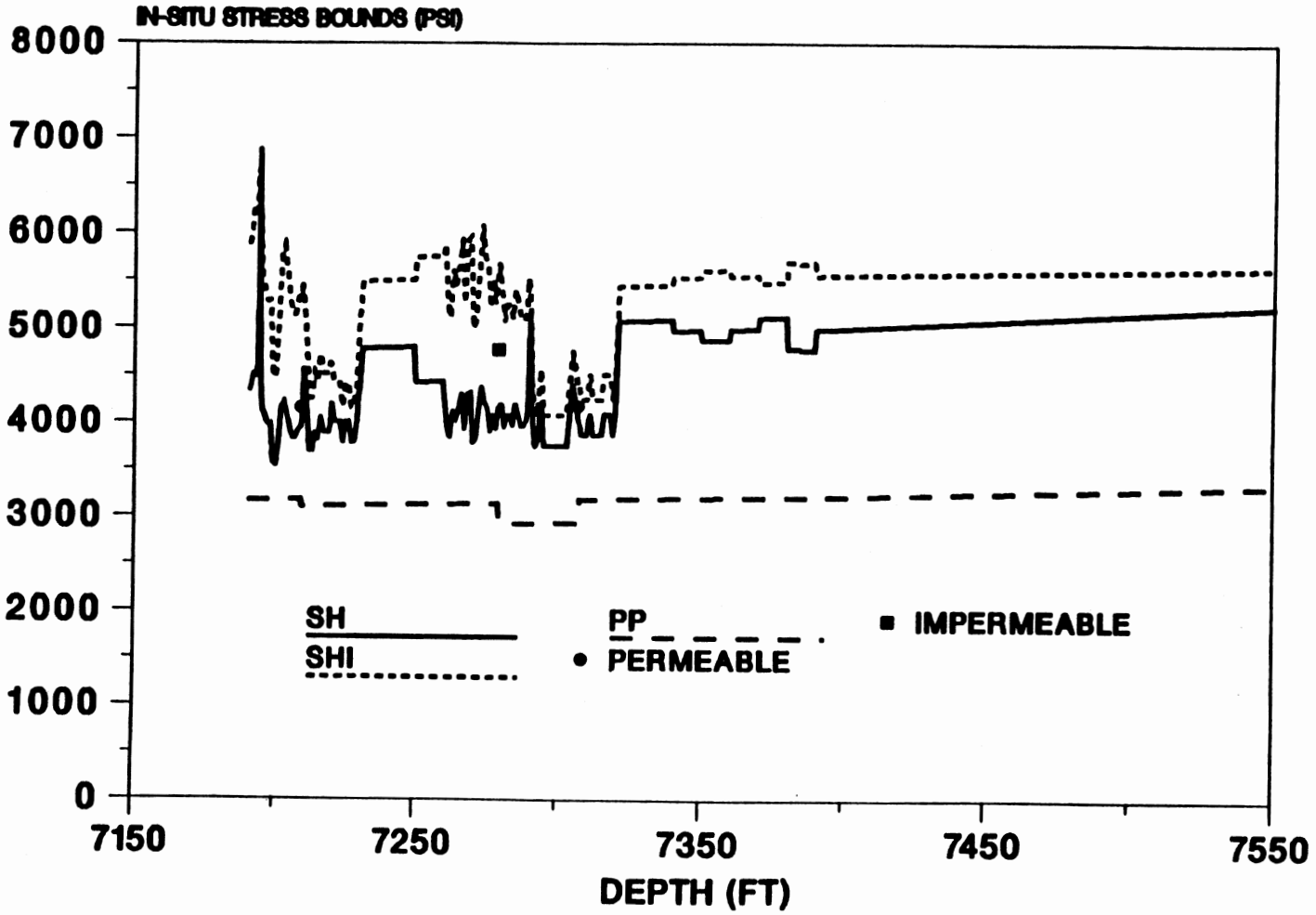

Figure 28. Section of Calculated In-Situ Stress Bounds and Stress Tests Versus Depth for Section of SFE #1 (7150 - 7550 Feet)

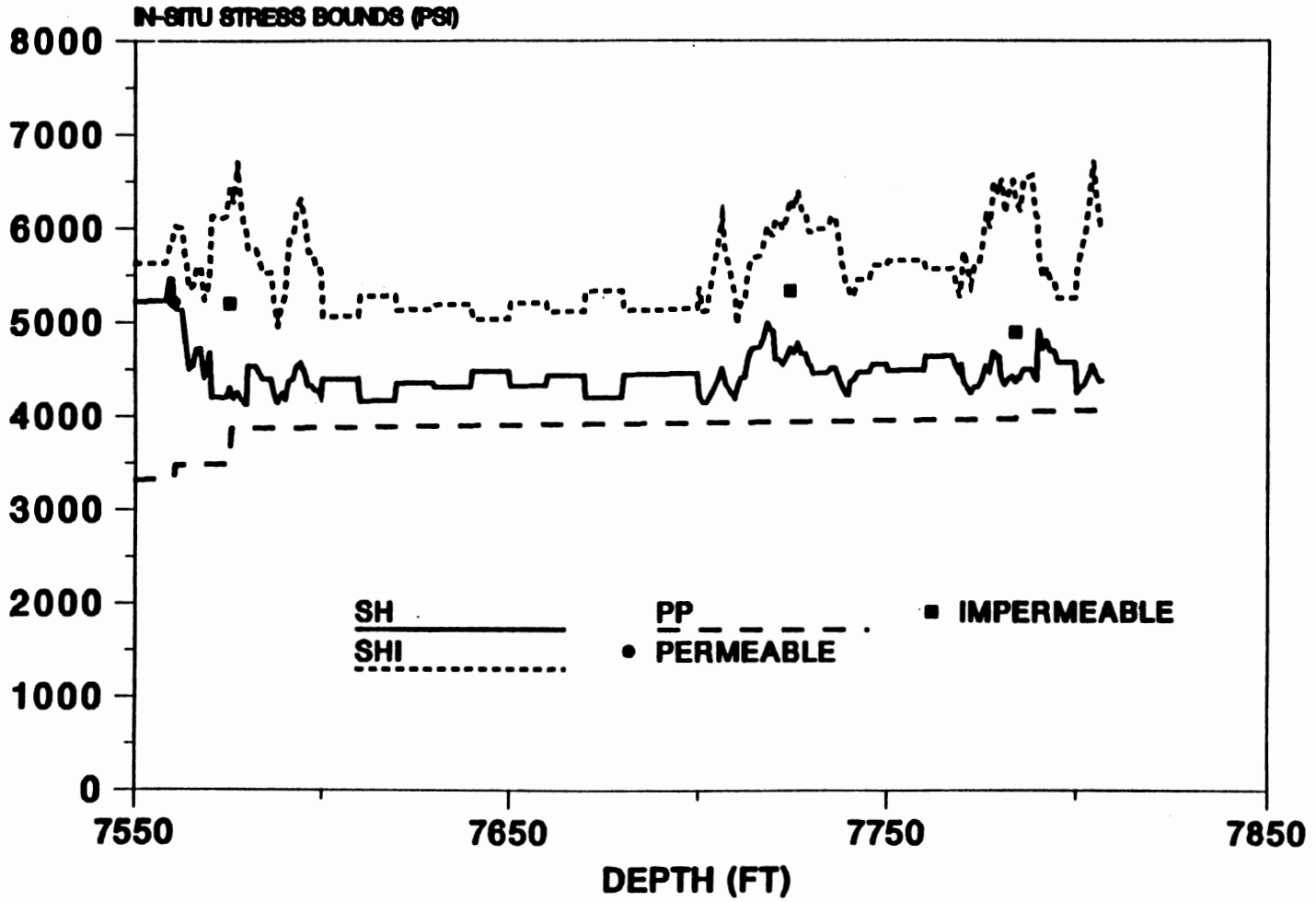

Figure 29. Section of Calculated In-Situ Stress Bounds and Stress Tests Versus Depth for Section of SFE #1 (7550 - 7850 Feet)

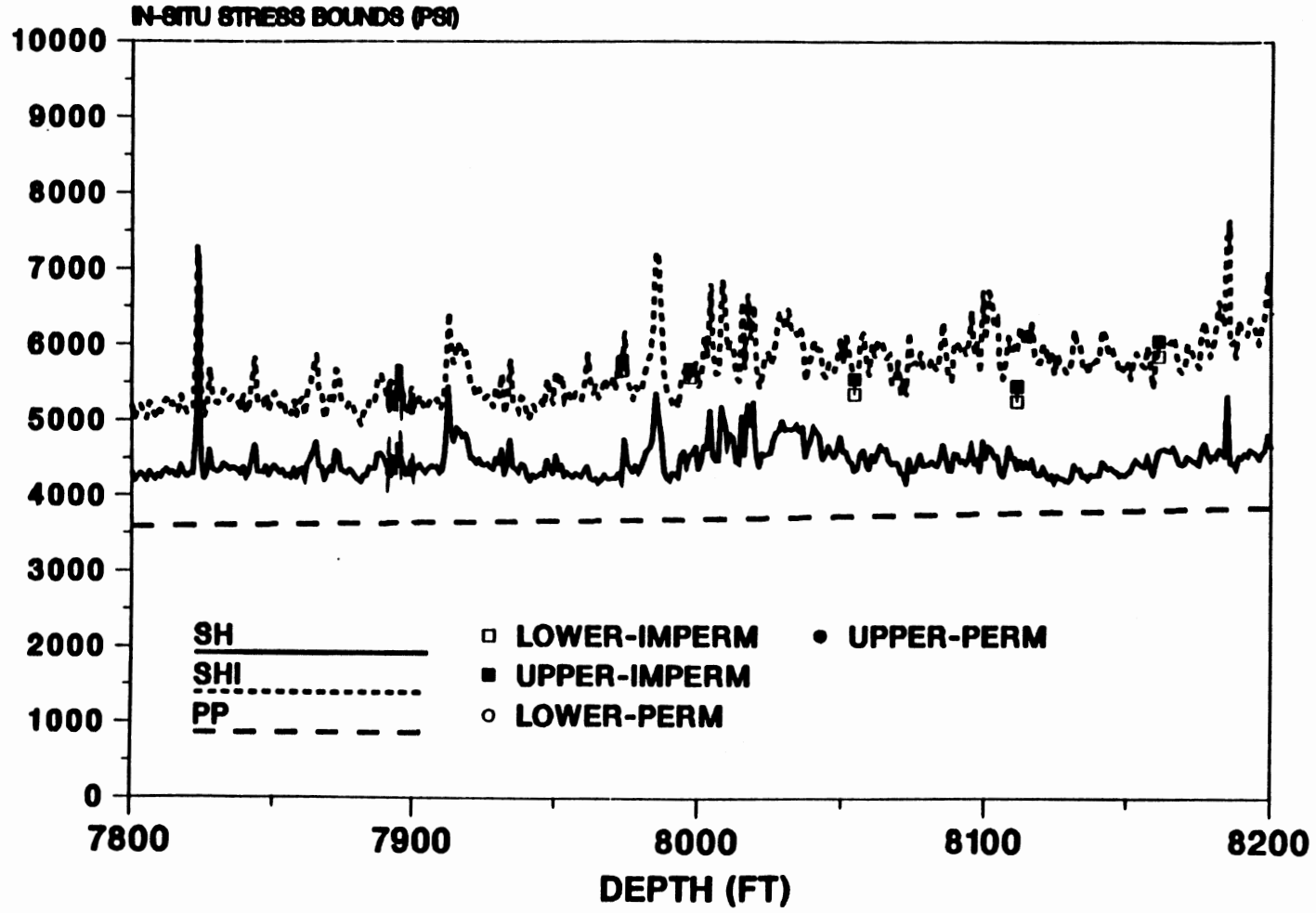

Figure 30. Section of Calculated In-Situ Stress Bounds and Stress Tests Versus Depth for Section of SFE #2 (7800 - 8200 Feet)

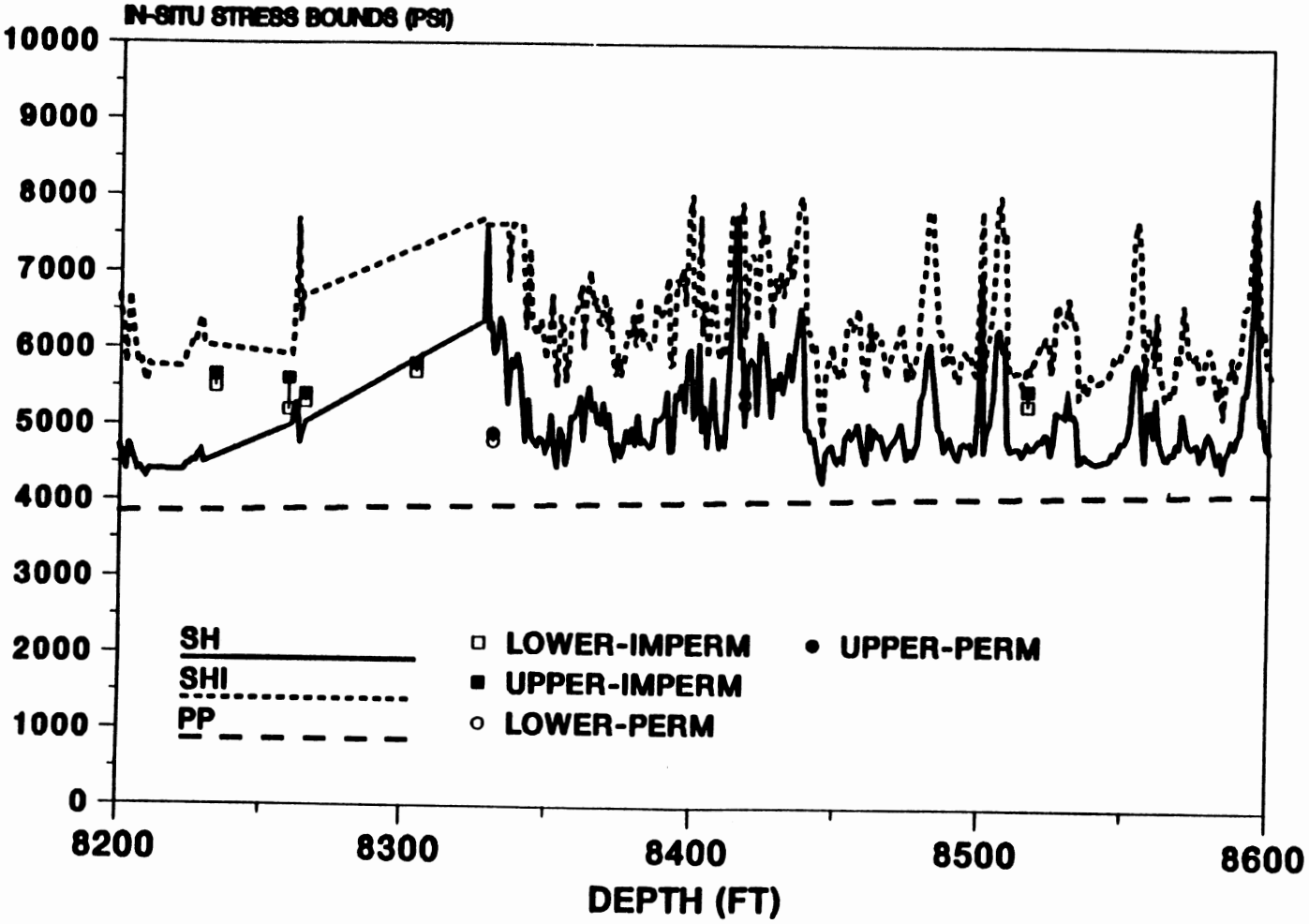

Figure 31. Section of Calculated In-Situ Stress Bounds and Stress Tests Versus Depth for Section of SFE #2 (8200 - 8600 Feet)

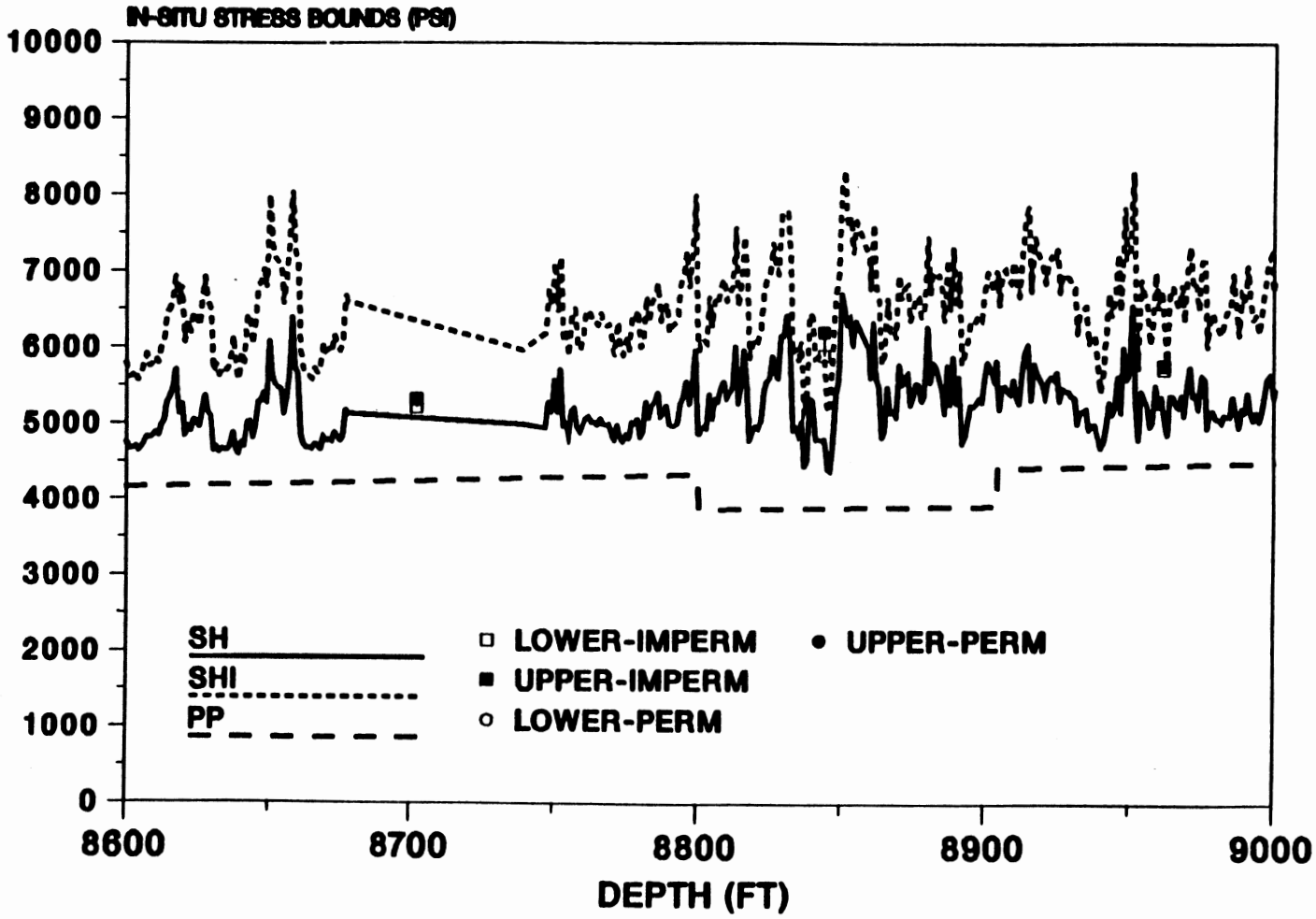

Figure 32. Section of Calculated In-Situ Stress Bounds and Stress Tests Versus Depth for Section of SFE #2 (8600 - 9000 Feet)

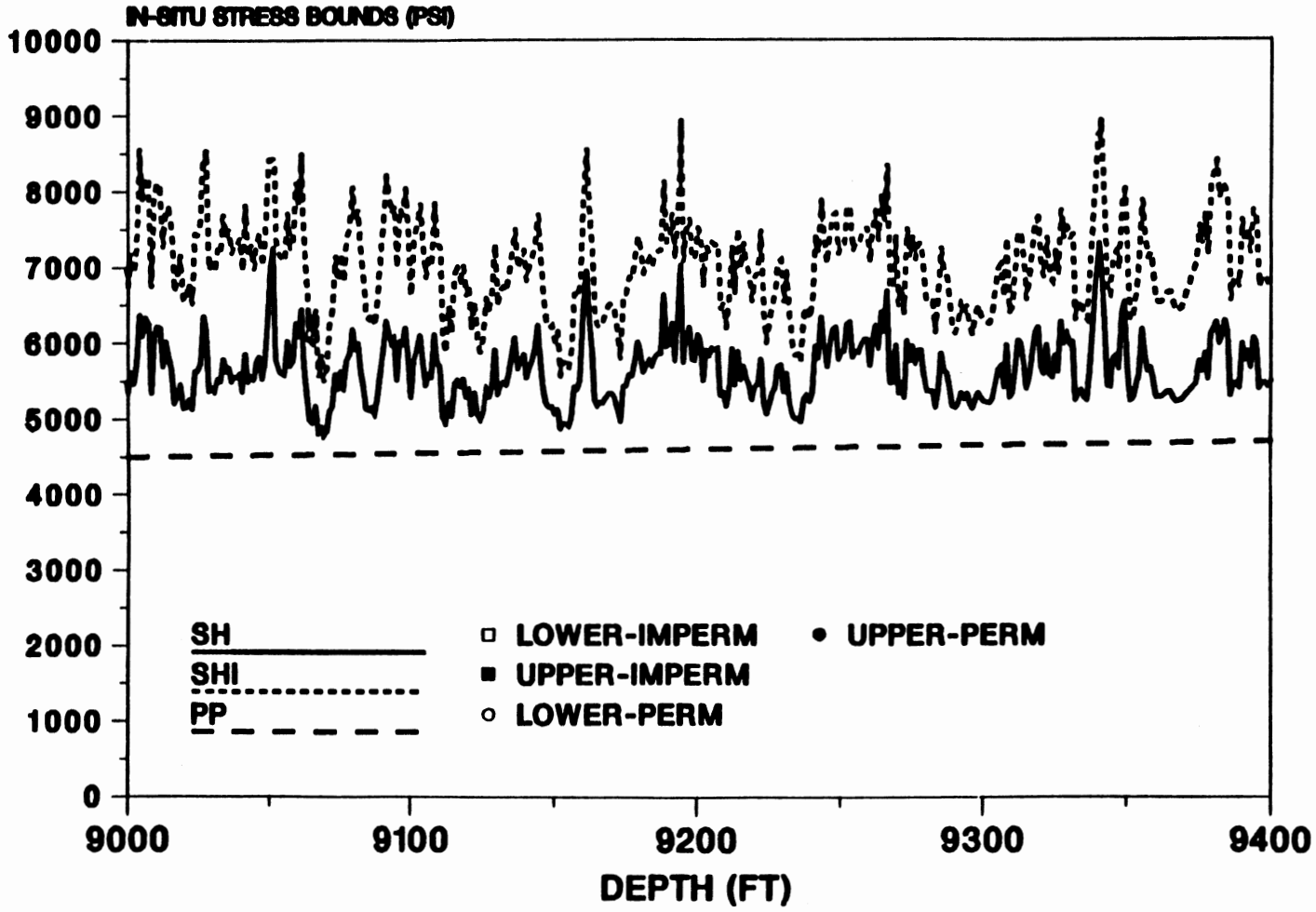

Figure 33. Section of Calculated In-Situ Stress Bounds and Stress Tests Versus Depth for Section of SFE #2 (9000 - 9400 Feet)

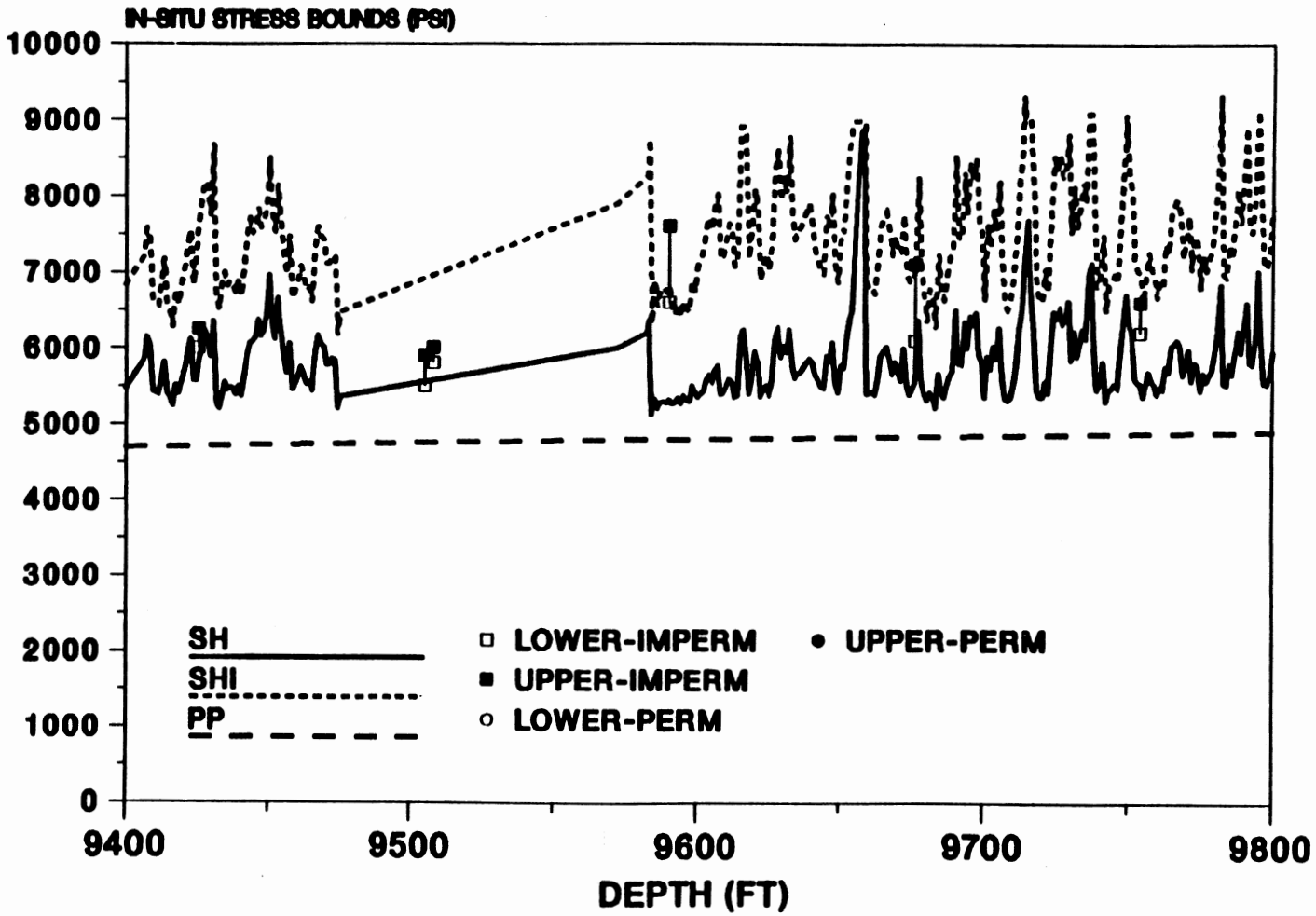

Figure 34. Section of Calculated In-Situ Stress Bounds and Stress Tests Versus Depth for Section of SFE #2 (9400 - 9800 Feet)

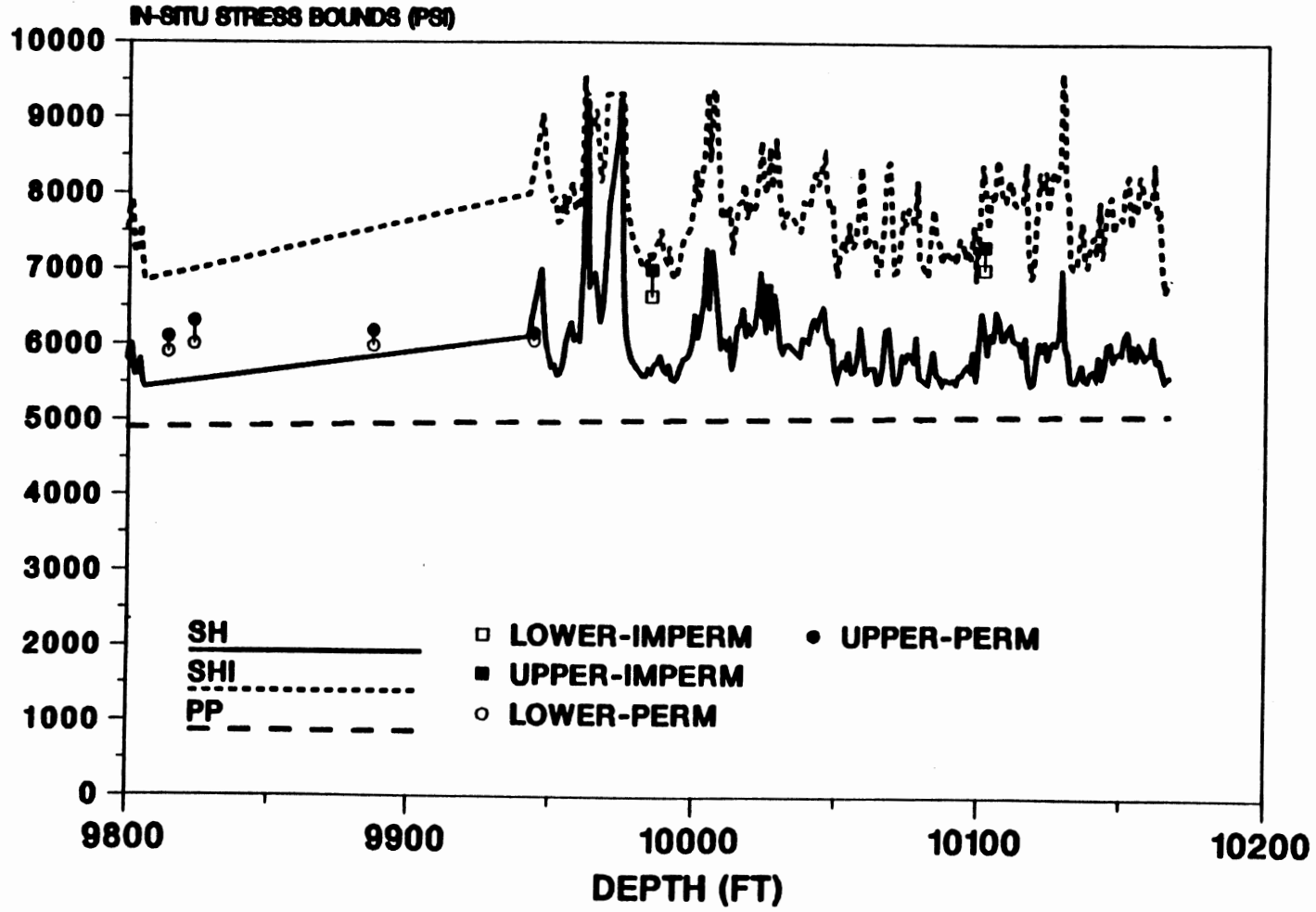

Figure 35. Section of Calculated In-Situ Stress Bounds and Stress Tests Versus Depth for Section of SFE #2 (9800 - 10200 Feet)

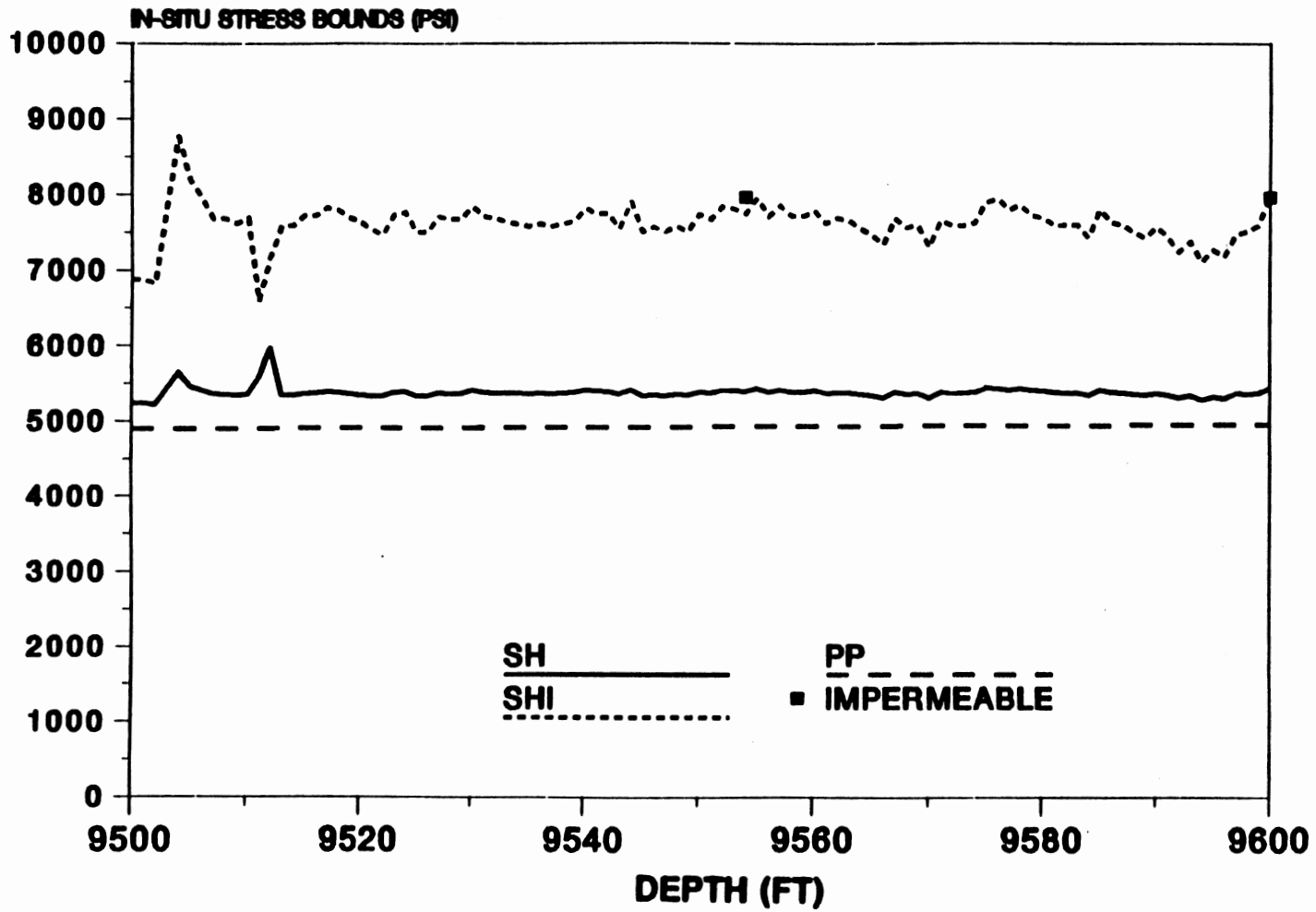

Figure 36. Section of Calculated In-Situ Stress Bounds and Stress Tests Versus Depth for Section of SFE #3 (9500 - 9600 Feet)

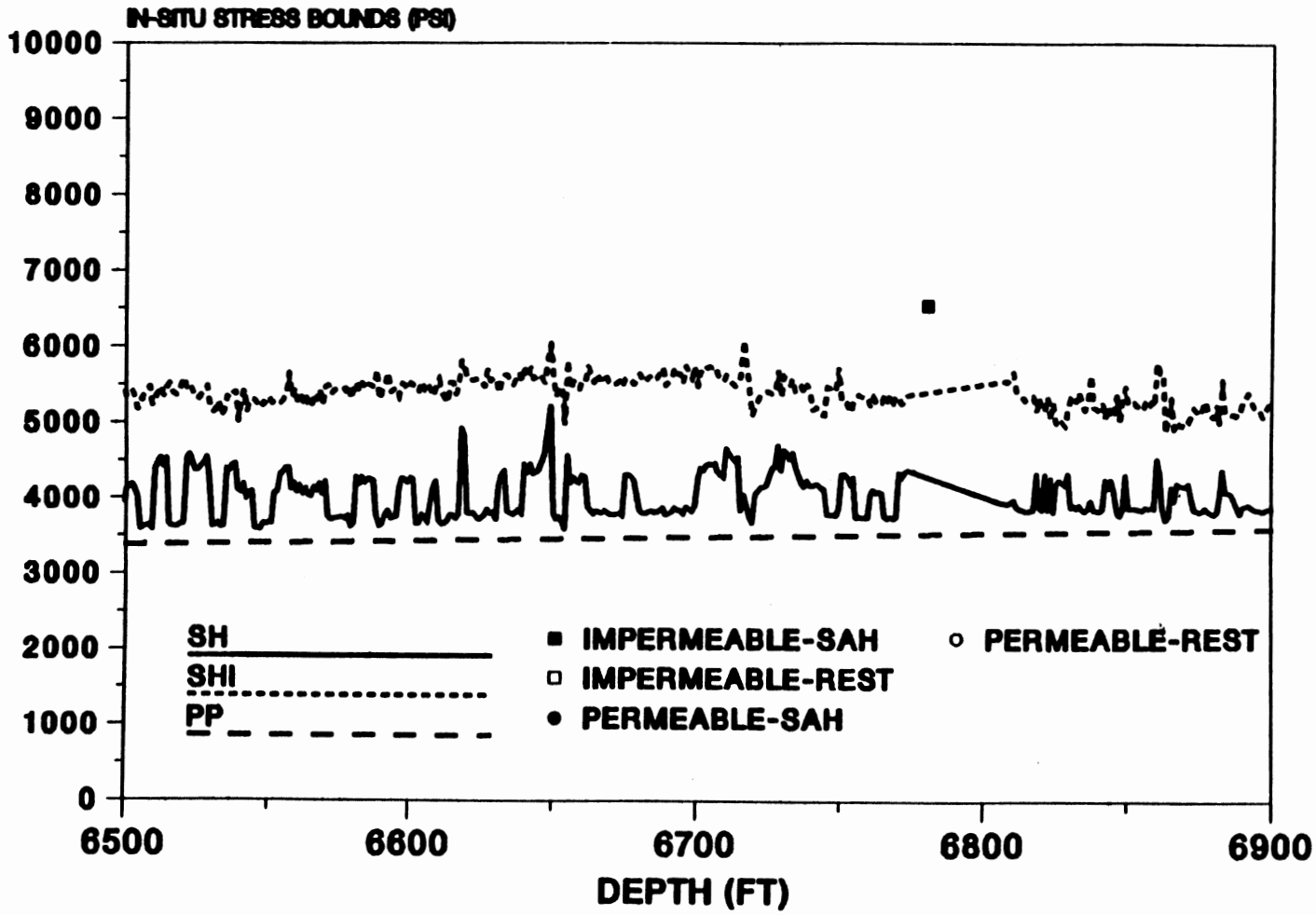

Figure 37. Section of Calculated In-Situ Stress Bounds and Stress Tests Versus Depth for Section of SFE #4 (6500 - 6900 Feet)

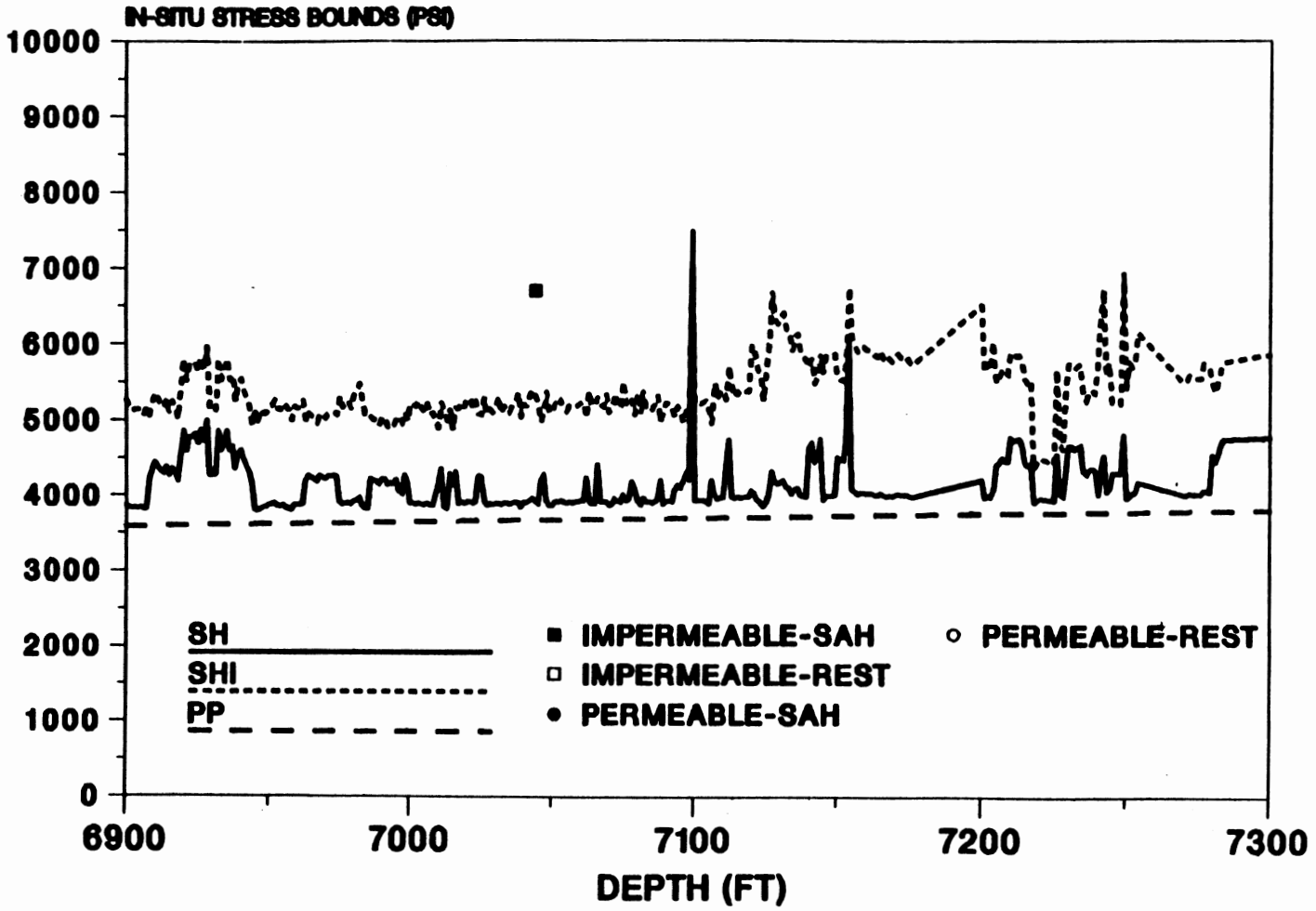

Figure 38. Section of Calculated In-Situ Stress Bounds and Stress Tests Versus Depth for Section of SFE #4 (6900 - 7300 Feet)

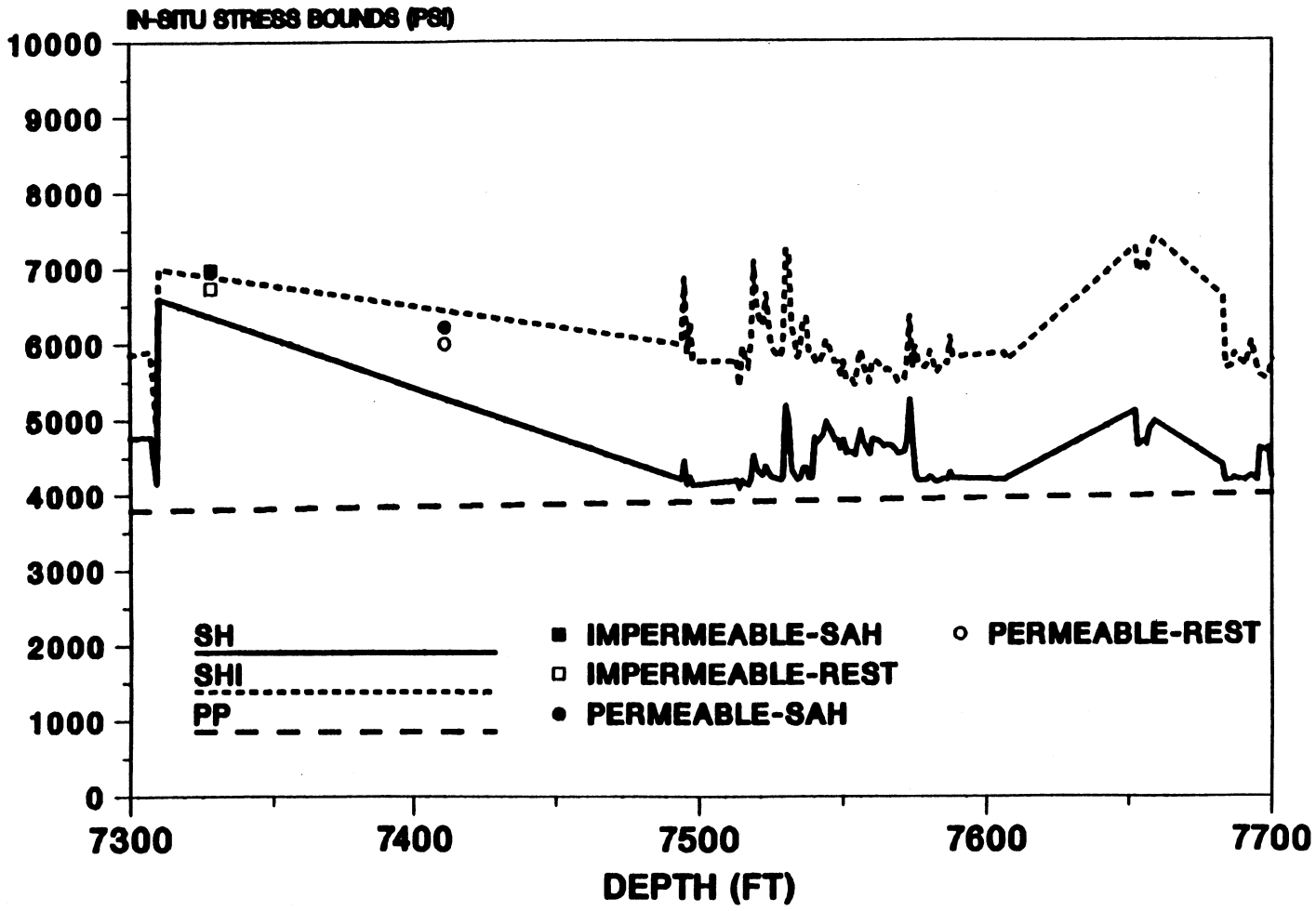

Figure 39. Section of Calculated In-Situ Stress Bounds and Stress Tests Versus Depth for Section of SFE #4 (7300 - 7700 Feet)

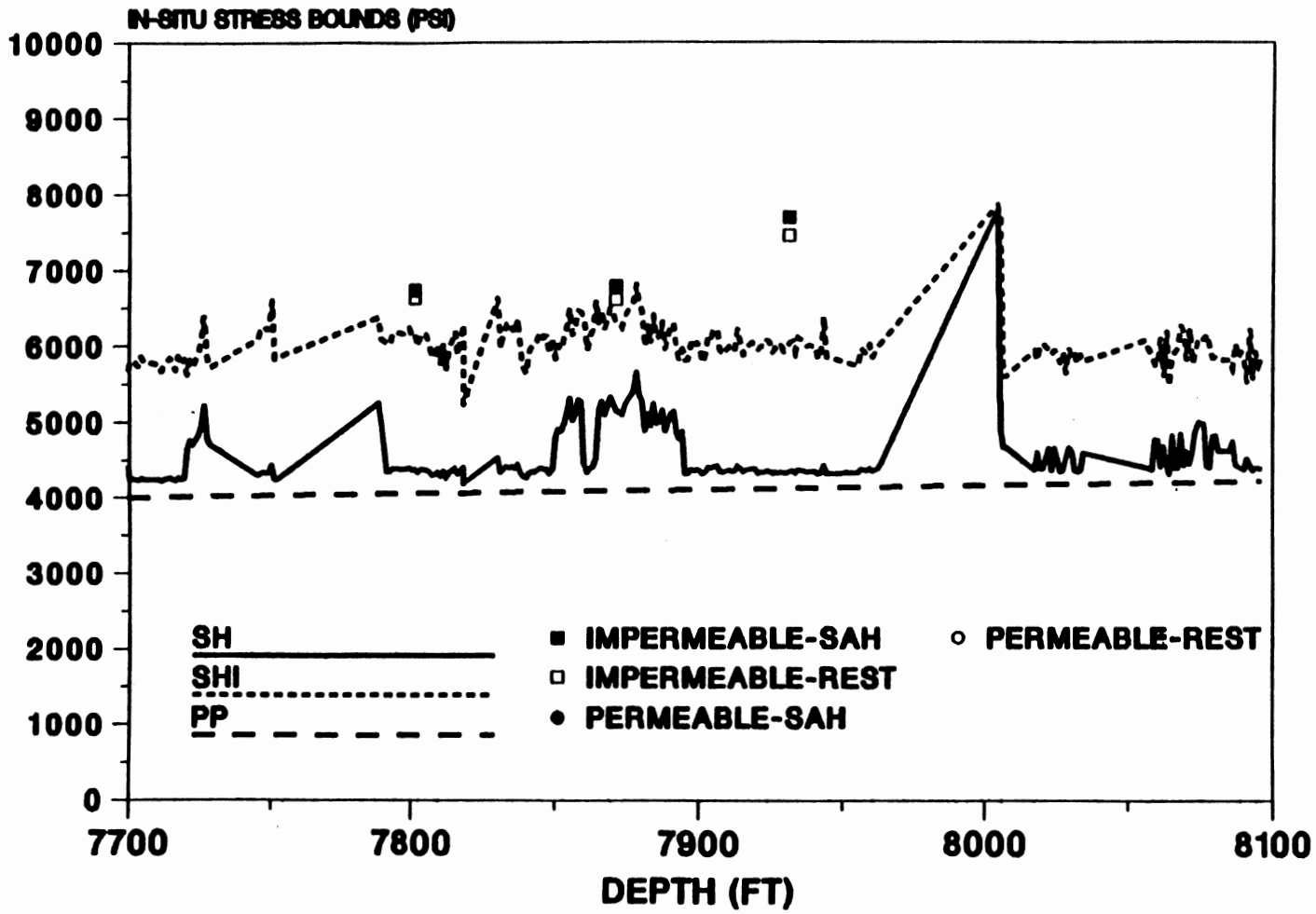

Figure 40. Section of Calculated In-Situ Stress Bounds and Stress Tests Versus Depth for Section of SFE #4 (7700 - 8100 Feet)

situ stress bound. The permeable stress test closure pressures lie on or below the calculated permeable upper bounds, but above the pore pressure (See Figures 28-36). These are encouraging results, since the calculated permeable and impermeable upper bounds seems to be the actual upper bounds. It can be seen that the "impermeable" upper bound serves as an upper bound on in-situ stress for all rock, whether permeable or impermeable. Pore pressure, of course, serves as a lower bound.

It is also important to note from this study that in-situ rock appears to typically be close to failure. It is concluded that much of the rock in the earth (at least in the vacinity of the SFE wells 1-3) is close to failure. We speculate that as rock is confined at higher stresses, which is the case with increased depth, it fails and becomes harder due to compaction. The continued compaction and hardening of earth rock with increasing depth suggests that deeply buried rock is frequently close to failure and fails more and more the deeper it is buried. This conclusion is supported by other evidence. E. Hunt observed [45] that in shales and sands there are various indications from core and log analysis of rock in the earth being close to or at failure. These are:

A. When shear velocity logs are run using polarized sources and three component receivers the shear velocity can be extracted in the three principal directions x, y, and z. When the x and y (horizontal velocities) are significantly different (birefringency) it is a strong indication of the presence of fractures in the formation. In the SFE wells a birefringency of 5-10 % was

observed. More than 6 % birefringency is indicative of presence of fractures.

B. There are large differences between measurements of the modulus of elasticity using dynamic and static loading on rock cores in the lab. Static loading on a core measures the modulus of elasticity from the stress-strain curve using a triaxial test. The dynamic loading test in the lab measures the shear and compressional velocities to obtain poissons ratio, and from which the modulus of elasticity is calculated. The large differences can not be explained by normal acoustical or static effects. It is believed that microfractures, which indicate rock at failure, open or close under static loading but are not closed under dynamic loading. These existing microfractures indicate that rock is close to or at failure.

C. When rock core thin sections are examined under a microscope, microcracks can frequently be seen crossing rock grains. Such microcracks, which ultimately sealed due to temperature and pressure effects, indicate in-situ rock failure.

For SFE #4 (Figures 37-40) it is seen that stress test results lie above the upper bounds calculated in our approach. This might have been expected since SFE #4 is located in a mountain area in western Wyoming near the "overthrust belt". Active tectonic stresses are know to exist in this area. Consider adding a constant term, T, to the R.H.S of (20) as proposed in (22) to account for horizontal tectonic stress. Then (20) becomes:

$$S_h = K_0(S_{ob} - P_P) + P_P + T \qquad (27)$$

By simple comparison of the results in Figures 37-40, it can be seen that a value of T given by;

$$T = 1500 \text{ psi} \tag{28}$$

will yield an upper bound in (27) such that all the stress test data lies on or below this new bound. This new upper bound is given in Figures 41-44. The value for T in (28) for SFE #4 can be explained partly by the well being located at the foot of a 700 ft mountain. An overburden gradient of 1.1 psi/ft indicates a 770 psi overburden increase due to this mountain, but this account for only about half of the needed 1500 psi. Z. Moschovidis [47] observed that values for T as high as 1250 psi have been seen in central mid-America fields located in mountain areas. Accordingly, we suspect that in mountainous areas, a non-zero value for T in (27) is needed to account for both tectonics stresses and nearby mountains. The value for T would then vary for each field. Unfortunately, as shown by Warpinski [42, 43, 44], calculating a value for T is extremely difficult.

Combination of the Two Upper Bounds

The two upper bounds calculated for the permeable and impermeable cases were combined into a single upper bound on stress by treating each foot of formation as either "impermeable" or "permeable" according to some measure of its permeability. The best results were obtained by assuming that permeable intervals were

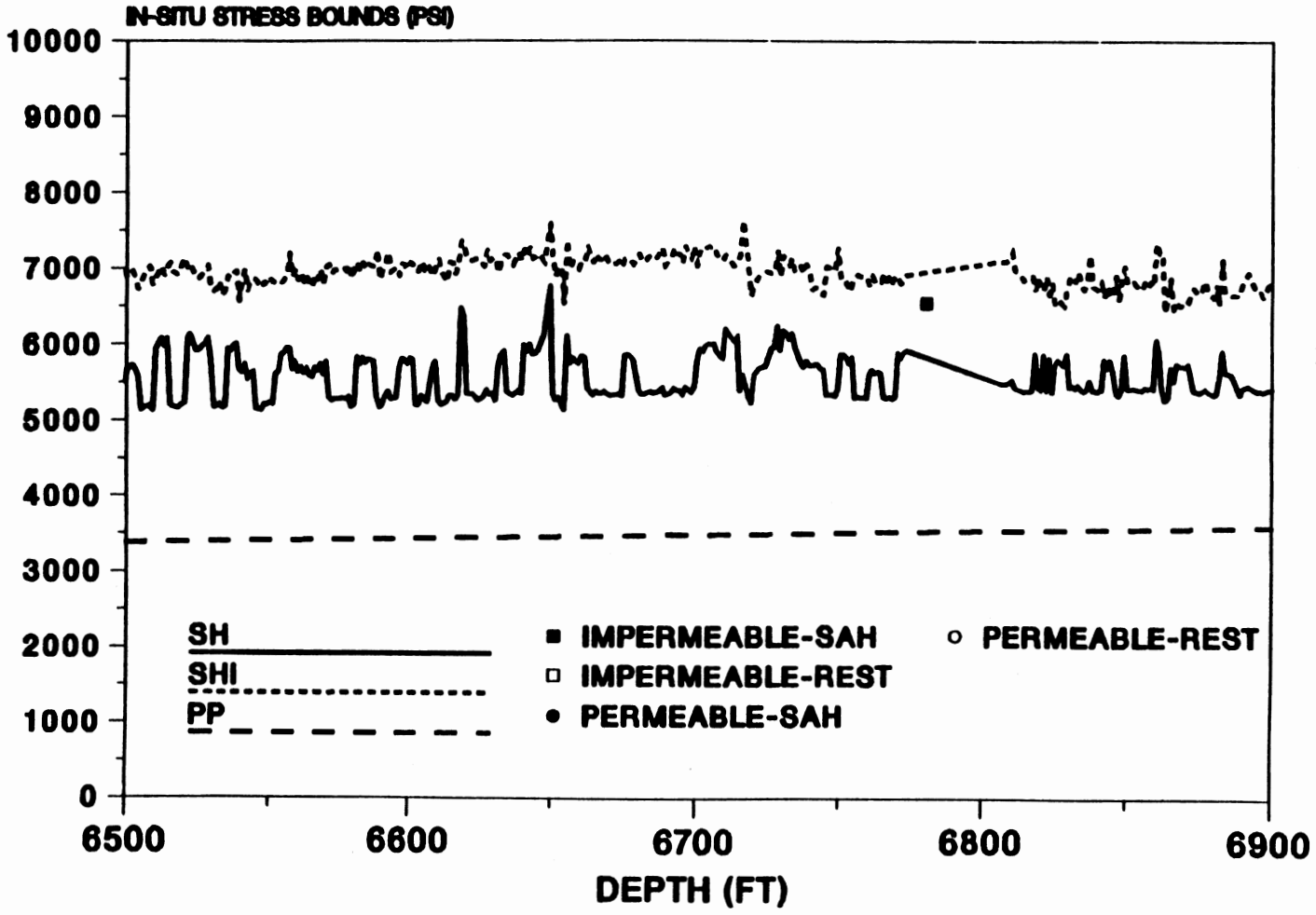

Figure 41. Section of Calculated In-Situ Stress Bounds and Stress Tests Versus Depth for Section of SFE #4 with T = 1500 psi (6500 - 6900 Feet)

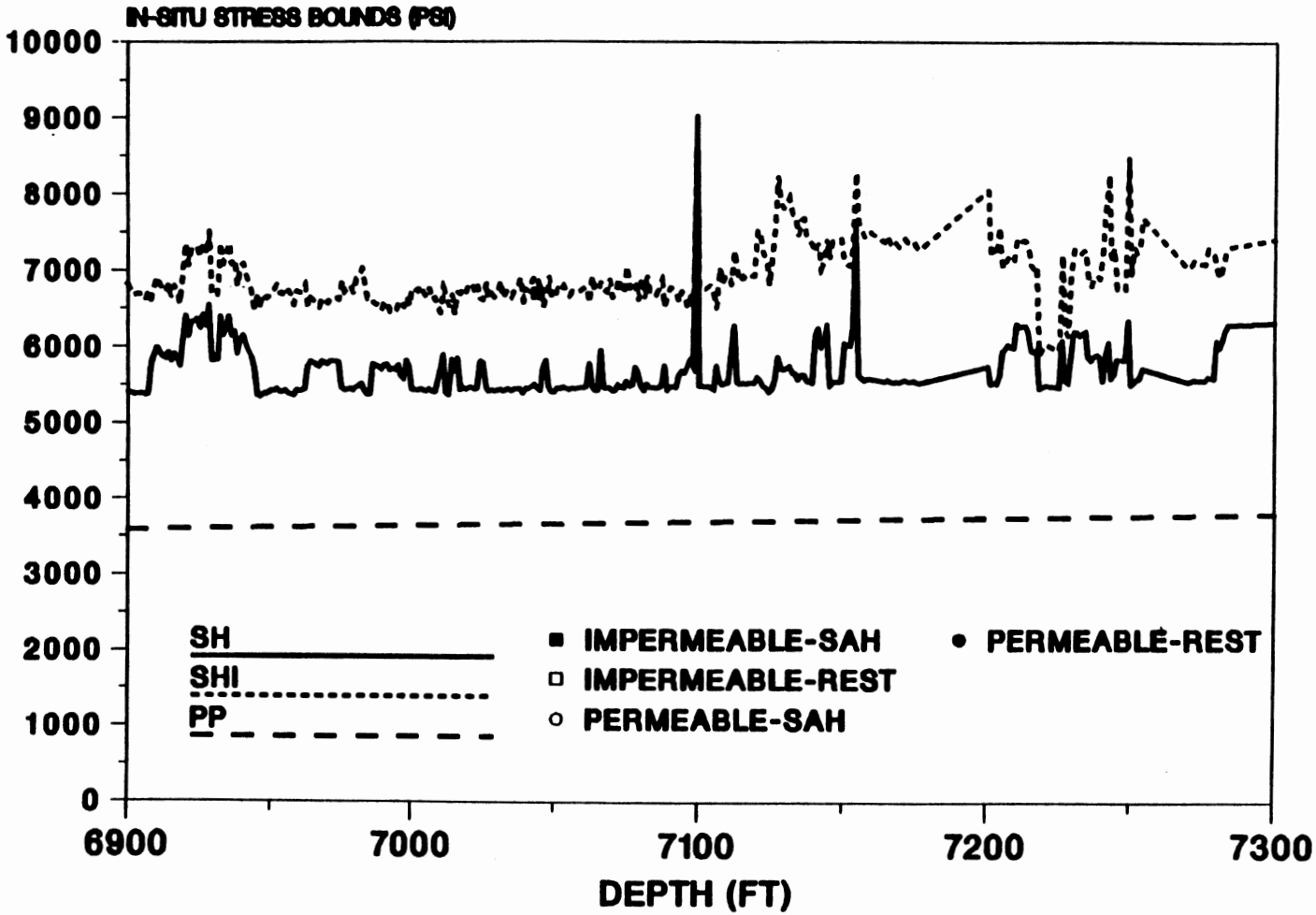

Figure 42. Section of Calculated In-Situ Stress Bounds and Stress Tests Versus Depth for Section of SFE #4 with T = 1500 psi (6900 - 7300 Feet)

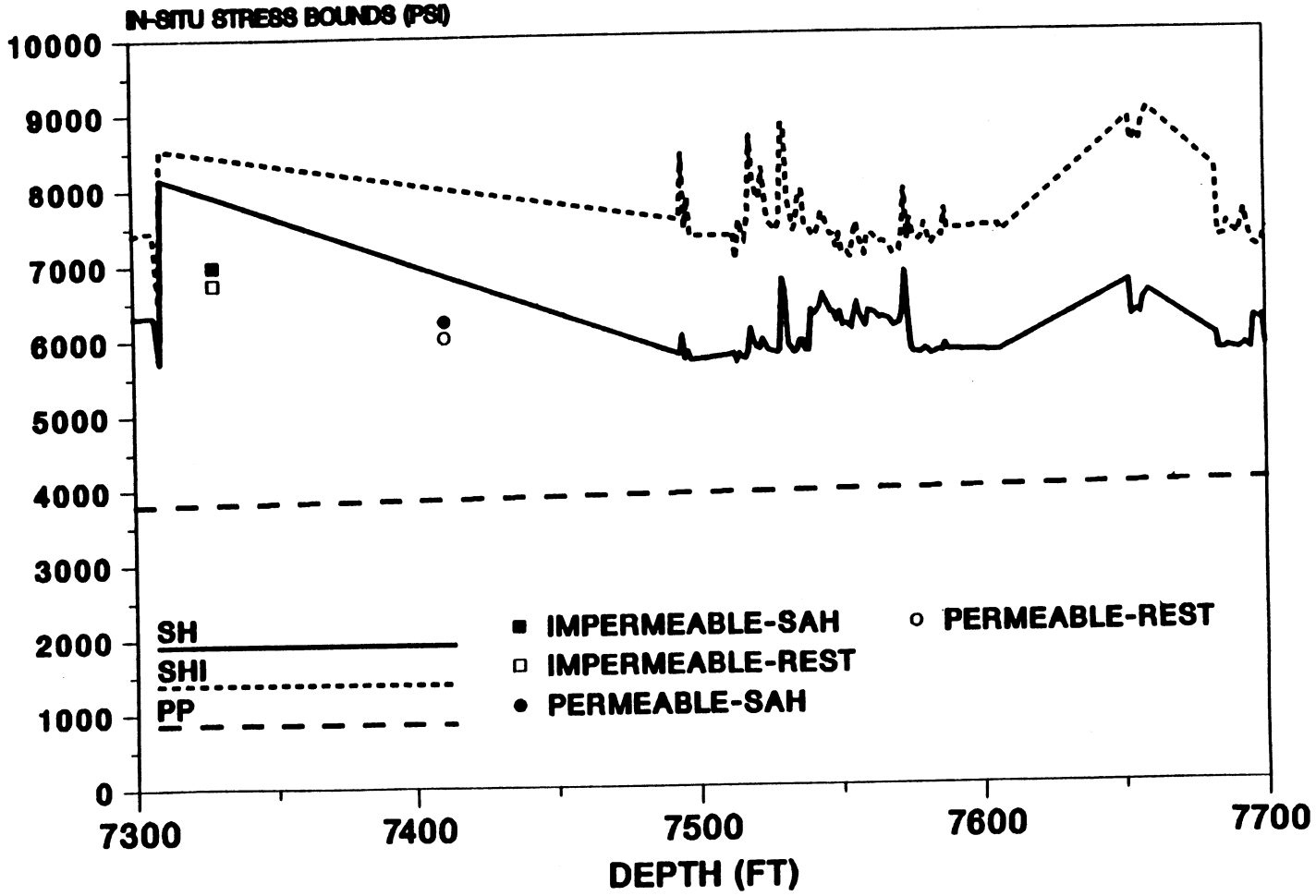

Figure 43. Section of Calculated In-Situ Stress Bounds and Stress Tests Versus Depth for Section of SFE #4 with T = 1500 psi (7300 - 7700 Feet)

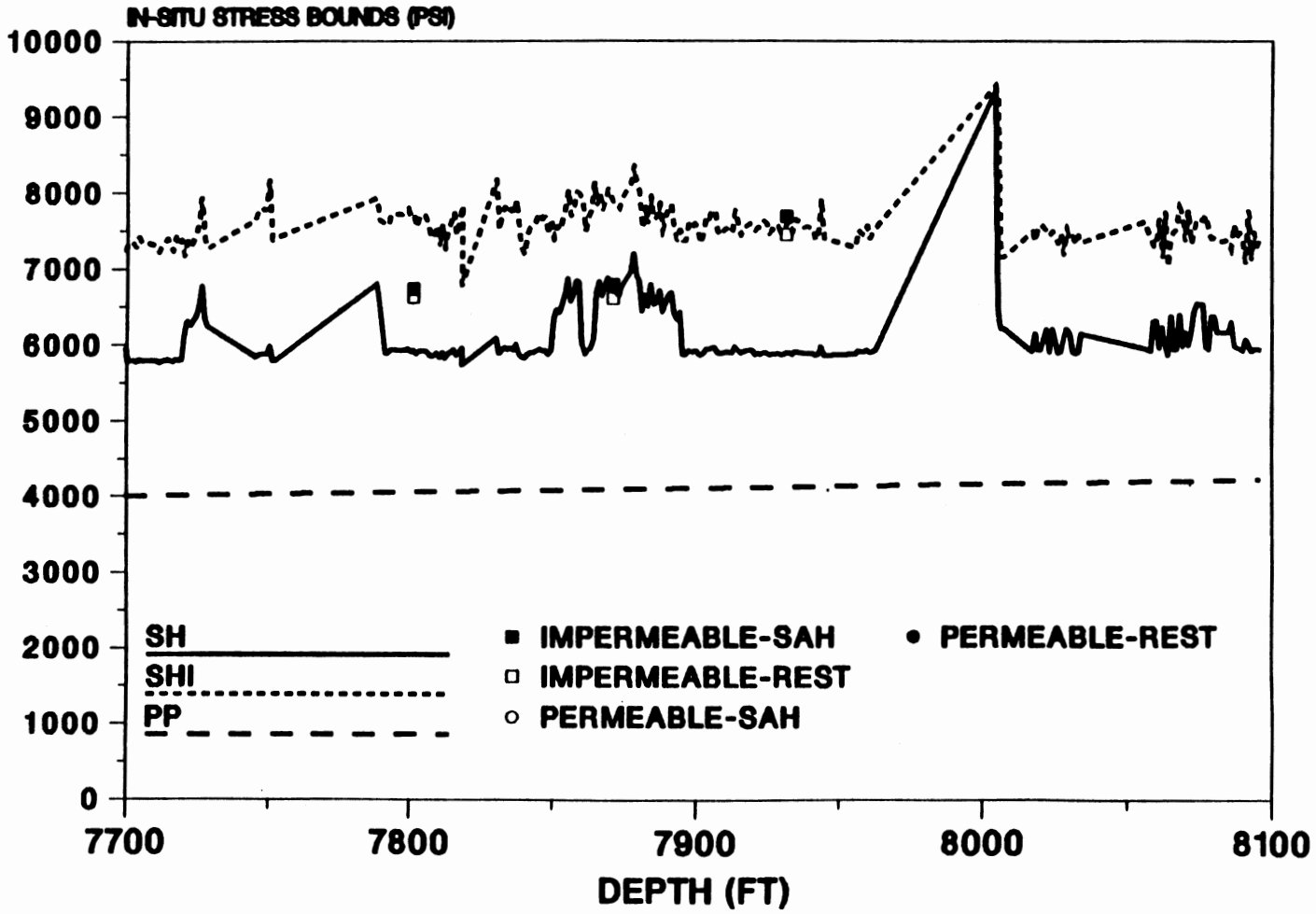

Figure 44. Section of Calculated In-Situ Stress Bounds and Stress Tests Versus Depth for Section of SFE #4 with T = 1500 psi (7700 - 8100 Feet)

those containing more than 90 percent sandstone, and that all other intervals were impermeable. The results of this approach are shown in Figures 45-57. It can be seen that all stress test data points are on or below this combined upper bound. Note that for SFE #4 a value of 1500 psi for T was included. Numerous other sandstone percentages were tried as the "switch value" for permeability, but the value of 90 % appeared optimum.

While it could be argued that volumetric percentage of sandstone is not necessarily a good measure of permeability, it is probably as good an indicator as can be obtained from data typically collected during drilling operations (ie, mud-logger lithology data). However, if one is willing to wait for an electric log to be run before this calculation is done, better permeability information can be obtained. Hunt [45] examined the electric logs from SFE # 1-4, and gave a rough estimate of permeabilities from the SP (Self Potential) logs. Formations were assumed permeable if permeability was larger than .01 md and impermeable if less than or equal to .01 md. Tables 22 and 23 present the results for SFE #1 and #2, respectively. For SFE #3 and 4 the intervals evaluated were impermeable. These new combined stress bounds are shown in Figures 58-70. This approach also yields all stress test data points on or below the calculated upper bound. It can be seen that the electric log approach yields less deviation of stress test data from the upper bound than does the 90 percent sandstone approach. Improved methods of combining the two upper bounds using drilling data would be possible if better knowledge of permeability could be obtained. One

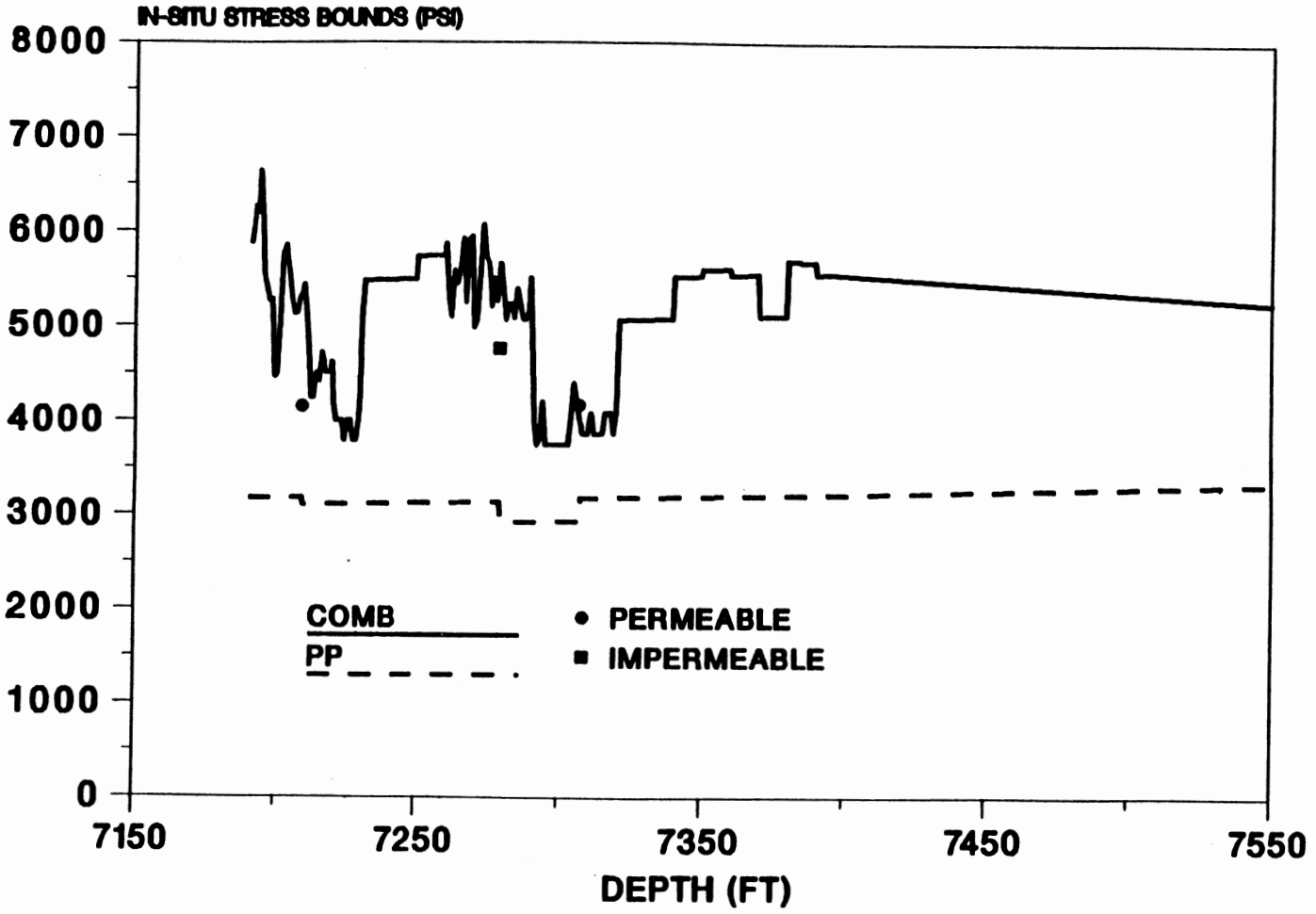

Figure 45. Section of Combined In-Situ Upper Stress Bounds with 90% Sand Permeability Switch for SFE #1 (7150 - 7550 Feet)

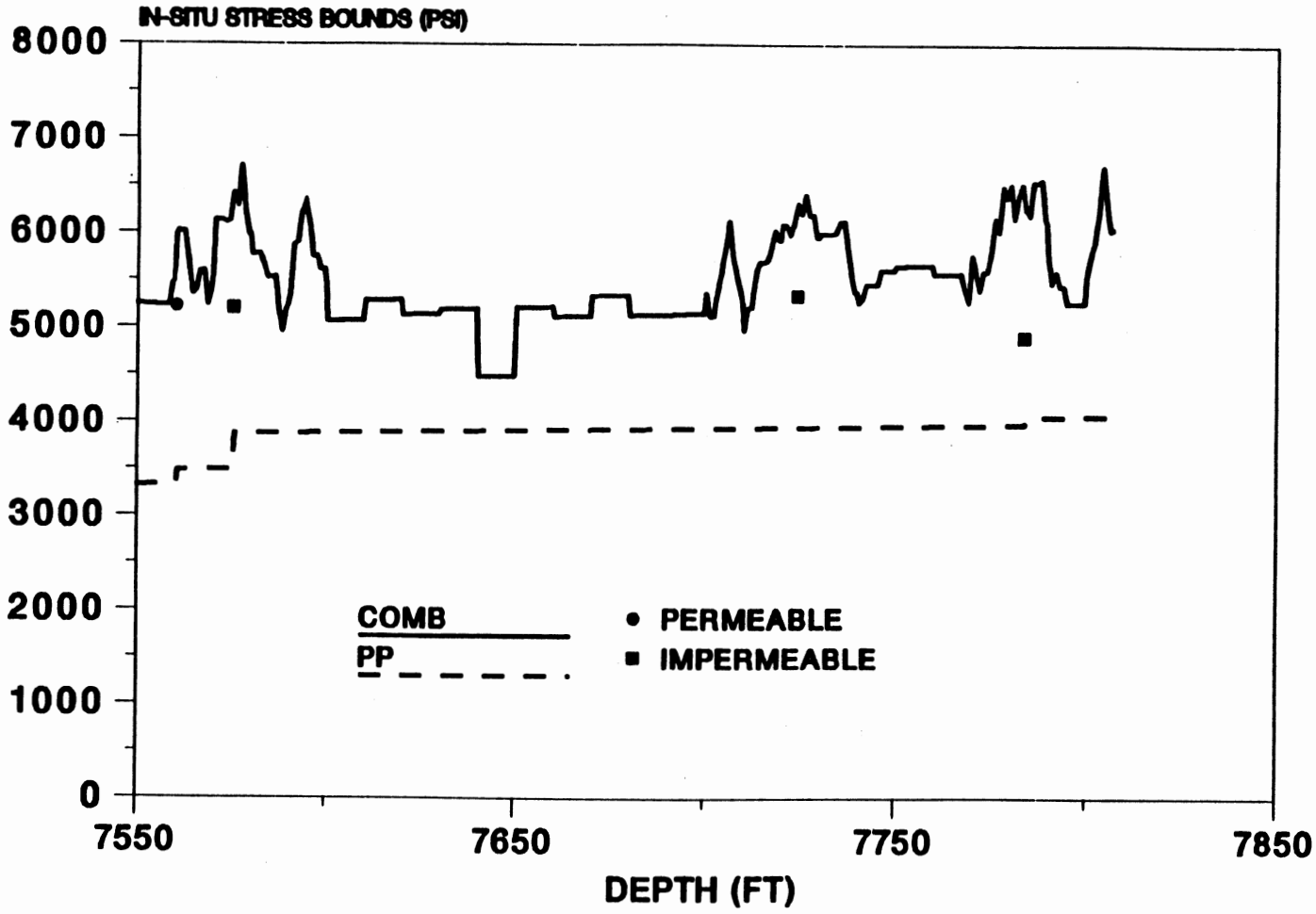

Figure 46. Section of Combined In-Situ Upper Stress Bounds with 90% Sand Permeability Switch for SFE #1 (7550 - 7850 Feet)

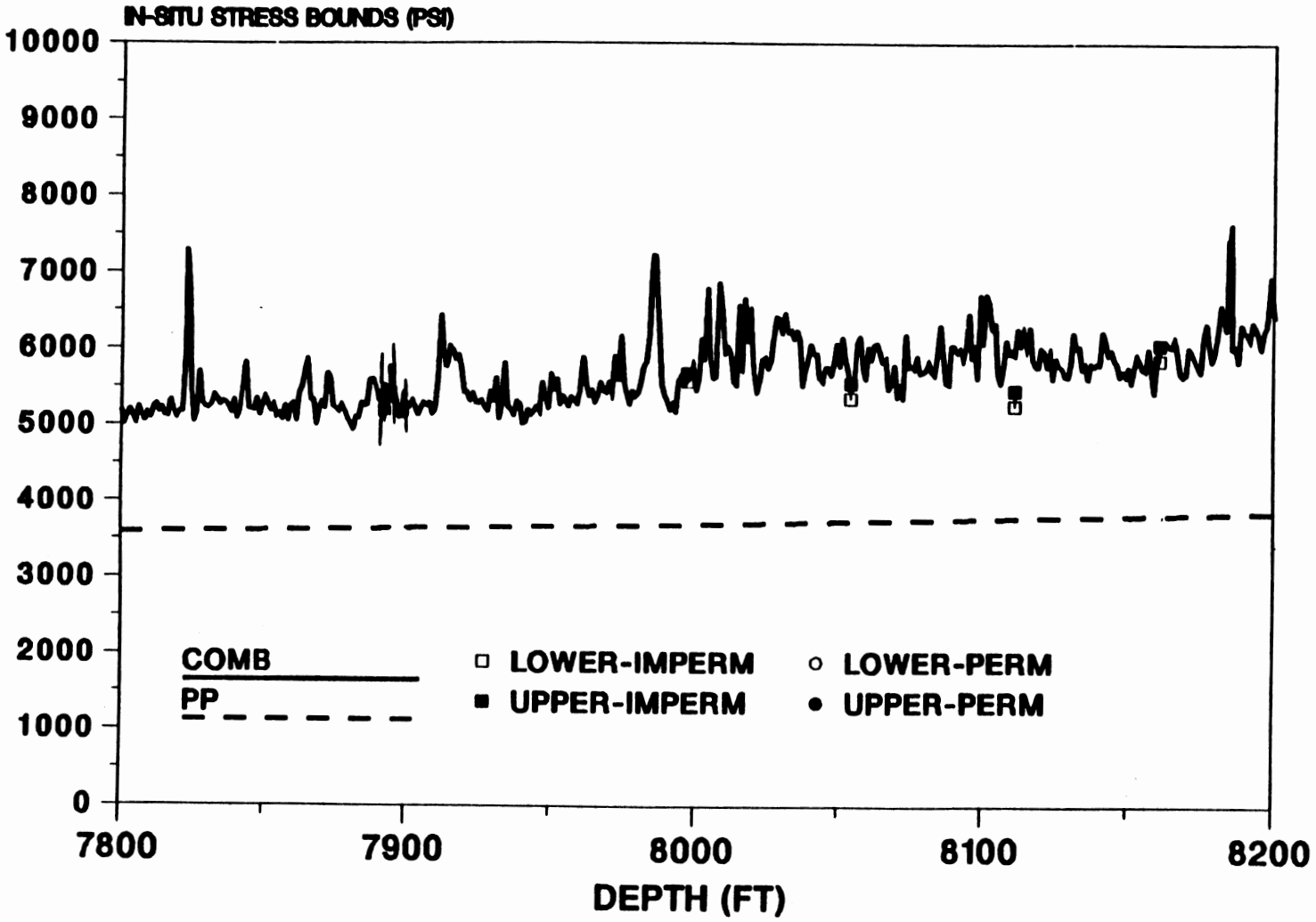

Figure 47. Section of Combined In-Situ Upper Stress Bounds with 90% Sand Permeability Switch for SFE #2 (7800 - 8200 Feet)

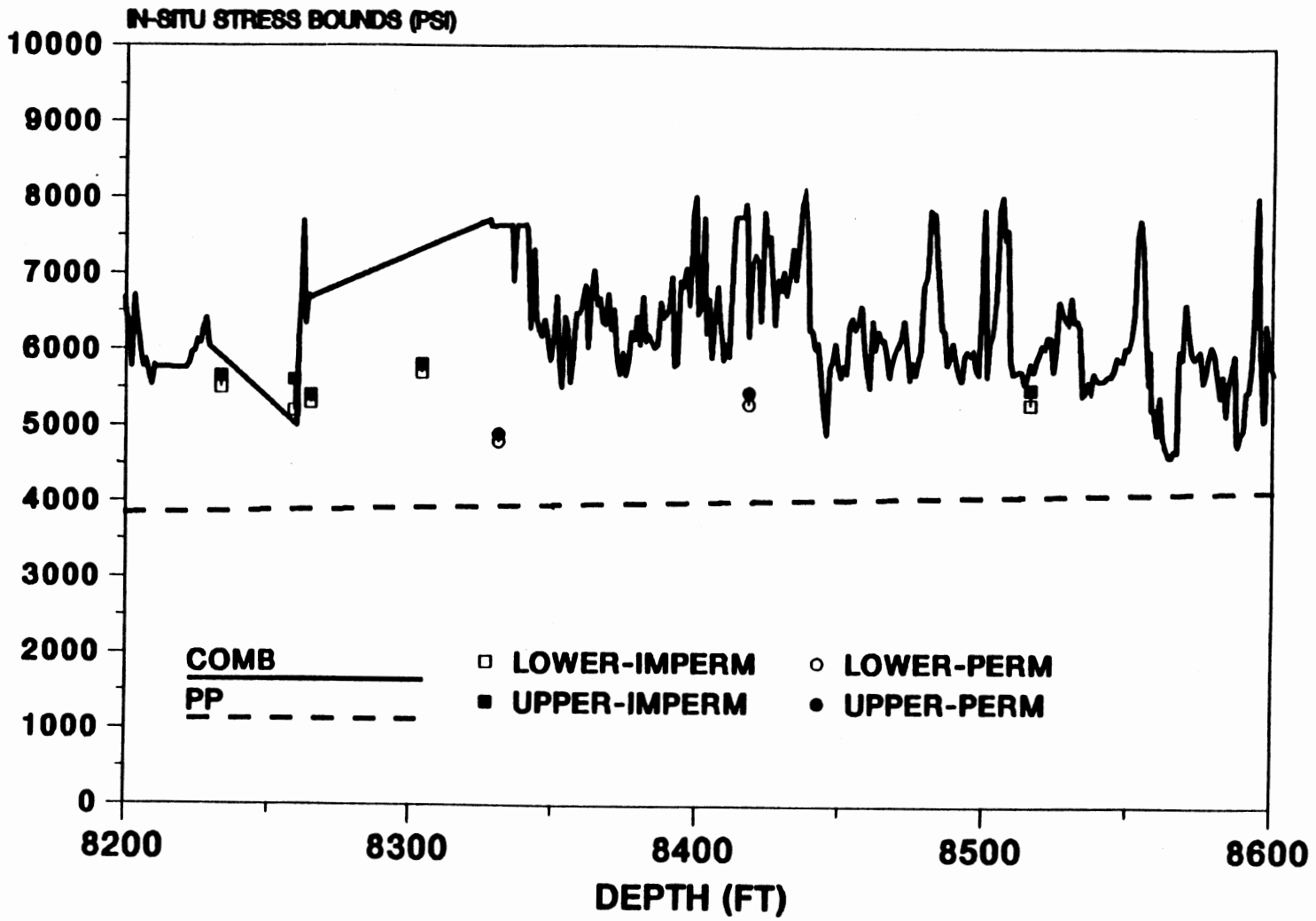

Figure 48. Section of Combined In-Situ Upper Stress Bounds with 90% Sand Permeability Switch for SFE #2 (8200 - 8600 Feet)

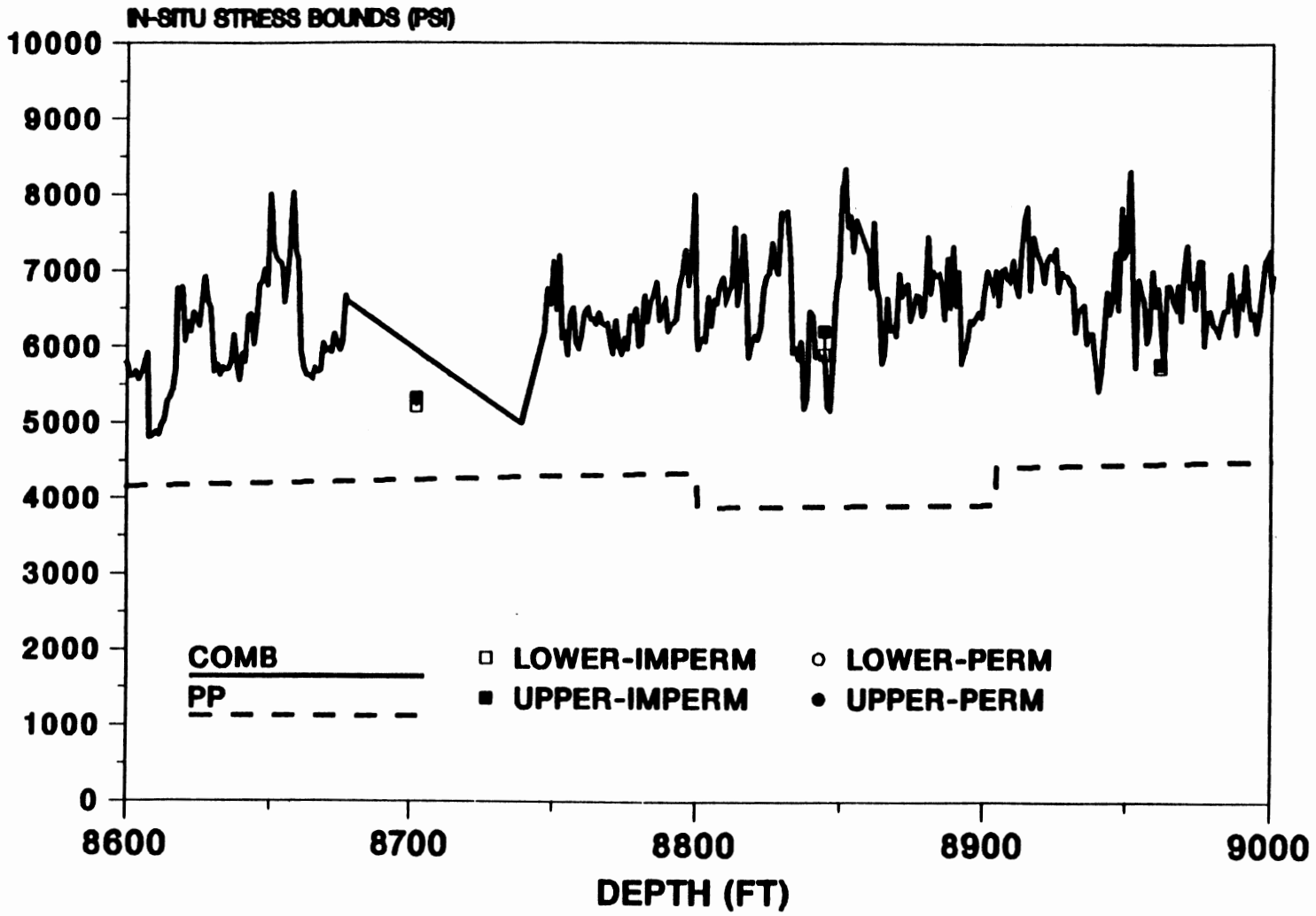

Figure 49. Section of Combined In-Situ Upper Stress Bounds with 90% Sand Permeability Switch for SFE #2 (8600 - 9000 Feet)

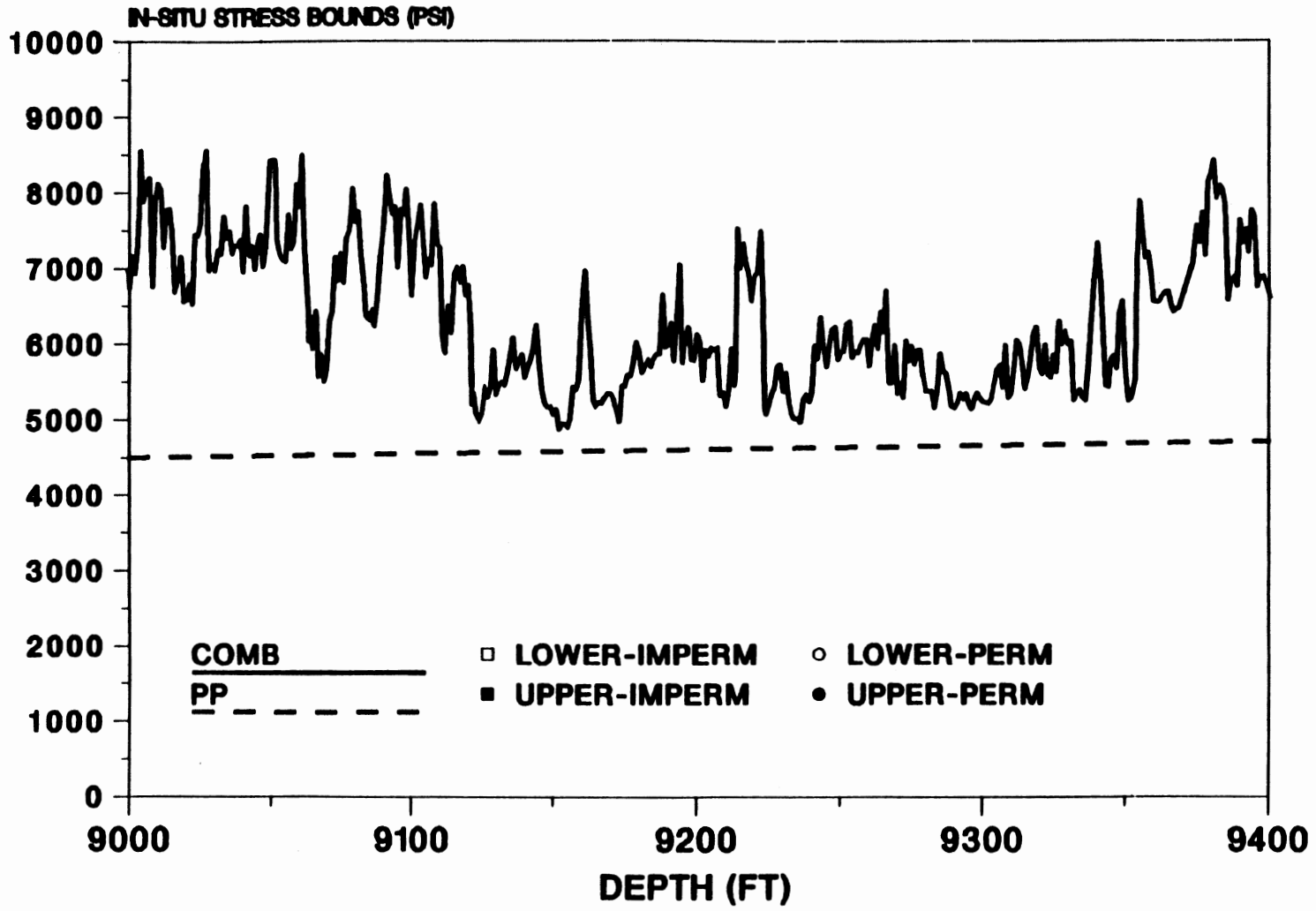

Figure 50. Section of Combined In-Situ Upper Stress Bounds with 90% Sand Permeability Switch for SFE #2 (9000 - 9400 Feet)

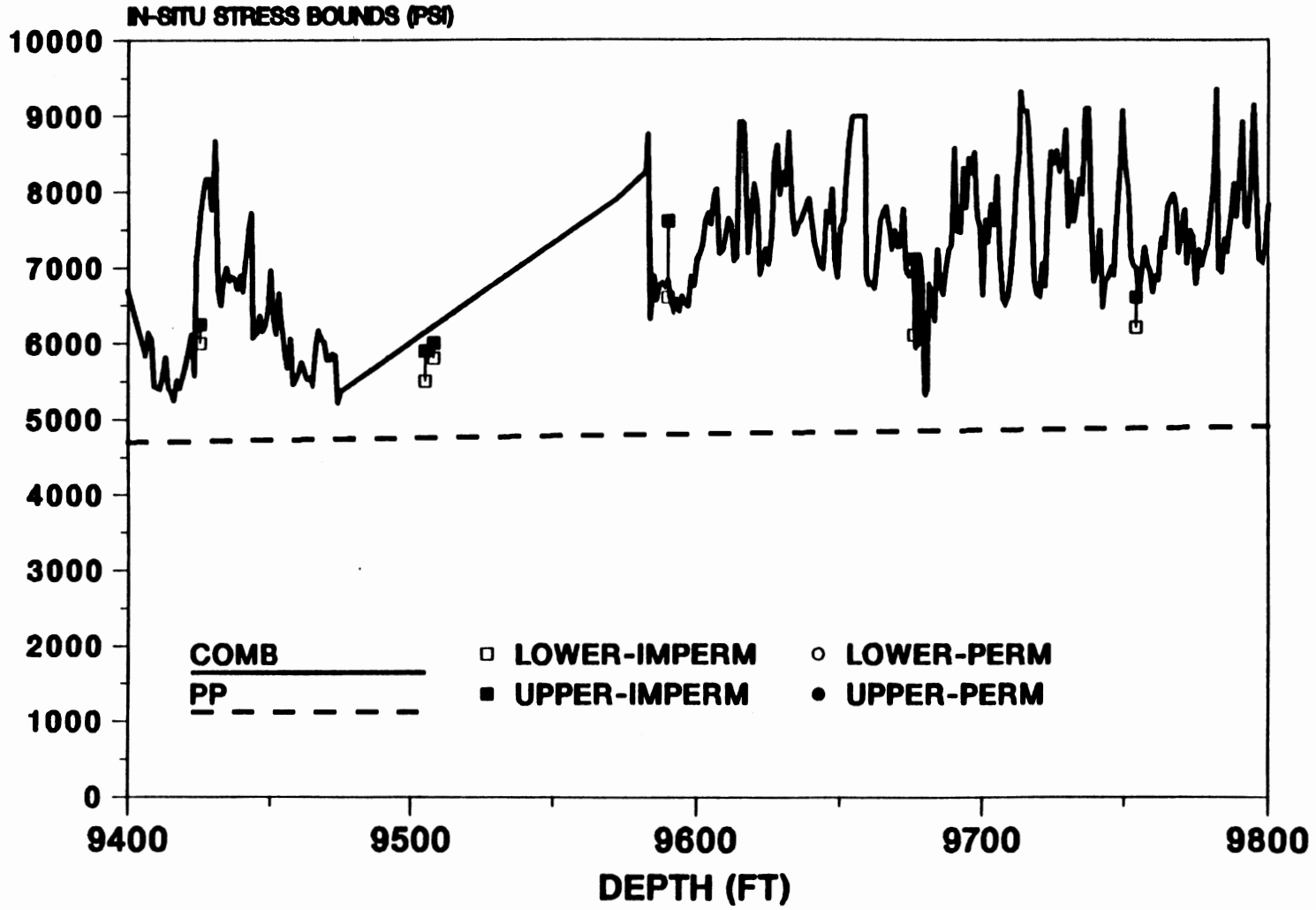

Figure 51. Section of Combined In-Situ Upper Stress Bounds with 90% Sand Permeability Switch for SFE #2 (9400 - 9800 Feet)

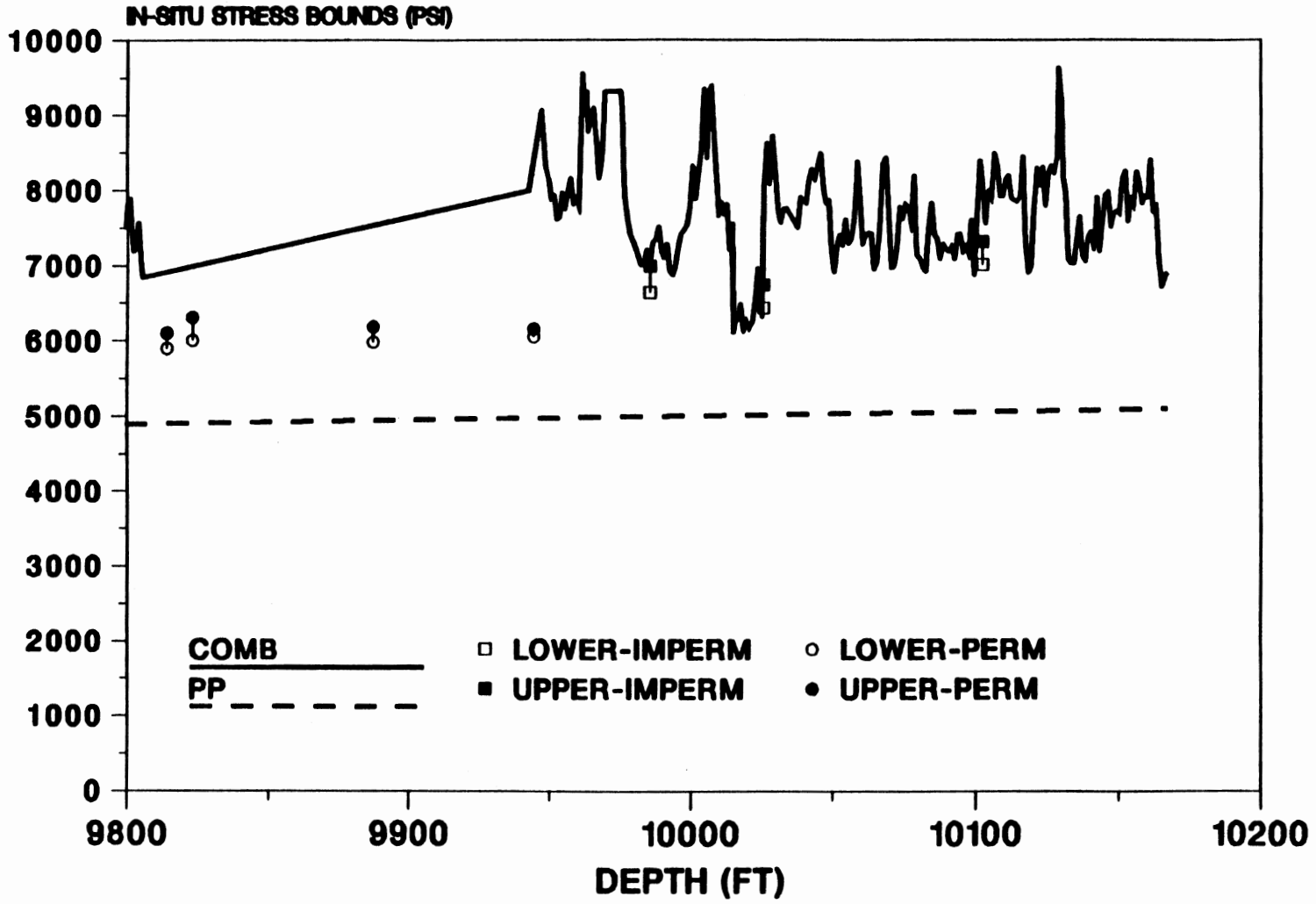

Figure 52. Section of Combined In-Situ Upper Stress Bounds with 90% Sand Permeability Switch for SFE #2 (9800 - 10200 Feet)

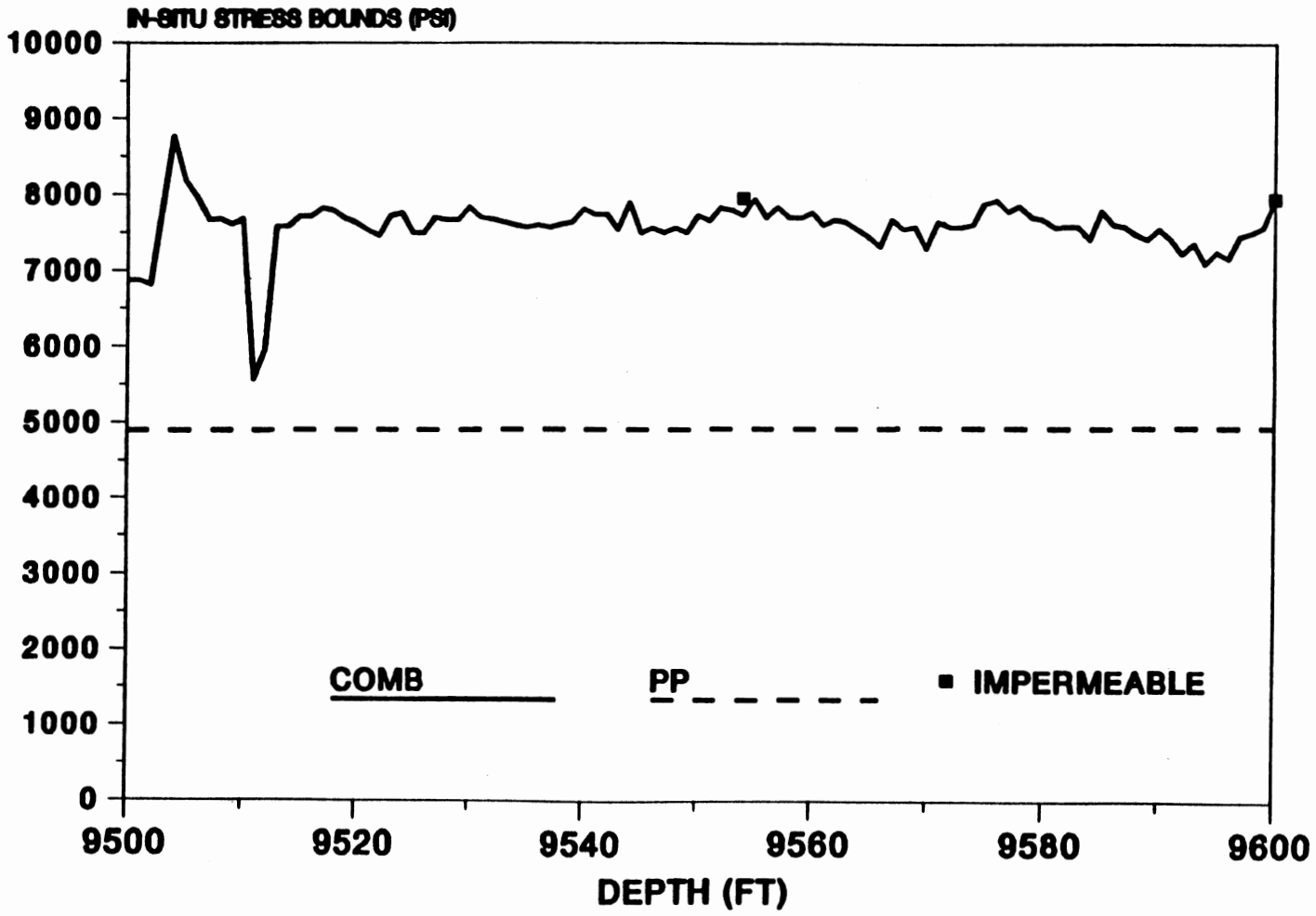

Figure 53. Section of Combined In-Situ Upper Stress Bounds with 90% Sand Permeability Switch for SFE #3 (9500 - 9600 Feet)

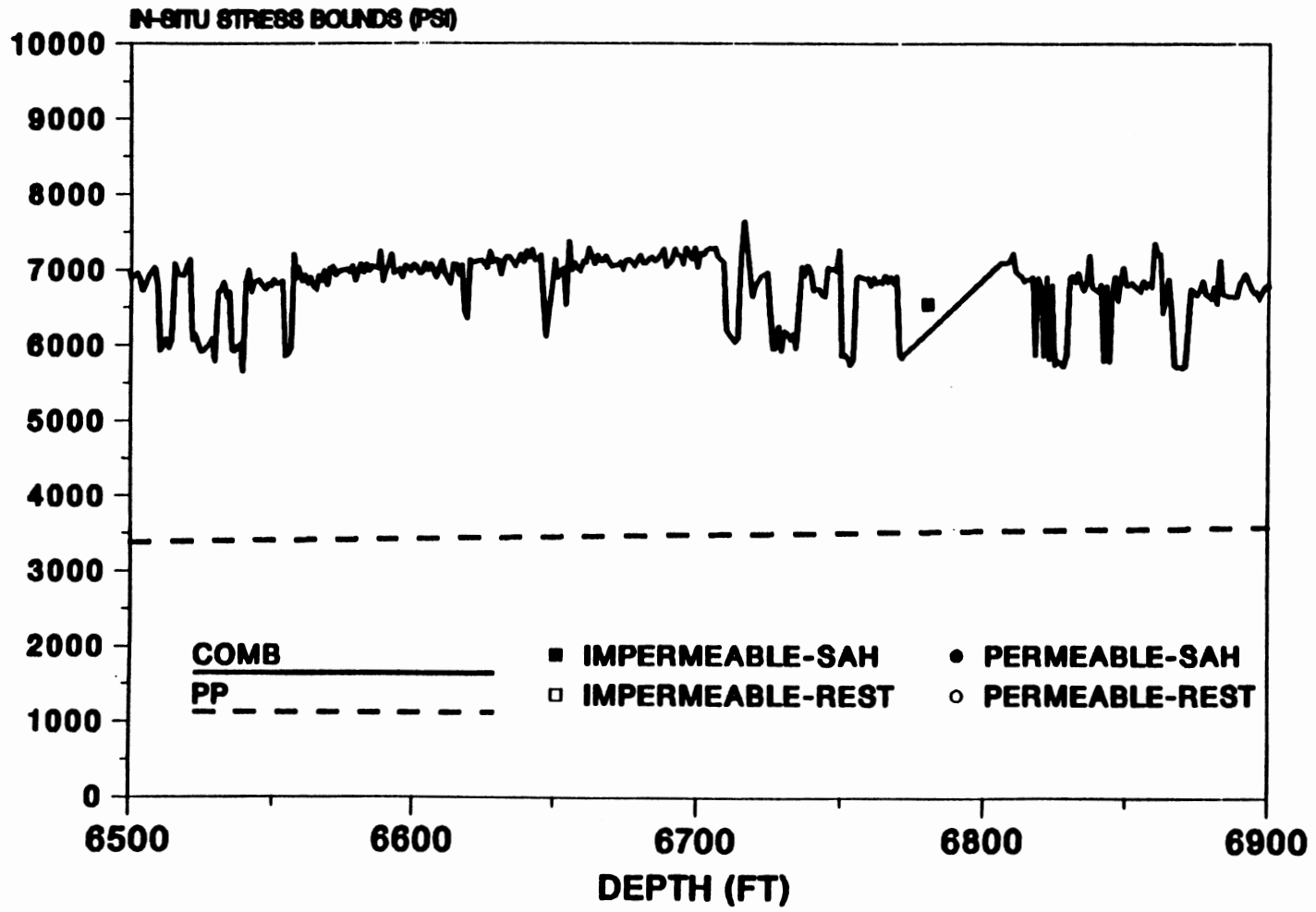

Figure 54. Section of Combined In-Situ Upper Stress Bounds with 90% Sand Permeability Switch for SFE #4 with T = 1500 psi (6500 - 6900 Feet)

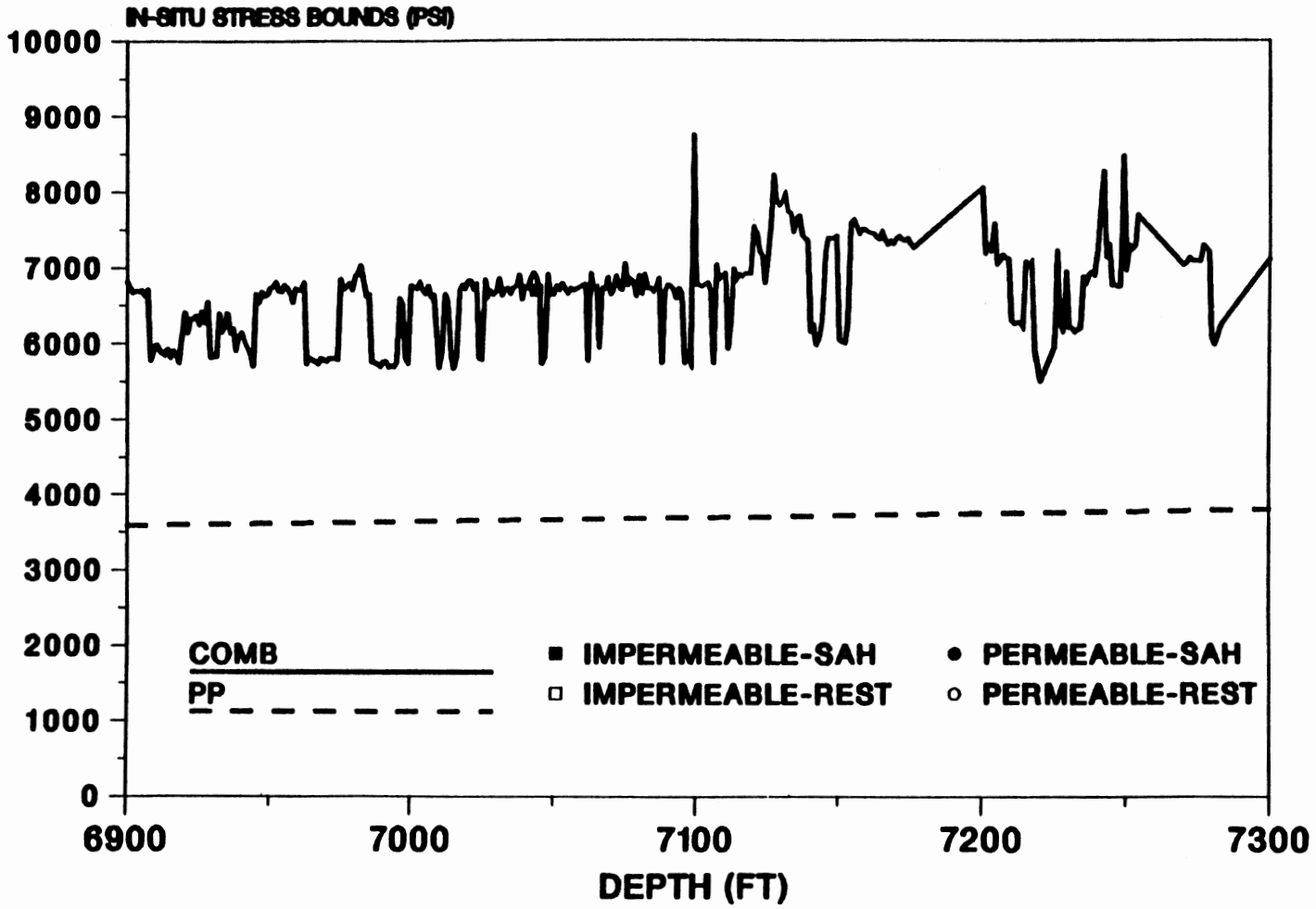

Figure 55. Section of Combined In-Situ Upper Stress Bounds with 90% Sand Permeability Switch for SFE #4 with T = 1500 psi (6900 - 7300 Feet)

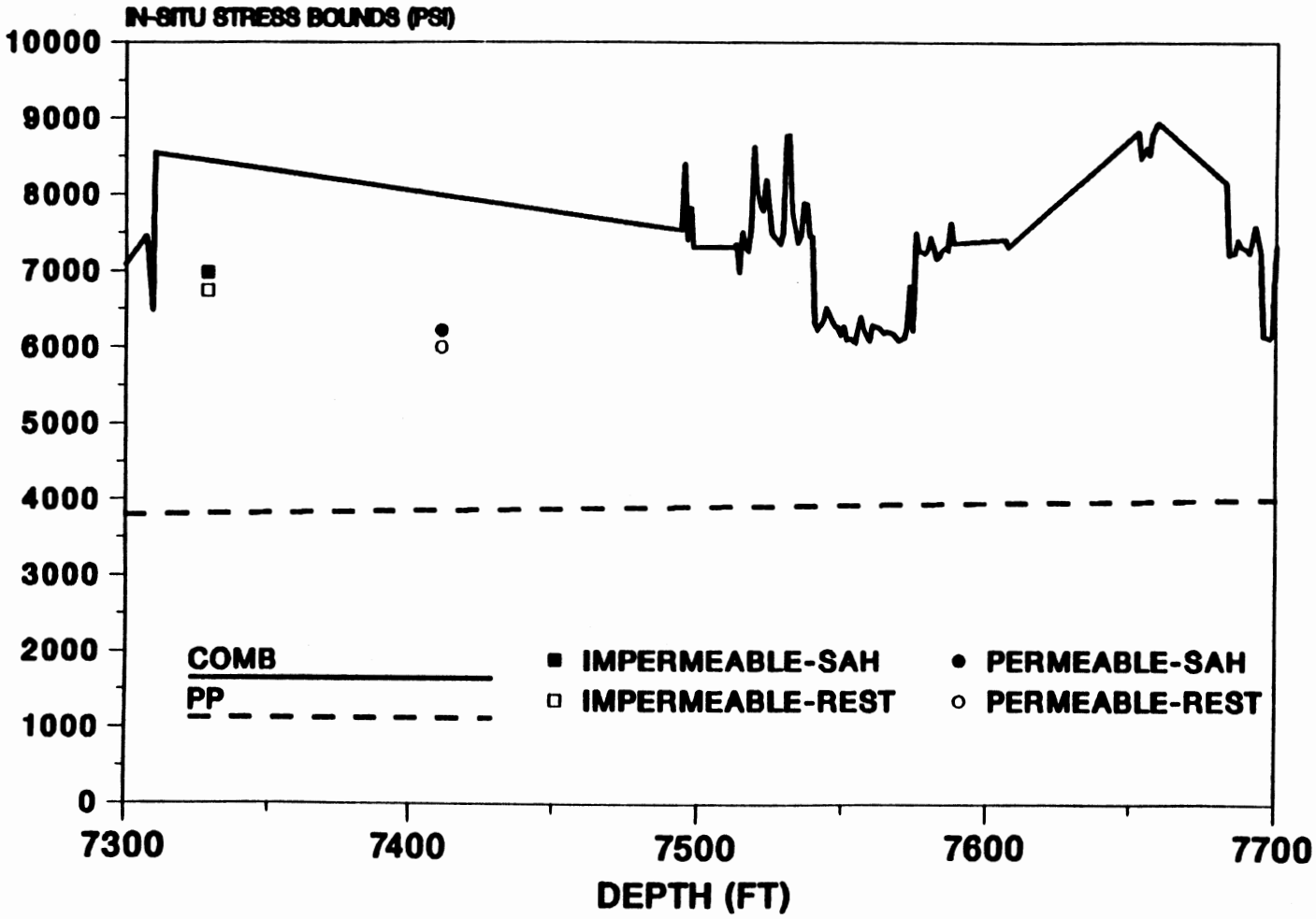

Figure 56. Section of Combined In-Situ Upper Stress Bounds with 90% Sand Permeability Switch for SFE #4 with T = 1500 psi (7300 - 7700 Feet)

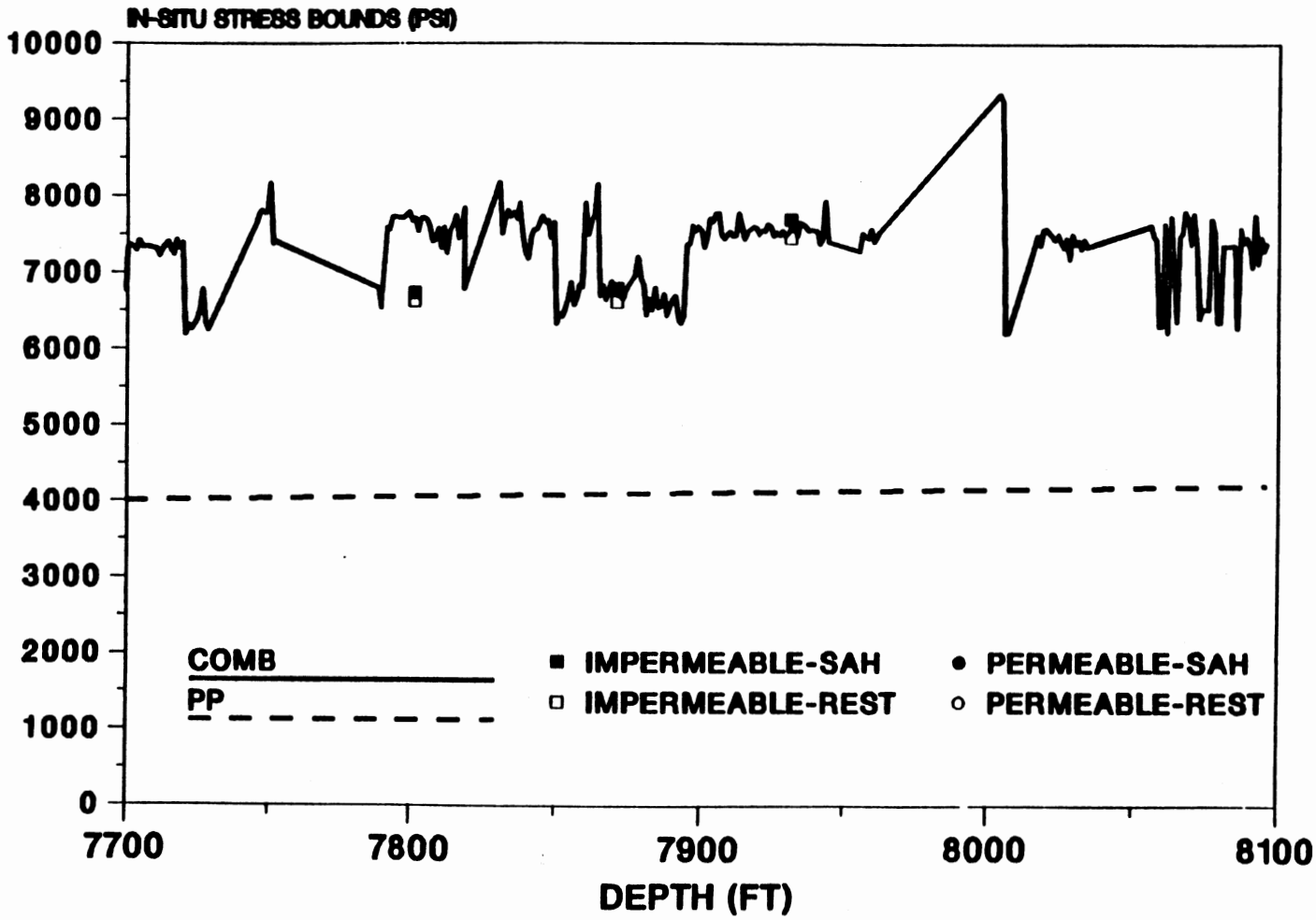

Figure 57. Section of Combined In-Situ Upper Stress Bounds with 90% Sand Permeability Switch for SFE #4 with T = 1500 psi (7700 - 8100 Feet)

TABLE XXII

PERMEABLE SECTIONS FOR SFE#1 WHERE PERMEABILITY IS LARGER THAN .01 MD.

Depth Interval (ft)
7210-7248
7251-7256
7292-7326
7332-7342
7360-7384
7392-7398
7420-7424
7442-7472
7496-7518
7586-7594
7600-7612
7628-7655
7663-7687
7698-7716
7740-7750
7766-7776
7794-7803
7815-7822
7826-7849

TABLE XXIII

PERMEABLE SECTIONS FOR SFE#2 WHERE PERMEABILITY IS LARGER THAN .01 MD.

Depth Interval (ft)
8263-8276
8324-8336
8396-8402
8414-8436
8646-8660
8806-8812
8853-8862
8870-8886
8896-8925
9004-9012
9021-9036
9090-9100
9183-9200
9244-9264
9824-9844

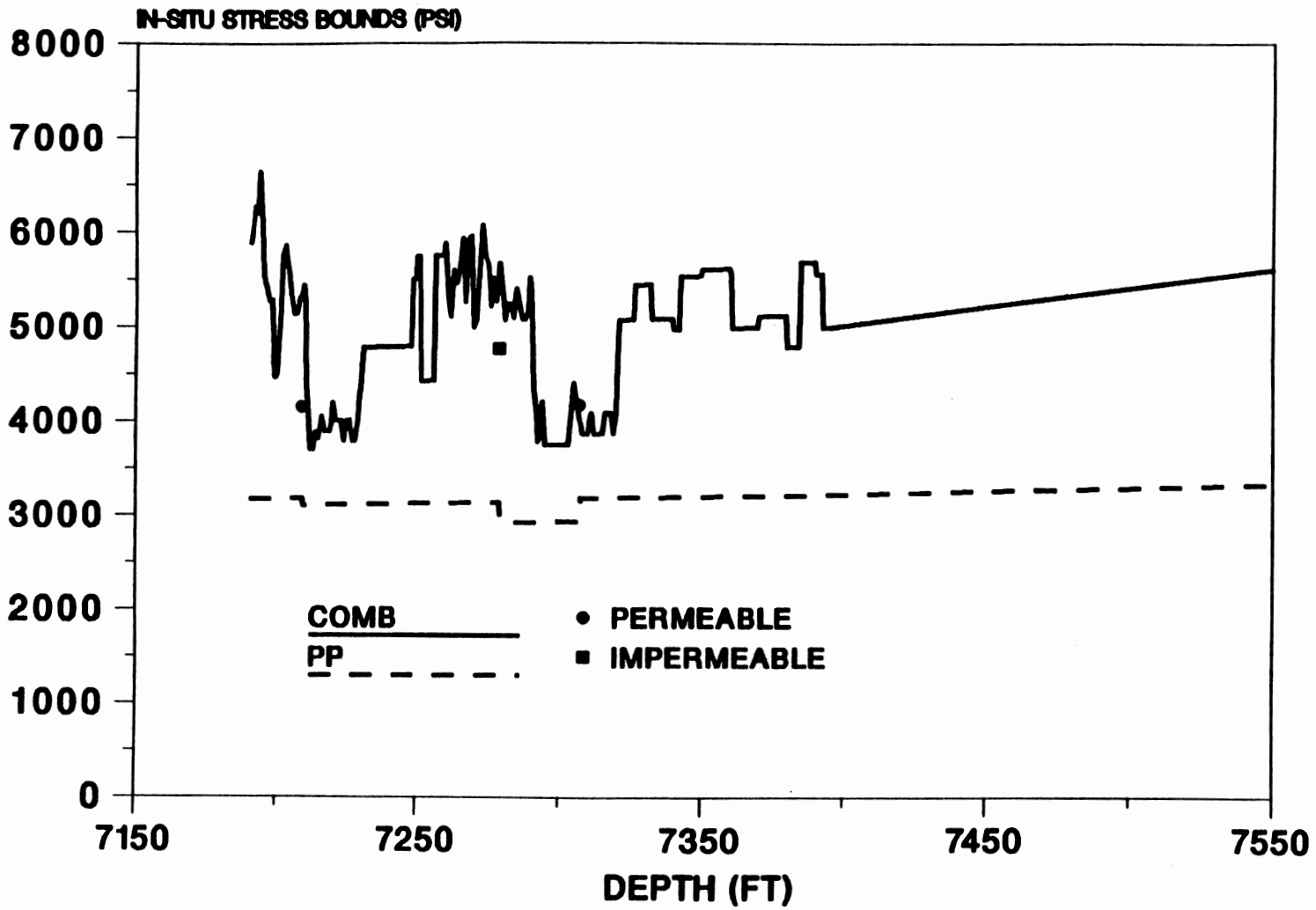

Figure 58. Section of Combined In-Situ Upper Stress Bounds with 0.1 md Permeability Switch from Electric Logs for SFE #1 (7150 - 7550 Feet)

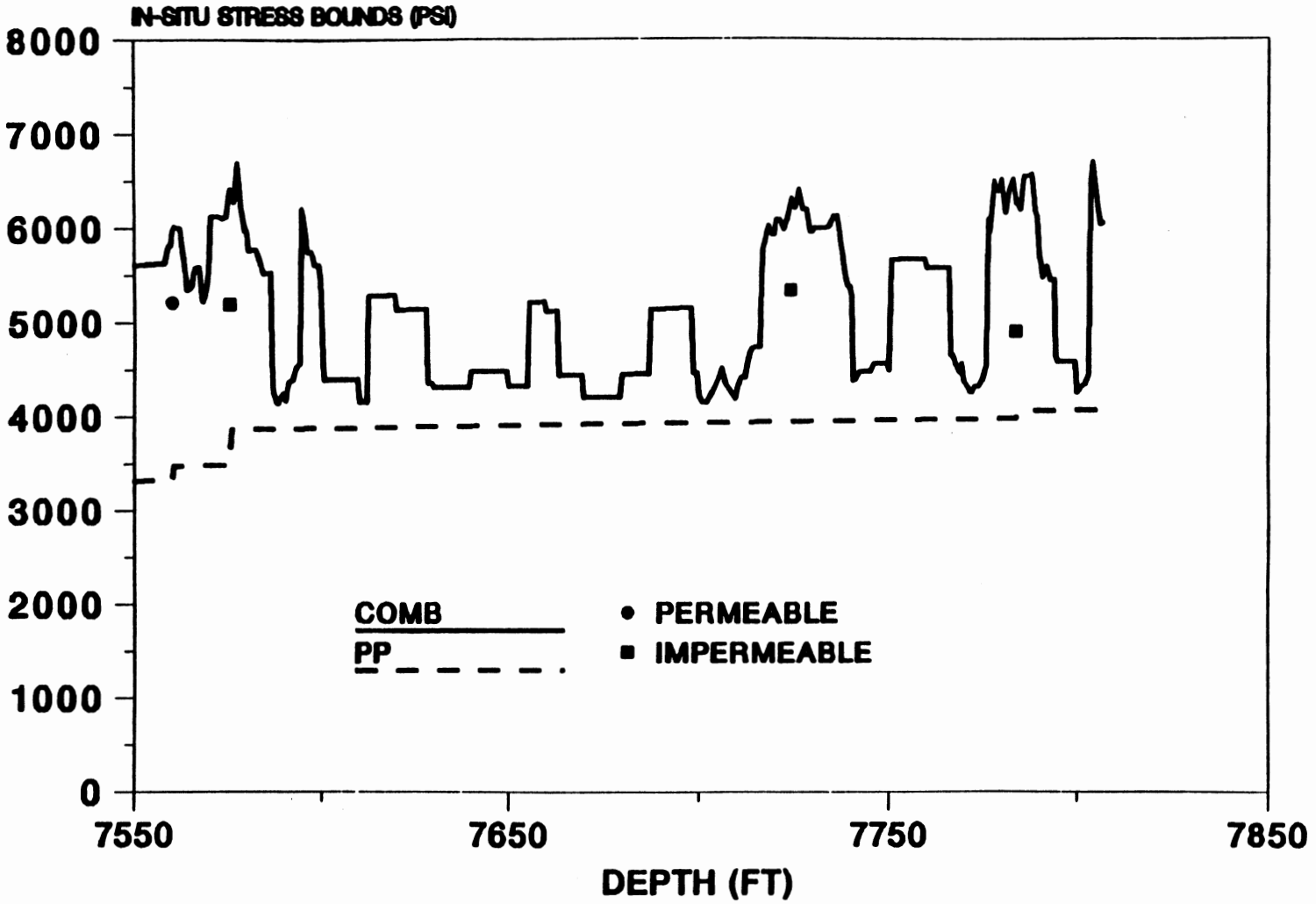

Figure 59. Section of Combined In-Situ Upper Stress Bounds with .01 md Permeability Switch from Electric Logs for SFE #1 (7550 - 7850 Feet)

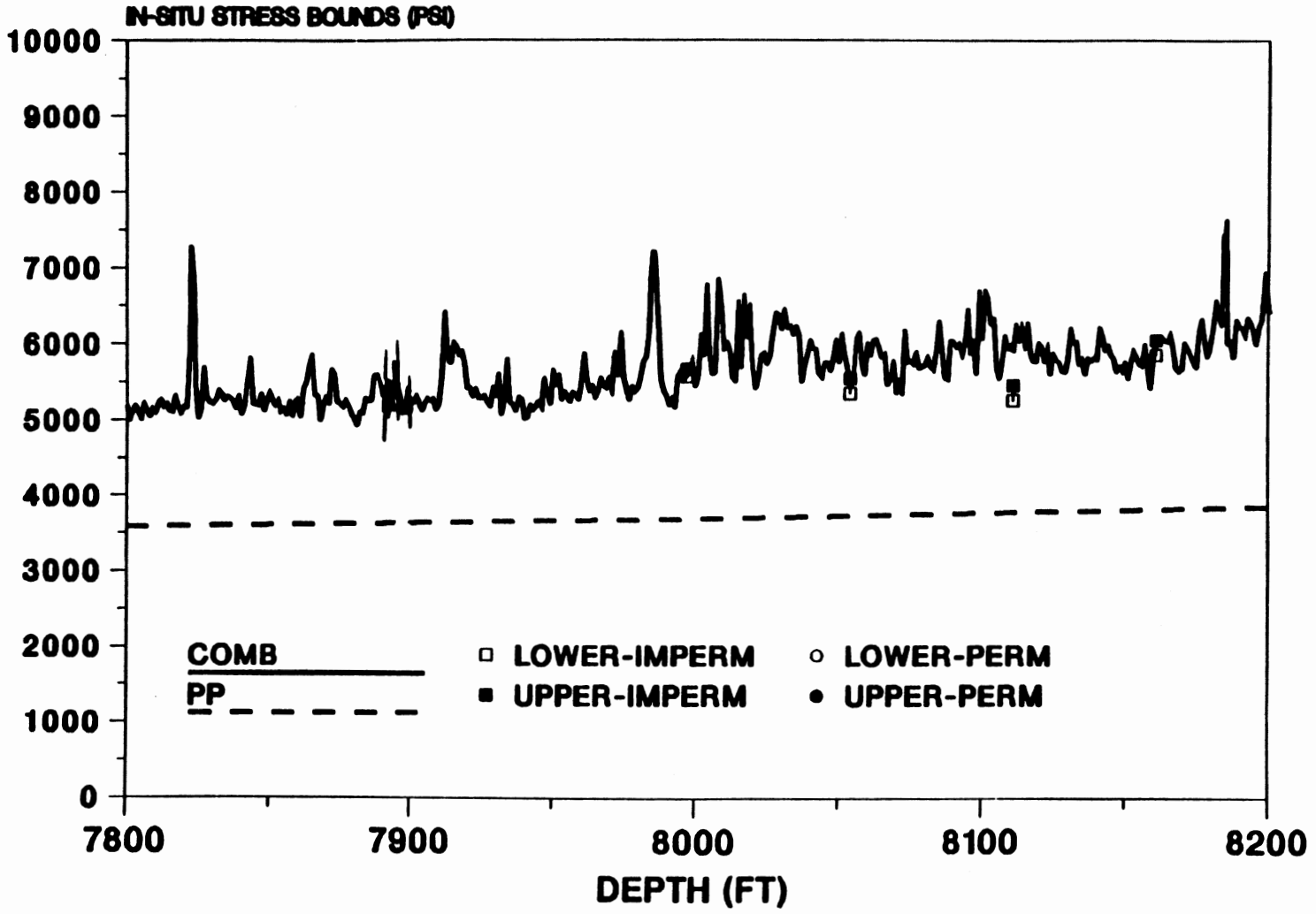

Figure 60. Section of Combined In-Situ Upper Stress Bounds with .01 md Permeability Switch from Electric Logs for SFE #2 (7800 - 8200 Feet)

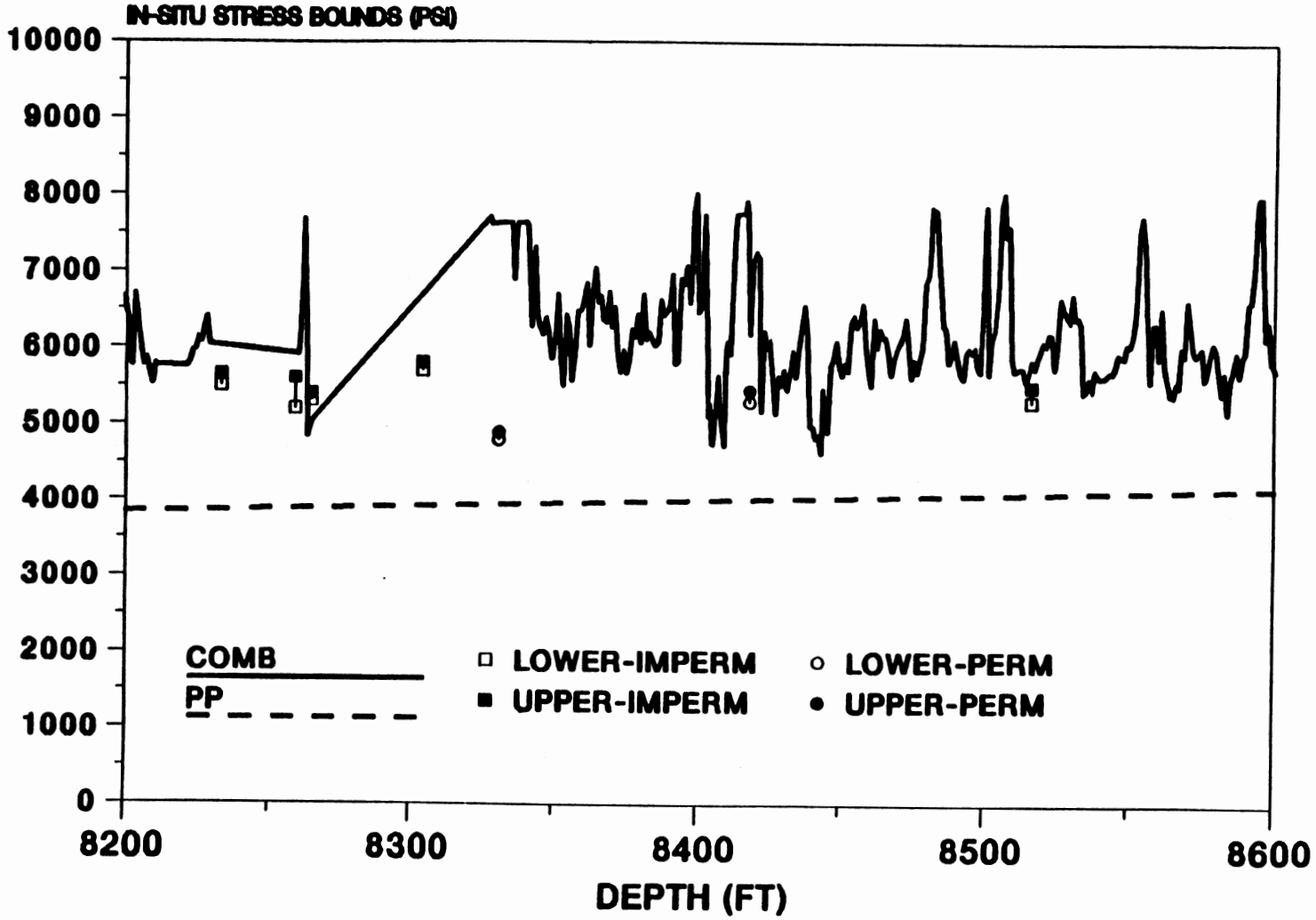

Figure 61. Section of Combined In-Situ Upper Stress Bounds with .01 md Permeability Switch from Electric Logs for SFE #2 (8200 - 8600 Feet)

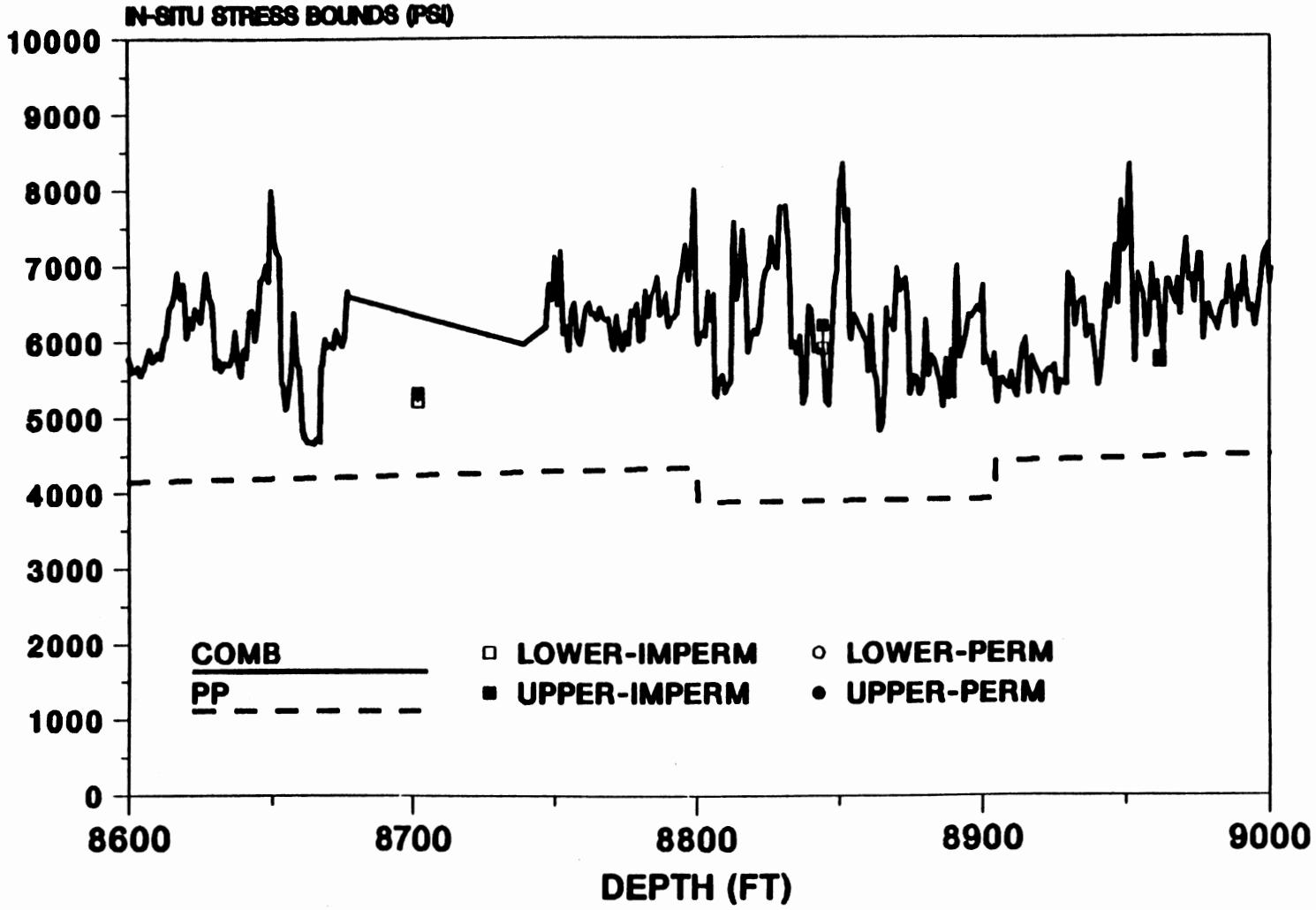

Figure 62. Section of Combined In-Situ Upper Stress Bounds with .01 md Permeability Switch from Electric Logs for SFE #2 (8600 - 9000 Feet)

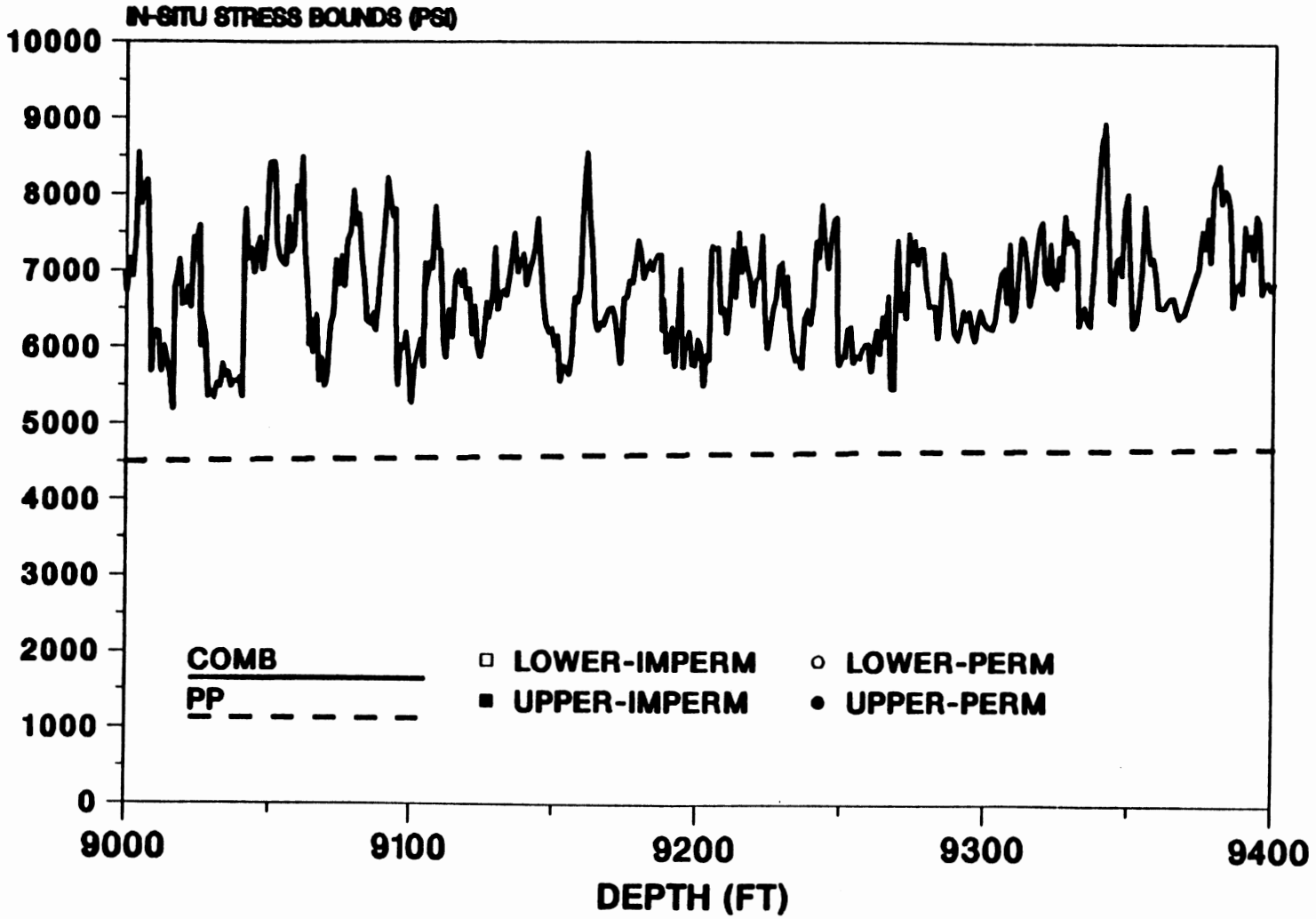

Figure 63. Section of Combined In-Situ Upper Stress Bounds with .01 md Permeability Switch from Electric Logs for SFE #2 (9000 - 9400 Feet)

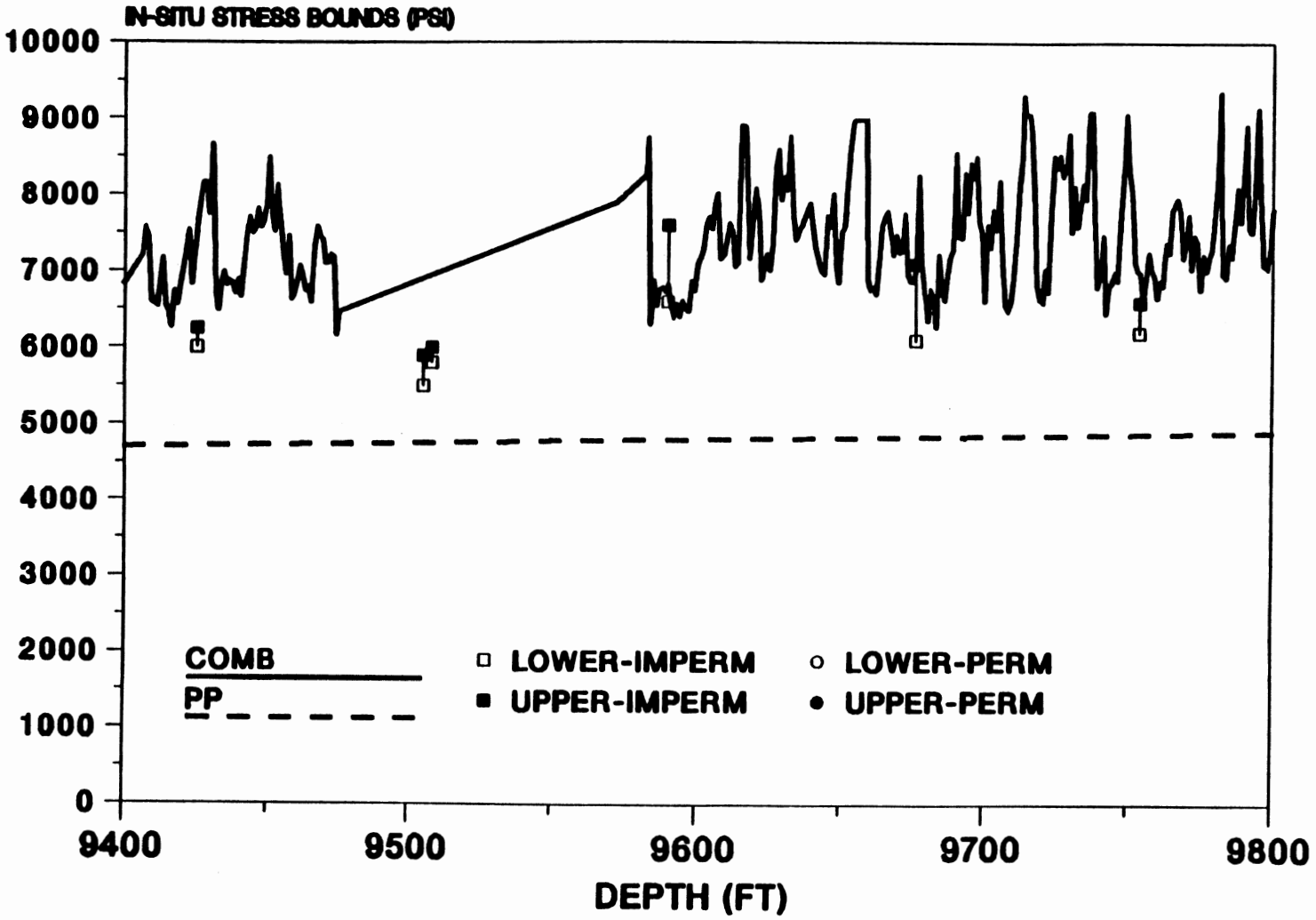

Figure 64. Section of Combined In-Situ Upper Stress Bounds with .01 md Permeability Switch from Electric Logs for SFE #2 (9400 - 9800 Feet)

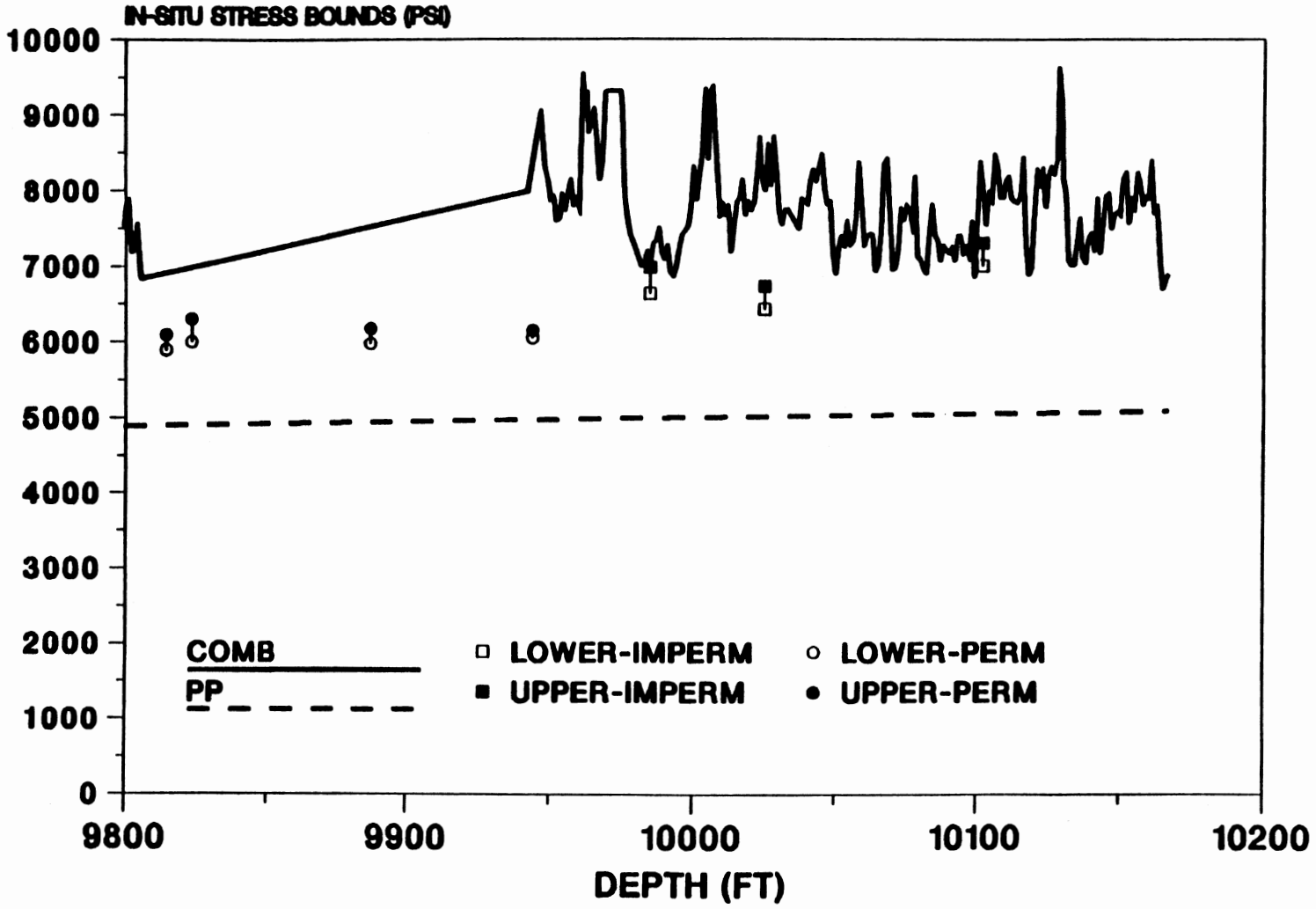

Figure 65. Section of Combined In-Situ Upper Stress Bounds with .01 md Permeability Switch from Electric Logs for SFE #2 (9800 - 10200 Feet)

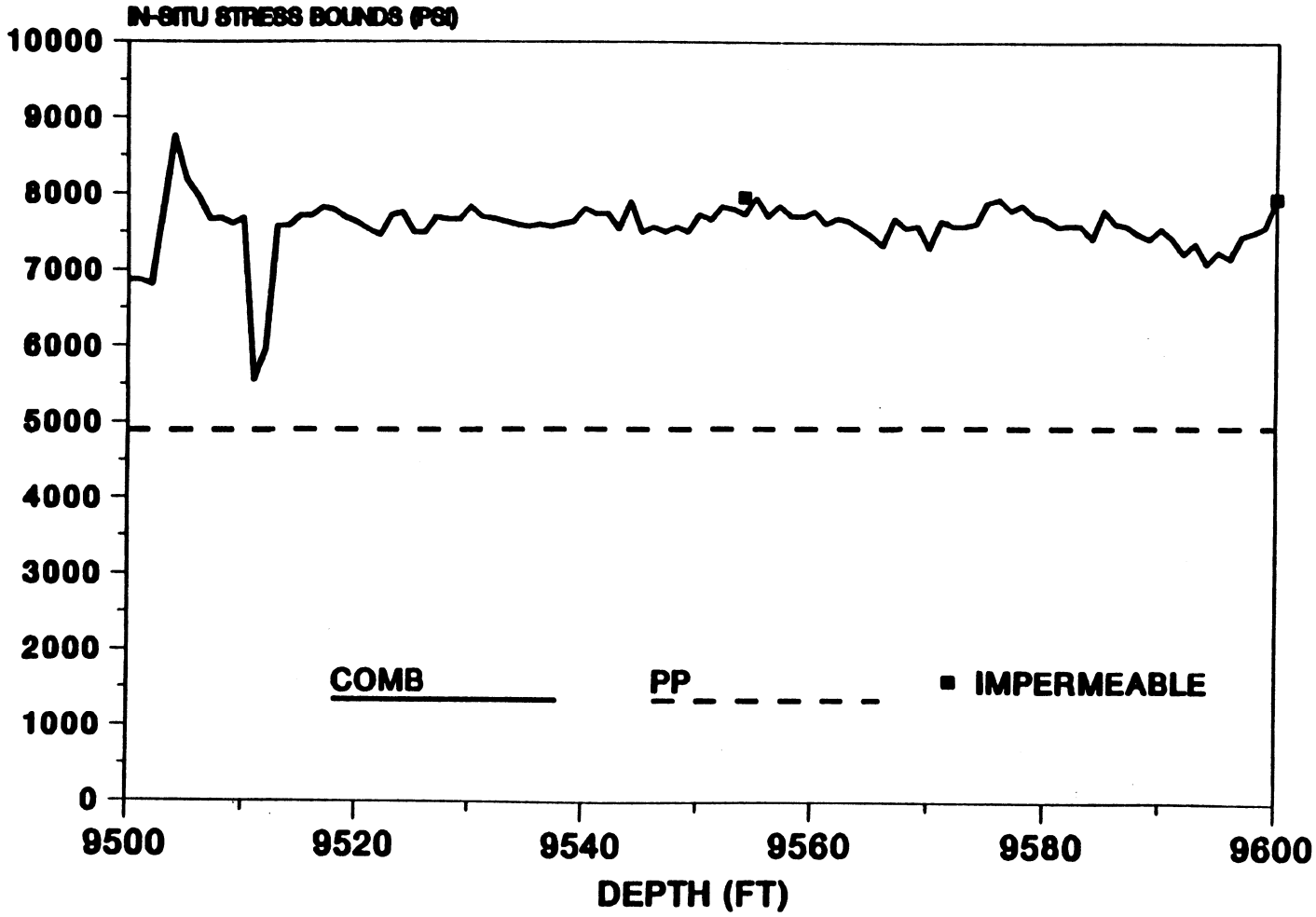

Figure 66. Section of Combined In-Situ Upper Stress Bounds with .01 md Permeability Switch from Electric Logs for SFE #3 (9500 - 9600 Feet)

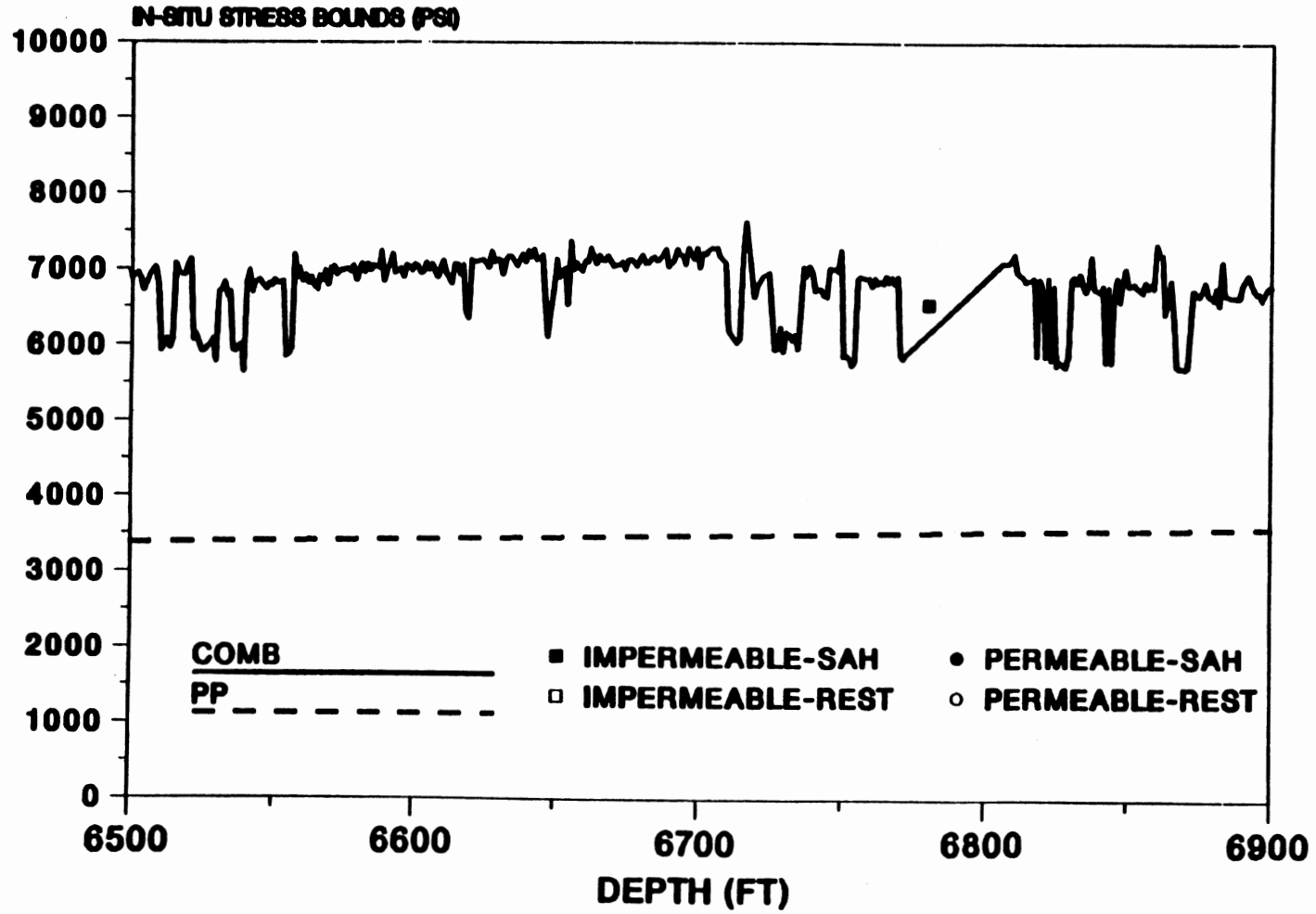

Figure 67. Section of Combined In-Situ Upper Stress Bounds with .01 md Permeability Switch from Electric Logs with T = 1500 psi for SFE #4 (6500 - 6900 Feet)

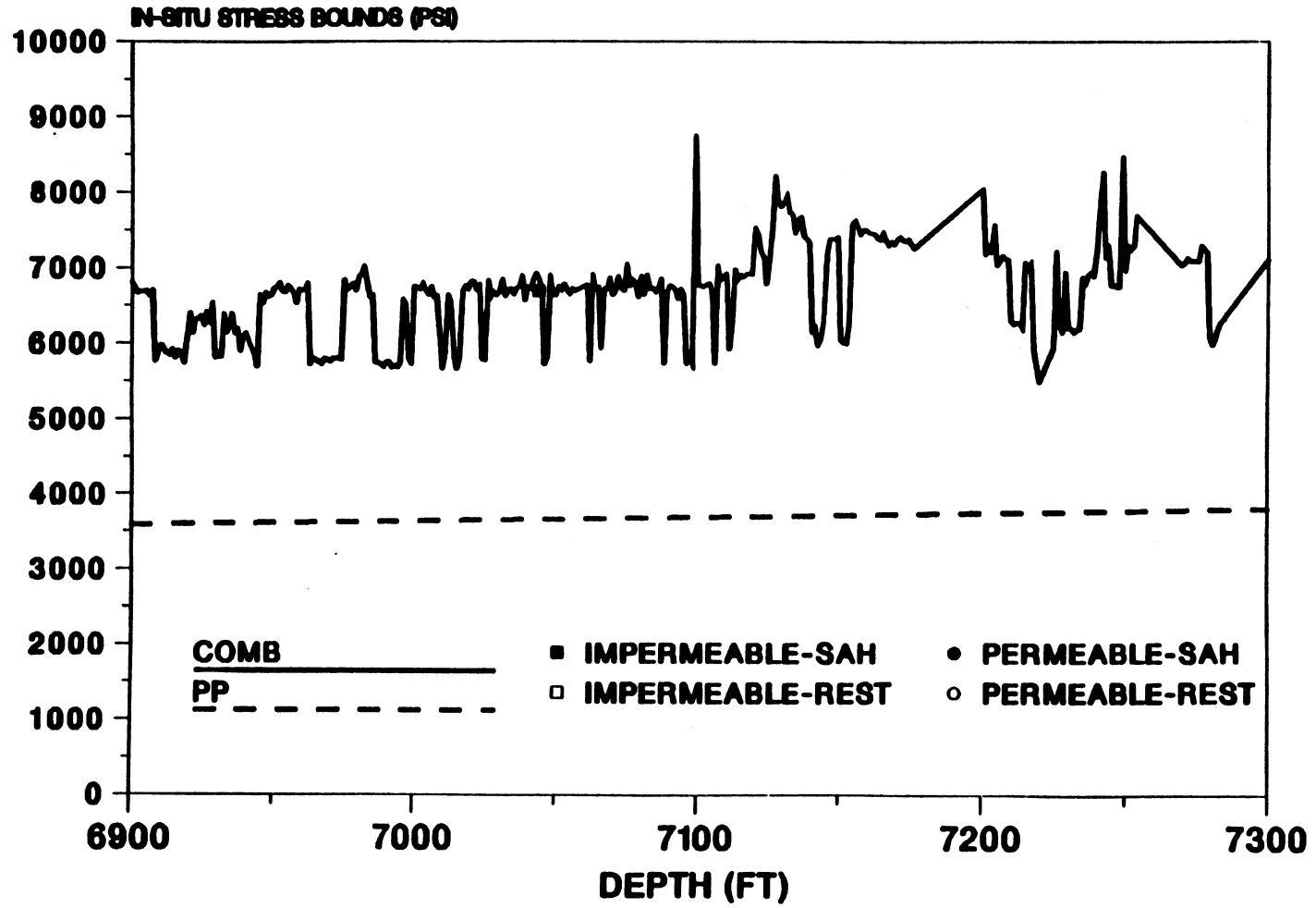

Figure 68. Section of Combined In-Situ Upper Stress Bounds with .01 md Permeability Switch from Electric Logs with T = 1500 psi for SFE #4 (6900 - 7300 Feet)

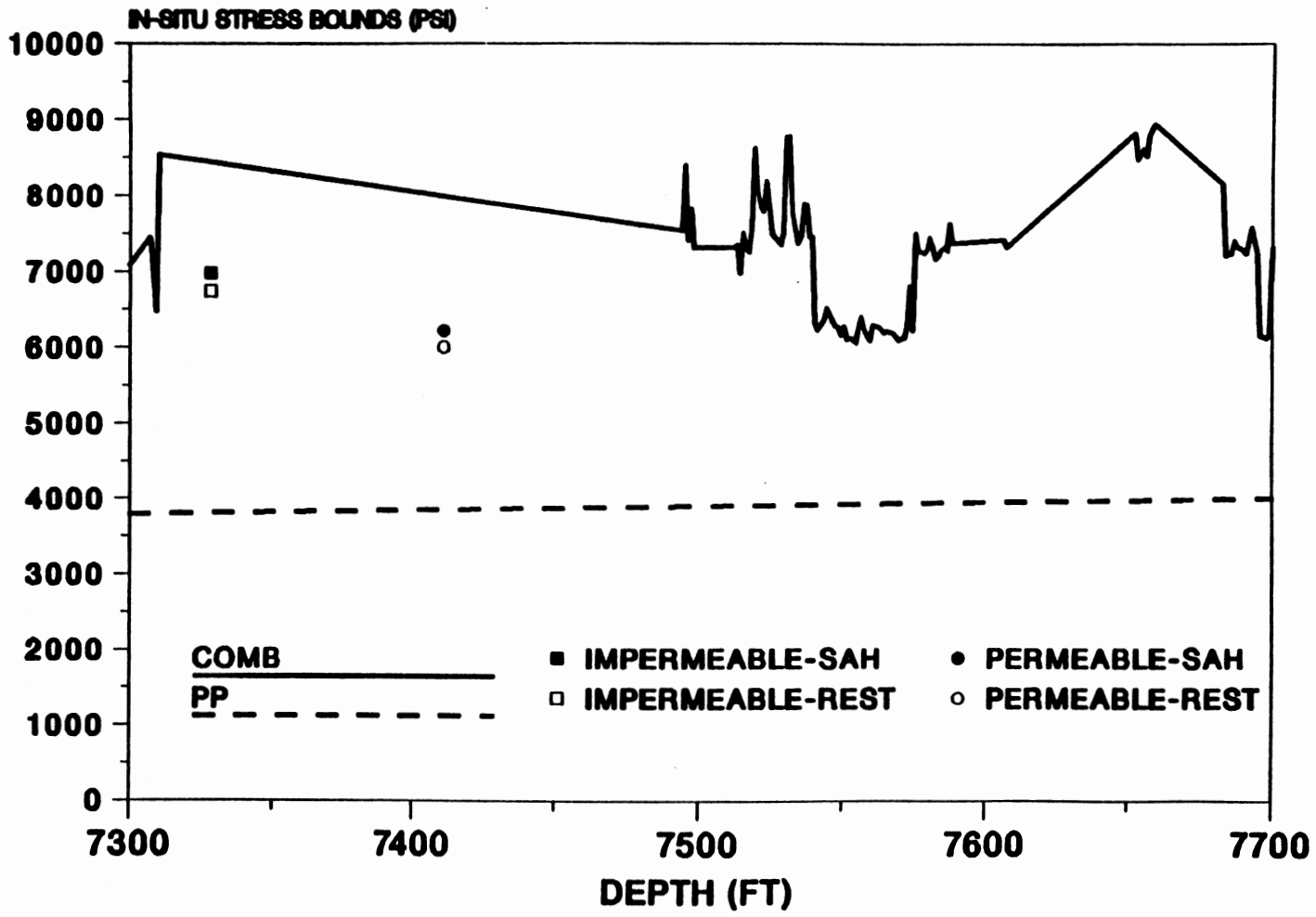

Figure 69. Section of Combined In-Situ Upper Stress Bounds with .01 md Permeability Switch from Electric Logs with T = 1500 psi for SFE #4 (7300 - 7700 Feet)

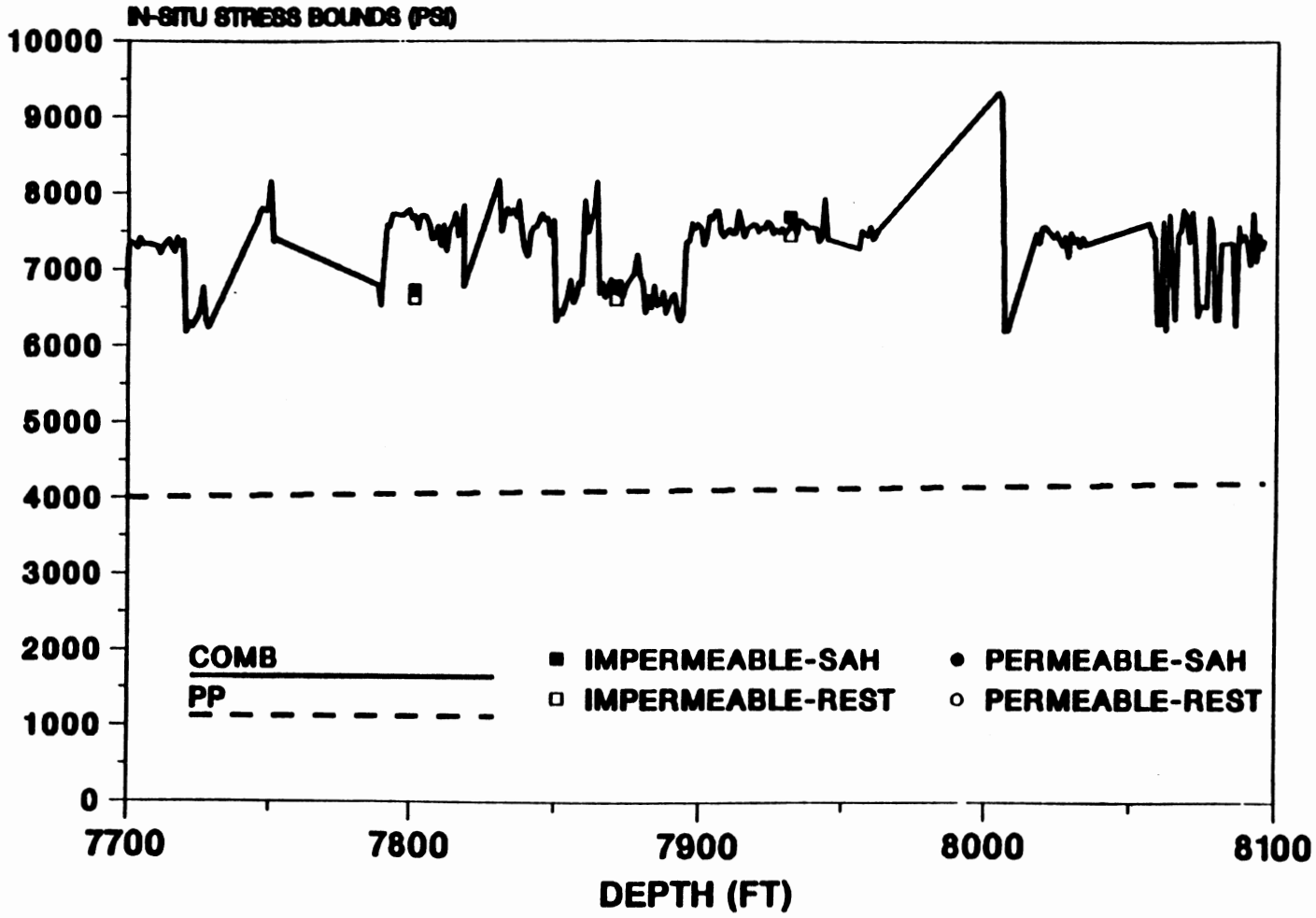

Figure 70. Section of Combined In-Situ Upper Stress Bounds with .01 md Permeability Switch from Electric Logs with T = 1500 psi for SFE #4 (7700 - 8100 Feet)

approach would be to devise a technique to determine permeabilities directly from drill cuttings at the wellsite.

An attempt to improve the electric log approach was made by changing the "impermeability switch" from .01 md to .005 md. This resulted in some stress test values being higher than the resulting upper in-situ stress bound. Accordingly, we recommend that .01 md be used as the "impermeability switch".

Sensitivity Analysis

The sensitivity of the calculated in-situ stress upper bound to variations in the various coefficients was investigated, together with the effect of using a smaller set of laboratory drilling data to obtain the bit coefficients. For the sensitivity analysis for stress bounds, two different sets of operating conditions and bits used on SFE #2 were investigated. The two sets of conditions, one in shale and one in sand, are presented, and detailed results given in Appendix K. The effect of changes from nominal values in coefficients was investigated for bit coefficients, rock strength coefficients, and chip hold down coefficients. It is concluded in Appendix K that reasonably bounded changes in any of these coefficients result in a change in the upper in-situ stress bound of substantially less than 20 percent. Accordingly, we conclude that the procedure presented here for determining bounds on in-situ stress is not unduly sensitive to the values of any coefficient.

An analysis was also performed on the procedure to calculate bit coefficients from laboratory drilling data. For this study, we

employed a subset of the available drilling data to generate bit coefficients, and then tested these coefficients against lab data that was not used to generate the coefficients. Appendix K presents the procedure and results. It can be concluded that using only a part of the drilling data yielded coefficients that produced a good match to the data that was not used to generate the coefficients in all cases but one. For this latter case, it appears that the employed data did not sufficiently span the penetration rate range for the complete data set. It can be concluded that the procedure used to determine the bit coefficients is reasonable, that the penetration rate model is reasonable, and that in general, larger data sets are preferable to smaller sets in determining bit coefficients.

Summary of Steps Needed to Obtain Upper Bounds on Horizontal Fracture Closure Stress

Step 1

Employ The modified Amoco 3-term drilling penetration rate model with foot-by foot drilling data to obtain drilling rock strength, S, versus depth, Equation(7).

Step 2

Obtain lithology description versus depth from the mudlogger data.

Step 3

From the laboratory-determined, lithology dependent correlations of rock strength with drilled rock confining pressure, use S from Step 1 to find unconfined rock strength, S_0 using Equation (8a). This calculation will be a strong function of the assumed or known permeability of the drilled rock.

Step 4

From Step 3, lithology dependent permeable and impermeable rock strengths, S_p and S_i may now be written as functions of in-situ confining pressure. (using Equations (9a) and (9b)).

Step 5

Using Step 4, construct Mohr failure envelopes for both the permeable and impermeable cases for each foot drilled. Confining pressure will be a parameter on each failure envelope curve. This envelope gives the stress state of rock at failure. Hence, it is an upper bound on in-situ rock stress.

Step 6

Assume a starting value for in-situ rock confining pressure. We use 0.65 (psi/ft)depth minus pore pressure (assumed known). Enter the failure envelope and determine the corresponding angle of

internal friction, β, of the rock at failure. This is done by applying Equation (11)

Step 7

From soil mechanics literature, calculate coefficient K_0. This is done by applying Equation (14) for sandstone (used when the lithology is more than 80 percent sandstone) and Equation (15) for all other lithologies.

Step 8

Using known overburden stress, S_{oB}, and pore pressure, P_p calculate a trial value for the upper bound on horizontal stress for both the permeable and impermeable cases as follows:

For the permeable case:

$$S_{pu} - P_p = K_{p0}(S_{oB} - P_p) \tag{29a}$$

For the impermeable case

$$S_{iu} - P_p = K_{i0}(S_{oB} - P_p) \tag{29b}$$

where the permeable and impermeable case uses different values for K_0 because each case has it own failure envelope, and therefore different angles of internal friction.

Step 9

Use the left sides of Equation (29a) and (29b) as a second guess for the true in-situ confining pressure, and repeat Steps 7 and 8 for both cases. Iterate until K_0 converges. S_{pu} and S_{iu} are then determined.

Step 10

Repeat steps 3-9 for each foot drilled depth and plot both permeable and impermeable horizontal stress bounds versus depth.

Step 11

Combine the two upper bounds into a single upper bound by using the permeable bound for intervals with more than 90 % sand, and using the impermeable bound otherwise. If permeability information is available from electric logs, combine the two bounds by using the permeable bound for intervals having more than .01 md permeability, and using the impermeable bound otherwise.

CHAPTER IV

CONCLUSIONS

1. A method for obtaining in-situ stress profile bounds from drilling data has been proposed and validated. The method uses a modified tricone bit drilling model to predict rock strengths, together with Mohr circles and equations for the coefficient of earth at rest to obtain bounds on the in-situ rock stress.
2. Bit coefficients and chip hold-down functions for the drilling model have been obtained from available laboratory data, for a limited number of bits and lithologies.
3. All data necessary to test the proposed procedure was collected, edited, and organized from SFE wells 1, 2, 3 and 4.
4. Both confined and unconfined rock strengths were predicted from the drilling model.
5. In-situ stress bounds were obtained from calculated rock strengths using Mohr circles and failure envelopes, together with published relationships for the "coefficient of earth at rest".
6. The predicted in-situ stress bounds were compared to data from actual stress tests performed on the four SFE wells. The calculated "upper" in-situ stress bound agrees well with the

stress test data for SFE #1-3. The closure pressures from stress tests performed in impermeable formations lie close to or on the impermeable upper bound. The closure pressures obtained in the permeable formations lie below the permeable upper stress bound.

7. The "impermeable" upper bound on in-situ stress serves as an upper bound for all rock, whether permeable or impermeable. Pore pressure is a lower bound.
8. Almost all impermeable rock in SFE #1-3 appears to be at or close to failure.
9. Upper bounds for in-situ stress on SFE #4 could be calculated only if an additional additive constant representing tectonic effects is included in the calculations. For SFE #4, this constant was 1500 psi.
10. The combined upper bound seems to be a reasonable approach to obtain a single upper bound profile on in-situ stress, and agrees well with the stress test data. If electric logs are available, .01 md can be used as a switch between the permeable and impermeable bounds. Otherwise mudlogger data can be used, with 90 % sandstone as the switch.
11. Sensitivity analysis of the empirically developed coefficients used in this study indicate that a +/- 20 percent change in most coefficients yields less than 20 percent change in the calculated in-situ stress bounds. Accordingly, the procedure is not unduly sensitive to variations in the various coefficients used.

CHAPTER V

RECOMMENDATIONS FOR FUTURE WORK

1. Develop and model the differential pressure effect more accurately than in the proposed approach. This would involve including the effects of fluid viscosity, mud solids content and type, pore fluid compressibility, rock permeability, mud spurt loss, and rate of penetration.
2. Conduct full scale laboratory drilling experiments on a suitable variety of homogeneous rock using various differential pressures to obtain chip hold-down function coefficients for various lithologies. Determine whether one function for permeable rock and another for impermeable rock can be used to adequately model all rock.
3. Conduct full scale laboratory drilling experiments on inhomogeneous rock to determine the accuracy of the "mixing" approach used herein, Equations (24a) and (24b).
4. Conduct suitable full-scale laboratory drilling experiments to determine bit coefficients for all potential tricone bits used to drill gas wells planned for hydraulic fracturing. Expand and update Table 6.
5. Evaluate current models with more drilling data and in-situ stress data. The MWX (Multi Well Experiments) wells could be

used because of the large amount of stress tests that were conducted. Other possibilities include data from SFE #4, GRI co-op wells, and GRI hydraulic fracture test site wells.

6. Investigate in-situ stress bound calculations in mountain areas. This will involve modeling of the tectonic stresses.
7. Evaluate whether the tricone bit model together with either a drilling torque model or other log-derived data can be used to predict pore pressure from drilling data.
8 Determine whether bit performance tests can be used for predicting the wear state of the bit and give bit life predictions. This will involve integrating a wear model into the tricone penetration rate model.
9. Evaluate the use of existing torque models for predictions of rock strength.
10. Evaluate and investigate a wear model for integration into the tricone bit model.
11. Evaluate and investigate possible drag bit models for use in predicting drilling rock strength and in-situ closure stress.

REFERENCES

1. Warren, T. M. and Sinor, L. A., "Drag Bit Performance Modeling", SPE 15618, 1986 SPE Annual Technical Conference, New Orleans, LA Oct. 5-8, 1986. SPE Drilling Engineering, May 1989.

2. Winters, W. J. and Warren, T. M., "Determining the True Weight-On-Bit for Diamond Bits", SPE Drilling Engineering, vol. 1, No. 4, August 1986.

3. Personal communication, Willie Iyoho, Willie Iyoho Technologies, Inc., Tulsa, OK, March 19, 1989.

4. Gnirk, P. F. and Cheatham, J. B., "A Theoretical Description of Rotary Drilling for Idealized Down-Hole Bit/Rock Conditions," SPEJ (December 1969) 443-450.

5. Eronini, E. I., "Rotary Drill Bit/Rock Model with Cutter Offset," Journal of Energy Resources Technology (September 1983) 356-361.

6. Ma, D. and Azar, J. J., "Dynamics of Roller Cone Bits," Journal of Energy Resources Technology (December 1985) 543-548.

7. Walker, B. H., et. al., "Roller Bit Penetration Rate Response as a Function of Rock Properties and Well Depth," SPE 15620, presented at the 61st Annual Fall Technical Conference, New Orleans, Louisiana, October 5-8, 1986.

8. Warren, T. M., "Drilling Model for Soft Formation Bits," JPT (December 1981) 963-970.

9. Warren, T. M. and Winters, W. J., "The Effect of Nozzle Diameter on Jet Impact for a Tricone Bit," SPEJ (February 1984) 9-18.

10. Warren, T. M., "Factors Affecting Torque for a Roller Cone Bit," JPT (September 1984) 1500-1508.

11. Warren, T. M. and Smith, M. B., "Bottomhole Stress Factors Affecting Drilling Rate at Depth," JPT (August 1985) 1523-1533.

12. Warren, T. M., "Penetration Rate Performance of Roller Cone Bits," SPE Drilling Engineering (March 1987) 9-18.

13. Winters, W. J., Warren, T. M., and Onyia, E. C., "Roller Bit Model With Rock Ductility and Cone Offset," SPE 16696, 1987 SPE Annual Technical Conference, Dallas, TX Sept. 27-30, 1987.

14. Onyia, E. C., "Geology Drilling Log (GDL): A Computer Database System for Drilling Simulation," SPE 13113, 1984 SPE Annual Technical Conference, Houston, TX, Sept. 16-19, 1984.

15. Onyia, E. C., "Relationships Between Formation Strength, Drilling Strength, and Electric Log Properties," SPE 18166, 1988 SPE Annual Technical Conference, Houston, TX Oct. 2-5, 1988.

16. Closmann, P. J. and Bradley W. B.,"Effect of Temperature on Tensile and Compressive Strengths and Young's Modulus of Oil Shale" SPE paper 6734, presented at SPE-AIME 52nd Annual Fall Technical Conference and Exhibition, Denver, Oct 9-12, 1977.

17. Darley, H. C., "Designing Fast Drilling Fluids", JPT, April 1965, 465-470.

18. Cheatham, J. B., "Tooth Penetration Into Dry Rock at Confining Pressures of 0 to 5000 psi", Texas Conference on Drilling and Rock Mechanics, Austin Texas, Jan. 20-21,1965.

19. SAS/STAT Language, First Edition (Statistical Analysis System Package) SAS Institute Inc., Cary, NC, USA, February 1990

20. Warren, T. M., Amoco Production Company, Tulsa, OK - Personal Communication, April 3, 1989.

21. Carmichael, R. S., e.d. (University of Iowa), Handbook of Physical Properties of Rock", Volume II, CRC Press, Boca Raton, Florida (1982).

22. Wuerker, R.G., "Annotated Tables of Strength and Elastic Properties of Rock", AIME paper 663-G (1956)

23. Daines, S. P., "Prediction Of Fracture Pressures for Wildcat Wells", JPT April 1982, p 863-872.

24. Holditch, S.A. and Associates, "Application of Advanced Geological Petrophysical and Engineering Technologies to Evaluate and Improve Gas Recovery from Low Permeability Sandstone Reservoirs", Vol. 1, GRI report 89/0140, June 1989.

25. Cheatham, J. B. Jr., and Gnirk, P. F., "Review of the Fundamental Aspects of Rock Deformation and Failure," Rock Mechanics in Oilfield Geology Drilling and Production, 1966, 3-26.

26. Massarsh, K. R., "New Method for Measurement of Lateral Earth Pressure in Cohesive Soils", Can. Geotech. J. Vol. 12, 1975, p142-146.

27. Jaky, J., "Talajmeckanika"("Soil Mechanics" in Hungarian), Budapest, 1944.

28. Fraser, A. M. "The Influence of Stress Ratio on Compressibility and Pore Pressure in Compacted Soils", Phd Thesis, London .U. 1957.

29. Kezdi, A., "Erddrucktheorien" ("Theories of Earth Pressure" in German), Springer Verlag, Berlin, 1962.

30. Brooker, E. W. and Ireland, H. O.,"Earth Pressures at Rest Related to Stress History", Canadian Geotech. J. , Vol. II, No.1(1-15), 1965.

31. Hubbert, K. M. and Willis, D. G., Mechanics Of Hydraulic Fracturing", AIME paper 686-G(1957).

32 Alkpan, I., "The Empirical Evaluation of the Coefficient Ko and Kor", Soil Mechanics , Vol VII, No. 1(31-40), 1967.

33. Howard G. C. and Fast C. R. "Hydraulic Fracturing" Monograph Vol. 2 of The H. L. Doherty Series SPE of AIME, New York 1970.

34. Fainthurst, C., "Measurement of In-Situ Rock Stresses, with Particular Reference to Hydraulic Fracturing," Rock Mech. Eng. Geol. (1964) 2,129.

35. Eaton, B. A., "Fracture Gradient Prediction and Its Application in Oilfield Operations," SPE 2163, 1968 SPE Annual Fall Meeting, Houston, TX, Sept. 29-Oct. 2, 1968.

36. Cheatham, J. B, Rice University, Houston, TX, Personal Communication, December, 1989.

37. Hubbert, M. King, "Mechanical Basis for Certain Familiar Geologic Structures," Bull. GSA (1951), 62, 355.

38. Kirsh, G, "Die Theorie der Elastizitat und die Bedurfnisse der Festigkeitslehre" Zeirschr. des Vereines Deutscher Ingenieure (1898) XLII, No. 29, 797.

39. Timoshenko, S., "Strength of Materials, 2nd ed., D. van Nostrand Co., Inc, New York (1941) Part I, 281-305; Part II, 474-476, 480.

40. Voight, B., "Stress History and Rock Stress", Proc; Third Intl. Congress of Soc. for Rock Mechanics (1974) 2. Part a, 580-582.

41. Prats, M., "Effect of Burial History on the Subsurface Horizontal Stresses of Formations Having Different Material Properties" SPEJ (Dec 1981) 658-62.

42. Warpiniski, N. R. and Teufel, L.W., "In-Situ Stresses in Low Permeability, Nonmarine Rocks" JPT April, 1989, p 405.

43. Warpiniski, N. R. and Teufel, L.W., "A Viscoelastic Constructive Model for Determining In-Situ Stress Magnitudes from Anelastic Strain Recovery of Core", paper SPE 8954 presented at the 1986 SPE Annual Technical Conference and Exhibition, New Orleans, Oct 5-8.

44. Gidley, J. L., Holditch, S. A., Nierode, D. E., and Veatch Jr., R. W., "Recent Advances in Hydraulic Fracturing", Chapter 3 by Warpinski et al,SPE Monograph Vol. 12, Henry L. Doherty Series, Chapter 3, p 59, 1989.

45. Hunt, E. E., E. Hunt and Associates, Houston, TX, Personal Communication, January, 1991.

46. Bourgoyne, Jr. A.T., Milleheim, K. K., Chenevert, M.E and Young, F. S., "Applied Drilling Engineering", Chapter 4, SPE Textbook Series, Vol. 2, SPE, Richardson, TX, 1986.

47. Moschovidis, Z, Amoco Production Company, Tulsa, OK, Personal Communication, July, 1991.

APPENDIXES

APPENDIX A

DEMONSTRATION THAT THE IMPERMABLE ROCK ASSUMPTION GIVES AN UPPER IN-SITU STRESS BOUND FOR ALL ROCK

This appendix shows that the impermeable or non penetrating calculated rock strength gives an upper in-situ stress bound for all rock, whether permeable or impermeable. Consider the following equations from the text:

$$\frac{S}{S_0} = 1.0 + a_s P_e^{b_s} \qquad \text{(A0) or (8a)}$$

$$F_c(P_e) = c_c + a_c(P_e - 120)^{b_c} \qquad \text{(A1) or (5)}$$

$$S = \left[\frac{NW^2}{aF_c(P_e)RD^3} - \frac{bW^2}{aD^4} - \frac{c\rho\mu NW^2}{aF_c(P_e)I_mD^2}\right]^{.5} \qquad \text{(A2) or (7)}$$

$$\sin(\beta) = \frac{S_{(P_e+\Delta)} - S_{(P_e-\Delta)}}{S_{(P_e+\Delta)} - S_{(P_e-\Delta)} + 4\Delta} \qquad \text{(A3) or (B9)}$$

$$K_0 = 1.0 - \sin(\beta) \qquad \text{(A4) or (14)}$$

$$S_h = (S_{ovb} - P_p)K_0 - P_p \qquad \text{(A5) or(20)}$$

Now by inspection, it can be seen from (A2) that with all other quantities fixed, S has its minimum value S_{min} when $F_c(P_e)$ is maximum. From (A1) we see that $F_c(P_e)$ achieves it's maximum value F_{max} when P_e is maximum at P_{max}, which will occur when the drilled rock is impermeable, hence we have:

$$S_{min} = \frac{W}{D}\left[\frac{N}{aF_{max}D} - \frac{b}{aD^2} - \frac{c\rho\mu N}{aF_{max}I_m}\right]^{0.5} \qquad \text{(A6)}$$

where

$$F_{max} = F_c(P_{max}) = c_c + a_c(P_{max} - 120)^{b_0} \qquad (A7)$$

Now solve (A0) for S_0 , using S_{min} for S from (A6):

$$S_0 = \frac{S_{min}}{1.0 + a_s P_{max}^{b_s}} \qquad (A8)$$

Substitute the right side of (A6) for S_{min} in (A8) yields:

$$S_0 = \left(\frac{1.0}{1.0 + a_s P_{max}^{b_s}}\right) \frac{W}{D} \left(\frac{N}{aF_{max}D} \frac{b}{aD^2} - \frac{c\rho\mu N}{aF_{max}I_m}\right)^{.5} \qquad (A9)$$

Now by inspection of (A9) and (A7), it can be seen that S_0 archives its minimum value S_{0min} when $P_e = P_{max}$, or when the rock is impermeable. Now consider (A0) with the confining pressure equal to the in-situ confining pressure (rather than the drilled rock confining pressure) and the unconfined rock strength given by (A9). The in-situ confining pressure from (12):

$$P_{e\text{-}is} = S_h - P_p \qquad (A10)$$

where P_{e-is} is the in-situ pressure, S_h is the horizontal stress upper bound, and P_p the pore pressure. Because the horizontal stress bound in (A10) is initially unknown, we use an initial guess for it of 0.65 psi/ft times depth. Then knowing pore pressure, we calculate a

first trial value of P_{e-is} from (A10), and substitute into (A0) which gives:

$$S = S_{0\text{-}min}(1.0 + a_s P_{e\text{-}is}{}^{b_s}) \qquad (A11)$$

Now calculate values for S from (A11) for two pressures, $P_{e-is\,+\,\Delta}$ and $P_{e-is\,-\,\Delta}$, where Δ is an arbitrary small pressure. Then by substituting from (A11), the angle of internal friction, given by (A3), may be written as:

$$\beta = \arcsin\left(\frac{1.0}{1.0 + \dfrac{4\Delta}{S_{0\text{-}min} a_s (P_{in\text{-}s\,+\,\Delta}{}^{b_s} - P_{in\text{-}s\,-\,\Delta}{}^{b_s})}}\right) \qquad (A12)$$

It can now be seen that since S_{0-min} is the minimum value for S_0, β in (A12) will be the minimum value for the angle of internal friction, other quantities being fixed. Accordingly, (A4) shows that for the impermeable case, the coefficient for earth at rest, K_0, is maximum. Finally, (A5) can be solved for the horizontal stress bound, which will be maximum, since K_0 is maximum.

The horizontal stress bound calculated from (A5) is then used in (A10), and the procedure to calculate the horizontal stress bound is iterated until the horizontal stress bound from (A5) changes little from the previous iteration. It was determined that for all cases of interest only 4 iterations were needed to obtain a change of less than 1 psi between the last two iterations. A graphic illustration of the iterative process is given in Figure 71. We conclude that under the assumption convergence occurs in this process, the impermeable rock

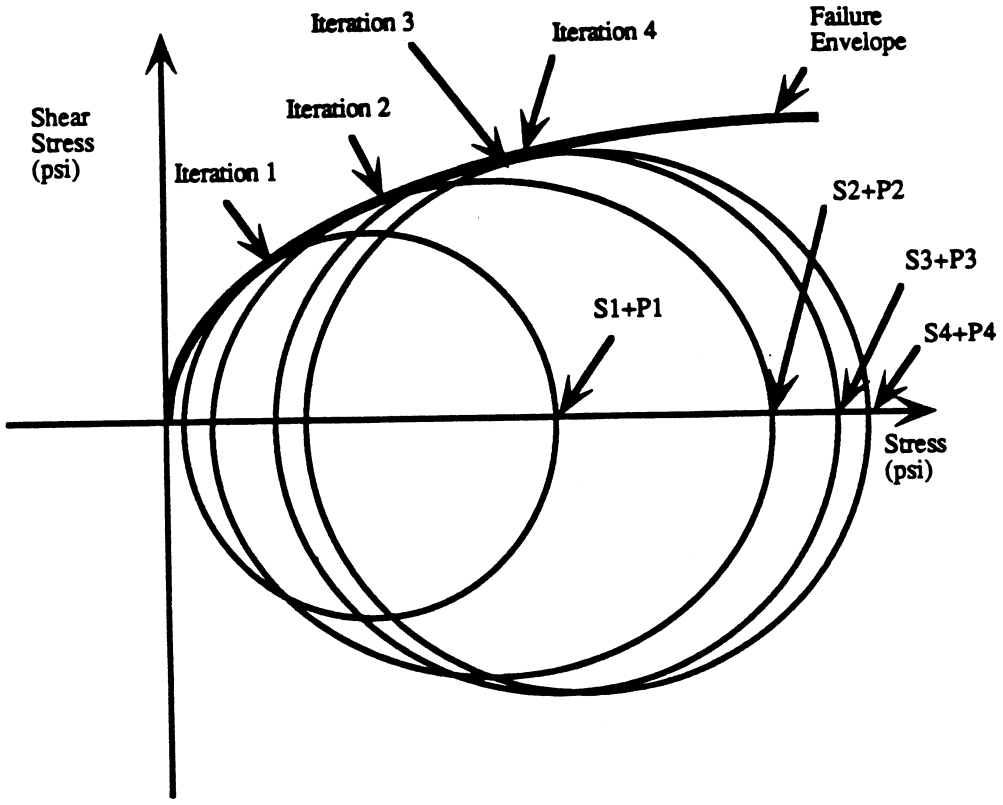

Figure 71. Graphic Illustration of Iterative Process on Failure Envelope to Obtain an In-Situ Horizontal Stress Bound

assumption yields an upper bound for in-situ stress for all rock, whether permeable or impermeable.

APPENDIX B

MATHEMATICAL SOLUTION FOR ANGLE OF INTERNAL FRICTION FROM TWO MOHR CIRCLES

This section show how the angle of internal friction, β, is obtained from the Mohr's failure envelope. Figure 72 shows that β is obtained by the use of similar triangle equalities. The two circles in the figure are Mohr circles at two different confining pressures. These two circles are obtained by using the equation for rock strength (8a) given by:

$$\frac{S}{S_0} = 1 + a_s P_e^{b_s} \tag{B0}$$

The tangent to the failure envelope where the Mohr circle touches the envelope defines the angle of internal friction as shown; A relationship for β. is obtained using two Mohr circles taken at two different pressures $P_e+\Delta$ and $P_e-\Delta$ where Δ is an arbitrarily small pressure. By using similar triangles, it is observed in Figure 72 that:

$$\frac{r_1}{r_2} = \frac{l_1}{l_2} \tag{B1}$$

and

$$l_2 = l_1 + (x_{c1} - x_{c2}) \tag{B2}$$

Now using (B2) in (B1) and solving for l_1 gives:

$$l_1 = \frac{r_1(x_{c1} + x_{c2})}{r_2 - r_1} \tag{B3}$$

It can be seen from Figure 46 that

$$\sin(\beta) = \frac{r_1}{l_1} = \frac{r_2 - r_1}{x_{c2} - x_{c1}} \tag{B4}$$

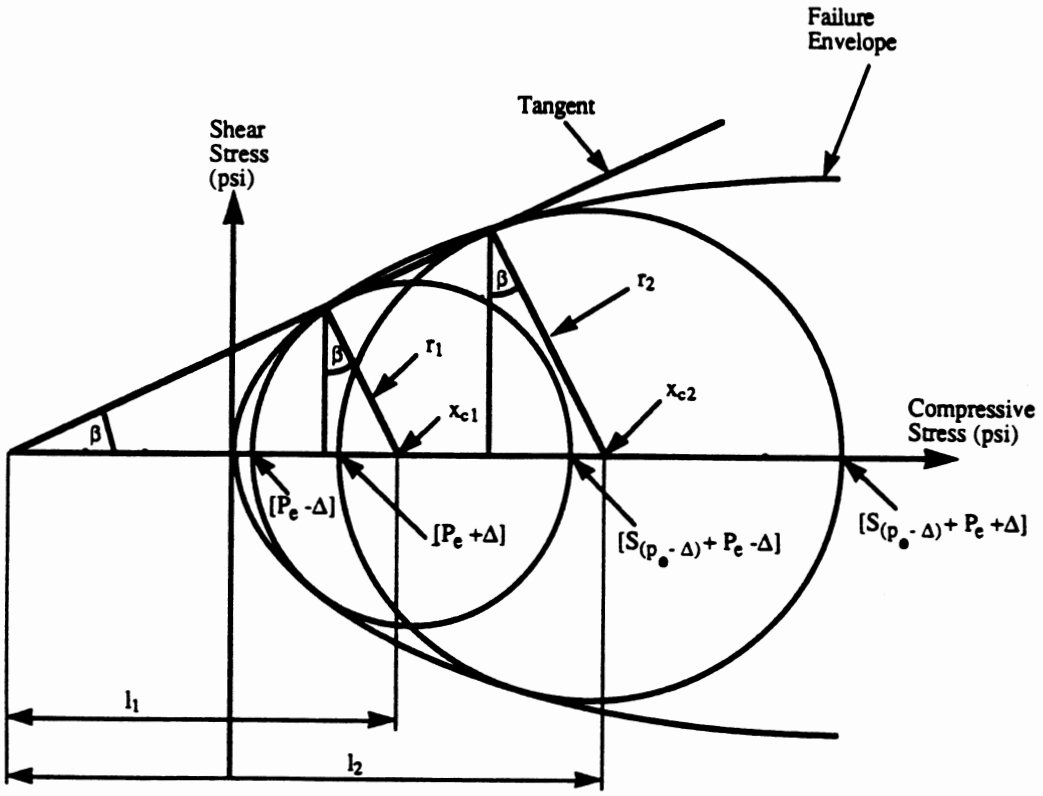

Figure 72. Angle of Internal Friction Obtained From Two Mohr Circles

Now, these geometric variables can be expressed as in terms of S from (B0) as:

$$r_1 = \frac{[S_{(P_e - \Delta)} + P_e - \Delta] - [P_e - \Delta]}{2} = \frac{S_{(P_e - \Delta)}}{2} \tag{B5}$$

$$r_2 = \frac{[S_{(P_e + \Delta)} + P_e + \Delta] - [P_e + \Delta]}{2} = \frac{S_{(P_e + \Delta)}}{2} \tag{B6}$$

$$x_{c2} = \frac{[S_{(P_e + \Delta)} + P_e + \Delta] + [P_e + \Delta]}{2} = \frac{S_{(P_e + \Delta)} + 2P_e + 2\Delta}{2} \tag{B7}$$

$$x_{c1} = \frac{[S_{(P_e - \Delta)} + P_e - \Delta] + [P_e - \Delta]}{2} = \frac{S_{(P_e + \Delta)} + 2P_e - 2\Delta}{2} \tag{B8}$$

Substituting the right sides of (B5)-(B8) in (B4) gives:

$$\sin(\beta) = \frac{S_{(P_e + \Delta)} - S_{(P_e - \Delta)}}{S_{(P_e + \Delta)} - S_{(P_e - \Delta)} + 4\Delta} \tag{B9}$$

The value for Δ used in this project was selected to be 50 psi.

APPENDIX C

SAS PROGRAM FOR DETERMINATION OF BIT COEFFICIENTS

```
CMS FILEDEF IN1 DISK 437 S82F A;
DATA INPUT2;
INFILE IN1 FIRSTOBS=05 LRECL=80;
INPUT OBS LITH GPM GPM1 PP BHP T RPM WOB TO TO1 ROP;
*INPUT WOB RPM GPM ROP BHP LITH;
*IF LITH=1. THEN DELETE;
J1=10;
J2=10;
J3=10;
MW=9.2;
PV=7;
DIA=8.75;

IF BHP<121 THEN DO; DELETE; END;


*LITH=1-LIME;
IF LITH=1 THEN DO; S0=9800;
SA=.004226119; SB=.67862975;
AF=.039222; BF=.33279; CF=.5654; END;

*LITH=2-SHALE;
IF LITH=2. THEN DO; S0=5000;
SA=.00241767; SB=.8033011;
AF=.241996; BF=.18645; CF=.1126; END;

*LITH=4-SAND;
IF LITH=4. THEN DO; S0=6100;
SA=.0183752; SB=.5293818;
AF=.03922; BF=.33279;  CF=.5493; END;

*LITH=3-BEDFORD;
IF LITH=3. THEN DO; S0=5500;
SA=.004226119; SB=.67862975;
AF=.039222; BF=.33279; CF=.5654; END;

LA=SA*BHP**SB;
SC=S0*(1+LA);
SC=SC/1000;
TERM1=SC**2.*DIA**3./(RPM*WOB**2.);
TERM2=1.0/(RPM*DIA);
AREAJ=.000767*(J1**2.+J2**2.+J3**2.);
AREAB=3.14159*(DIA**2.)/4.;
IF=.000516*MW*GPM*(.32086*GPM/AREAJ);
ALF=.15*AREAB/AREAJ;
IM=(1.-ALF**(-0.122))*IF;
TERM3=DIA*MW*PV/IM;
K=(1.0-AF*(BHP-120)**BF)/CF;
*PROC NLIN OUTEST=COEF METHOD=DUD;
PROC NLIN OUTEST=COEF METHOD=MARQUARDT;
PARAMETERS A=.02 B=4.0 C=.004;
POR=(1./K)*(A*TERM1+B*TERM2)+C*TERM3;
POR2=POR*POR;
DER.A=-TERM1/POR2*K;
DER.B=-TERM2/POR2*K;
DER.C=-TERM3/POR2;
MODEL ROP=1./POR;
BOUNDS 0<C, 0<B, 0<A;
OUTPUT OUT=TANF PREDICTED=PRED RESIDUAL=RESID PARMS=A B C;
PROC PRINT DATA=TANF;
VAR K S0 SC BHP ROP PRED RESID WOB RPM;
```

APPENDIX D

POWER LAW HYDRAULICS MODEL FOR CALCULATION OF ANNULAR PRESSURE DROP

This section gives the equations used to calculate the annular pressure drop due to the flow of the drilling fluid [46]. The non-newtonian power law model uses the measured rheological properties from the fan VG viscometer, as well as flow rate and wellbore geometry. The procedure for calculating the pressure drop in each of the annular sections is listed below. An annular section is defined as a section of the annulus where the annular cross-sectional geometry does not change. Typical annular sections occur opposite drill collars, heavy weight drill pipe, and regular drill pipe. Pressure drops for each of these sections are calculated separately and shown below.

The non-newtonian power law model is given by [46]:

$$\tau = K|\zeta|^{n-1}\zeta \qquad \text{(D1)}$$

where

τ = Shear Stress (dynes/cm**2)

ζ = Shear Rate (1/sec)

n = Flow behavior index of power law model (dimensionless)

K = Consistency index of power law model (dynes*sec**n /cm**2)

The values for n and K may be calculated from [46]:

$$n = 3.32 \log\left(\frac{\theta_{600}}{\theta_{300}}\right) \qquad \text{(D2)}$$

$$K = \frac{510\ \theta_{300}}{(511)^n} \qquad \text{(D3)}$$

where

θ_{300} = Dial reading of fann viscometer at 300 rpm (centipoise)

θ_{600} = Dial reading of fann viscometer at 600 rpm (centipoise)

The Reynolds number is calculated for each of the annular sections by [46]:

$$N_{re} = \frac{109{,}000\ \rho(\bar{v})^{2-n}}{K}\left(\frac{0.0208(d_2 - d_1)}{2 + \frac{1}{n}}\right)^n \qquad \text{(D4)}$$

where

$$\bar{v} = \frac{q}{2.448(d_2 - d_1)} \qquad \text{(D4)}$$

N_{re} = Reynolds number (dimensionless)

ρ = Mud weight (ppg)

$\bar{v}$ = Average annular fluid velocity (ft/sec)

q = Flow rate (gpm)

d_2 = Annular outer diameter (inches)

d_1 = Annular inner diameter (inches)

The Reynolds is used to determine if the flow is laminar or turbulent, depending upon whether it is less or greater than 2100, respectively.

If the flow is laminar, the pressure drop per unit length for each section is given by:

$$\frac{dp_f}{dL} = \frac{k\bar{v}^n\left(\frac{2 + 1/n}{0.0208}\right)^n}{144{,}000\ (d_2 - d_1)^{1+n}}, \qquad N_{re} \leq 2100 \tag{D6}$$

If turbulent the result is:

$$\frac{dp_f}{dL} = \frac{f\rho\bar{v}^2}{21.1\ (d_2 - d_1)}, \qquad N_{re} > 2100 \tag{D7}$$

where

$$f = \frac{0.0791}{N_{re}^{0.25}} \tag{D8}$$

$\frac{dp_f}{dL}$ = Pressure drop in annular section (psi/ft)

f = Turbulent friction coefficient (dimensionless)

The lengths for each of the annular sections are multiplied by the pressure drop per unit length for each section. Finally, pressure drops for all annular sections are added up to obtain the total annular pressure drop.

APPENDIX E

SAMPLE DAILY DRILLING WIRE

S. A. HOLDITCH & ASSOCIATES, INC.
DAILY DRILLING REPORT

DATE 5/13/90

LEASE & WELL SFE #4 DAYS FROM SPUD 3

DEPTH 980 FOOTAGE LAST 24 HOURS 762

ACTIVITY @ REPORT TIME Trying to run pipe

	Daily	Cumulative
Drilling Cost	4708	95306
Mud Cost	705	3094
Evaluation Cost		
Completion Cost		
Facilities Cost		
TOTAL COST	5413	98400

OPERATIONS PREVIOUS 24 HOURS

1 1/2 hours lay down HWDP & pick up drill collars

1 + 1/2 hours drilling

'2 hour survey at 442' - 1°

'2 hour circulate

. hour short trip back to collars

1 2 hour circulate

1 1/2 hour POOH

2 hours rigging up casing crew

1/2 hour rig service

1 1/2 hours trying to run casing

Hit bridge at 160'

DRILLING MUD PROPERTIES MUD COMPANY

Wt. 9.2 Vis. 33 WL NC Gels 6/14 % Solids 4 PV 9 YP 8 pH 10.5

% Oil 0 % Sand 2 Cake 2/32 PPMCL 12000 $PPMC_a$ 120

MUD USED: 30 Bar 65 Gel

BIT RECORD:

BIT NO	SIZE	TYPE	SER NO	JETS · 32nd 1	2	3	DEPTH OUT	FEET	HRS.	CUM. HRS.	FT/HR	COND DULL T	B	G
1	17.5	HP11	143437	14	14	14	980	940	22	22	43	7	7	I

BIT NO	WT. ON BIT	RPM	STROKE LENGTH	SPM	LINER	GPM	ANN VEL	JET VEL	SURF PSI	BIT PSI	%HHP @ BIT	DEVIATION SURVEYS
1	30000	120	9	160	6	524	45	372	1700	1048	61	442'-1°, 980'-1°

DP SIZE & TYPE 4 1/2 X-Hole NO. DC 6 OD ID 3 THD 7 5/8 reg LENGTH 179

EFF WT 30000 STAB POSITION KILL RATE (GPM) PUMP PRESSURE @ KILL RATE

APPENDIX F

SAS ROUTINE FOR CALCULATION OF PERMEABLE AND IMPERMEABLE ROCK STRENGTH AND STRESS BOUNDS

```
data hello1;
CMS FILEDEF IN1 DISK SFE2 DRI A;
INFILE IN1 FIRSTOBS=10 LRECL=256;
input depth shale silt sand congl lime dolo coal;
data hello2;
CMS FILEDEF IN2 DISK SFE2 LOG A;
INFILE IN2 FIRSTOBS=10 LRECL=256;
input depth idph dtc dts rhob pef npss rop tor wob rpm spm;
data both;
merge hello1(in=n1) hello2(in=n2); by depth;
if n1 and n2;

IF DEPTH<8000.1 THEN DO; PG=.46; END;
IF DEPTH>8000.1 AND DEPTH<8800.1 THEN DO;
PG=.46+.04*(DEPTH-8000.)/1000.; END;
IF DEPTH>8800.1 AND DEPTH<8900.1 THEN DO;
PG=.44; END;
IF DEPTH>8900.1 AND DEPTH<9000.1 THEN DO;
PG=.46+.04*(DEPTH-8000.)/1000.; END;
IF DEPTH>9000 THEN DO; PG=.50; END;

IF DEPTH>1 AND DEPTH<11000 THEN YP=8;

IF DEPTH>1 AND DEPTH<7896.1 THEN DO; MW=9.9; PV=9; GPM=321; END;
IF DEPTH>7896.1 AND DEPTH<8082.1 THEN DO;MW=9.9;PV=9; GPM=321; END;
IF DEPTH>8082.1 AND DEPTH<8183.1 THEN DO;MW=10.;PV=9; GPM=320; END;
IF DEPTH>8183.1 AND DEPTH<8251.1 THEN DO;MW=10.1;PV=8; GPM=322; END;
IF DEPTH>8251.1 AND DEPTH<8457.1 THEN DO;MW=10.;PV=6; GPM=297; END;
IF DEPTH>8457.1 AND DEPTH<8591.1 THEN DO;MW=10.;PV=5; GPM=328; END;
IF DEPTH>8591.1 AND DEPTH<8709.1 THEN DO;MW=9.9;PV=6; GPM=328; END;
IF DEPTH>8709.1 AND DEPTH<8770.1 THEN DO;MW=10.;PV=6; GPM=292; END;
IF DEPTH>8770.1 AND DEPTH<8949.1 THEN DO;MW=9.9;PV=6; GPM=325; END;
IF DEPTH>8949.1 AND DEPTH<9122.1 THEN DO;MW=10.;PV=8; GPM=325; END;
IF DEPTH>9122.1 AND DEPTH<9377.1 THEN DO;MW=10.;PV=6; GPM=325; END;
IF DEPTH>9377.1 AND DEPTH<9481.1 THEN DO;MW=10.;PV=6; GPM=325; END;
IF DEPTH>9481.1 AND DEPTH<9640.1 THEN DO;MW=10.;PV=7; GPM=325; END;
IF DEPTH>9640.1 AND DEPTH<9780.1 THEN DO;MW=9.9;PV=9; GPM=325; END;
IF DEPTH>9780.1 AND DEPTH<9942.1 THEN DO;MW=9.8;PV=8; GPM=306; END;
IF DEPTH>9942.1 AND DEPTH<11000.1 THEN DO;MW=9.9;PV=14; GPM=285; END;

IF DEPTH<8116.1 THEN DO; J1=10; J2=10; J3=10; BTYPE=537; END;
IF DEPTH>8116.1 AND DEPTH<8229.1 THEN DO; J1=11; J2=11; J3=11;
BTYPE=537; END;
IF DEPTH>8259.9 AND DEPTH<8265.1 THEN DO; J1=11; J2=11; J3=11;
BTYPE=537; END;
IF DEPTH>8320.1 AND DEPTH<8677.9 THEN DO; J1=11; J2=11; J3=11;
BTYPE=737; END;
IF DEPTH>8738.9 AND DEPTH<9479.9 THEN DO; J1=11; J2=11; J3=11;
BTYPE=737; END;
IF DEPTH>9571.9 AND DEPTH<9805.9 THEN DO; J1=11; J2=11; J3=11;
BTYPE=737; END;
IF DEPTH>9941.9 THEN DO; J1=11; J2=11; J3=11;
BTYPE=737; END;

sand=silt+sand+congl;
shal=shale+coal;
lime=lime+dolo;
LIMESA=.0043188; LIMESB=.74191; AFL=.01413; BFL=.4702; CFL=.6595;
SHALSA=.0043188; SHALSB=.74191; AFSH=.00496; BFSH=.7572; CFSH=.1025;
SANDSA=.01331 ; SANDSB=.57106; AFSA=0.01413; BFSA=.4702; CFSA=.6595;
IF BTYPE=437 THEN DO; A=.01817;   B=3.0709;  C=.002094; END;
IF BTYPE=517 THEN DO; A=.02587;   B=4.2149;  C=.003350; END;
```

```
IF BTYPE=537 THEN DO; A=.01383;   B=9.7704;  C=.002231; END;
IF BTYPE=617 THEN DO; A=.01902;   B=13.4527; C=.003256; END;
IF BTYPE=627 THEN DO; A=.01953;   B=3.2536; C=.01441;  END;
IF BTYPE=737 THEN DO; A=.01684; B=9.314; C=.007988; END;
*IF BTYPE=737 THEN DO;*A=.03224;*B=3.02;*C=.0033;*END;
dia=8.75;
COLDIA=6.75;
PIPDIA=5.0;
IF DEPTH<11000 AND DEPTH>1 THEN DO; DRC=554; DRP=DEPTH-DRC;
ANCVEL=GPM/(2.448*(DIA**2.0-COLDIA**2.0));
ANPVEL=GPM/(2.448*(DIA**2.0-PIPDIA**2.0));
FAN3=PV+YP;
FAN6=FAN3+PV;
PLN=3.32*LOG(FAN6/FAN3);
PLK=(510*FAN3)/((511)**PLN);
REYAC=109000*MW*((ANCVEL)**(2-PLN))/PLK;
REYBC=(.0208*(DIA-COLDIA)/(2+1/PLN))**PLN;
REYNC=REYAC*REYBC;

REYAP=109000*MW*((ANPVEL)**(2-PLN))/PLK;
REYBP=(.0208*(DIA-PIPDIA)/(2+1/PLN))**PLN;
REYNP=REYAP*REYBP;

IF REYNC>2100.1 THEN DO;
FRICKC=.0791/(REYNC**.25);
PRESSC=DRC*(FRICKC*MW*ANCVEL**2.)/(21.1*(DIA-COLDIA));
END;


IF REYNC<2100.1 THEN DO;
PRESSCA=DRC*(PLK*ANCVEL**PLN);
PRESSCB=((2+1/PLN)/.0208)**PLN;
PRESSCC=144000*(DIA-COLDIA)**(1-PLN);
PRESSC=PRESSCA*PRESSCB/PRESSCC;
END;

IF REYNP>2100.1 THEN DO;
FRICKP=.0791/(REYNP**.25);
PRESSP=DRP*(FRICKP*MW*ANPVEL**2.)/(21.1*(DIA-PIPDIA));
END;


IF REYNP<2100.1 THEN DO;
PRESSPA=DRP*(PLK*ANPVEL**PLN);
PRESSPB=((2+1/PLN)/.0208)**PLN;
PRESSPC=144000*(DIA-PIPDIA)**(1-PLN);
PRESSP=PRESSPA*PRESSPB/PRESSPC;
END;


ANTOT=PRESSC+PRESSP;
BET=1.0;

BHPI=.052*MW*DEPTH+ANTOT;
PP=PG*DEPTH;
BHP=.052*MW*DEPTH-BET*PG*DEPTH+ANTOT;

IF BHP<120 THEN BHP=120;
AREAJ=.000767*(J1**2.+J2**2.+J3**2.);
AREAB=3.14159*(DIA**2)/4.;
IF=.000516*MW*GPM*(.32086*GPM/AREAJ);
ALF=.15*AREAB/AREAJ;
```

```
IM=(1. - ALF**(-0.122))*IF;

KLI=(CFL+AFL*(BHP-120)**BFL);
KLII=(CFL+AFL*(BHPI-120)**BFL);
KSH=(CFSH+AFSH*(BHP-120)**BFSH);
KSHI=(CFSH+AFSH*(BHPI-120)**BFSH);
KSA=(CFSA+AFSA*(BHP-120)**BFSA);
KSAI=(CFSA+AFSA*(BHPI-120)**BFSA);
K=KLI*LIME+KSH*SHAL+KSA*SAND;
KI=KLII*LIME+KSHI*SHAL+KSAI*SAND;
TERM1=(RPM*WOB**2.0)/(A*K*ROP*DIA**3.0);
TERM1I=(RPM*WOB**2.0)/(A*KI*ROP*DIA**3.0);
TERM2=(B*WOB**2.0)/(A*DIA**4.0);
TERM3=(C*RPM*MW*PV*WOB**2.0)/(IM*K*A*DIA**2);
TERM3I=(C*RPM*MW*PV*WOB**2.0)/(IM*KI*A*DIA**2);
ROCKY=(TERM1-TERM2-TERM3);
ROCKYI=(TERM1I-TERM2-TERM3I);
ROCK=(TERM1-TERM2-TERM3)**.5;
ROCKI=(TERM1I-TERM2-TERM3I)**.5;
IF ROCKY<0.5 THEN DO; ROCK=3; END;
IF ROCKYI<0.5 THEN DO; ROCKI=3; END;
ROCK=ROCK*1000;
ROCKI=ROCKI*1000;
IF DEPTH>7900.1 AND DEPTH<8220.9 THEN DO; DEPTH=DEPTH-10; END;
IF DEPTH>8320.1 AND DEPTH<8678.9 THEN DO; DEPTH=DEPTH+7; END;
IF DEPTH>8855.1 AND DEPTH<9480.9 THEN DO; DEPTH=DEPTH+4; END;
IF DEPTH>9572.1 AND DEPTH<9806.9 THEN DO; DEPTH=DEPTH+10; END;
IF DEPTH>9942.1 AND DEPTH<10163.9 THEN DO; DEPTH=DEPTH+4; END;
IF DEPTH>8229.1 AND DEPTH<8259.9 THEN DO; DELETE; END;
IF DEPTH>8265.1 AND DEPTH<8320.1 THEN DO; DELETE; END;
IF DEPTH>8677.9 AND DEPTH<8738.9 THEN DO; DELETE; END;
IF DEPTH>9479.9 AND DEPTH<9571.9 THEN DO; DELETE; END;
IF DEPTH>9805.9 AND DEPTH<9941.9 THEN DO; DELETE; END;

PERSAND=SAND;
PERSHALE=SHAL;
PERLIME=LIME;



*A1=0.0043188 ;* B1=0.74191;
A1=0.01331 ;B1=0.57106 ; A2=0.0043188 ; B2=0.74191 ;
A3=0.0043188 ; B3=0.74191;

SAND0=PERSAND*(1+A1*BHP**B1);
SAND0I=PERSAND*(1+A1*BHPI**B1);
LIME0=PERLIME*(1+A2*BHP**B2);
LIME0I=PERLIME*(1+A2*BHPI**B2);
SHALE0=PERSHALE*(1+A3*BHP**B3);
SHALE0I=PERSHALE*(1+A3*BHPI**B3);
SOC=ROCK/(SAND0+LIME0+SHALE0);
SOCI=ROCKI/(SAND0I+LIME0I+SHALE0I);

CPR=.65*DEPTH-PP;
GAMMA=CPR+50;
ZETA=CPR-50;
SAND1=PERSAND*(1+A1*ZETA**B1);
LIME1=PERLIME*(1+A2*ZETA**B2);
SHALE1=PERSHALE*(1+A3*ZETA**B3);

SC1=SOC*(SAND1+LIME1+SHALE1);
SC1I=SOCI*(SAND1+LIME1+SHALE1);
```

```
SAND2=PERSAND*(1+A1*GAMMA**B1);
LIME2=PERLIME*(1+A2*GAMMA**B2);
SHALE2=PERSHALE*(1+A3*GAMMA**B3);
SC2=SOC*(SAND2+LIME2+SHALE2);
SC2I=SOCI*(SAND2+LIME2+SHALE2);

delta=sc2-sc1;
DELTAI=SC2I-SC1I;
N=DELTA/(DELTA+200);
NI=DELTAI/(DELTAI+200);
beta1=arsin(n);
BETA1I=ARSIN(NI);
BETA2=BETA1*180/(3.141593);
BETA2I=BETA1I*180/(3.141593);
KO=1-N;
KOI=.9*(1-NI);
SOVB=1.04*DEPTH;
sh=ko*(sovb-Pp)+Pp;
SHI=KOI*(SOVB-PP)+PP;

CPRP=SH-PP;
CPRI=SHI-PP;
GAMMAP=CPRP+50;
GAMMAI=CPRI+50;
ZETAP=CPRP-50;
ZETAI=CPRI-50;
SAND1P=PERSAND*(1+A1*ZETAP**B1);
SAND1I=PERSAND*(1+A1*ZETAI**B1);
LIME1P=PERLIME*(1+A2*ZETAP**B2);
LIME1I=PERLIME*(1+A2*ZETAI**B2);
SHALE1P=PERSHALE*(1+A3*ZETAP**B3);
SHALE1I=PERSHALE*(1+A3*ZETAI**B3);
SC1P=SOC*(SAND1P+LIME1P+SHALE1P);
SC1IM=SOCI*(SAND1I+LIME1I+SHALE1I);
SAND2P=PERSAND*(1+A1*GAMMAP**B1);
SAND2I=PERSAND*(1+A1*GAMMAI**B1);
LIME2P=PERLIME*(1+A2*GAMMAP**B2);
LIME2I=PERLIME*(1+A2*GAMMAI**B2);
SHALE2P=PERSHALE*(1+A3*GAMMAP**B3);
SHALE2I=PERSHALE*(1+A3*GAMMAI**B3);
SC2P=SOC*(SAND2P+LIME2P+SHALE2P);
SC2IM=SOCI*(SAND2I+LIME2I+SHALE2I);

DELTAP=SC2P-SC1P;
DELTAIM=SC2IM-SC1IM;
NP=DELTAP/(DELTAP+200);
NIM=DELTAIM/(DELTAIM+200);
BETA1P=ARSIN(NP);
BETA1IM=ARSIN(NIM);
BETA2P=BETA1P*180/(3.141593);
BETA2IM=BETA1IM*180/(3.141593);
KOP=1-NP;
KOIM=.9*(1-NIM);
SHP=KOP*(SOVB-PP)+PP;
SHIM=KOIM*(SOVB-PP)+PP;

CPRP2=SHP-PP;
CPRI2=SHIM-PP;
GAMMAP2=CPRP2+50;
GAMMAI2=CPRI2+50;
ZETAP2=CPRP2-50;
ZETAI2=CPRI2-50;
```

```
SAND1P2=PERSAND*(1+A1*ZETAP2**B1);
SAND1I2=PERSAND*(1+A1*ZETAI2**B1);
LIME1P2=PERLIME*(1+A2*ZETAP2**B2);
LIME1I2=PERLIME*(1+A2*ZETAI2**B2);
SHALE1P2=PERSHALE*(1+A3*ZETAP2**B3);
SHALE1I2=PERSHALE*(1+A3*ZETAI2**B3);

SC1P2=SOC*(SAND1P2+LIME1P2+SHALE1P2);
SC1IM2=SOCI*(SAND1I2+LIME1I2+SHALE1I2);

SAND2P2=PERSAND*(1+A1*GAMMAP2**B1);
SAND2I2=PERSAND*(1+A1*GAMMAI2**B1);
LIME2P2=PERLIME*(1+A2*GAMMAP2**B2);
LIME2I2=PERLIME*(1+A2*GAMMAI2**B2);
SHALE2P2=PERSHALE*(1+A3*GAMMAP2**B3);
SHALE2I2=PERSHALE*(1+A3*GAMMAI2**B3);

SC2P2=SOC*(SAND2P2+LIME2P2+SHALE2P2);
SC2IM2=SOCI*(SAND2I2+LIME2I2+SHALE2I2);

DELTAP2=SC2P2-SC1P2;
DELTAIM2=SC2IM2-SC1IM2;
NP2=DELTAP2/(DELTAP2+200);
NIM2=DELTAIM2/(DELTAIM2+200);
BETA1P2=ARSIN(NP2);
BETA1IM2=ARSIN(NIM2);
BETA2P2=BETA1P2*180/(3.141593);
BETA2IM2=BETA1IM2*180/(3.141593);
KOP2=1-NP2;
KOIM2=.9*(1-NIM2);
SHP2=KOP2*(SOVB-PP)+PP;
SHIM2=KOIM2*(SOVB-PP)+PP;

CPRP3=SHP2-PP;
CPRI3=SHIM2-PP;
GAMMAP3=CPRP3+50;
GAMMAI3=CPRI3+50;
ZETAP3=CPRP3-50;
ZETAI3=CPRI3-50;
SAND1P3=PERSAND*(1+A1*ZETAP3**B1);
SAND1I3=PERSAND*(1+A1*ZETAI3**B1);
LIME1P3=PERLIME*(1+A2*ZETAP3**B2);
LIME1I3=PERLIME*(1+A2*ZETAI3**B2);
SHALE1P3=PERSHALE*(1+A3*ZETAP3**B3);
SHALE1I3=PERSHALE*(1+A3*ZETAI3**B3);

SC1P3=SOC*(SAND1P3+LIME1P3+SHALE1P3);
SC1IM3=SOCI*(SAND1I3+LIME1I3+SHALE1I3);

SAND2P3=PERSAND*(1+A1*GAMMAP3**B1);
SAND2I3=PERSAND*(1+A1*GAMMAI3**B1);
LIME2P3=PERLIME*(1+A2*GAMMAP3**B2);
LIME2I3=PERLIME*(1+A2*GAMMAI3**B2);
SHALE2P3=PERSHALE*(1+A3*GAMMAP3**B3);
SHALE2I3=PERSHALE*(1+A3*GAMMAI3**B3);

SC2P3=SOC*(SAND2P3+LIME2P3+SHALE2P3);
SC2IM3=SOCI*(SAND2I3+LIME2I3+SHALE2I3);

DELTAP3=SC2P3-SC1P3;
DELTAIM3=SC2IM3-SC1IM3;
NP3=DELTAP3/(DELTAP3+200);
```

```
NIM3=DELTAIM3/(DELTAIM3+200);
BETA1P3=ARSIN(NP3);
BETA1IM3=ARSIN(NIM3);
BETA2P3=BETA1P3*180/(3.141593);
BETA2IM3=BETA1IM3*180/(3.141593);
KOP3=1-NP3;
KOIM3=.9*(1-NIM3);
SHP3=KOP3*(SOVB-PP)+PP;
SHIM3=KOIM3*(SOVB-PP)+PP;

CPRP4=SHP3-PP;
CPRI4=SHIM3-PP;
GAMMAP4=CPRP4+50;
GAMMAI4=CPRI4+50;
ZETAP4=CPRP4-50;
ZETAI4=CPRI4-50;
SAND1P4=PERSAND*(1+A1*ZETAP4**B1);
SAND1I4=PERSAND*(1+A1*ZETAI4**B1);
LIME1P4=PERLIME*(1+A2*ZETAP4**B2);
LIME1I4=PERLIME*(1+A2*ZETAI4**B2);
SHALE1P4=PERSHALE*(1+A3*ZETAP4**B3);
SHALE1I4=PERSHALE*(1+A3*ZETAI4**B3);

SC1P4=SOC*(SAND1P4+LIME1P4+SHALE1P4);
SC1IM4=SOCI*(SAND1I4+LIME1I4+SHALE1I4);

SAND2P4=PERSAND*(1+A1*GAMMAP4**B1);
SAND2I4=PERSAND*(1+A1*GAMMAI4**B1);
LIME2P4=PERLIME*(1+A2*GAMMAP4**B2);
LIME2I4=PERLIME*(1+A2*GAMMAI4**B2);
SHALE2P4=PERSHALE*(1+A3*GAMMAP4**B3);
SHALE2I4=PERSHALE*(1+A3*GAMMAI4**B3);

SC2P4=SOC*(SAND2P4+LIME2P4+SHALE2P4);
SC2IM4=SOCI*(SAND2I4+LIME2I4+SHALE2I4);

DELTAP4=SC2P4-SC1P4;
DELTAIM4=SC2IM4-SC1IM4;
NP4=DELTAP4/(DELTAP4+200);
NIM4=DELTAIM4/(DELTAIM4+200);
BETA1P4=ARSIN(NP4);
BETA1IM4=ARSIN(NIM4);
PI=3.141593;
BETA2P4=BETA1P4*180/PI;
BETA2IM4=BETA1IM4*180/PI;
KOP4=1-NP4;
KOIM4=.9*(1-NIM4);
SHP4=KOP4*(SOVB-PP)+PP;
SHIM4=KOIM4*(SOVB-PP)+PP;
*IF PERSAND>.901 THEN COMB=SHP4;
*IF PERSAND<.901 THEN COMB=SHIM4;

proc print;
VAR DEPTH ROCK ROCKI SHIM4 SHP4 PP KOP4 KOIM4 BETA2P4 BETA2IM4;
 TITLE 'BOUND2 DATA ';
*;
  CMS FI TAGOUT DISK BOUND2 DATA A (LRECL 80 RECFM F BLOCK 80);
PROC TAG;  PARMCARDS4;
  GENERATE A FANCY PLOT.
  FRAME ON.
  TITLE 'ANGLE OF INTERNAL FRICTION FOR SFE#2'
        ,STYLE DUPLEX, ALPHABET ITALIC.
```

```
  SAS DATA.
  USE X=DEPTH Y=SHIM4.
  USE X=DEPTH Y=SHP4.
  USE X=DEPTH Y=PP.
  END OF DATA.
  Y AXIS LABEL "ANGLE OF INTERNAL FRICTION (DEGREES)",STYLE DUPLEX,
  ALPHABET ITALIC.
  X AXIS LABEL "DEPTH (FT)",STYLE DUPLEX,ALPHABET ITALIC.
  X AXIS MAX 10200, MIN 7800, TICK 2, STEP 100.0.
  X AXIS LENGTH 8.2.
  X PAGE 10.
  Y AXIS MAX 90., MIN 0, TICK 2, STEP 10.
  EVERY MSG STYLE DUPLEX, ALPHABET ITALIC, HEIGHT .15.
EVERY CURVE SYMBOL SIZE  1, SYMBOL BLANKING OFF.
  EVERY MESSAGE BLANKING ON.
  CURVE 1 SYMBOL COUNT 0,COLOR BLUE , SYMBOL TYPE 17.
  CURVE 2 SYMBOL COUNT 0,COLOR RED , SYMBOL TYPE 15.
  LEGEND EXISTENCE ON.
  LEGEND IS UNITS COORDINATE.
  LEGEND CONNECT LC, X=8000  Y=2000.
  LEGEND HEIGHT .12.
  LEGEND TEXT "  ", STYLE DUPLEX, ALPHABET ITALIC.
  CURVE 1 LABEL 'PERMEABLE'.
  CURVE 2 LABEL 'IMPERMEABLE'.
GO.
C.
SEND.
```

APPENDIX G

SAMPLE OUTPUT FROM SAS PROGRAM IN APPENDIX F

Depth (feet)	Permeable Rock Strength (psi)	Impermeable Rock Strength (psi)	Horizontal Stress (Impermeable) Forth Iteration (psi)	Horizontal Stress (Permeable) Forth Iteration (psi)	Pore Pressure (psi)
8000.0	30021.0	18858.8	5449.23	4354.58	3687.80
8001.0	28654.8	17774.3	5598.90	4459.81	3688.58
8002.0	23226.1	11561.1	6126.86	4662.96	3689.37
8003.0	25121.8	14895.4	5853.43	4616.84	3690.15
8004.0	16311.2	6340.8	6780.53	5123.26	3690.93
8005.0	27054.0	14746.6	5867.91	4544.40	3691.71
8006.0	28531.7	17666.6	5611.43	4467.38	3692.49
8007.0	26879.2	16677.9	5630.26	4470.42	3693.27
8008.0	14539.3	5508.6	6852.05	5172.46	3694.05

APPENDIX H

PERMEABLE AND IMPERMEABLE ROCK STRENGTH PLOTS FOR SFE #1-4

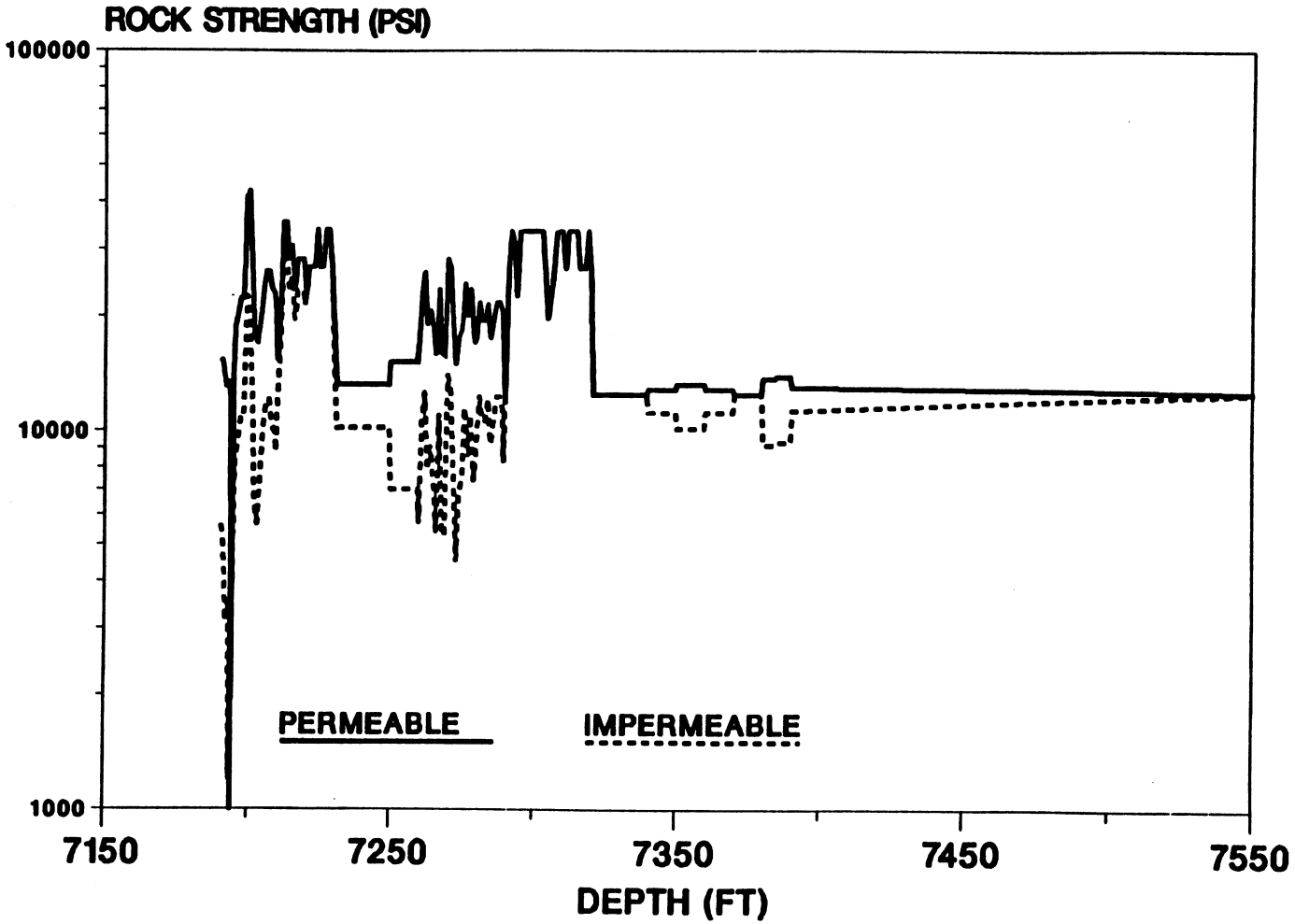

Figure 73. Section of Permeable and Impermeable Rock Strength for SFE #1 (7150 - 7550 Feet)

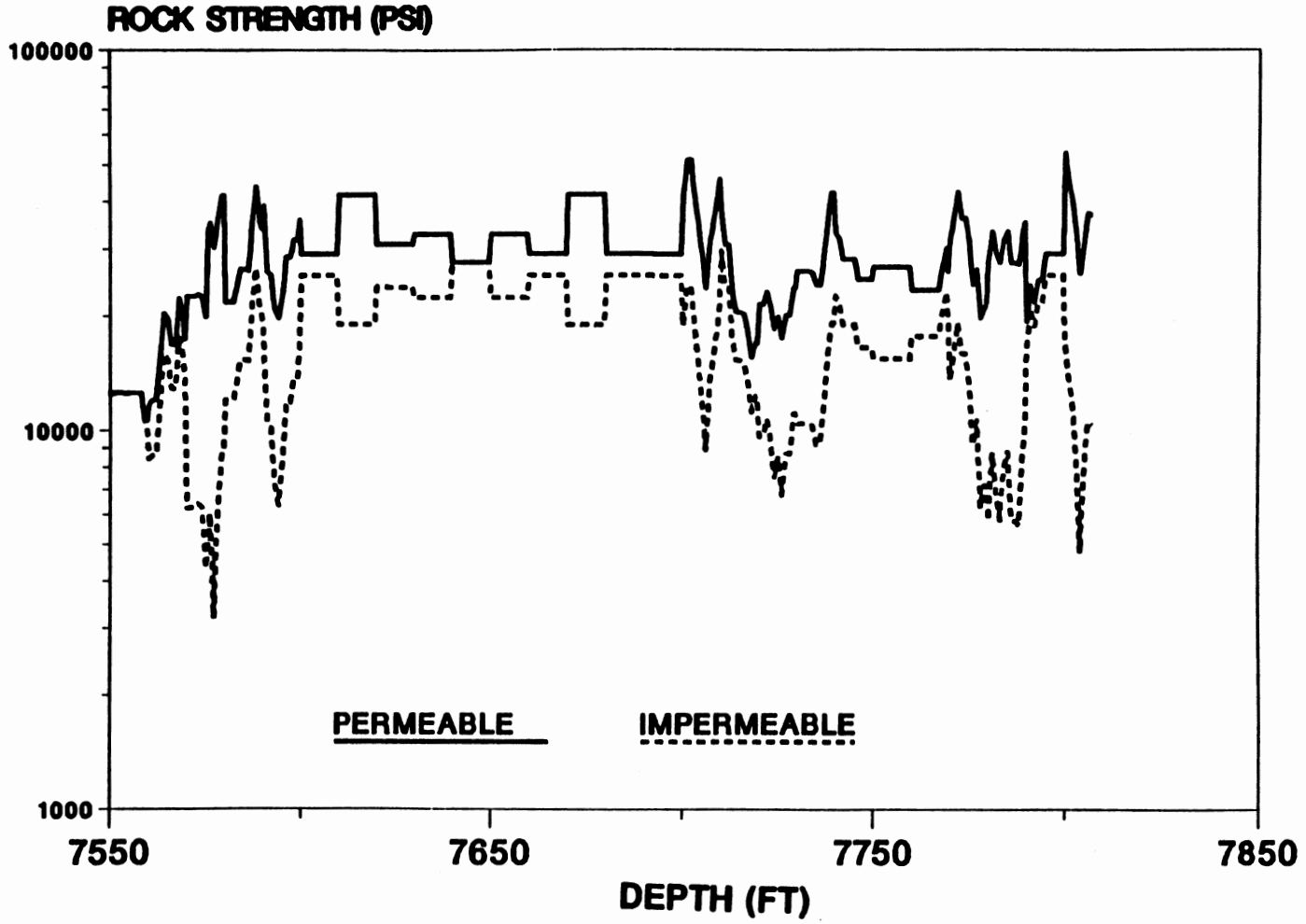

Figure 74. Section of Permeable and Impermeable Rock Strength for SFE #1 (7550 - 7850 Feet)

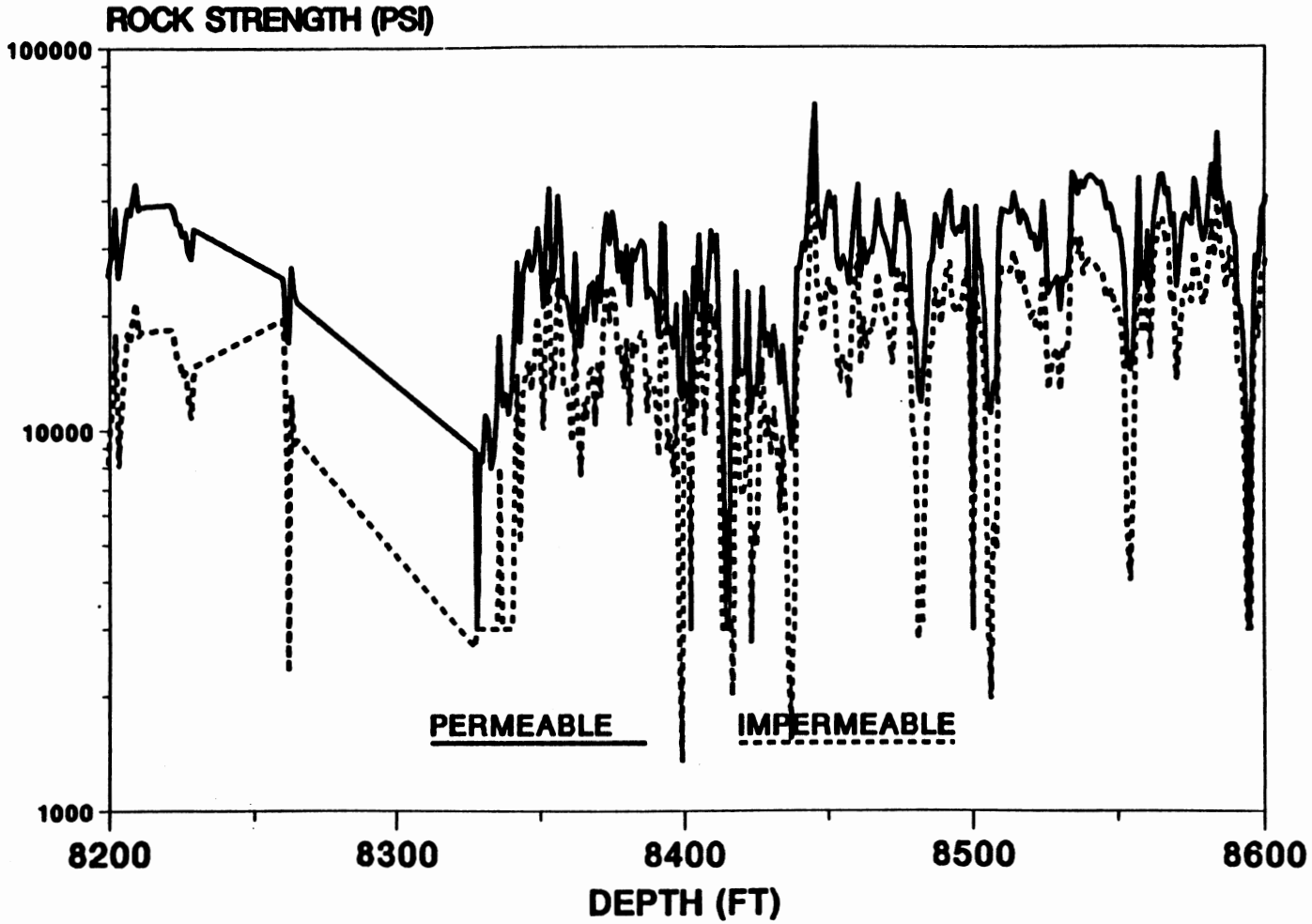

Figure 75. Section of Permeable and Impermeable Rock Strength for SFE #2 (8200 - 8600 Feet)

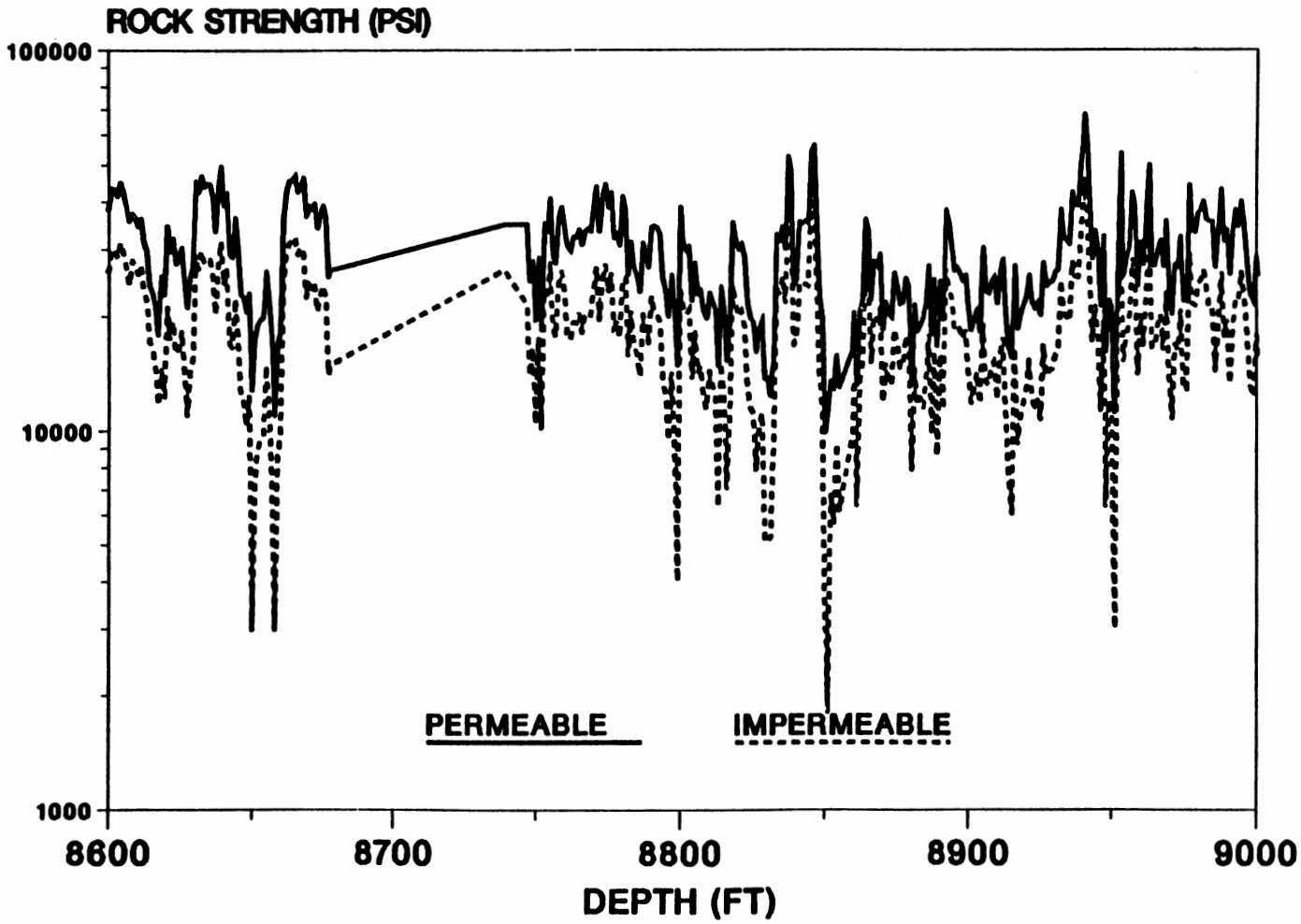

Figure 76. Section of Permeable and Impermeable Rock Strength for SFE #2 (8600 - 9000 Feet)

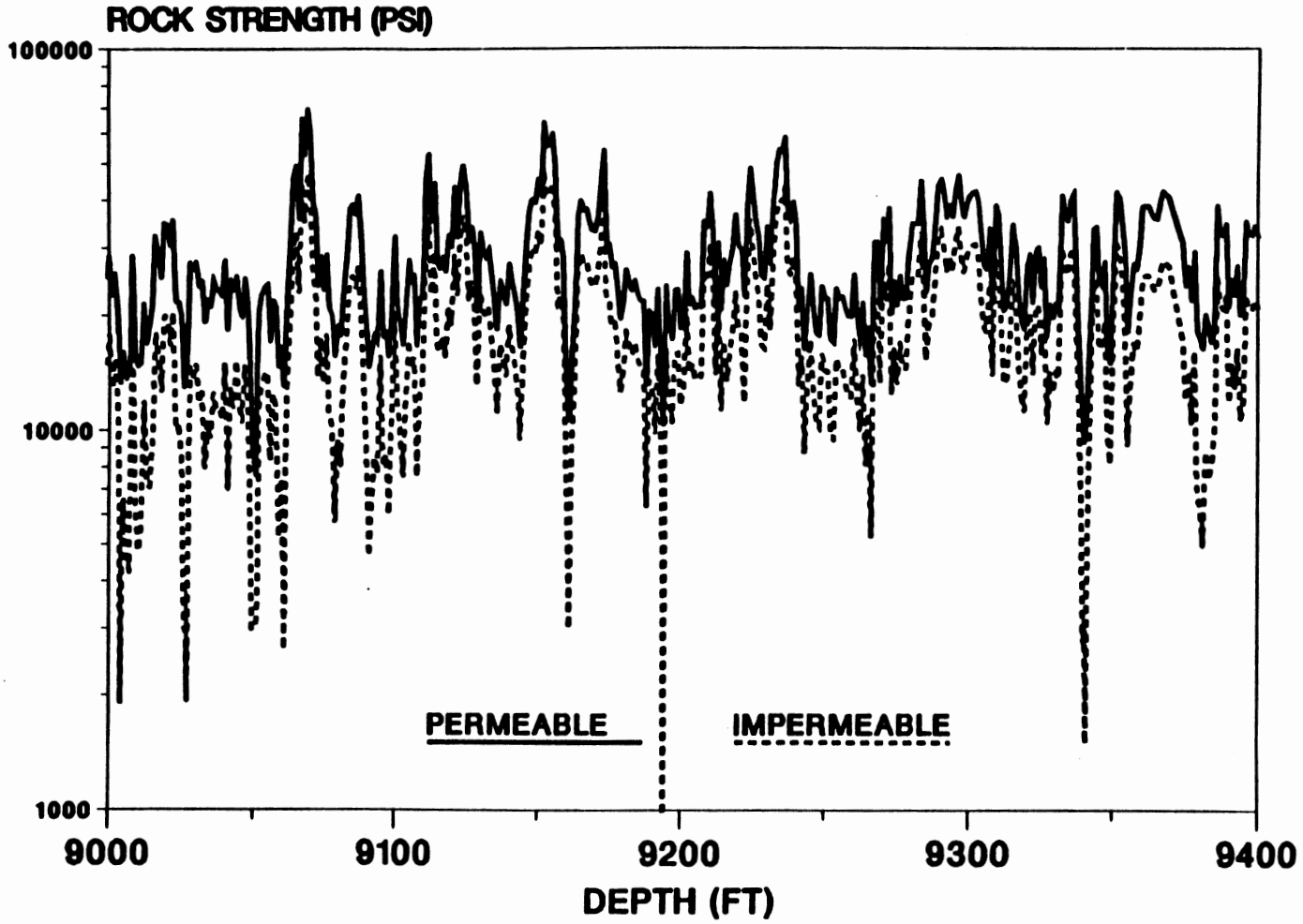

Figure 77. Section of Permeable and Impermeable Rock Strength for SFE #2 (9000 - 9400 Feet)

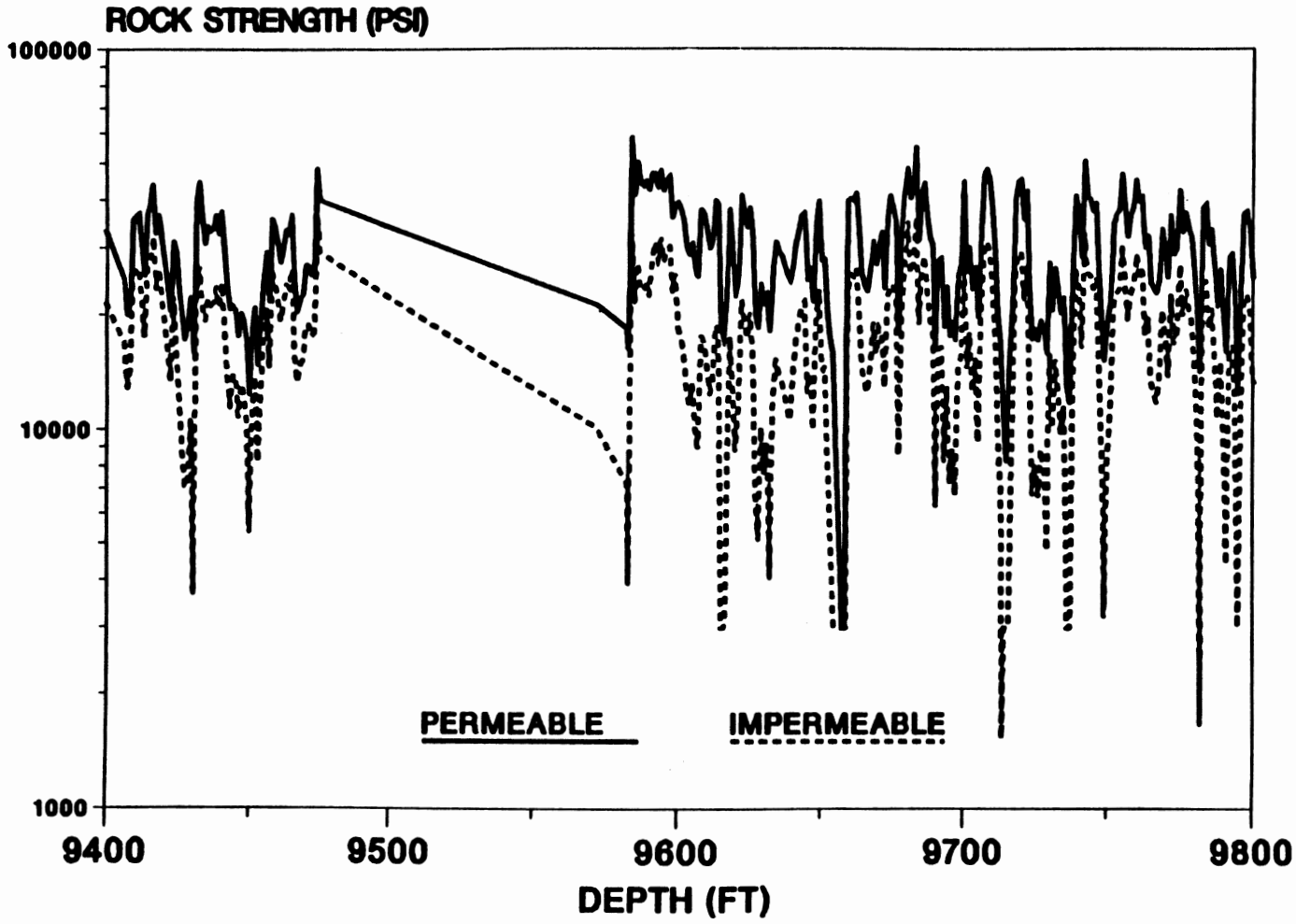

Figure 78. Section of Permeable and Impermeable Rock Strength for SFE #2 (9400 - 9800 Feet)

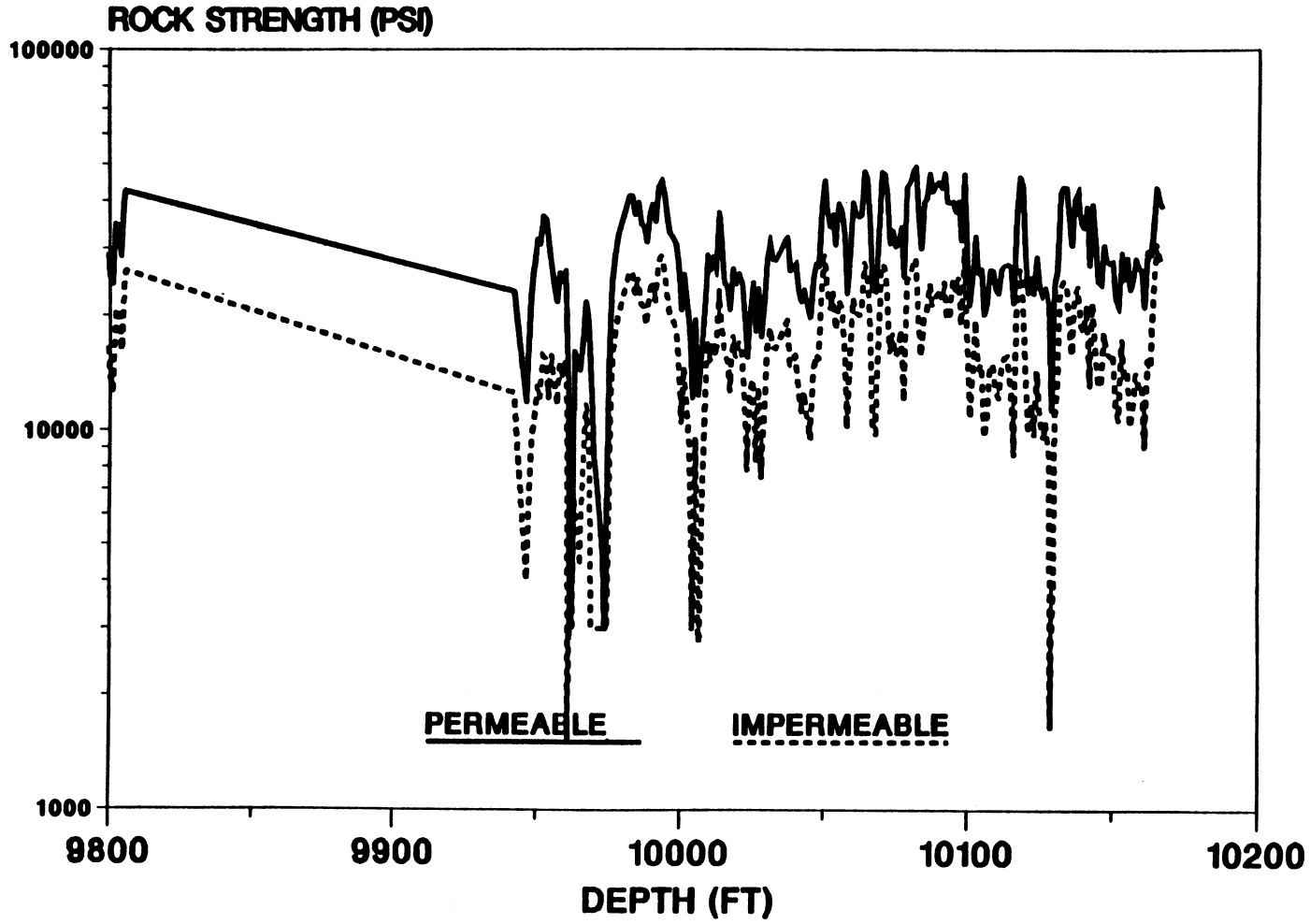

Figure 79. Section of Permeable and Impermeable Rock Strength for SFE #2 (9800 - 10200 Feet)

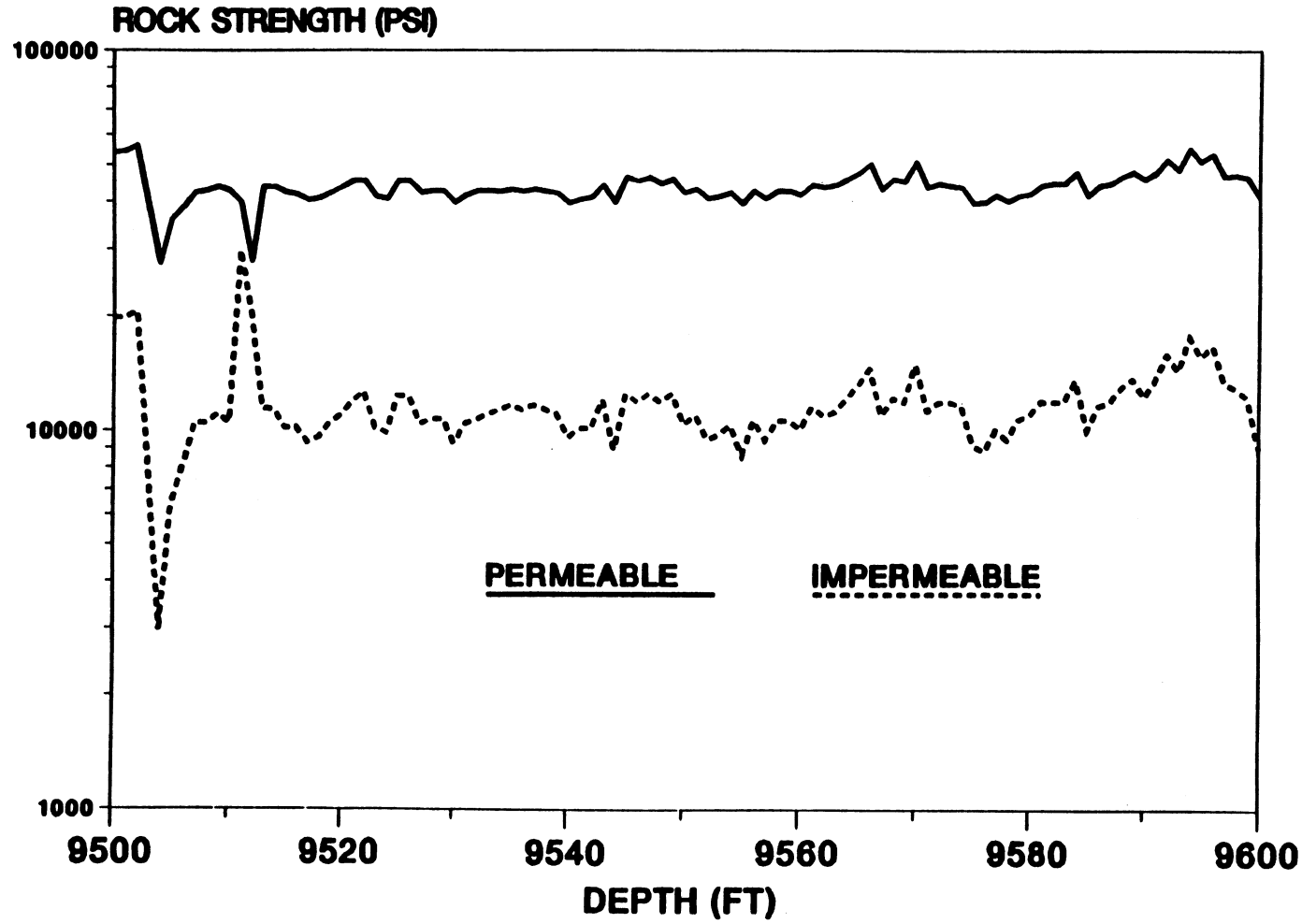

Figure 80. Section of Permeable and Impermeable Rock Strength for SFE #3 (9500 - 9600 Feet)

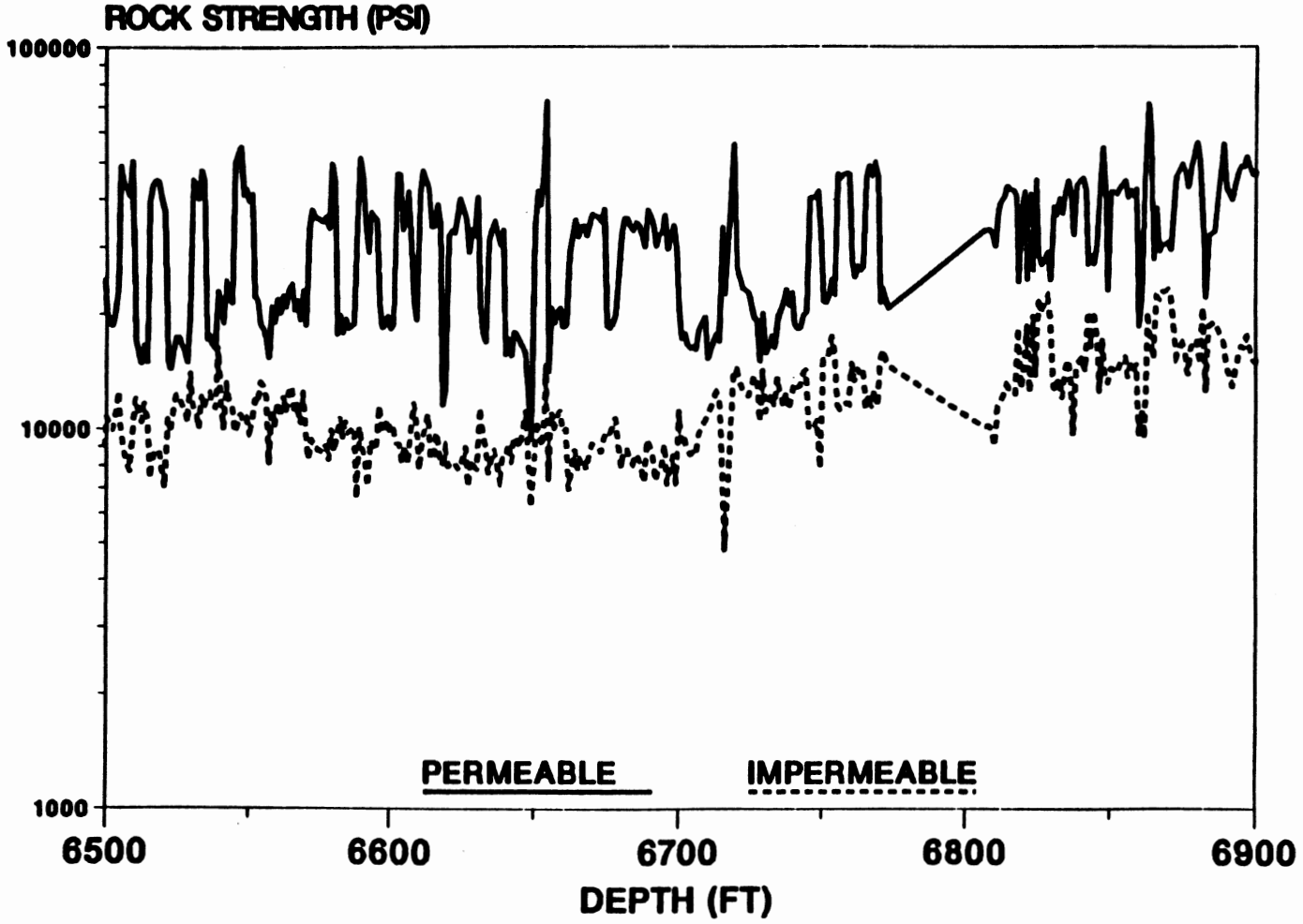

Figure 81. Section of Permeable and Impermeable Rock Strength for SFE #4 (6500 - 6900 Feet)

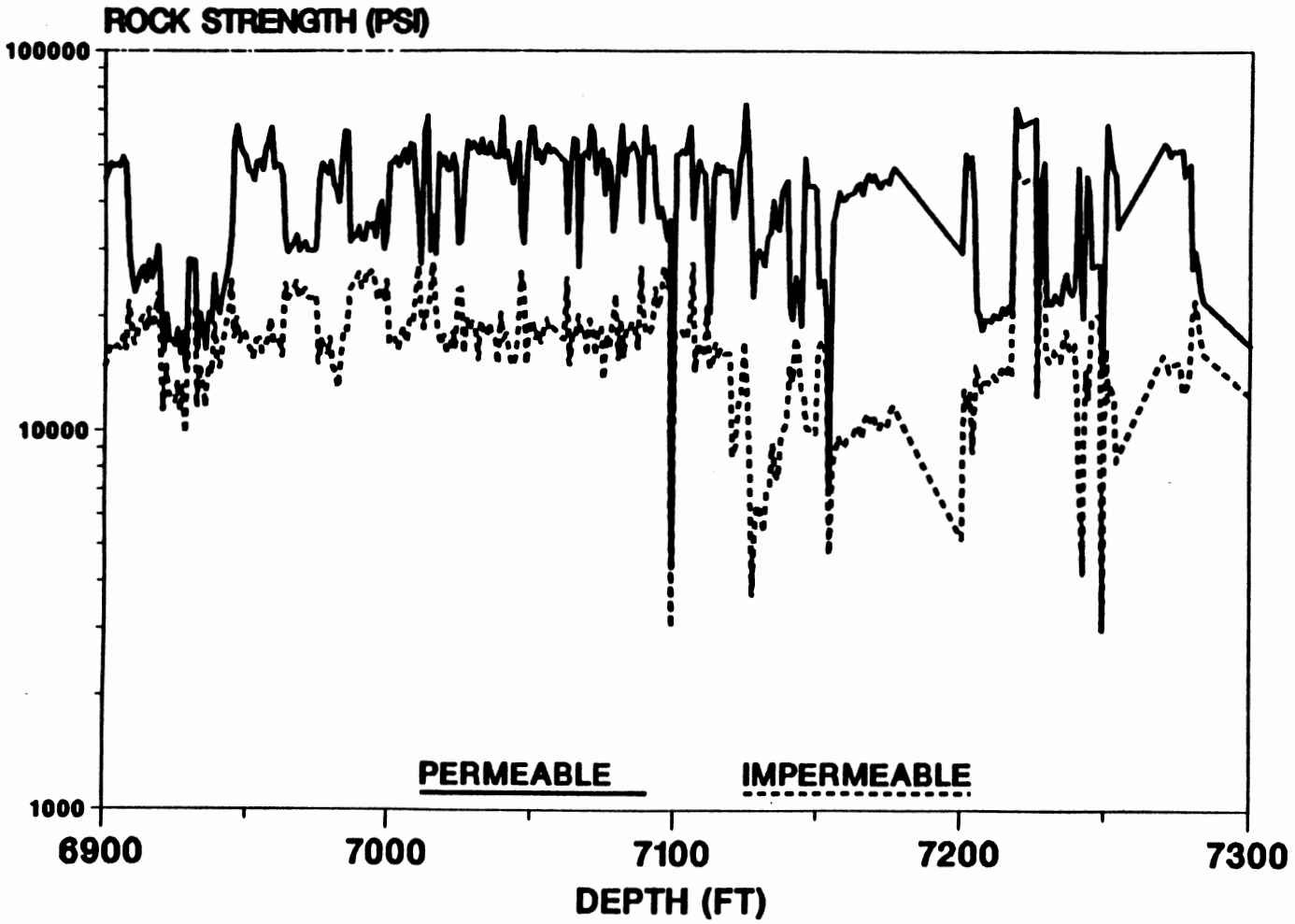

Figure 82. Section of Permeable and Impermeable Rock Strength for SFE #4 (6900 - 7300 Feet)

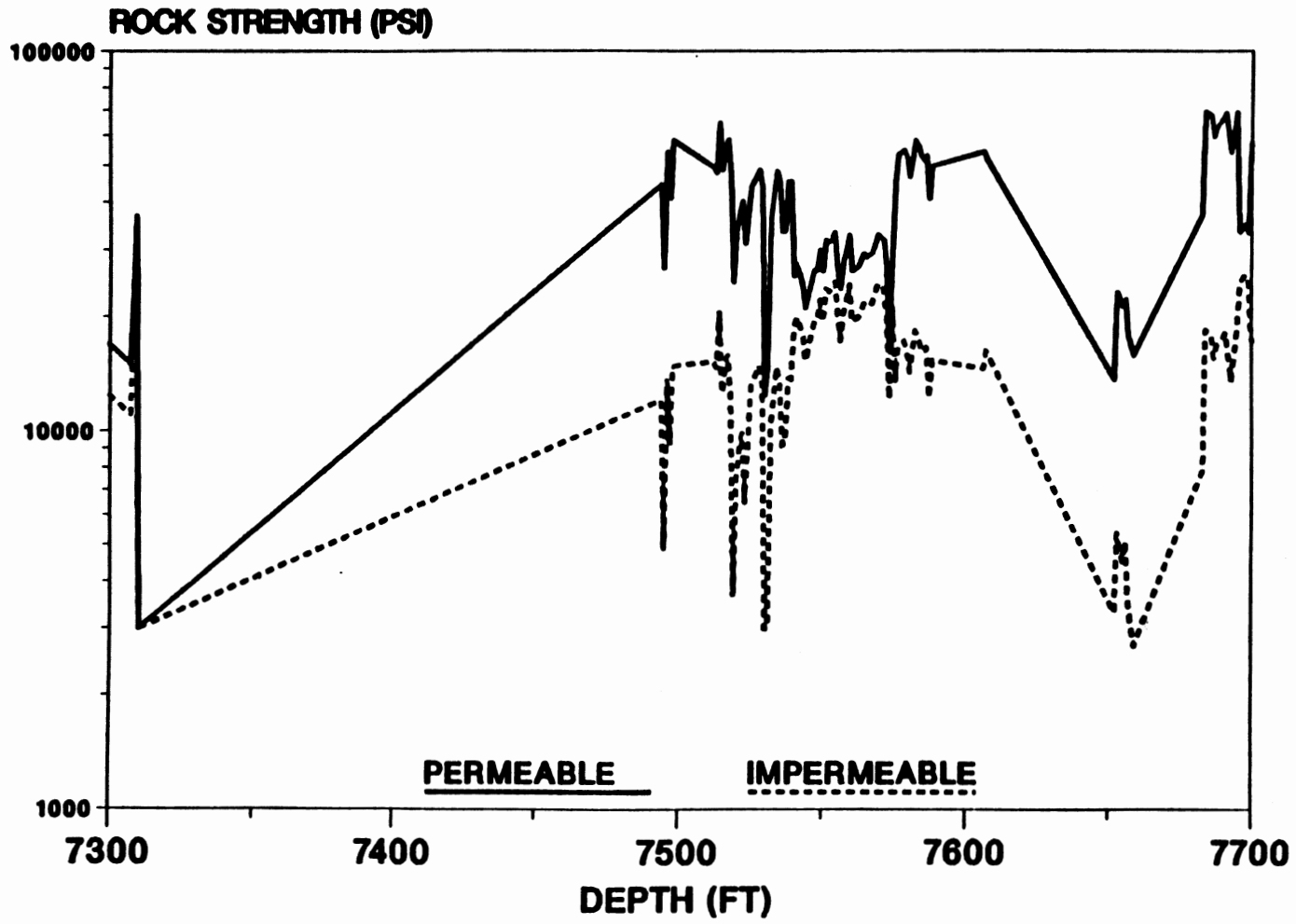

Figure 83. Section of Permeable and Impermeable Rock Strength for SFE #4 (7300 - 7700 Feet)

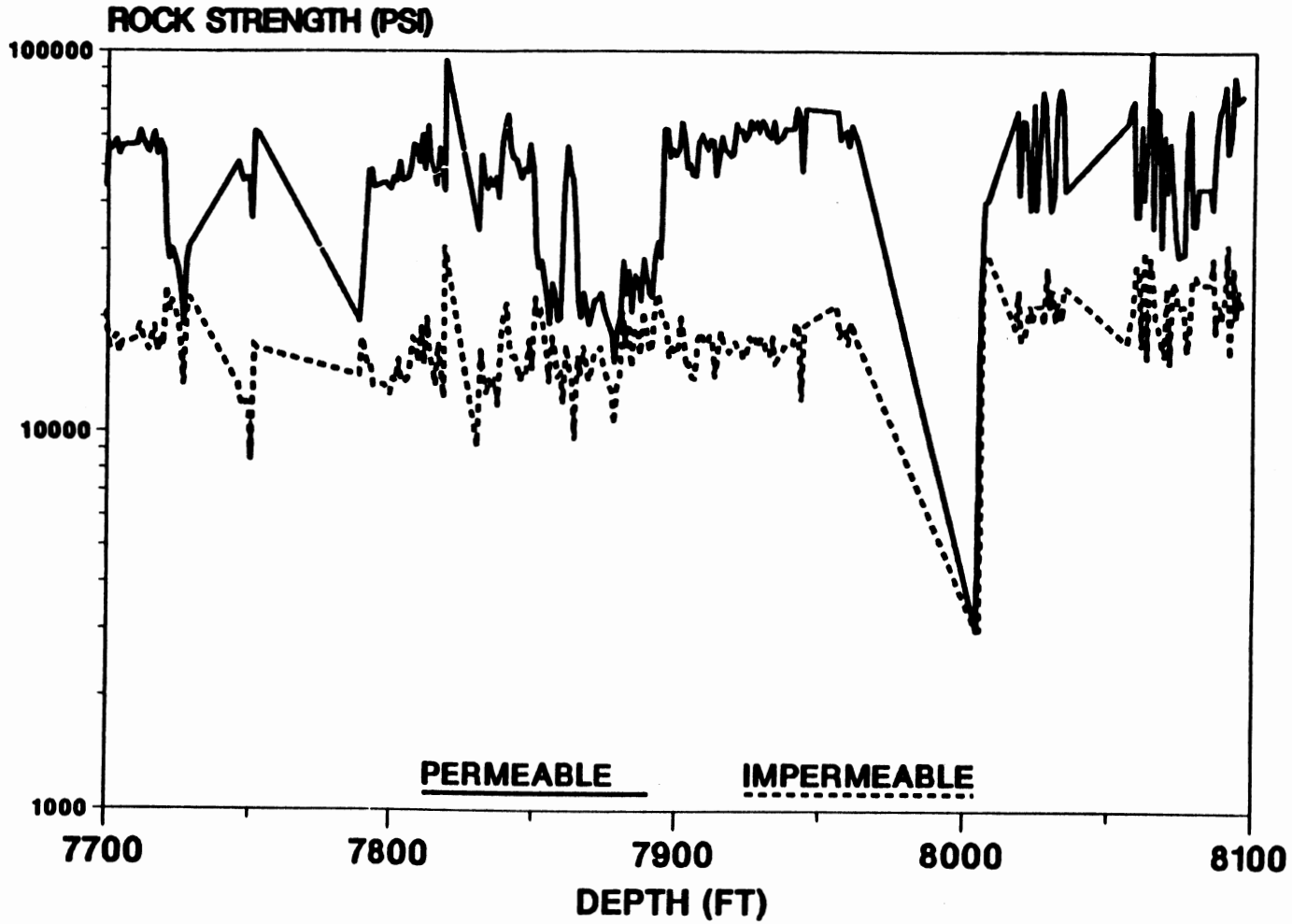

Figure 84. Section of Permeable and Impermeable Rock Strength for SFE #4 (7700 - 8100 Feet)

APPENDIX I

PERMEABLE AND IMPERMEABLE COEFFICIENT FOR EARTH AT REST PLOTS FOR SFE #1-4

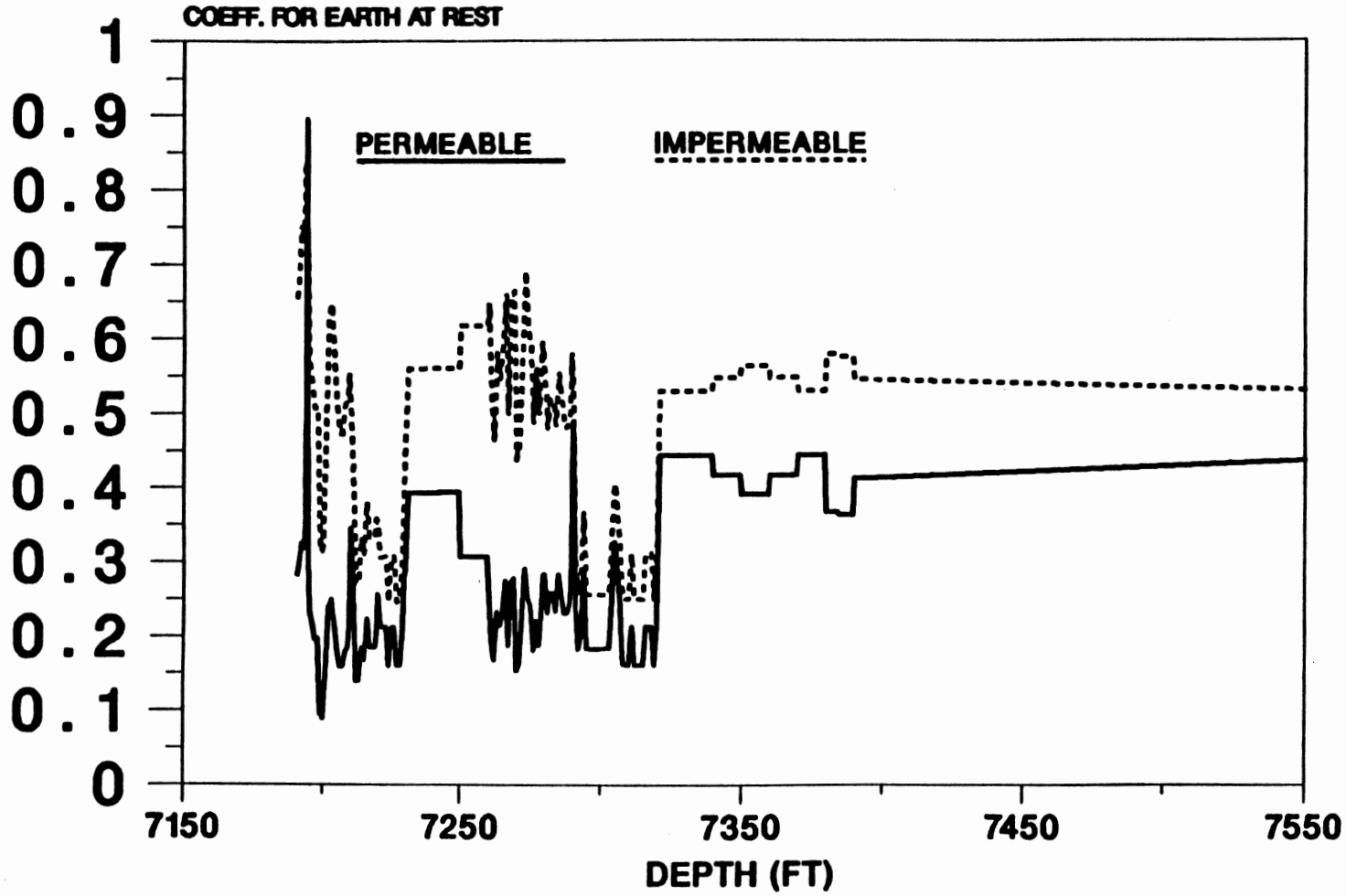

Figure 85. Section of Permeable and Impermeable Coefficient for Earth at Rest for SFE #1 (7150 - 7550 Feet)

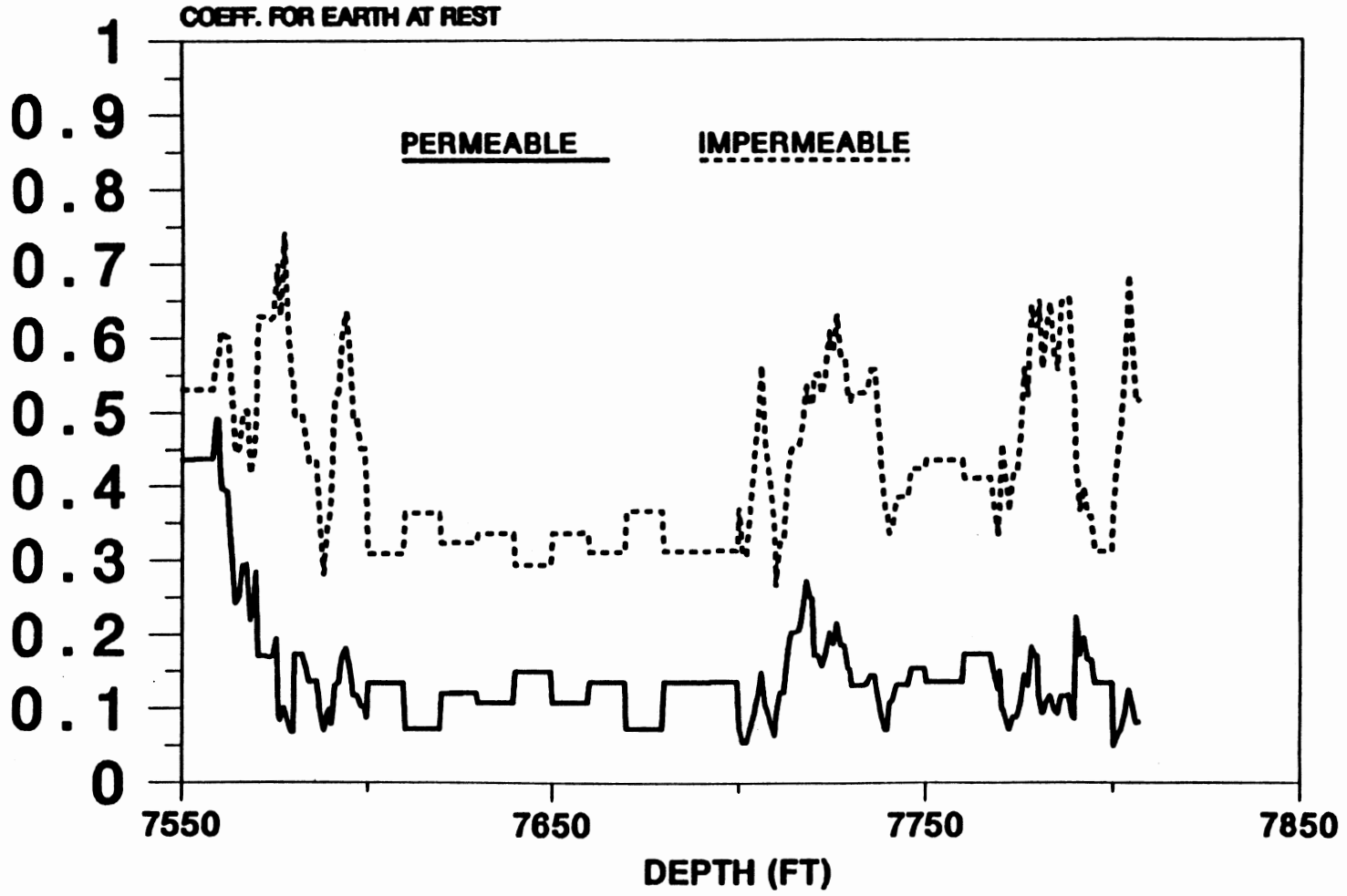

Figure 86. Section of Permeable and Impermeable Coefficient for Earth at Rest for SFE #1 (7550 - 7850 Feet)

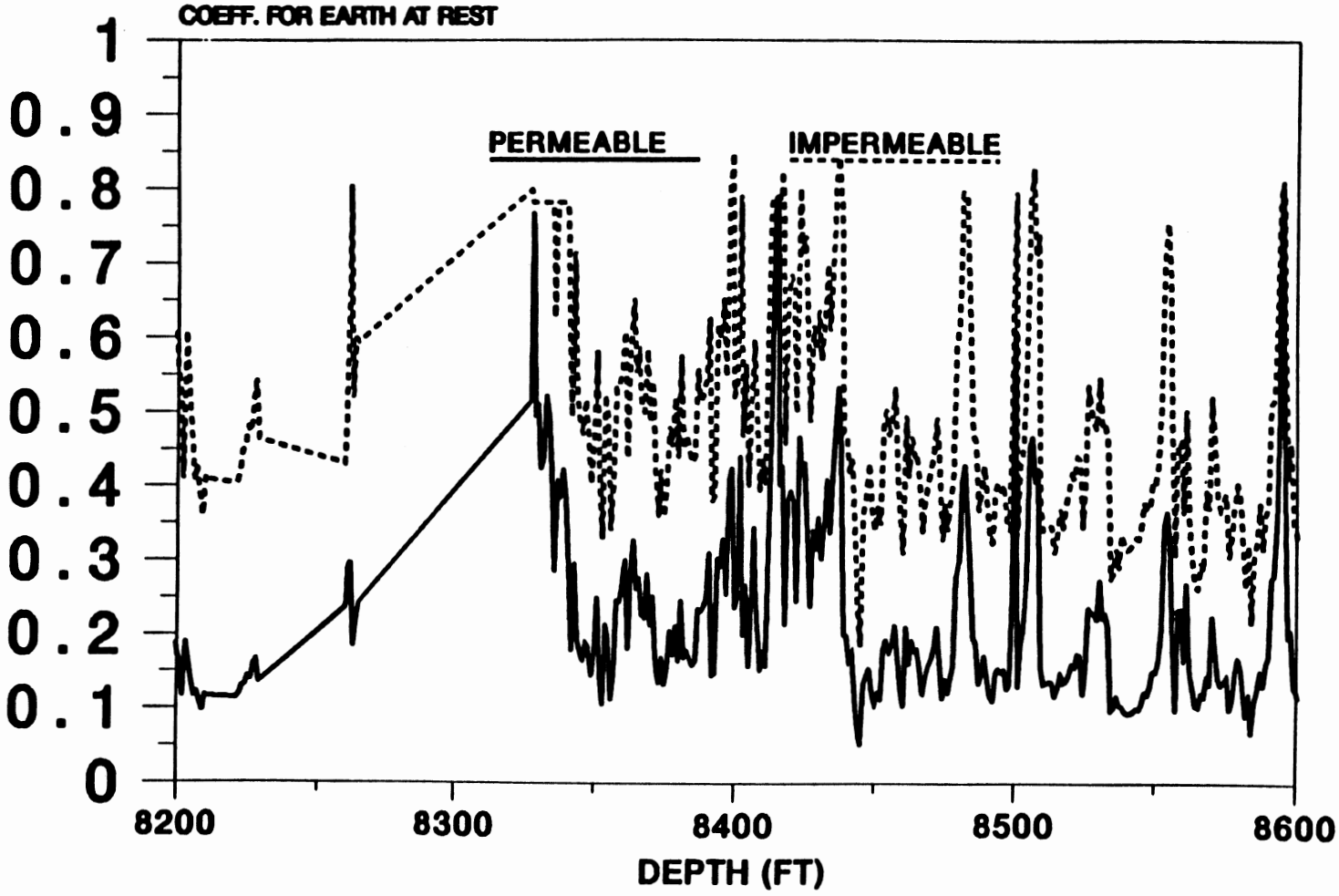

Figure 87. Section of Permeable and Impermeable Coefficient for Earth at Rest for SFE #2 (8200 - 8600 Feet)

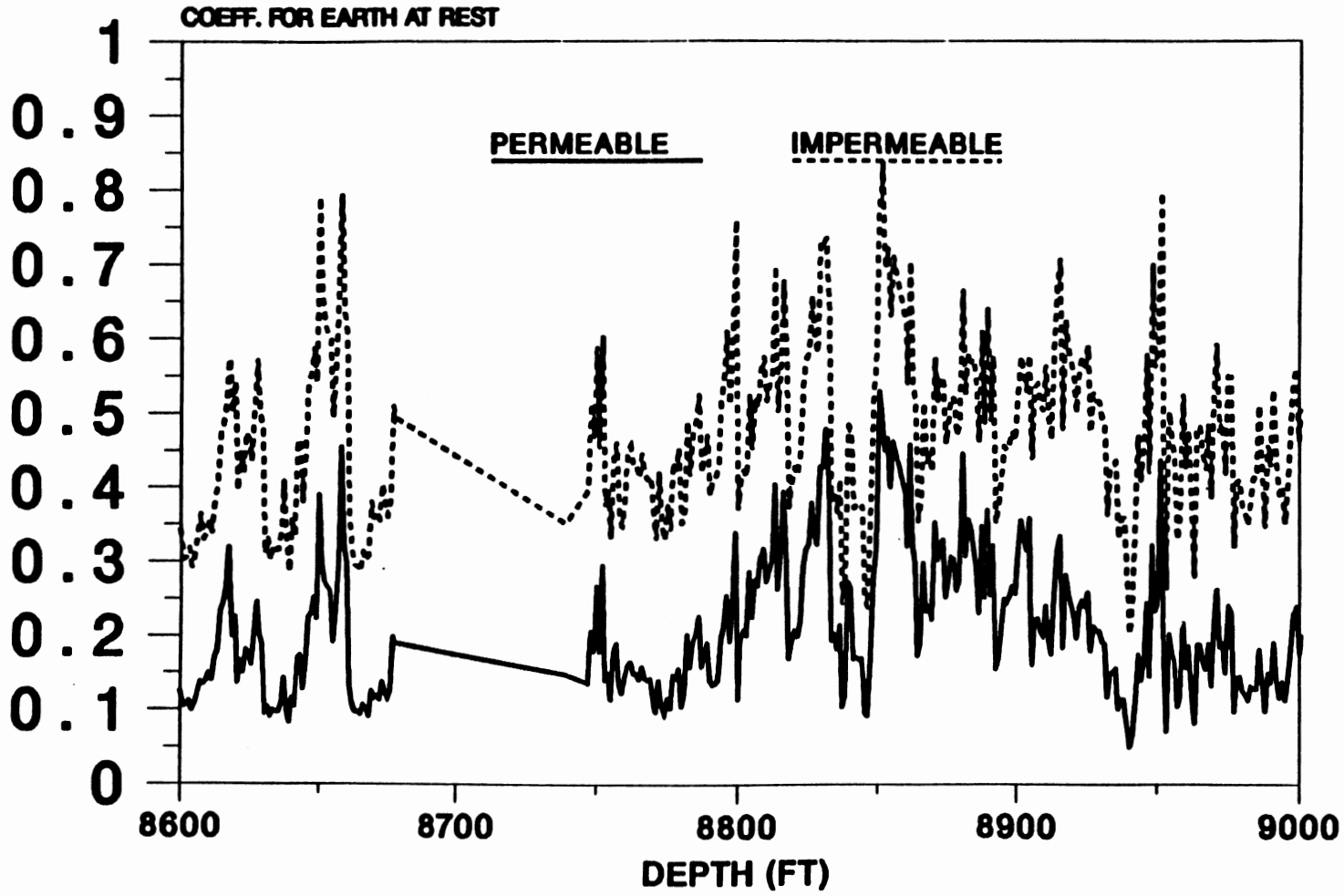

Figure 88. Section of Permeable and Impermeable Coefficient for Earth at Rest for SFE #2 (8600 - 9000 Feet)

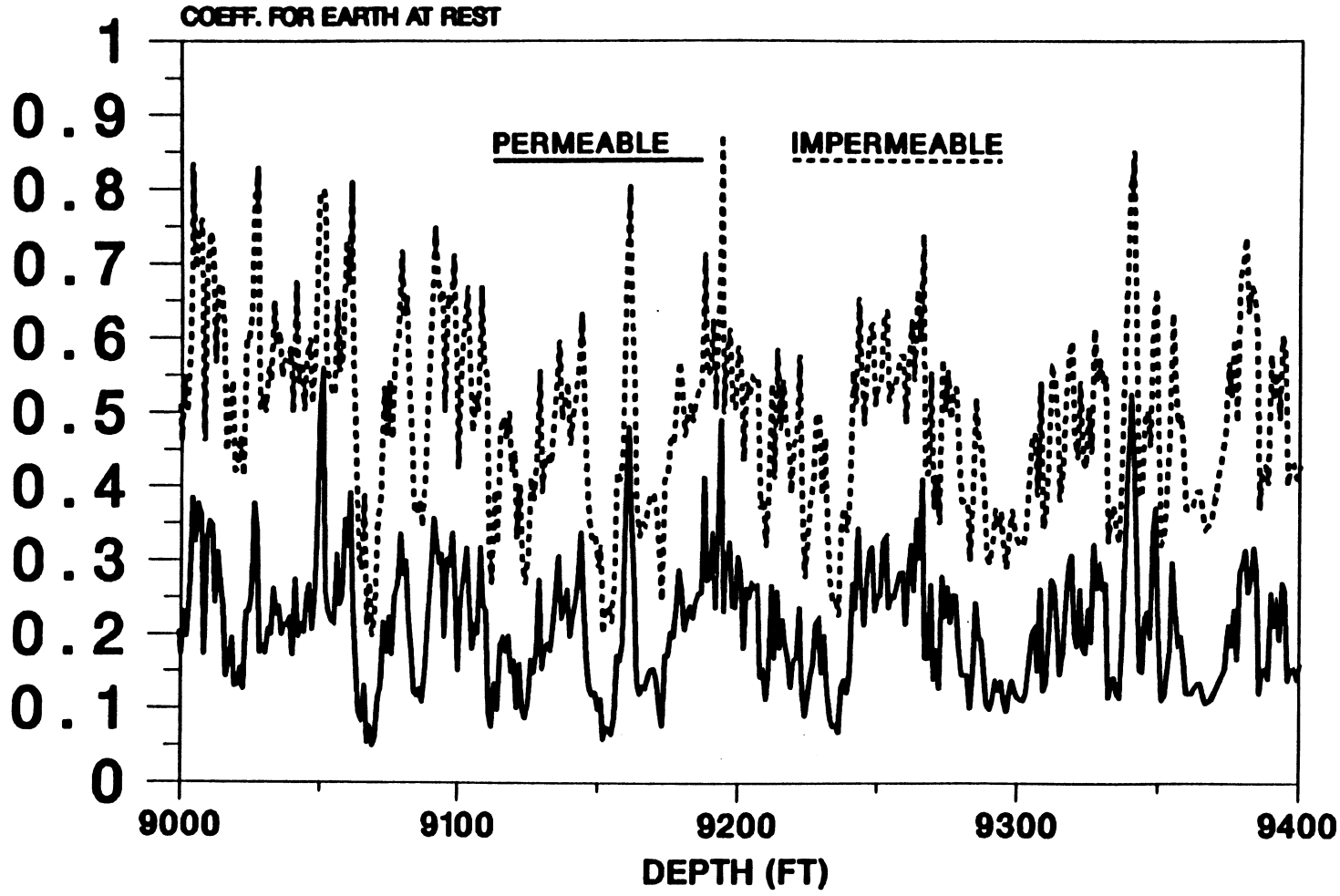

Figure 89. Section of Permeable and Impermeable Coefficient for Earth at Rest for SFE #2 (9000 - 9400 Feet)

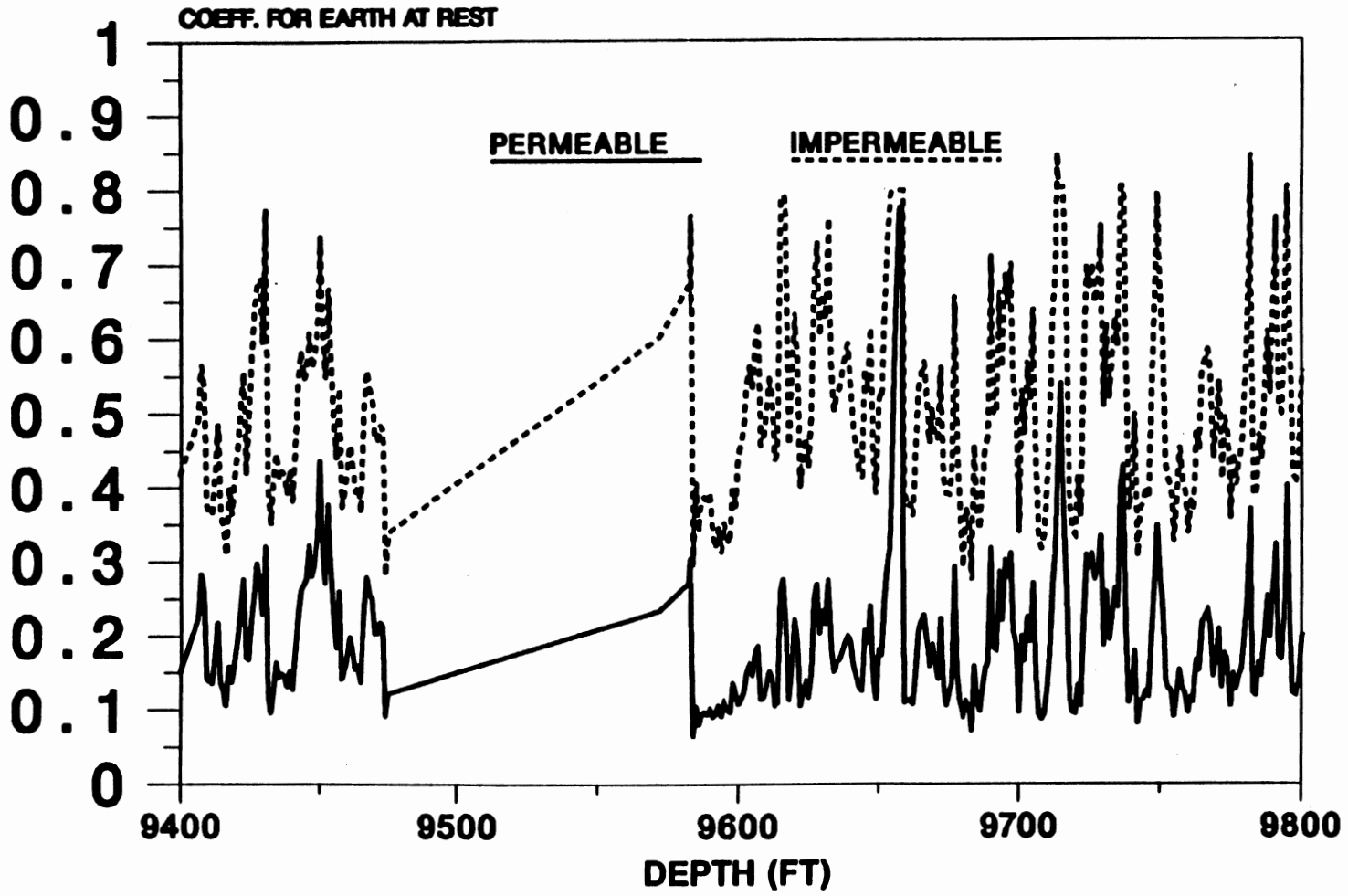

Figure 90. Section of Permeable and Impermeable Coefficient for Earth at Rest for SFE #2 (9400 - 9800 Feet)

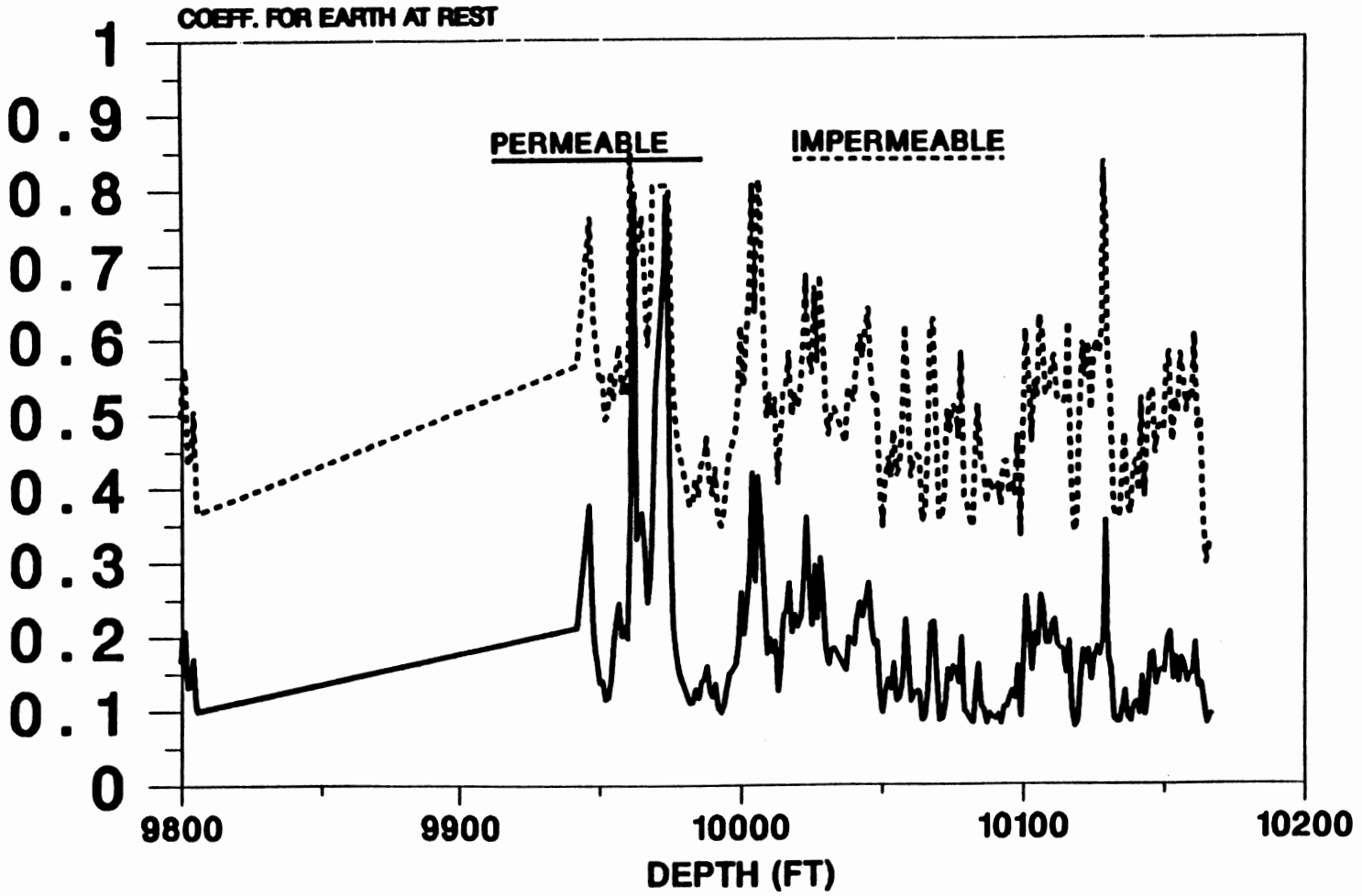

Figure 91. Section of Permeable and Impermeable Coefficient for Earth at Rest for SFE #2 (9800 - 10200 Feet)

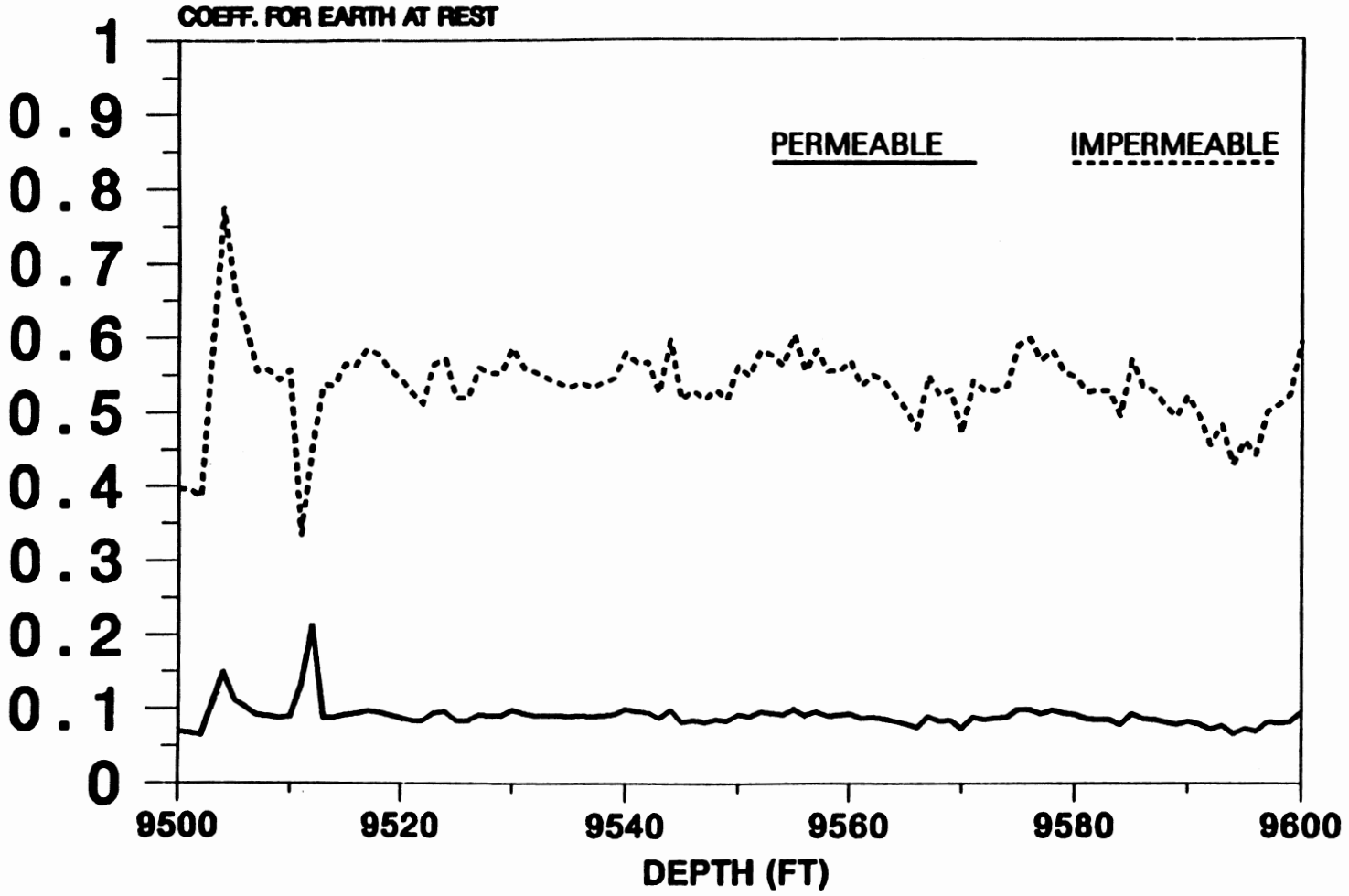

Figure 92. Section of Permeable and Impermeable Coefficient for Earth at Rest for SFE #3 (9500 - 9600 Feet)

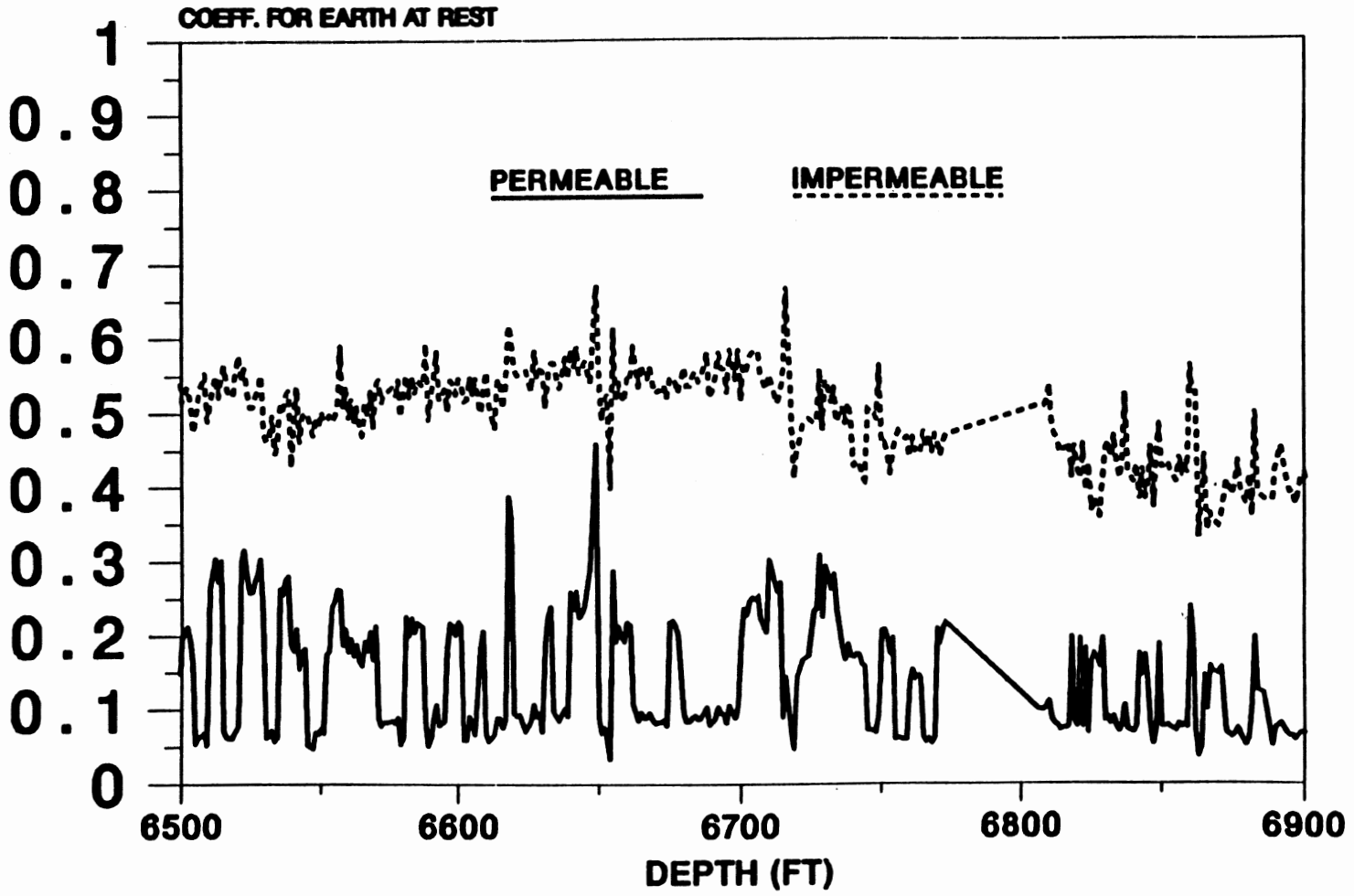

Figure 93. Section of Permeable and Impermeable Coefficient for Earth at Rest for SFE #4 (6500 - 6900 Feet)

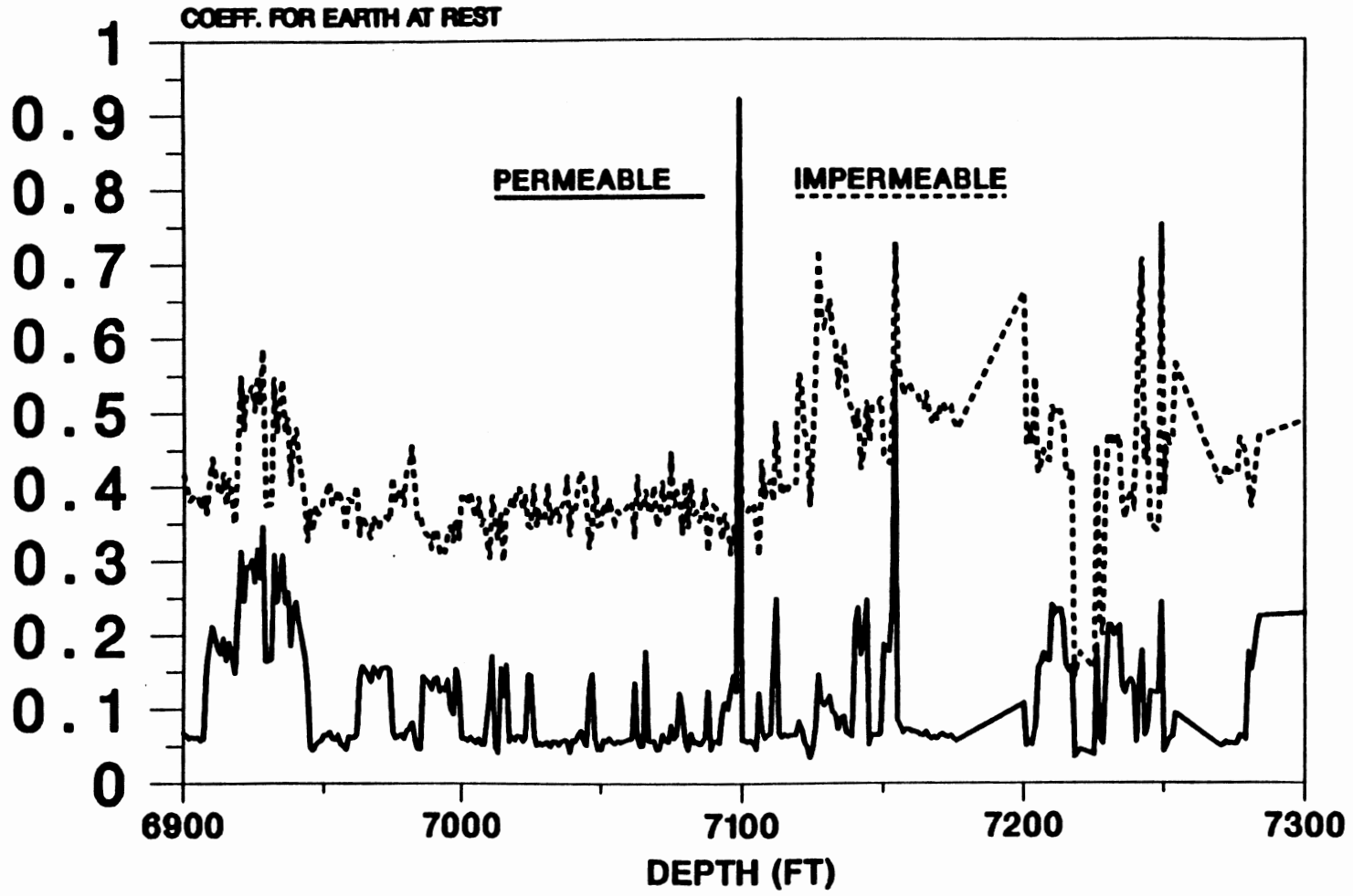

Figure 94. Section of Permeable and Impermeable Coefficient for Earth at Rest for SFE #4 (6900 - 7300 Feet)

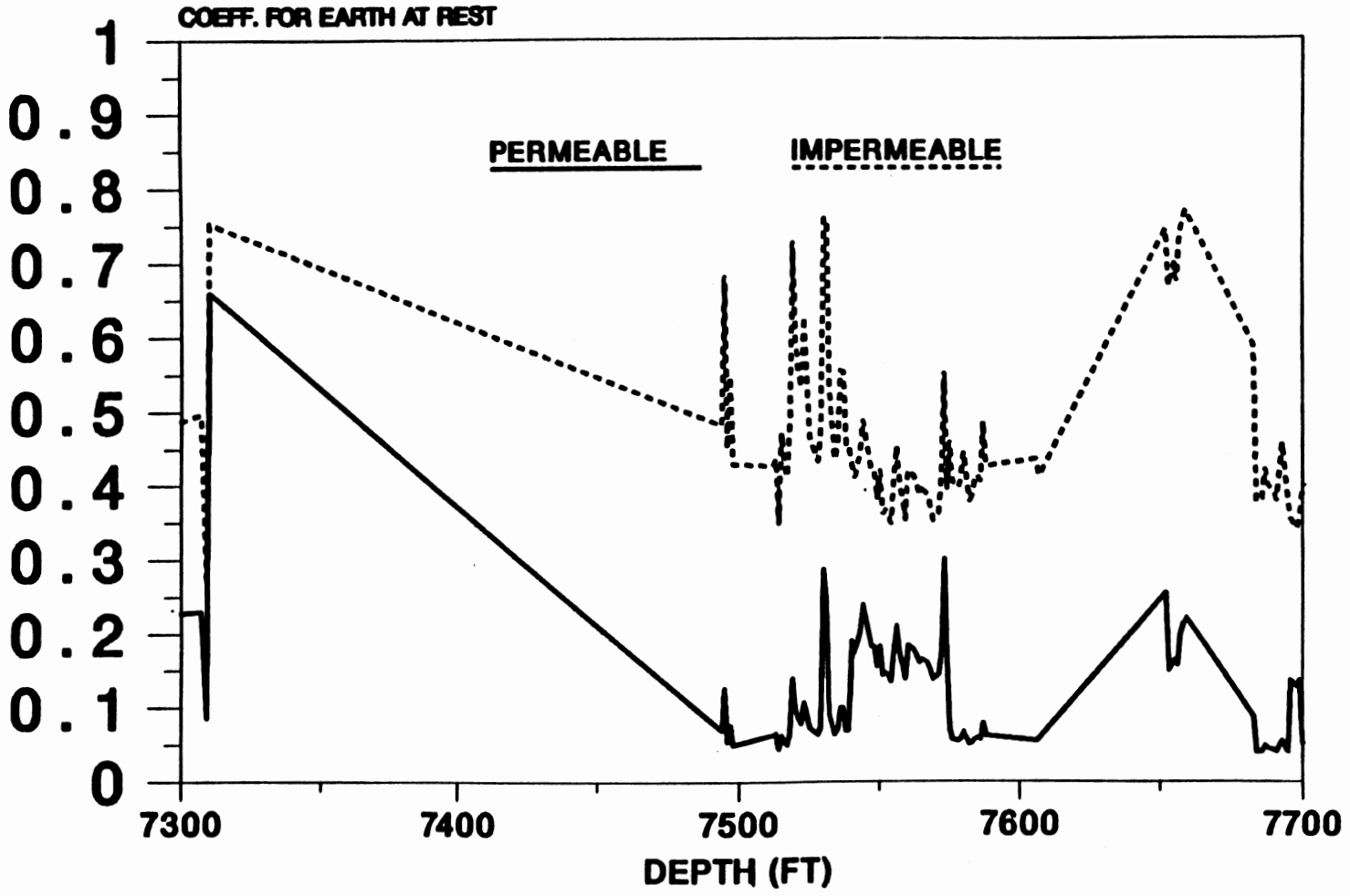

Figure 95. Section of Permeable and Impermeable Coefficient for Earth at Rest for SFE #4 (7300 - 7700 Feet)

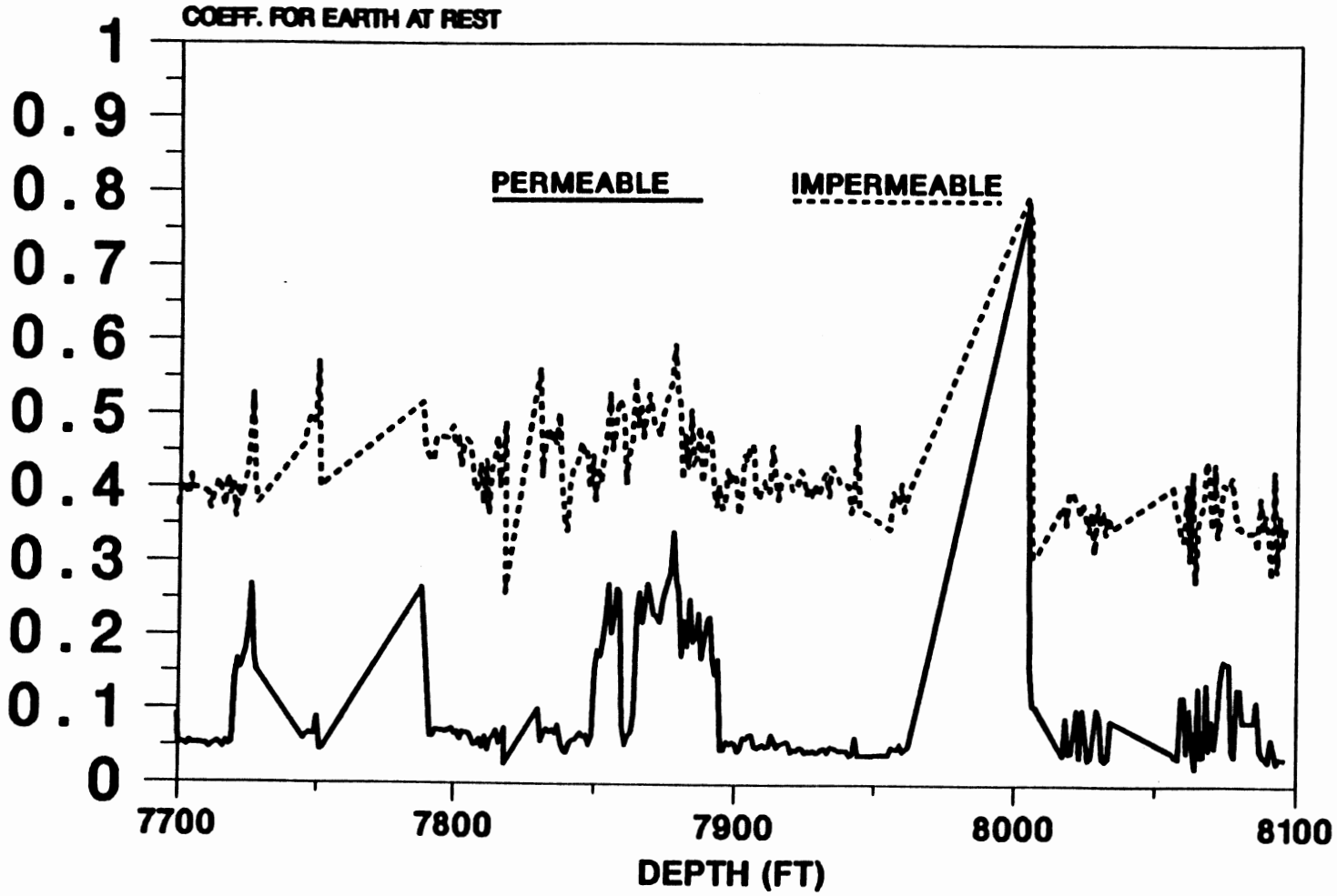

Figure 96. Section of Permeable and Impermeable Coefficient for Earth at Rest for SFE #4 (7700 - 8100 Feet)

APPENDIX J

PERMEABLE AND IMPERMEABLE ANGLE OF INTERNAL FRICTION PLOTS FOR SFE #1-4

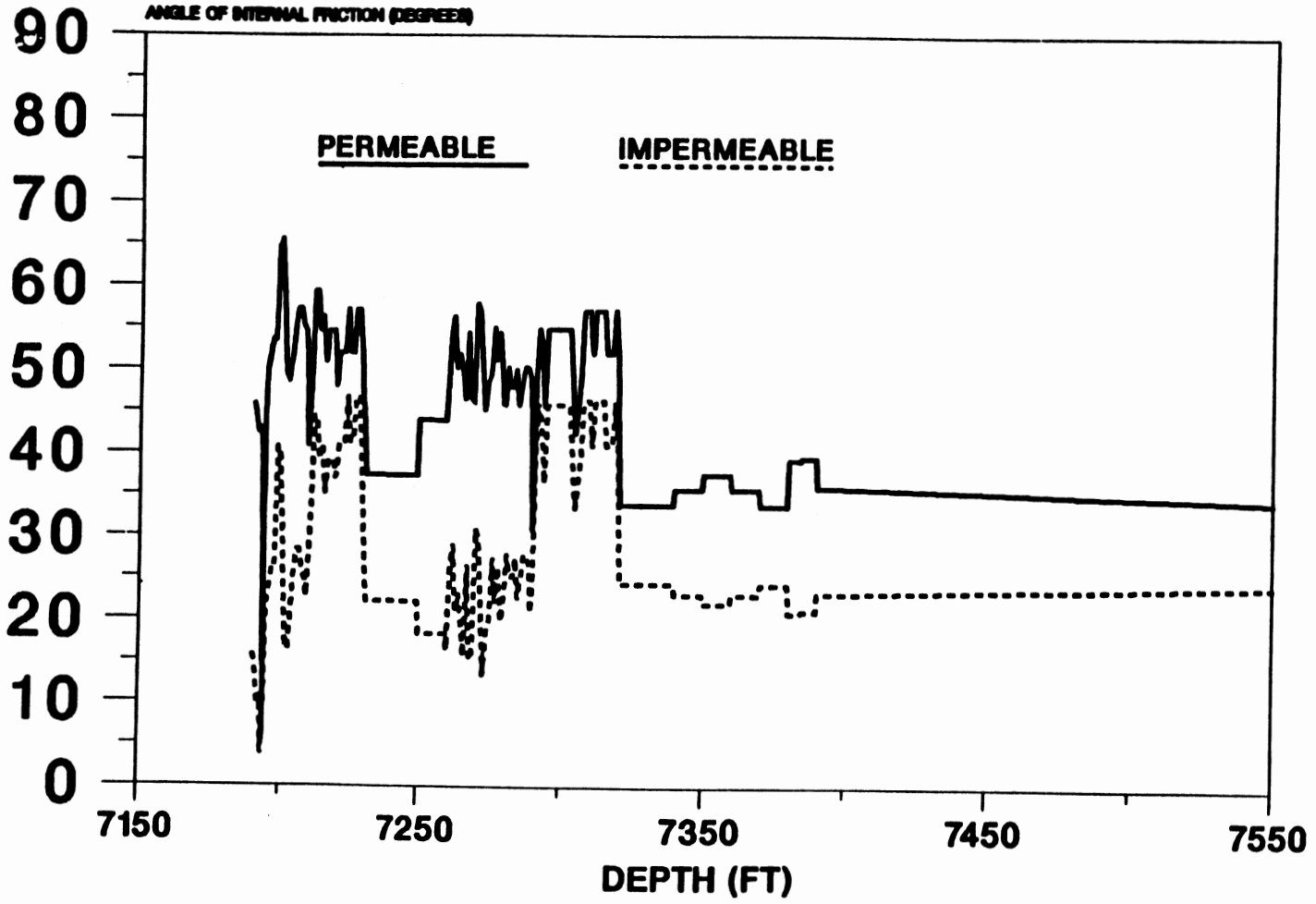

Figure 97. Section of Permeable and Impermeable Angle of Internal Friction for SFE #1 (7150 - 7550 Feet)

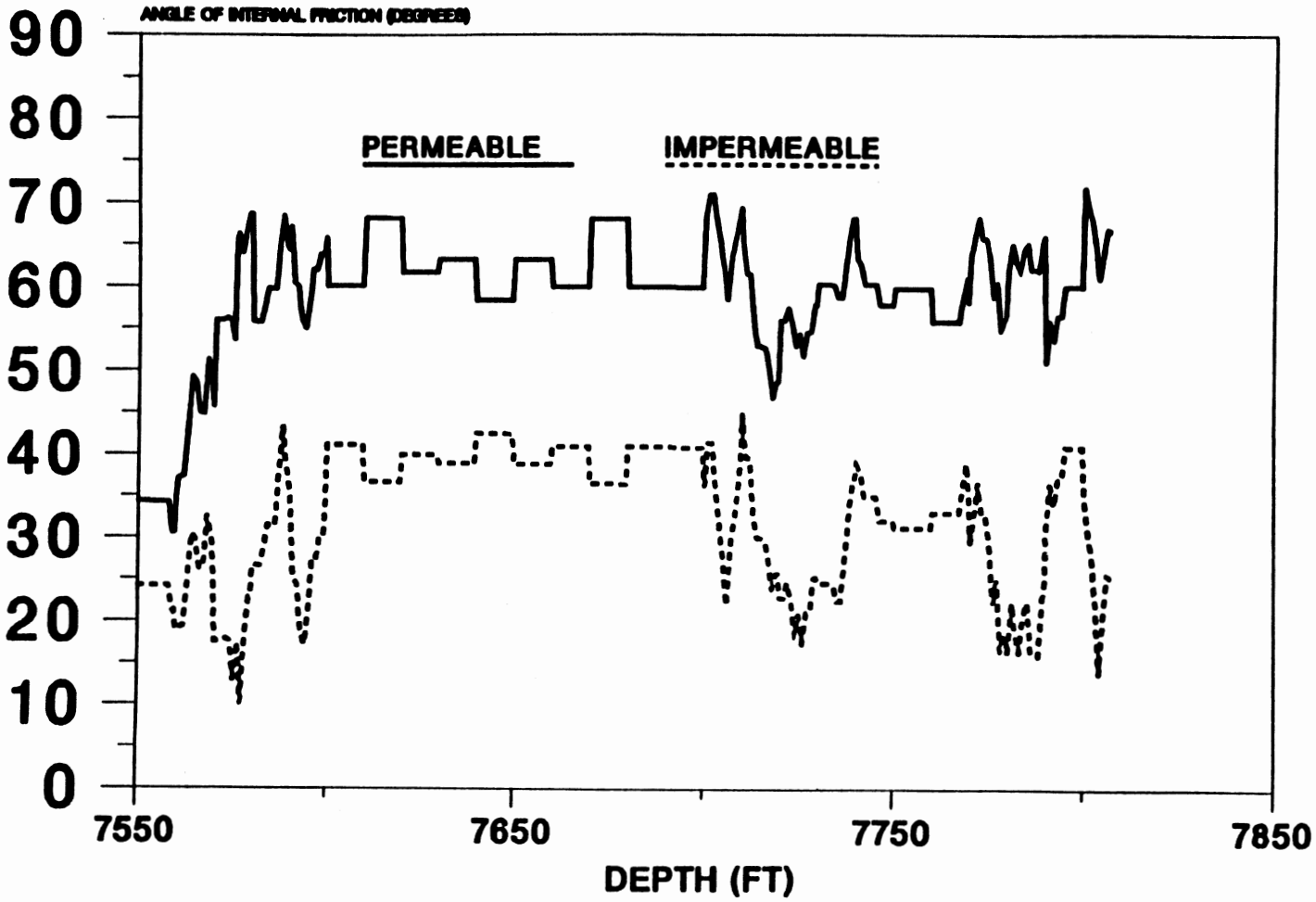

Figure 98. Section of Permeable and Impermeable Angle of Internal Friction for SFE #1 (7550 - 7850 Feet)

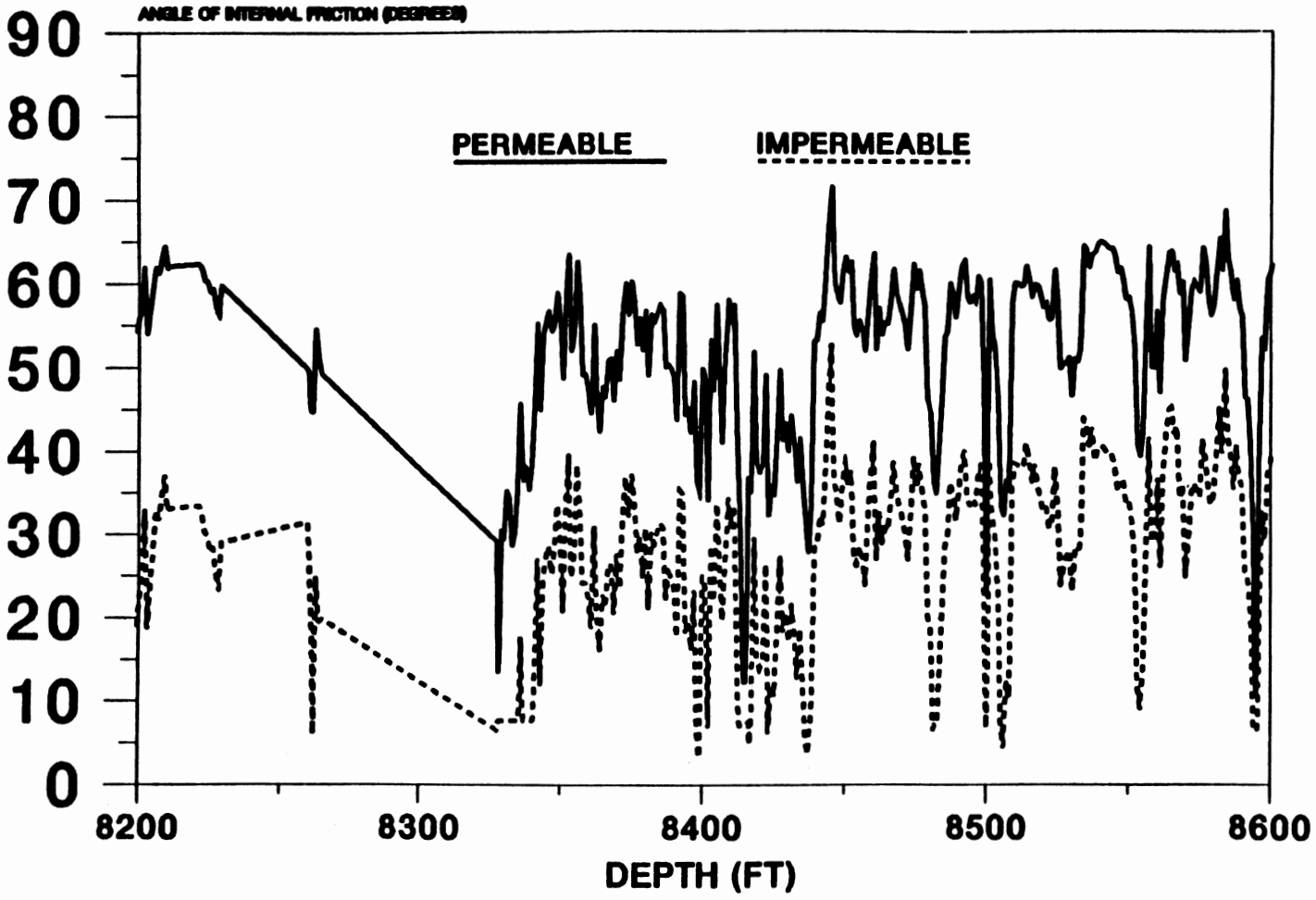

Figure 99. Section of Permeable and Impermeable Angle of Internal Friction for SFE #2 (8200 - 8600 Feet)

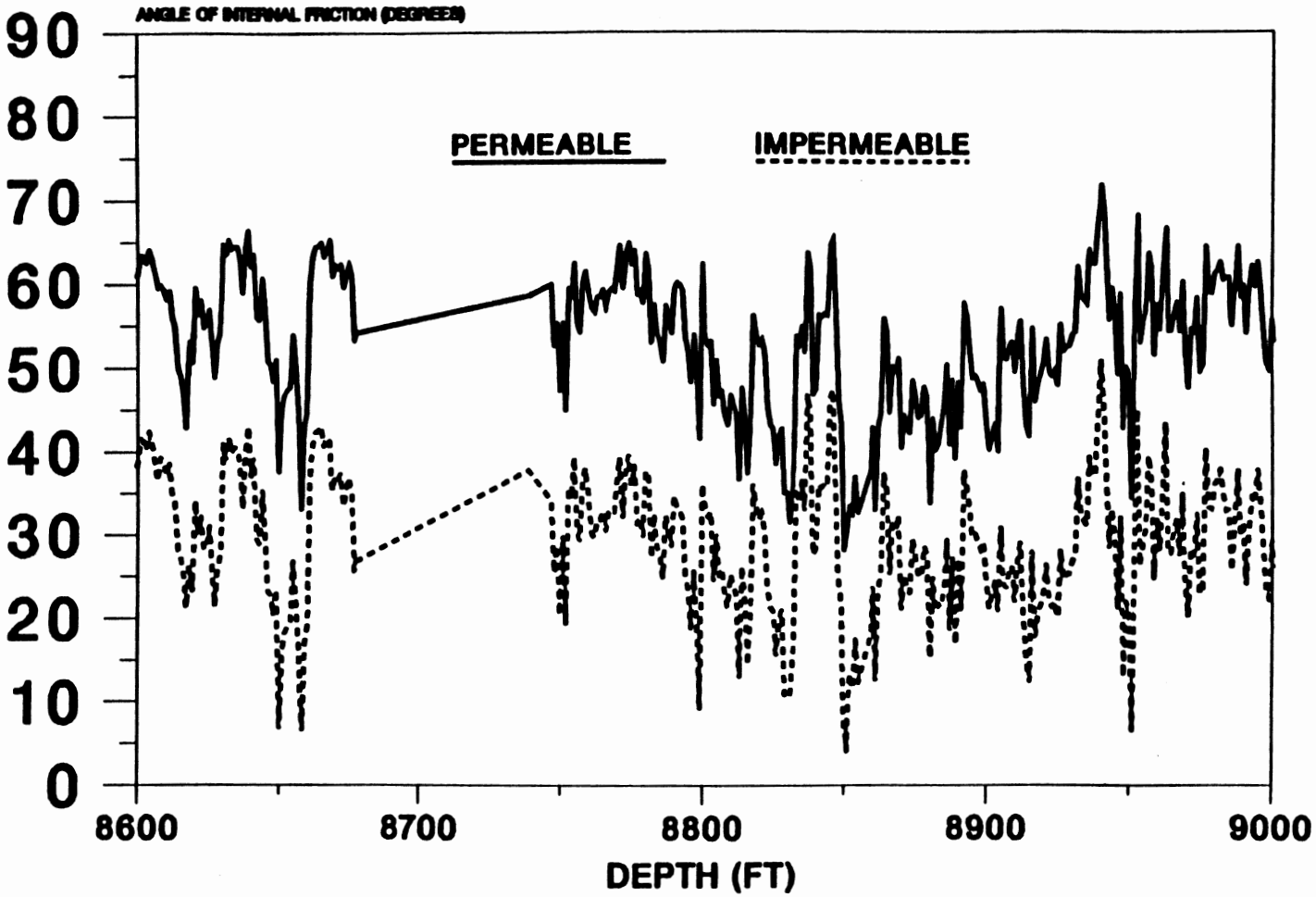

Figure 100. Section of Permeable and Impermeable Angle of Internal Friction for SFE #2 (8600 - 9000 Feet)

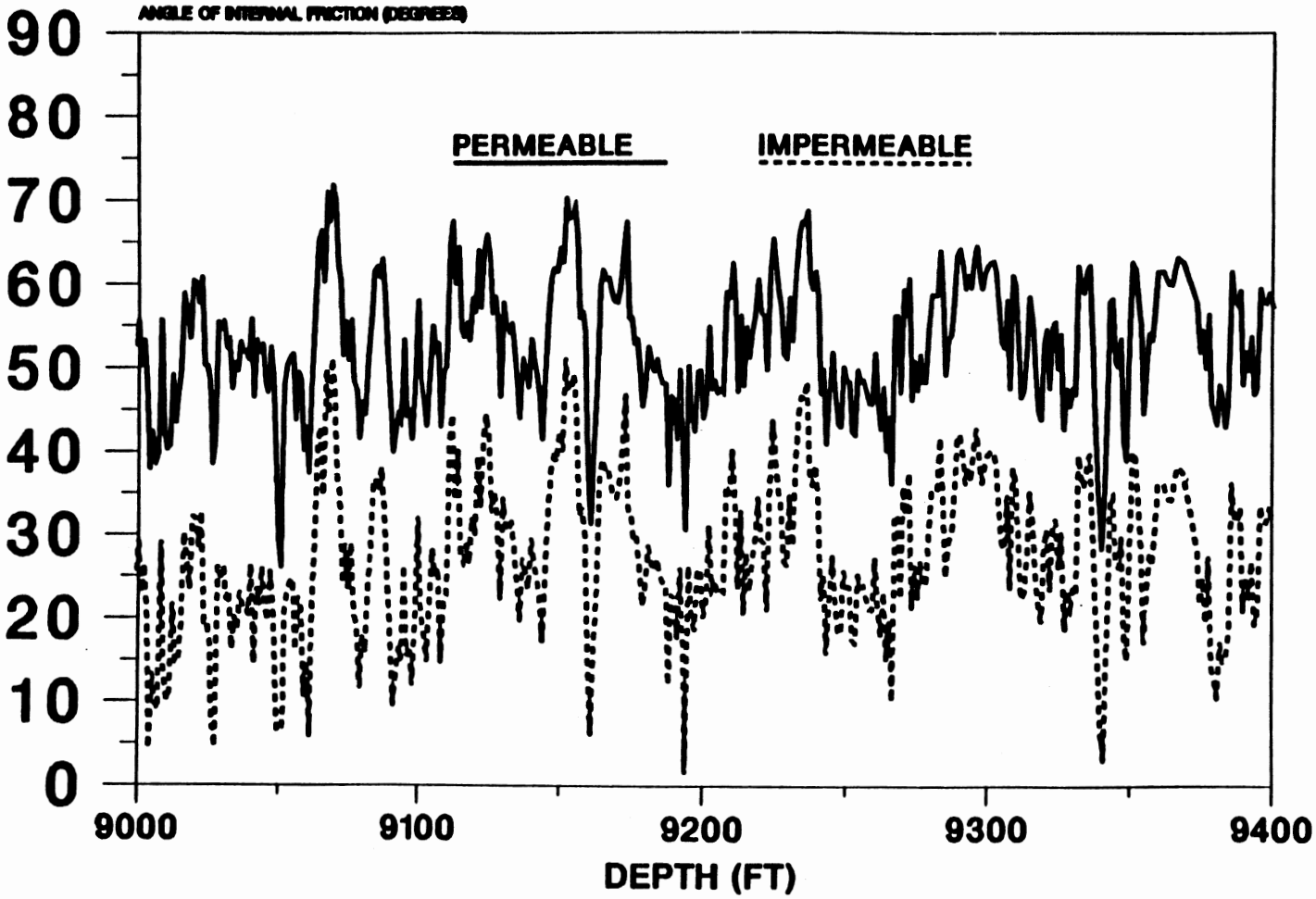

Figure 101. Section of Permeable and Impermeable Angle of Internal Friction for SFE #2 (9000 - 9400 Feet)

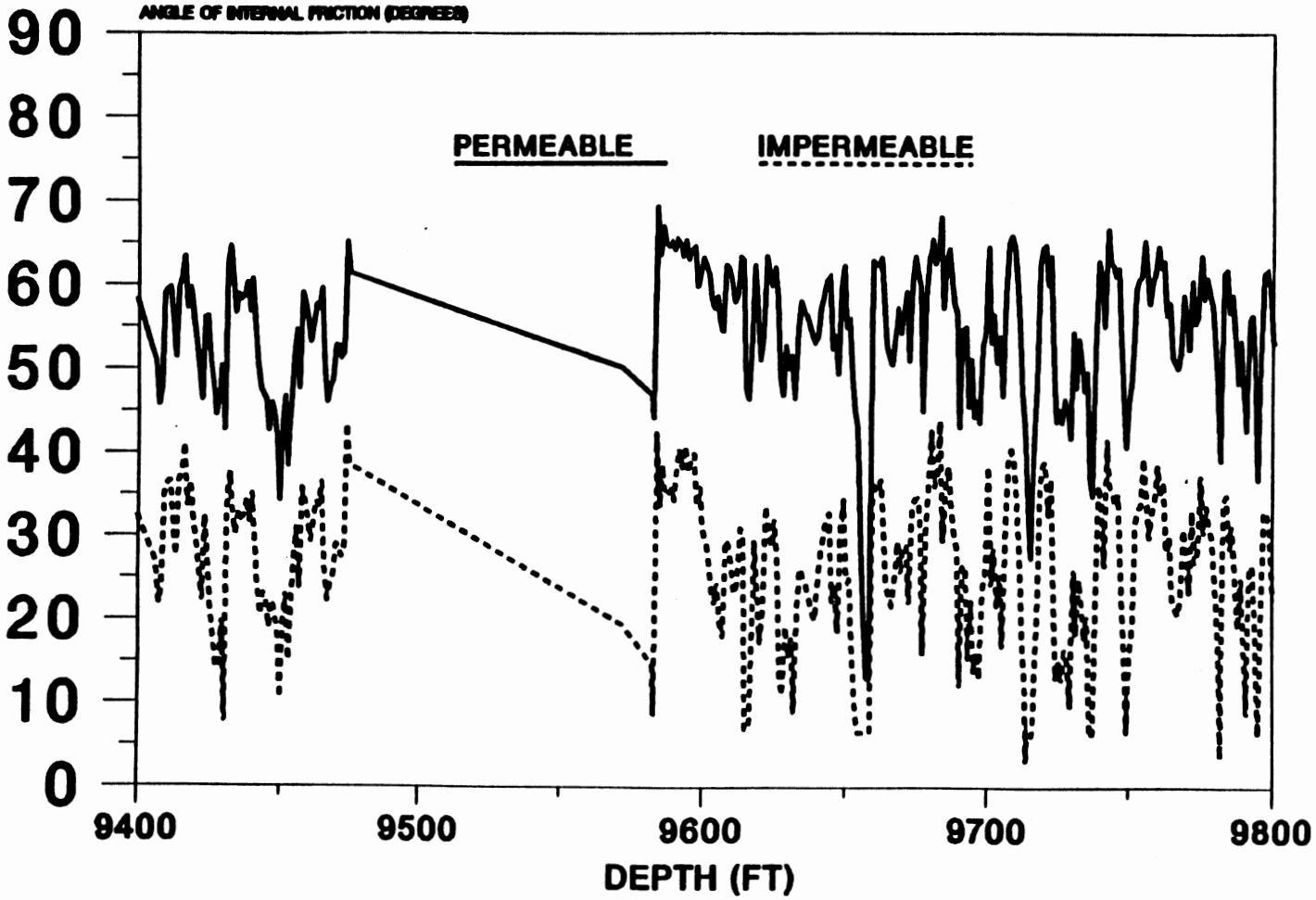

Figure 102. Section of Permeable and Impermeable Angle of Internal Friction for SFE #2 (9400 - 9800 Feet)

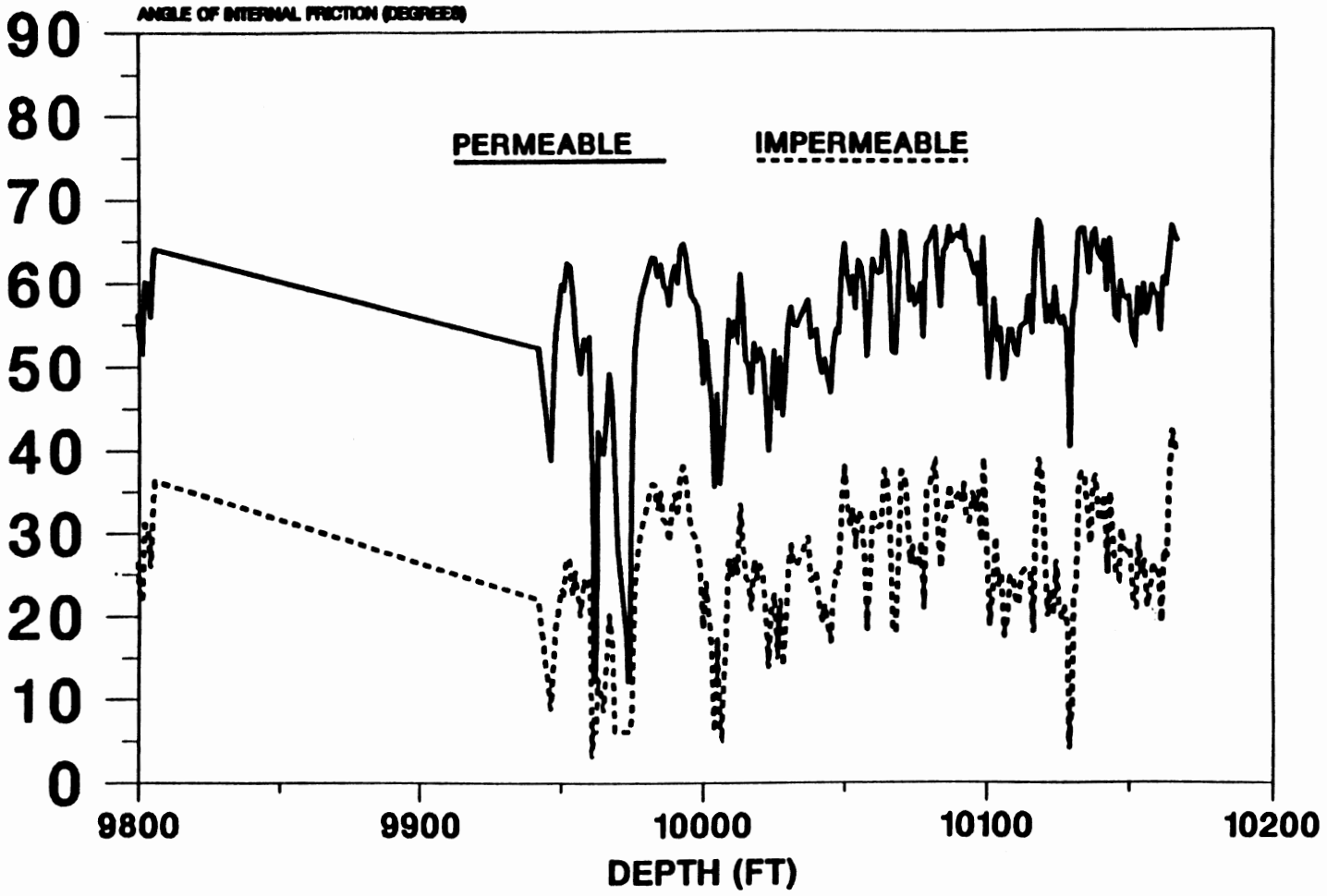

Figure 103. Section of Permeable and Impermeable Angle of Internal Friction for SFE #2 (9800 - 10200 Feet)

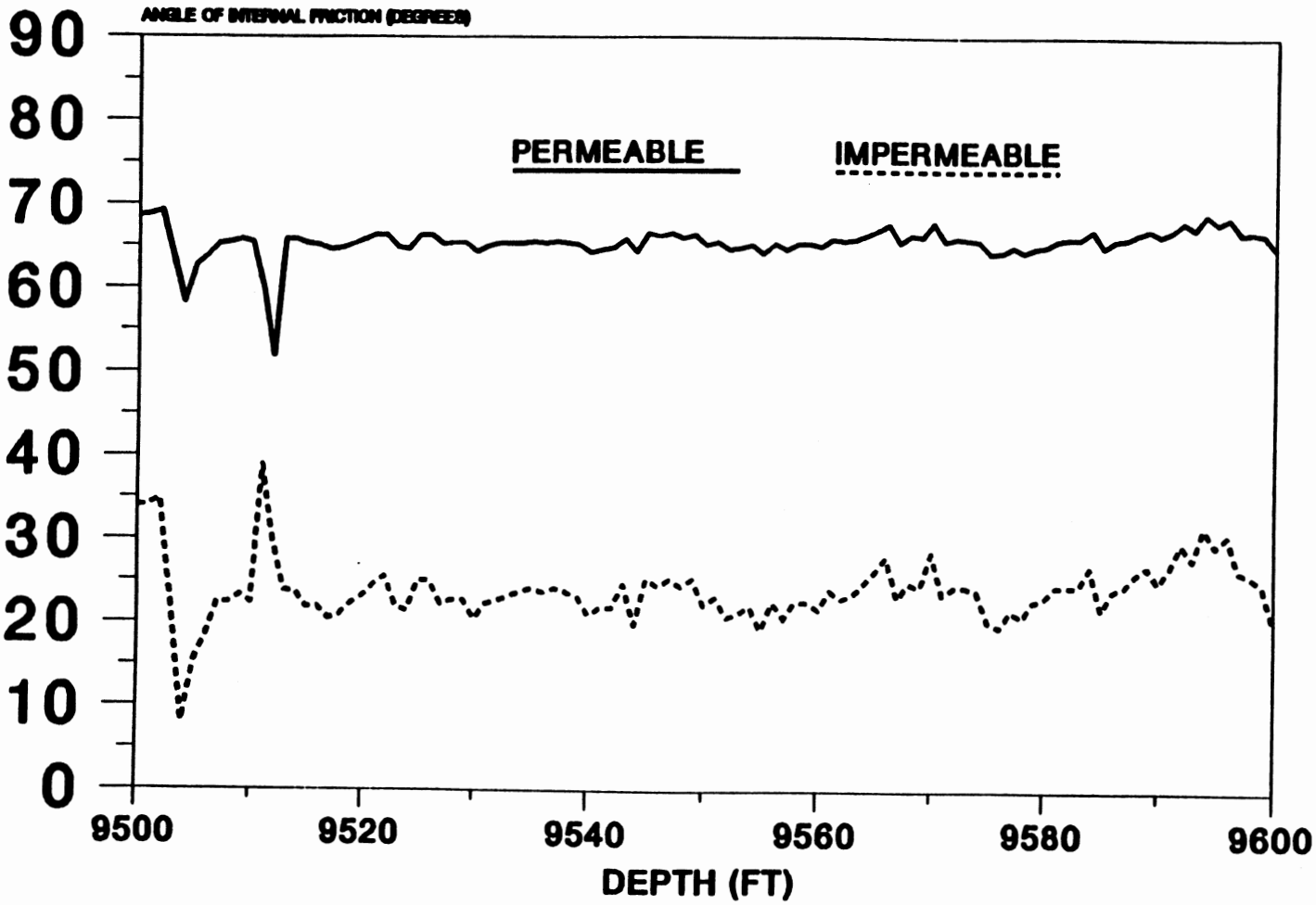

Figure 104. Section of Permeable and Impermeable Angle of Internal Friction for SFE #3 (9500 - 9600 Feet)

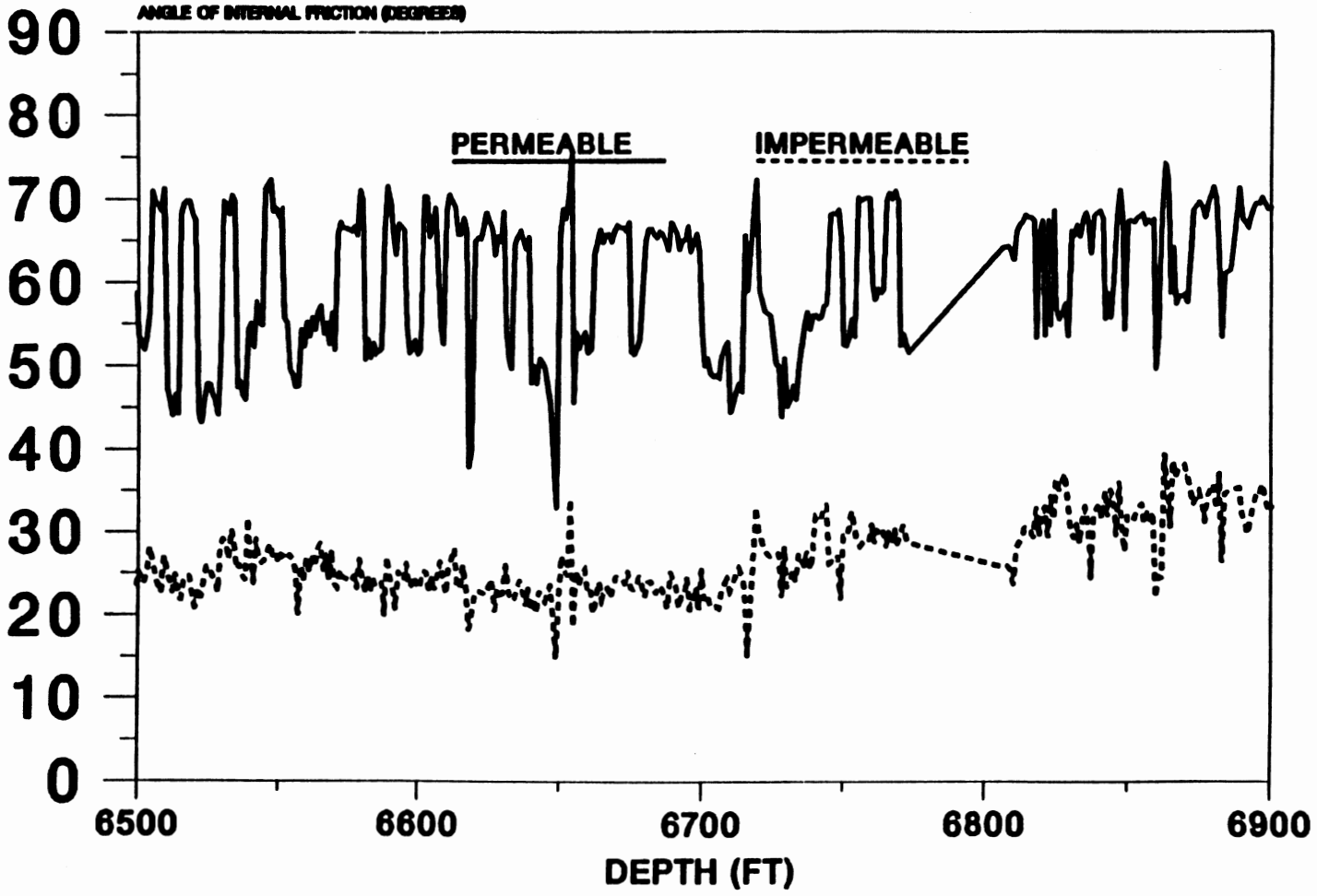

Figure 105. Section of Permeable and Impermeable Angle of Internal Friction for SFE #4 (6500 - 6900 Feet)

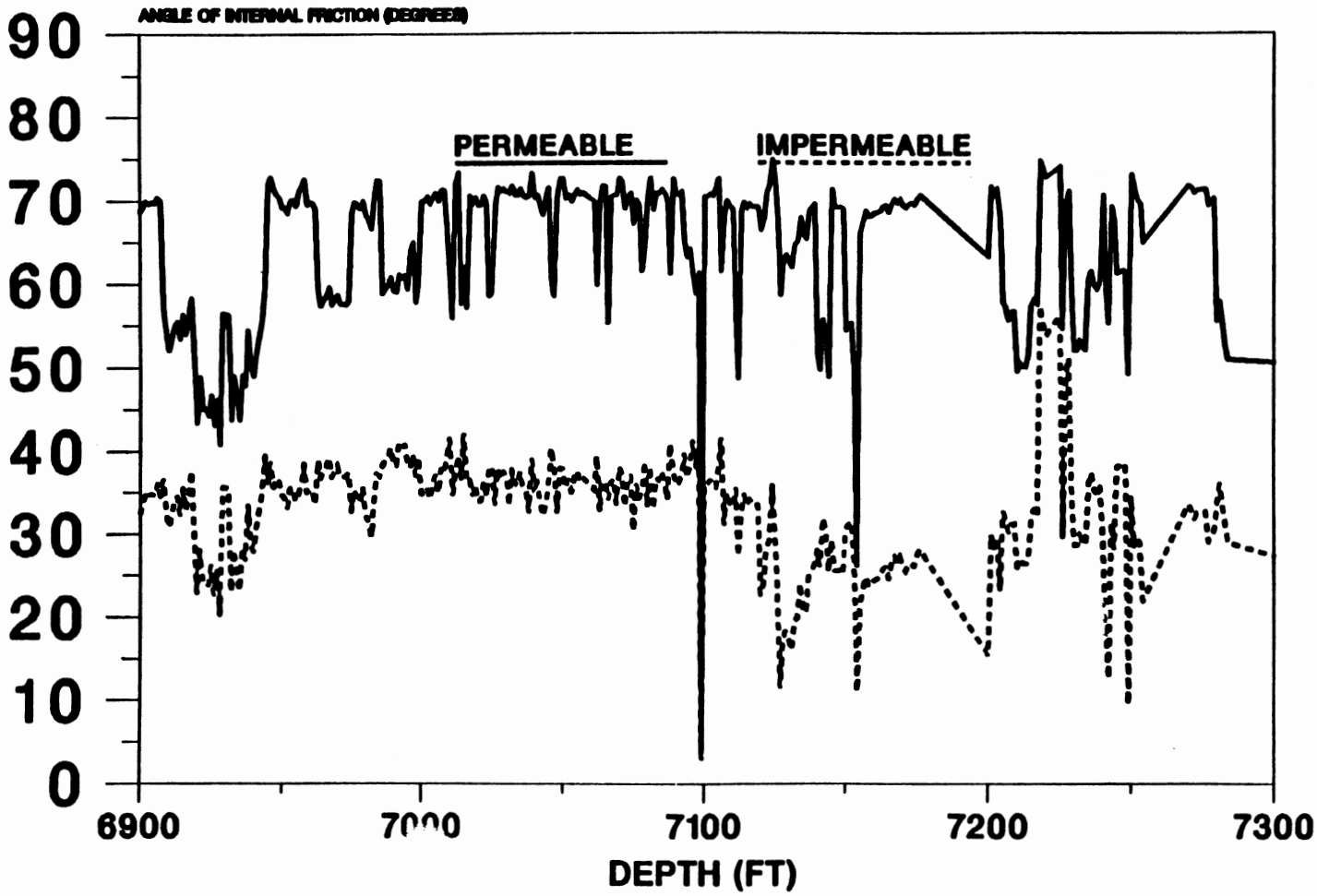

Figure 106. Section of Permeable and Impermeable Angle of Internal Friction for SFE #4 (6900 - 7300 Feet)

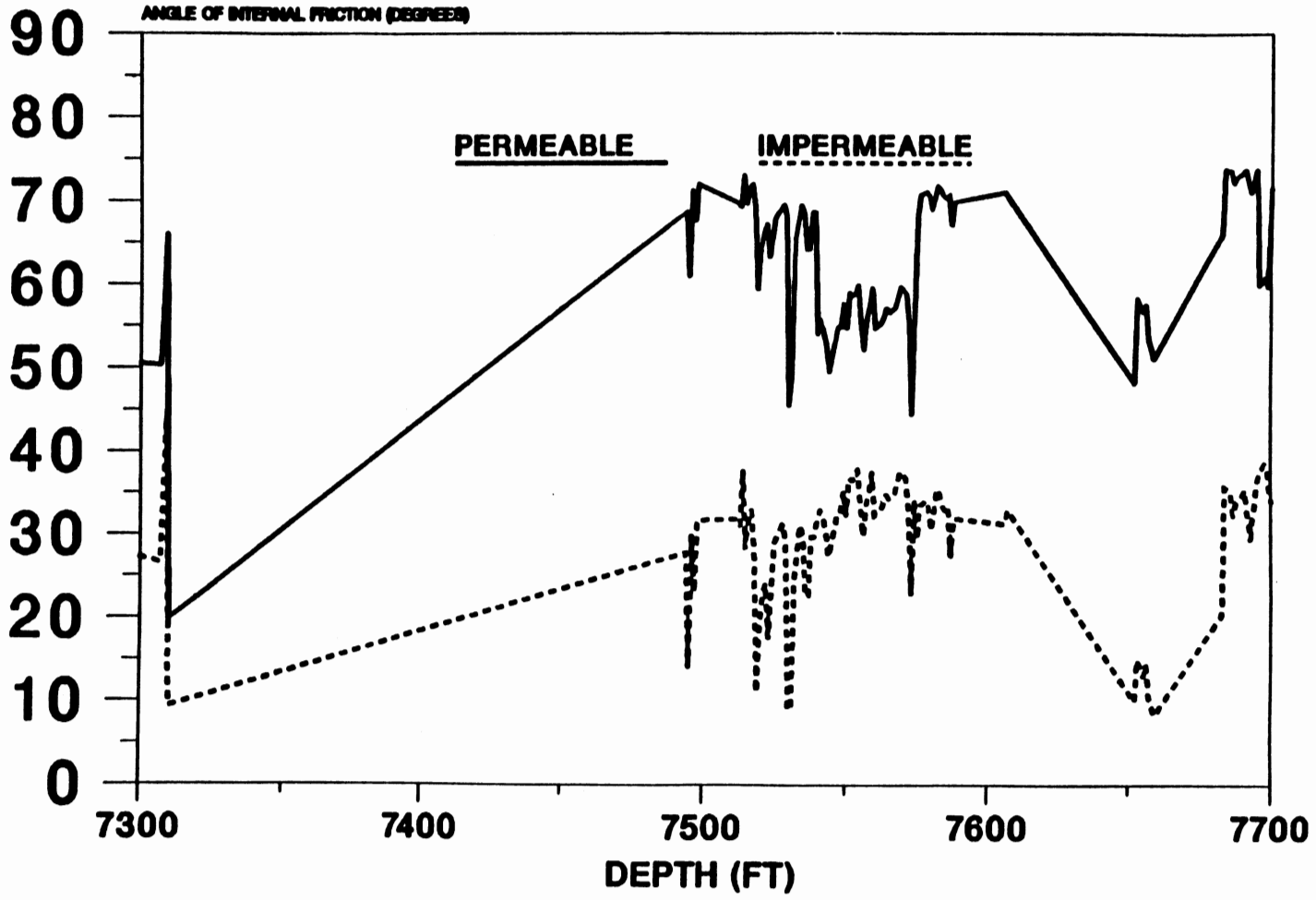

Figure 107. Section of Permeable and Impermeable Angle of Internal Friction for SFE #4 (7300 - 7700 Feet)

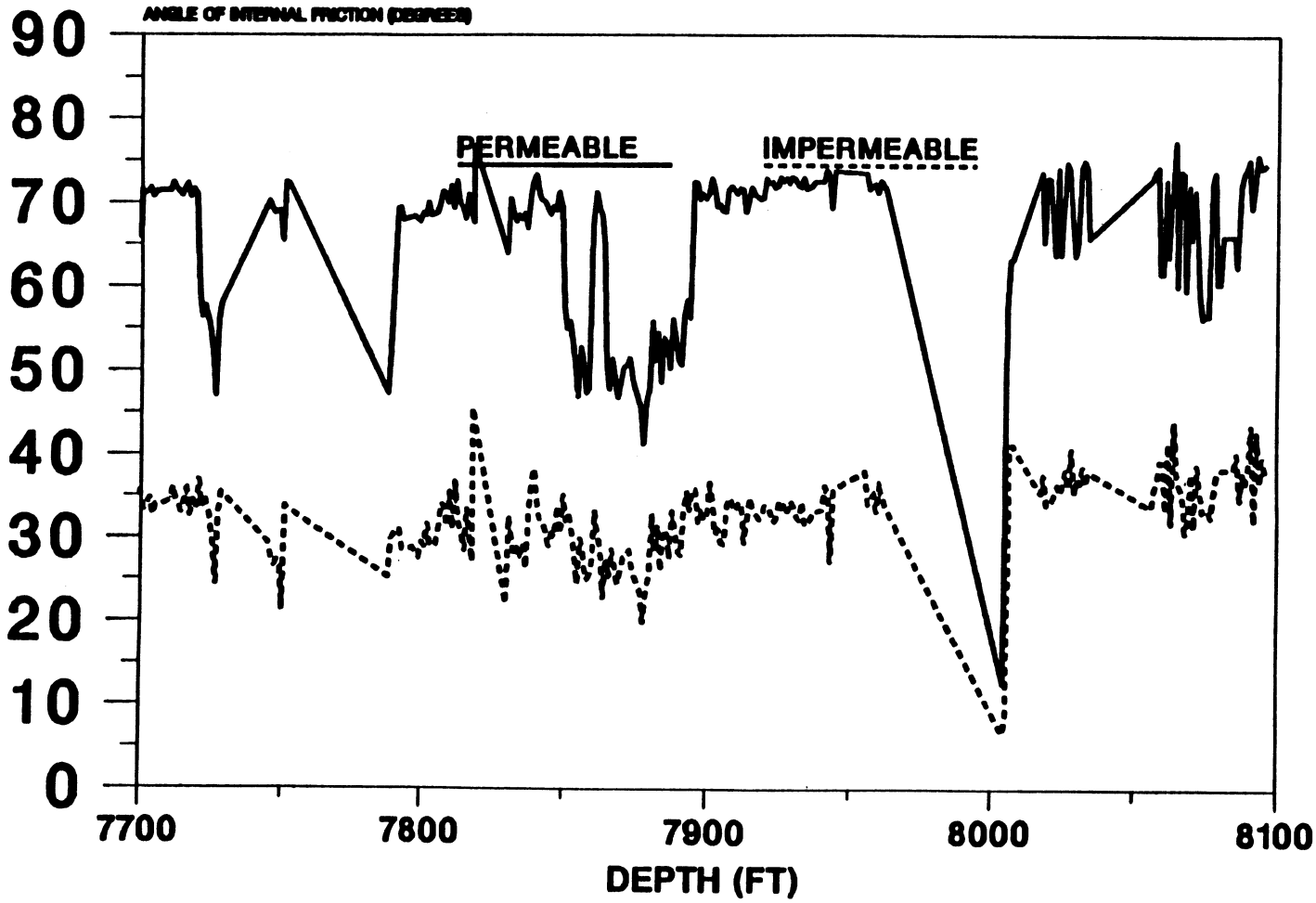

Figure 108. Section of Permeable and Impermeable Angle of Internal Friction for SFE #4 (7700 - 8100 Feet)

APPENDIX K

SENSITIVITY ANALYSIS FOR EMPIRICALLY DEVELOPED COEFFICIENTS

Sensitivity analyses were performed on the empirically developed coefficients used in the proposed approach to obtain in-situ stress bounds. Evaluations were also performed on the amount and type of laboratory drilling data used to obtain the bit coefficients.

The Amount and Type of Laboratory Drilling Data Needed for Bit Coefficients

This investigation involved using a subset of the available laboratory drilling data to obtain bit coefficients for two IADC bits, namely the 437 and the 617, to "test" against the laboratory drilling data not used to generate the bit coefficients. The "test" consisted of employing the values of the bit coefficients in the modified three term penetration rate model (6) and using this model to predict penetration rates for the conditions associated with each lab drilling data point.

For the 437 IADC code bit, three different scenarios were studied:

1) Employ part of the available laboratory drilling data in both Catoosa Shale and Carthage Limestone and test against the remaining data. The results are shown in Figure 109. The dark symbols indicate the laboratory drilling data employed, and the open symbols indicate the laboratory drilling data it was tested against. The bit coefficient values obtained using this data are listed in

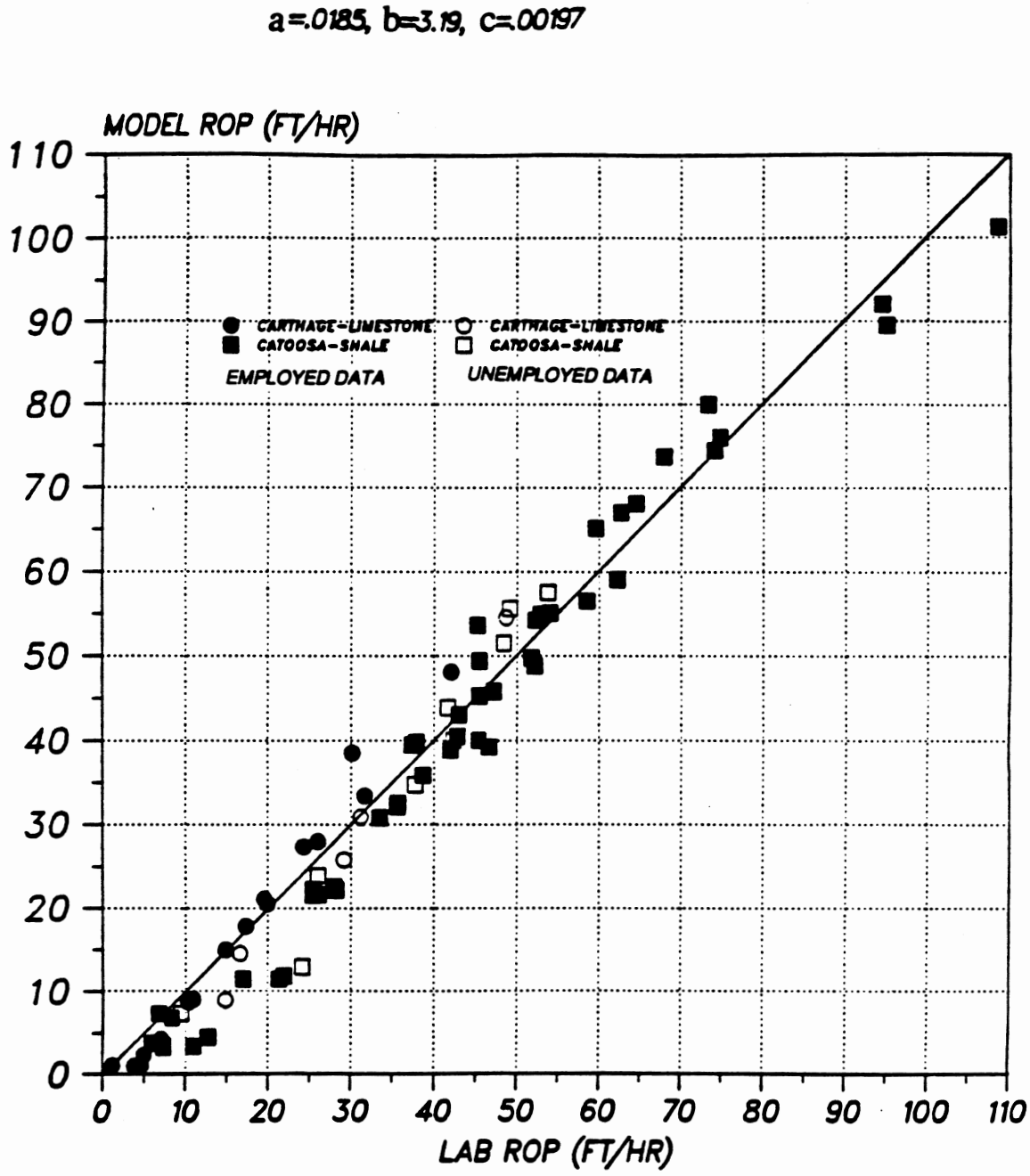

Figure 109. Bit Coefficients Developed from Part of Carthage Limestone and Catoosa Shale Drilling Data Tested Against the Other Part of the Carthage Limestone and Catoosa Shale Data for a 437 IADC Bit

Figure 109. It is seen that the unused data matched the model very well.

2) Employ the available Catoosa Shale drilling data and test against the Carthage Limestone drilling data. The results are shown in Figure 110, and it is observed that a very good match is obtained.

3) Employ the Carthage Limestone data and test against the Catoosa shale. The results are shown in Figure 111, and it can be seen that a poor match results. The bit coefficients employed for this scenario yield underpredicted values for ROP in the Catoosa Shale. This may be due to insufficiently high ROP values in the "employed" data set, such that high ROP values are not predicted well.

For the 617 IADC bit, two scenarios were investigated:

4) Employ the Catoosa Shale and Bedford Limestone data, and test against the Carthage Limestone data. The results in Figure 112 show a reasonable match.

5) Employ the Carthage Limestone and Catoosa Shale data and test against the Bedford Limestone data. The results in Figure 113 shows a reasonable match.

Sensitivity of In-Situ Stress Bounds, Coefficient for Earth at Rest and Rock Strength to Changes in Empirically Developed Coefficients

The evaluation of empirically developed coefficients for the bit, rock strength, and chip hold-down was accomplished by varying the

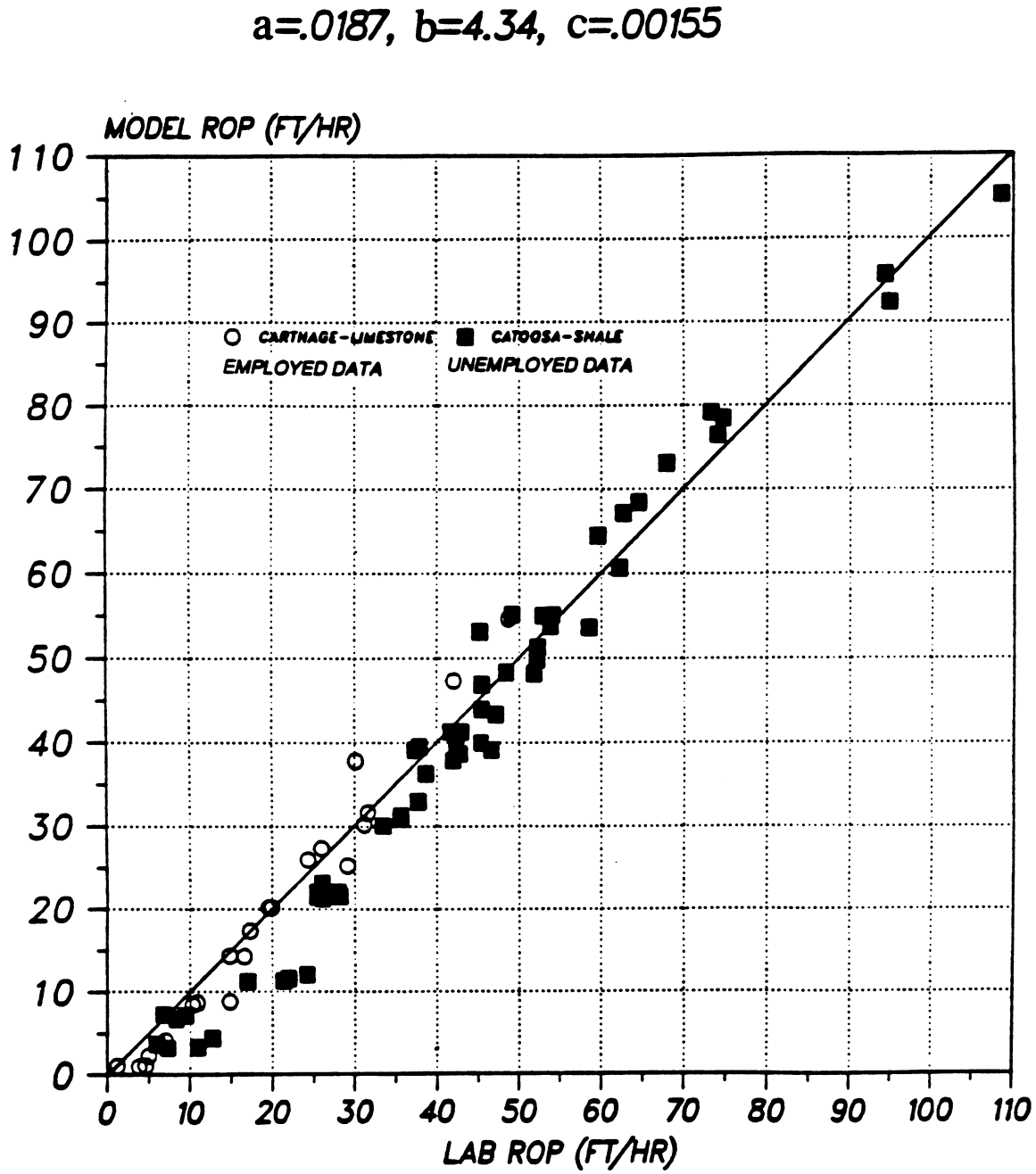

Figure 110. Bit Coefficients Developed from Catoosa Shale Drilling Data Tested Against Carthage Limestone Drilling Data for a 437 IADC Bit

a=.0166, b=1.76, c=.00392

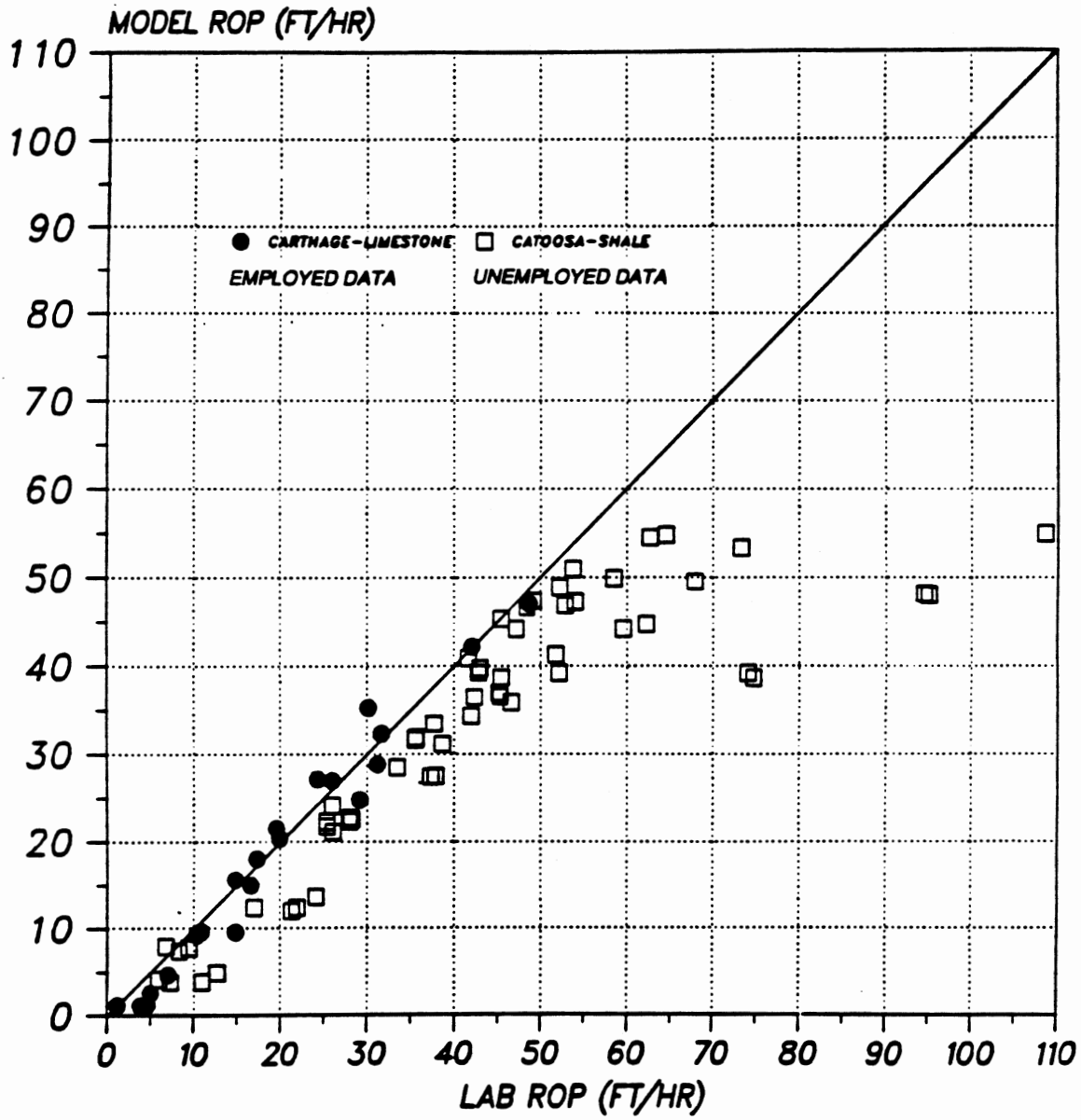

Figure 111. Bit Coefficients Developed from Carthage Limestone Drilling Data Tested Against Catoosa Shale Drilling Data for a 437 IADC Bit

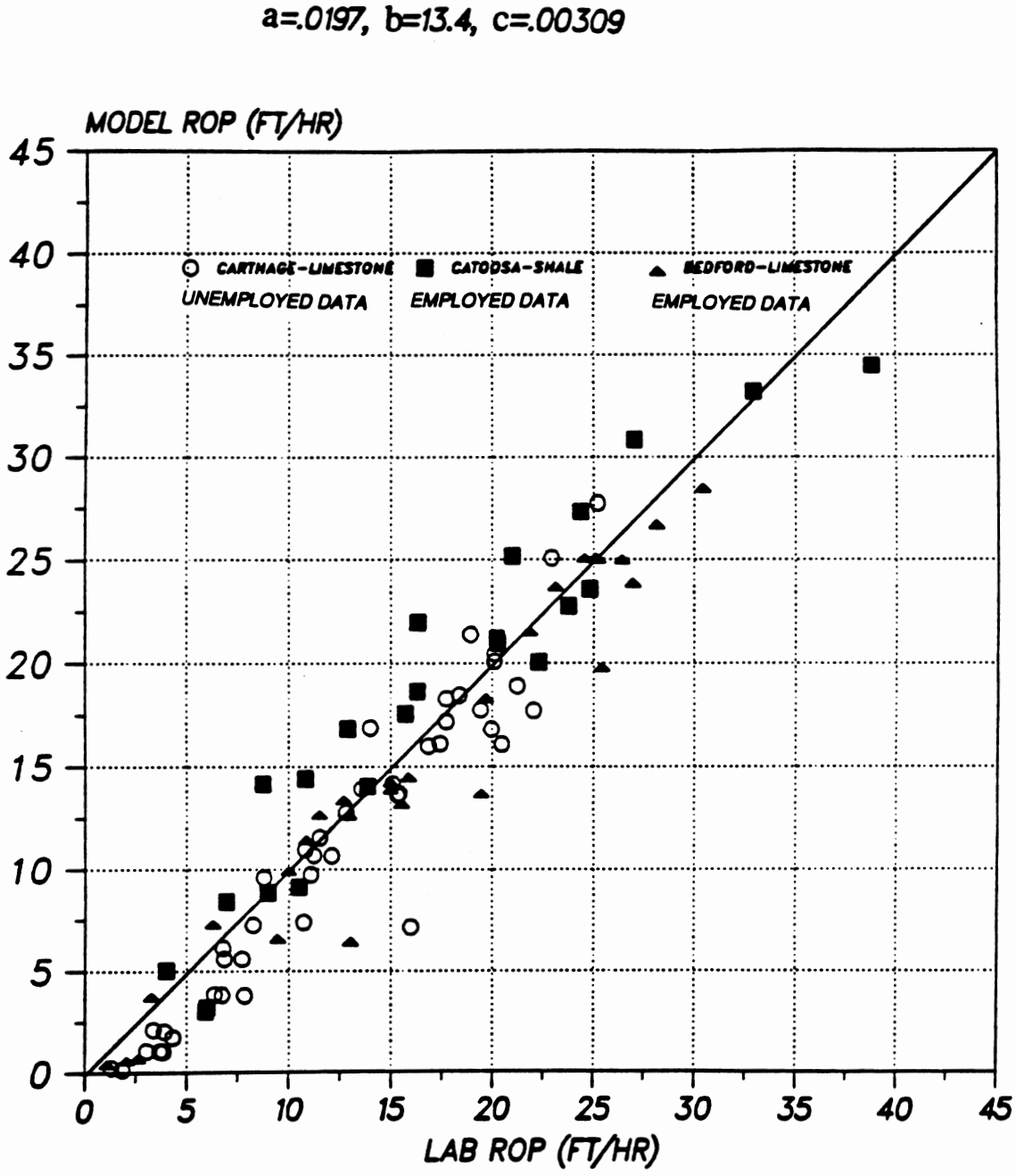

Figure 112. Bit Coefficients Developed from Bedford Limestone and Catoosa Shale Drilling Data Tested Against Carthage Limestone Drilling Data for a 617 IADC Bit

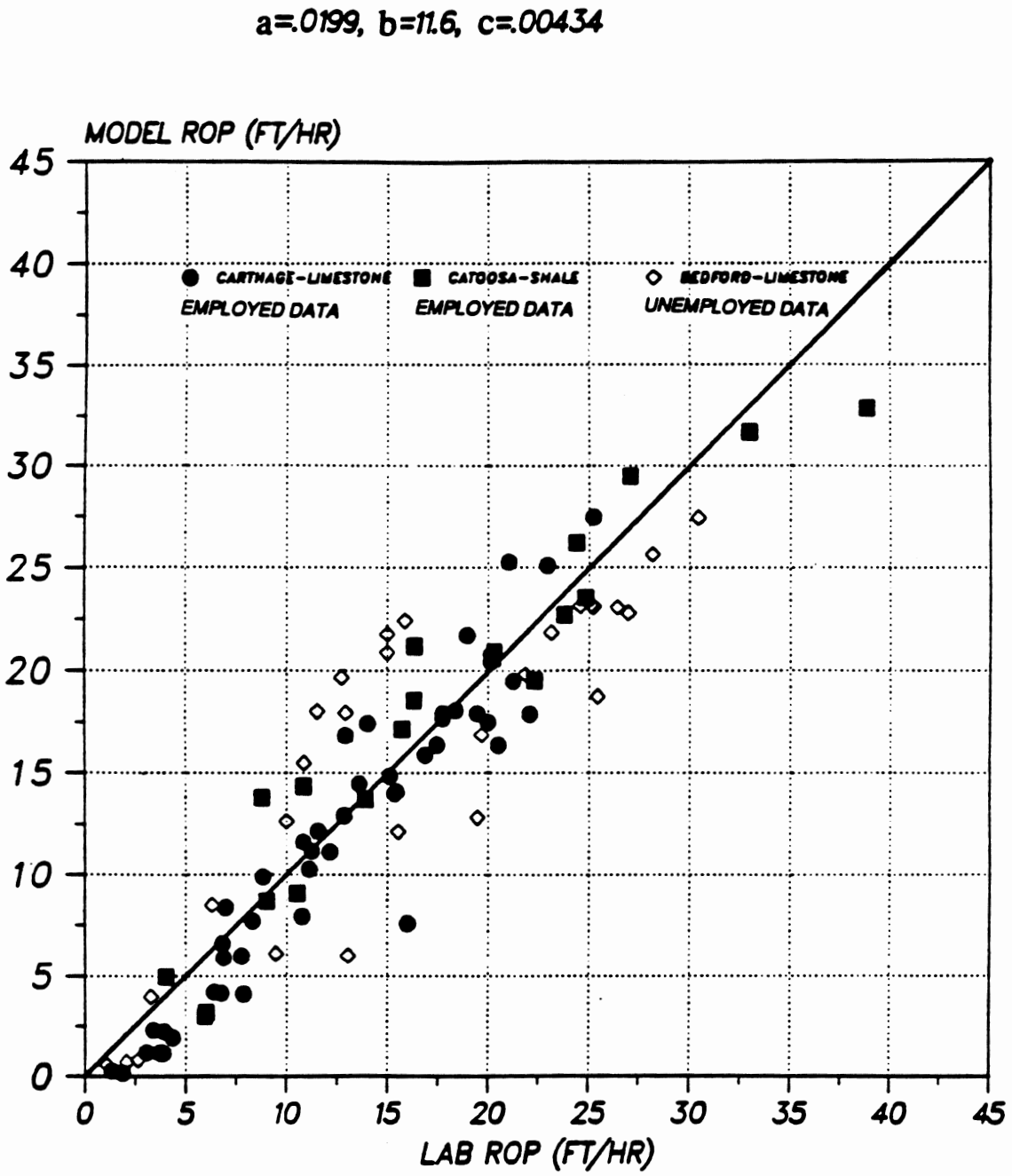

Figure 113. Bit Coefficients Developed from Carthage Limestone and Catoosa Shale Drilling Data Tested Against Bedford Limestone Drilling Data for a 617 IADC Bit

coefficients by +/-20 percent about selected nominal values. This amount of coefficient variation appeared to span what could be reasonably be expected in practice.

Two sets of typical operating conditions were taken from the SFE #2 well. These were:

Case 1:	Depth	-	8139 ft.
	Bit IADC	-	537
	Lithology	-	100% Shale
	ROP	-	7.087 ft/hr
	WOB	-	37.675 klbs
	RPM	-	64.6 RPM
	PV	-	9 cp

Case 2:	Depth	-	9000 ft.
	Bit IADC	-	737
	Lithology	-	100% Sandstone
	ROP	-	13.025 ft/hr
	WOB	-	40.621 klbs
	RPM	-	52.3 RPM
	PV	-	15 cp

For Case 1 Figure 114 shows the sensitivity of calculated rock strength to a +/- 20 percent change from nominal of the bit coefficients. Figure 115 shows the sensitivity of the impermeable upper bound on in-situ stress to the same coefficient variation. It can be seen that rock strength changes remain less than 12 % of nominal and stress bound changes remain less than 2.5 % of nominal. The same approach was used to evaluate the sensitivity of the

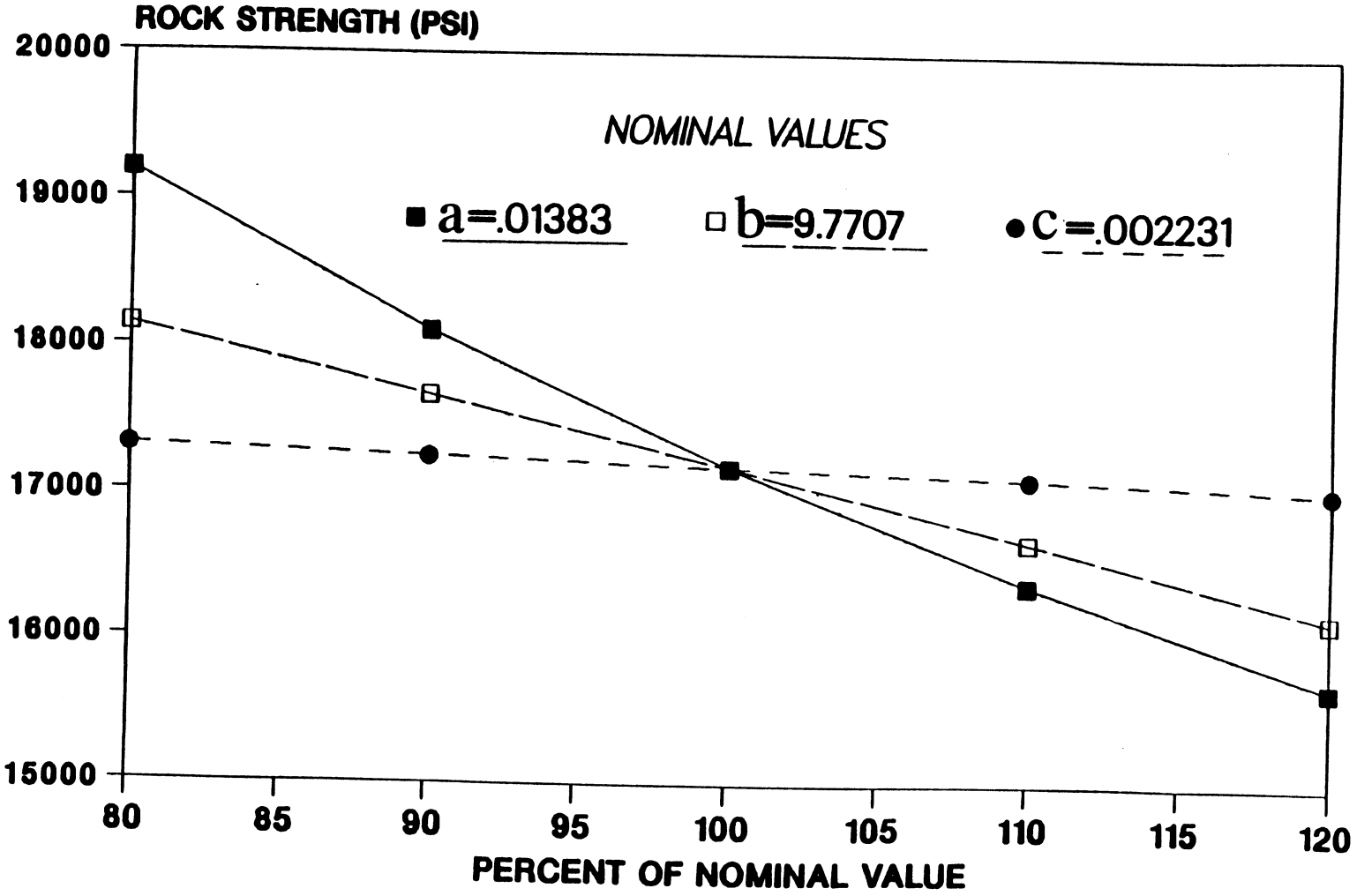

Figure 114. Sensitivity to Bit Coefficients of Impermeable Rock Strength in Shale for a 537 IADC Bit

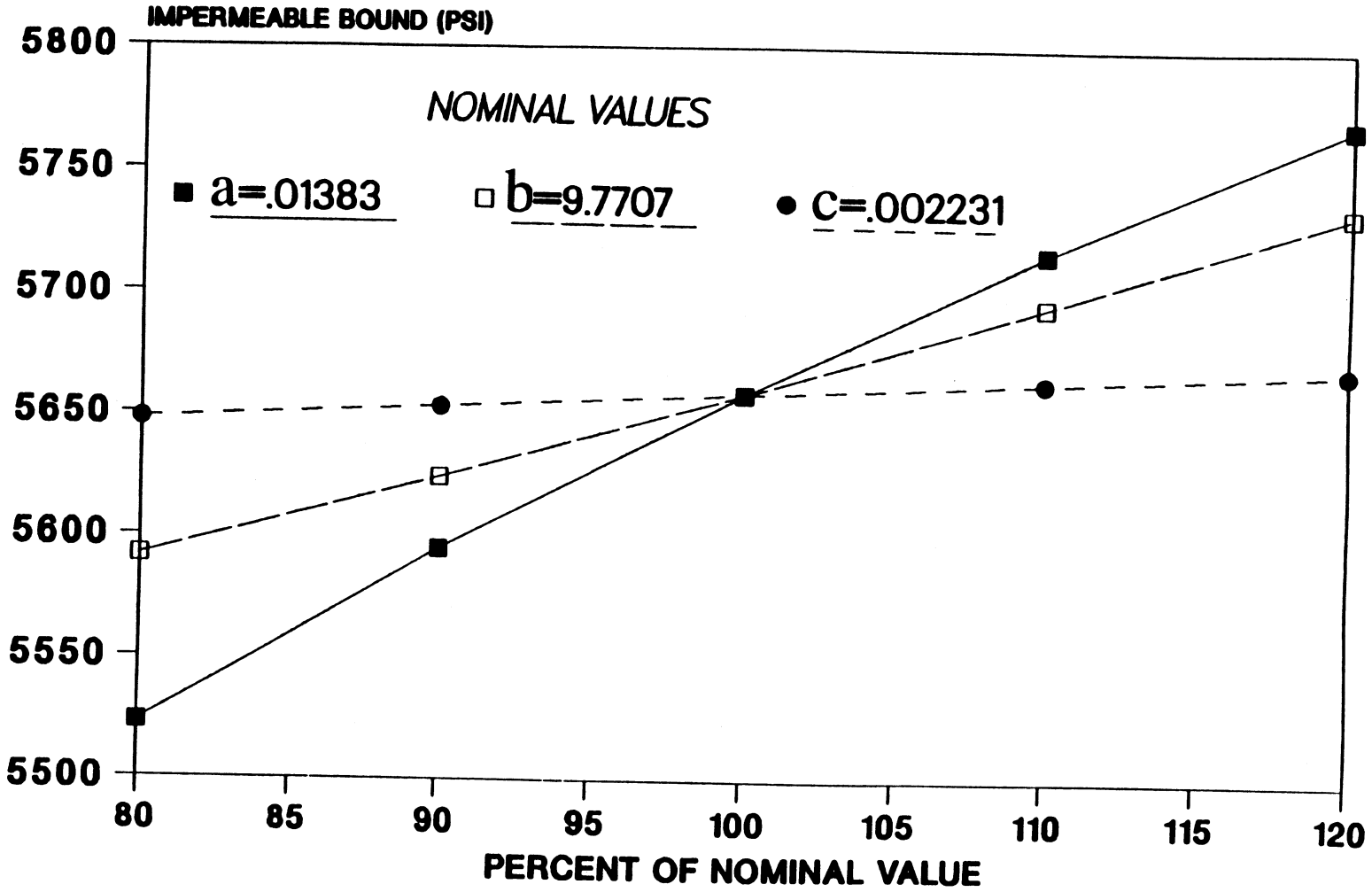

Figure 115. Sensitivity to Bit Coefficients of Impermeable Upper In-Situ Stress Bound for a 537 IADC Bit

coefficient of earth at rest, K_o, and the impermeable in-situ stress bound to a =/- 20 percent variation about nominal values of the chip hold-down coefficients. Figures 116 and 117 shows the results. It can be seen that while there is little sensitivity to the coefficients a_c and c_c, strong sensitivity to b_c exists. This is perhaps expected since b_c is an exponent in the confining pressure term. In order for the in-situ stress bound to vary less than 20 % from nominal, the coefficient b_c should vary less than 10 % from nominal. This does not appear to be an unreasonable expectation.

For Case 1 Figure 118 shows the sensitivity of the impermeable upper bound on in-situ stress to a +/- 20 percent change from nominal of the shale rock strength coefficients. It can be seen that impermeable stress bound changes remain less than 14 % of nominal. Little or no sensitivity is shown to the coefficient a_s (less than 1 %), while a stronger sensitivity to the coefficient b_s exists. This is perhaps expected since b_s is an exponent in the confining pressure term.

For Case 2 Figure 119 and 120 show the sensitivity of the rock strength and the permeable upper bound on in-situ stress to a +/- 20 percent change from nominal of the bit coefficients. It can be seen that rock strength changes remain less than 13 % of nominal, and stress bound changes remain less than 4 % of nominal.

The same approach was used to evaluate the sensitivity of rock strength, coefficient of earth at rest, and permeable upper bound on in-situ stress to a +/- 20 percent change of nominal of the chip hold-down coefficients. It can be seen from Figure 121 that rock strength

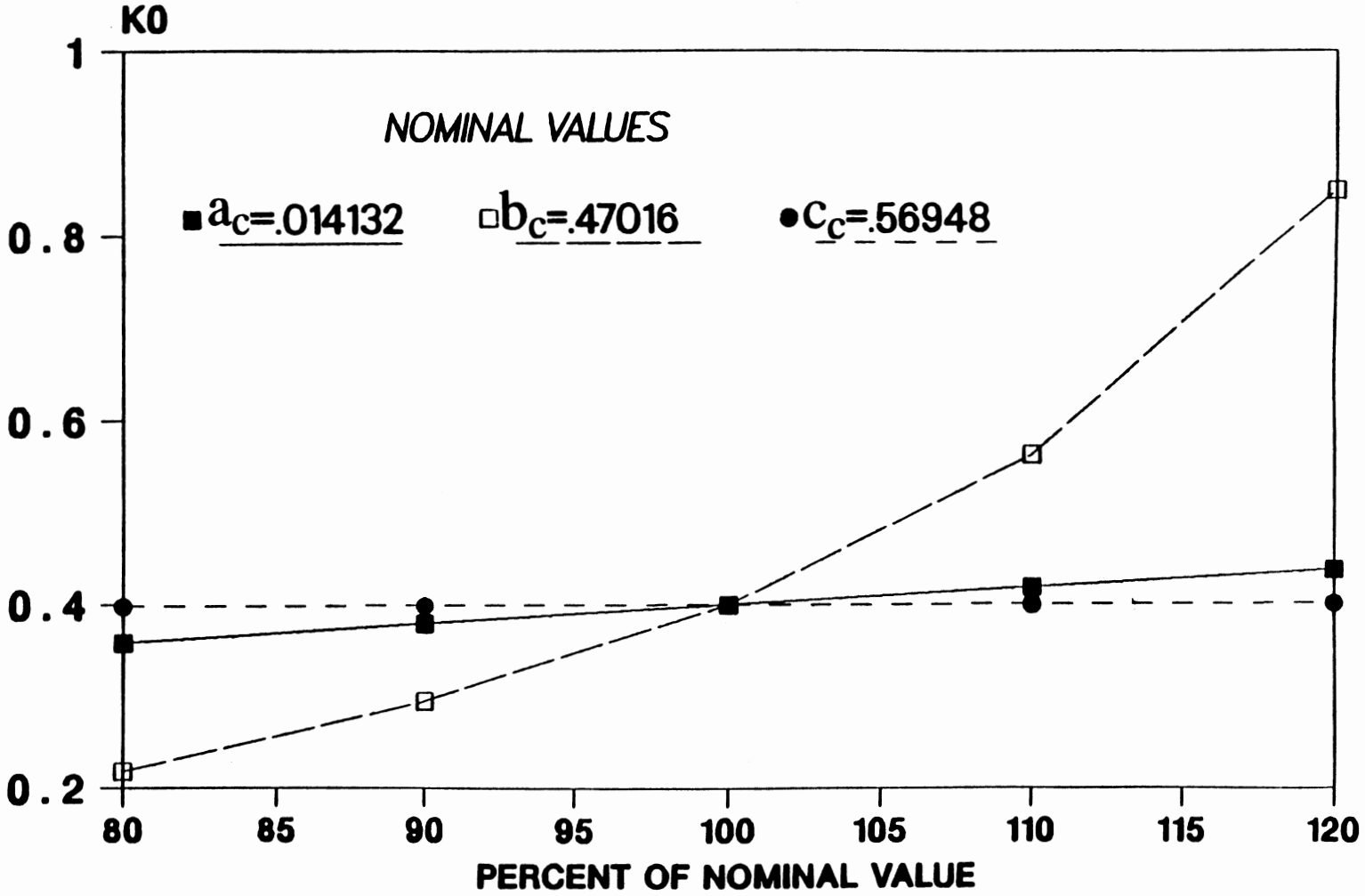

Figure 116. Sensitivity to Chip Hold-Down Coefficients of Impermeable Coefficient for Earth at Rest in Shale for a 537 IADC Bit

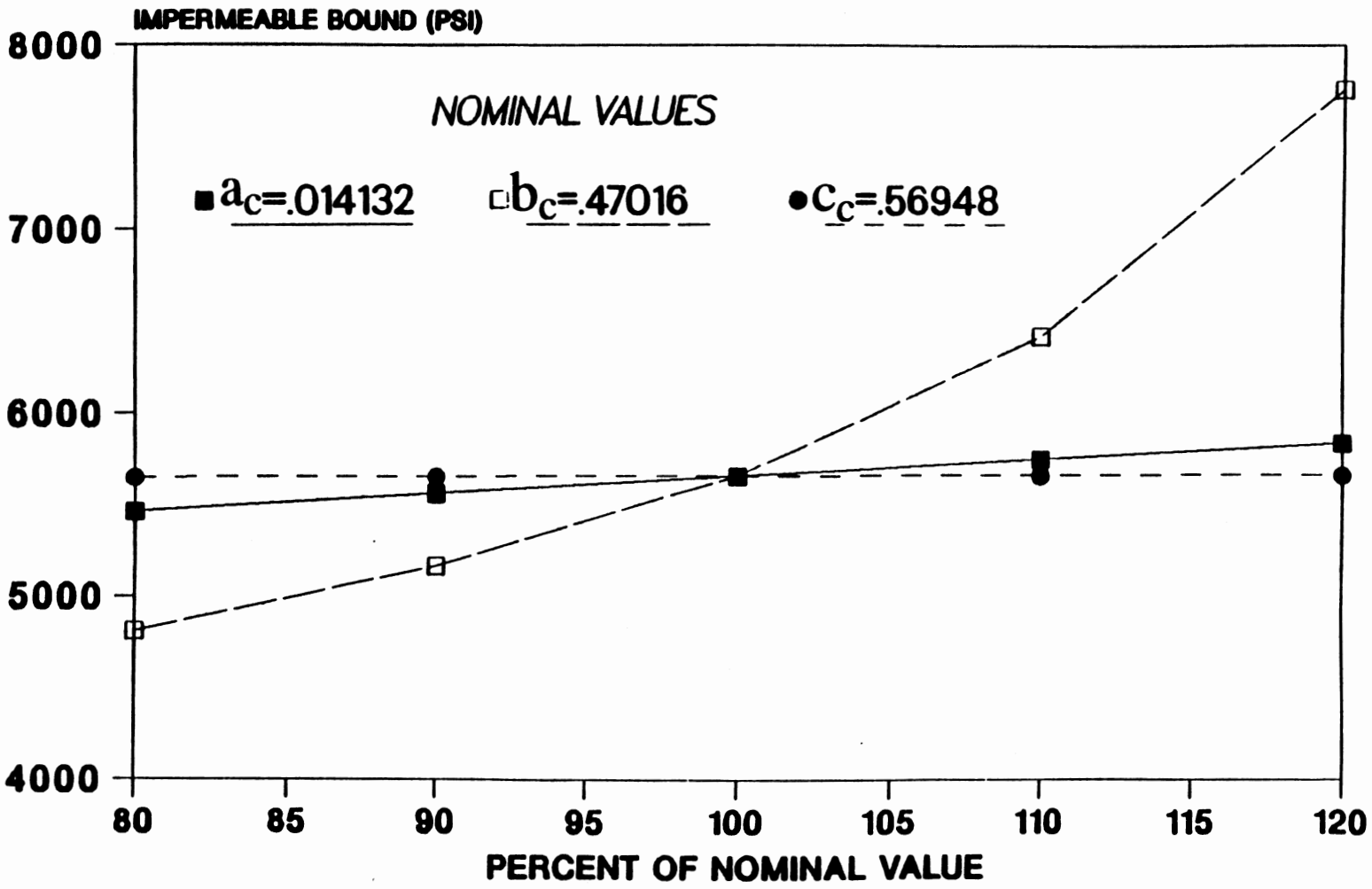

Figure 117. Sensitivity to Chip Hold-Down Coefficients of Impermeable Upper In-Situ Stress Bound for a 537 IADC Bit

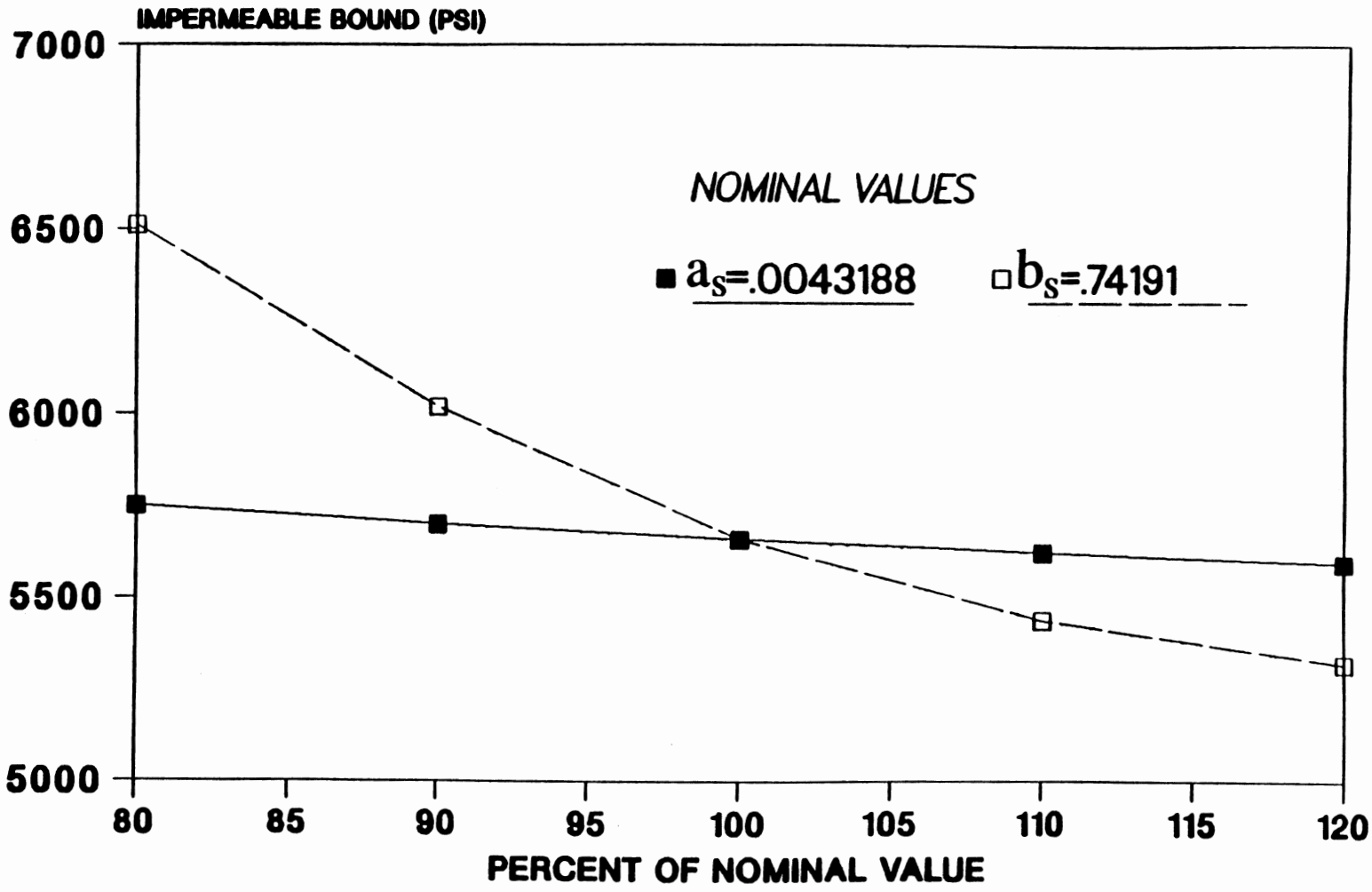

Figure 118. Sensitivity to Rock Strength Coefficients of Impermeable Upper In-Situ Stress Bound for a 537 IADC Bit

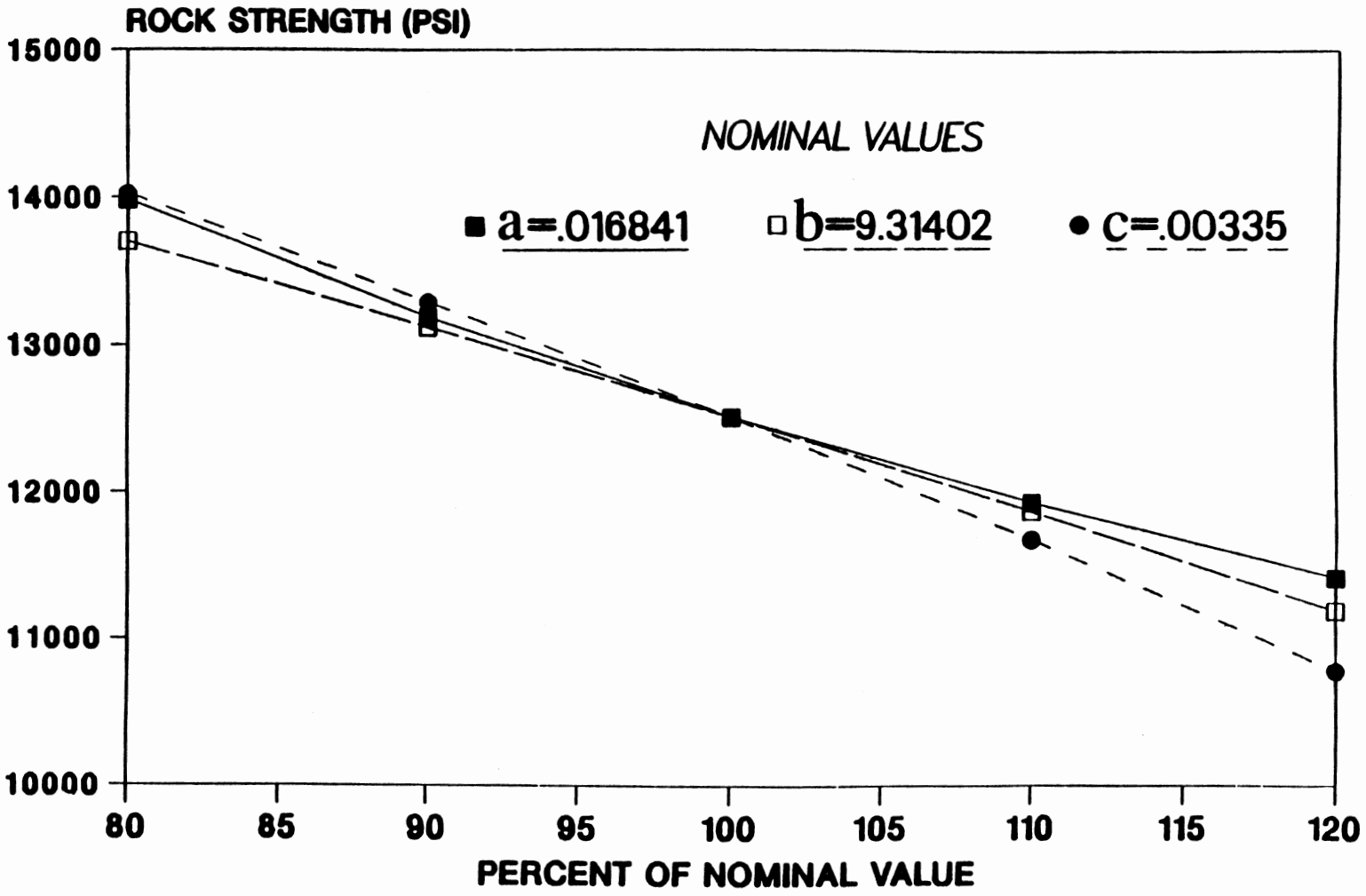

Figure 119. Sensitivity to Bit Coefficients of Permeable Rock Strength in Sandstone for a 737 IADC Bit

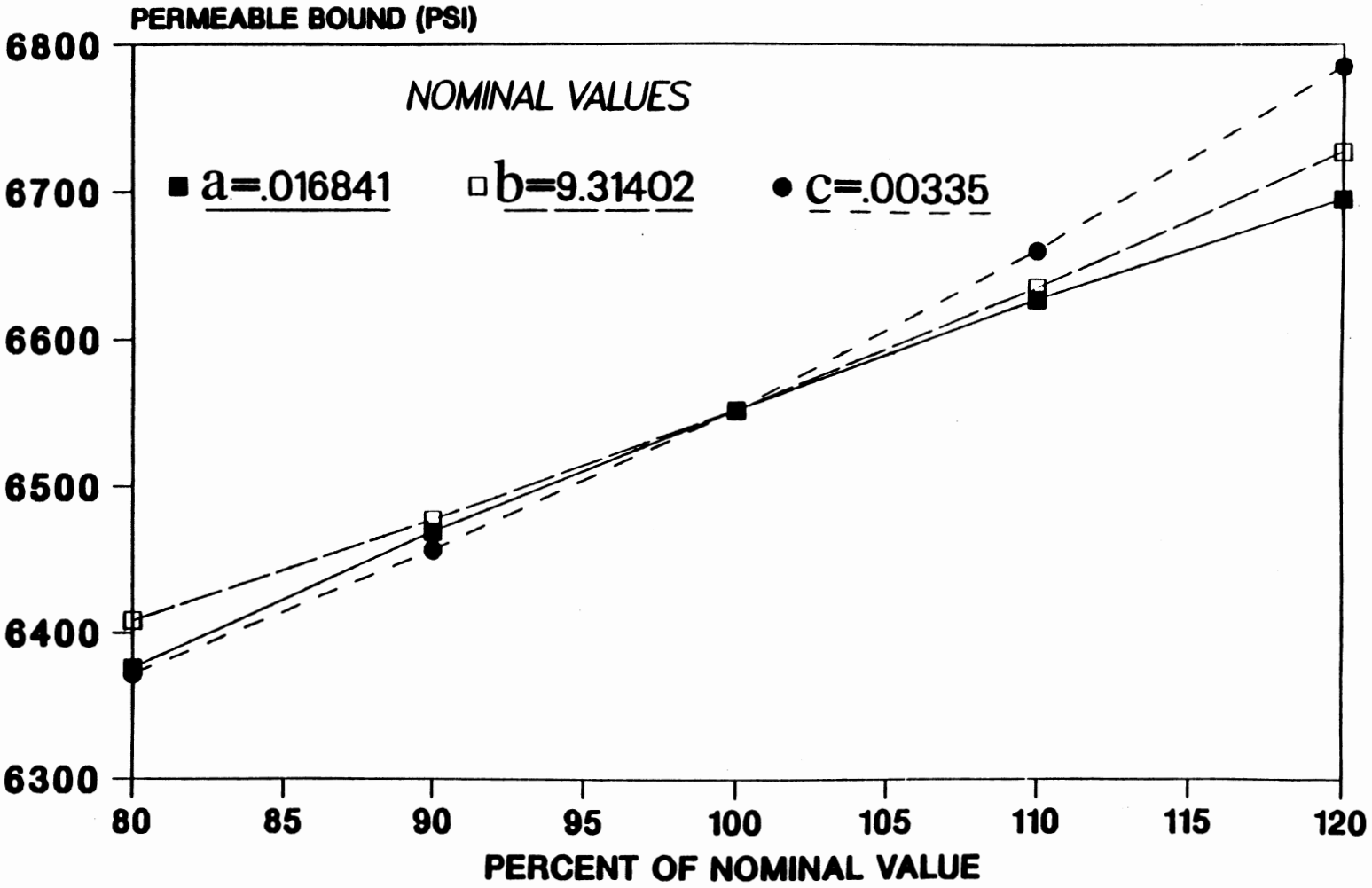

Figure 120. Sensitivity to Bit Coefficients of Permeable Upper In-Situ Stress Bound for a 737 IADC Bit

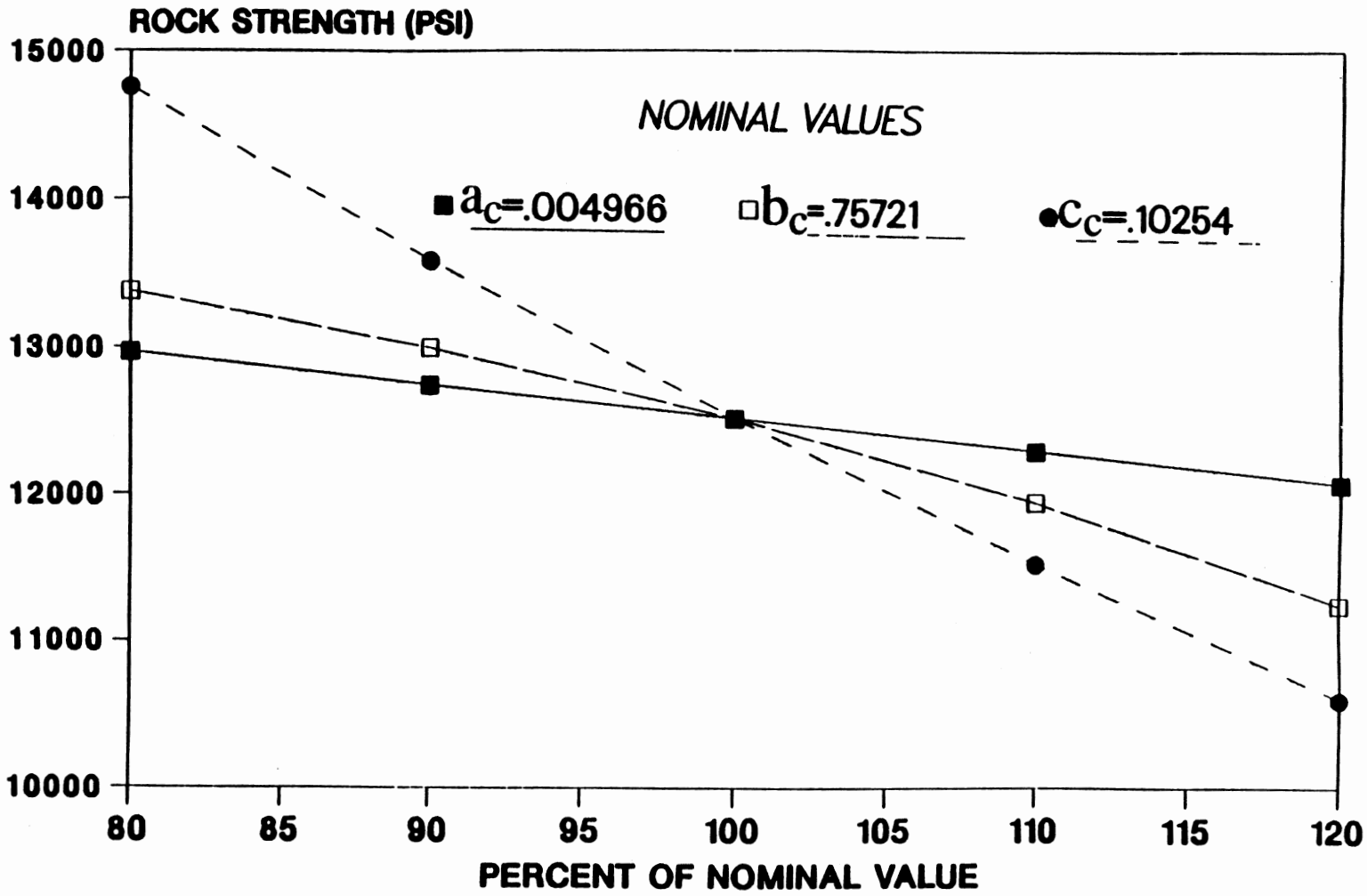

Figure 121. Sensitivity to Chip Hold-Down Coefficients of Permeable Rock Strength in Sandstone for a 737 IADC Bit

changes remain less than 18 % of nominal; from Figure 122 that changes in the coefficient for earth at rest remain less than 13 % of nominal; and from Figure 123 that changes in the permeable bound on in-situ stress remain less than 5 % of nominal.

It can be concluded that three significant digits in the bit coefficients gives less than 0.5 percent possible error in the in-situ stress bound calculation. This is based on the results above, in which a change of less than 20 percent in nominal bit coefficients values yields a change of less than 20 percent in in-situ stress bounds. Since three significant digits gives a maximum possible error of 0.5 percent in the bit coefficient, we estimate from the curves in Figure 115 and 120 that the maximum error in in-situ bounds due to error in the bit coefficients would be less than 0.5 percent.

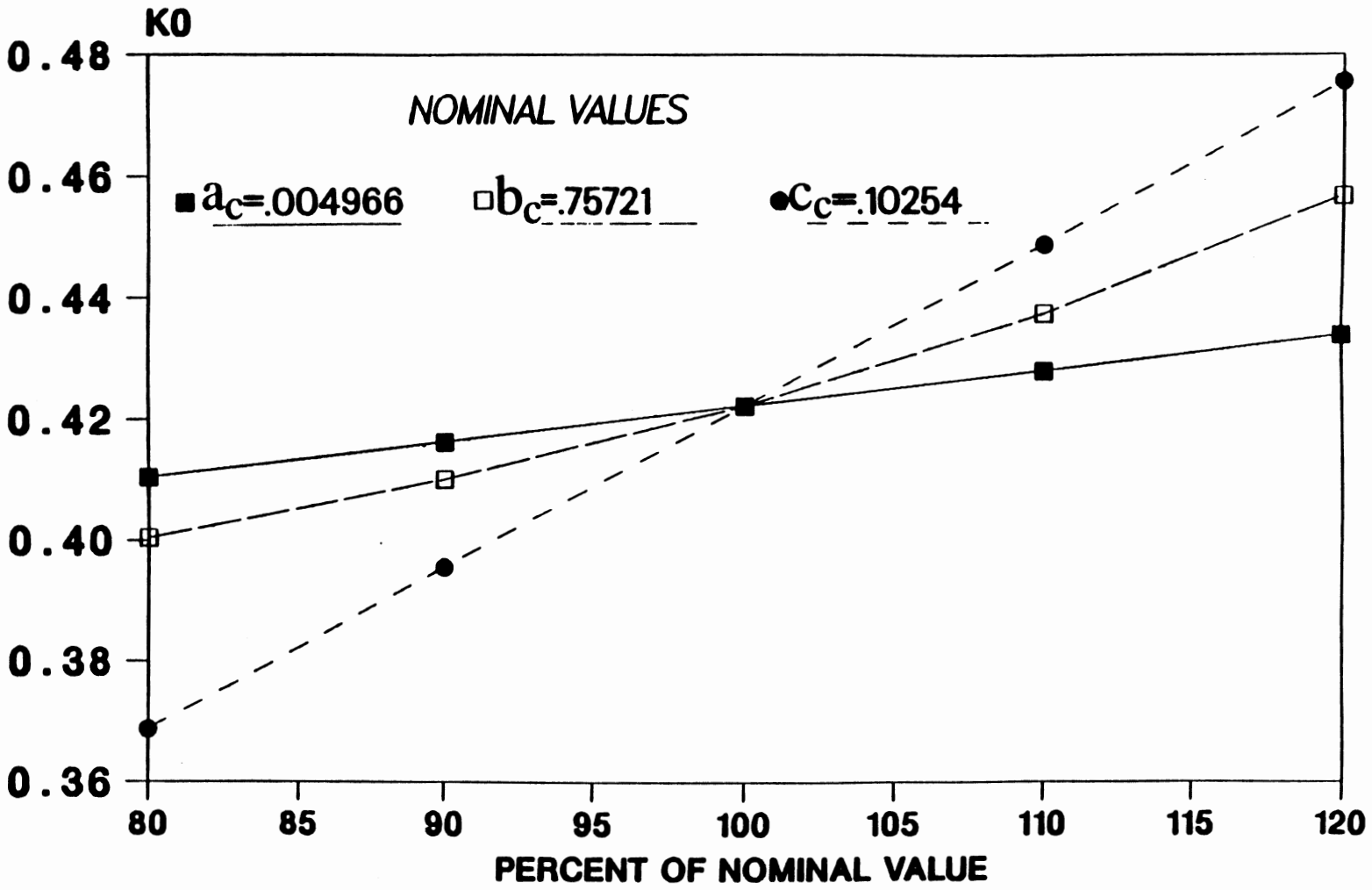

Figure 122. Sensitivity to Chip Hold-Down Coefficients of Permeable Coefficient for Earth at Rest in Sandstone for a 737 IADC Bit

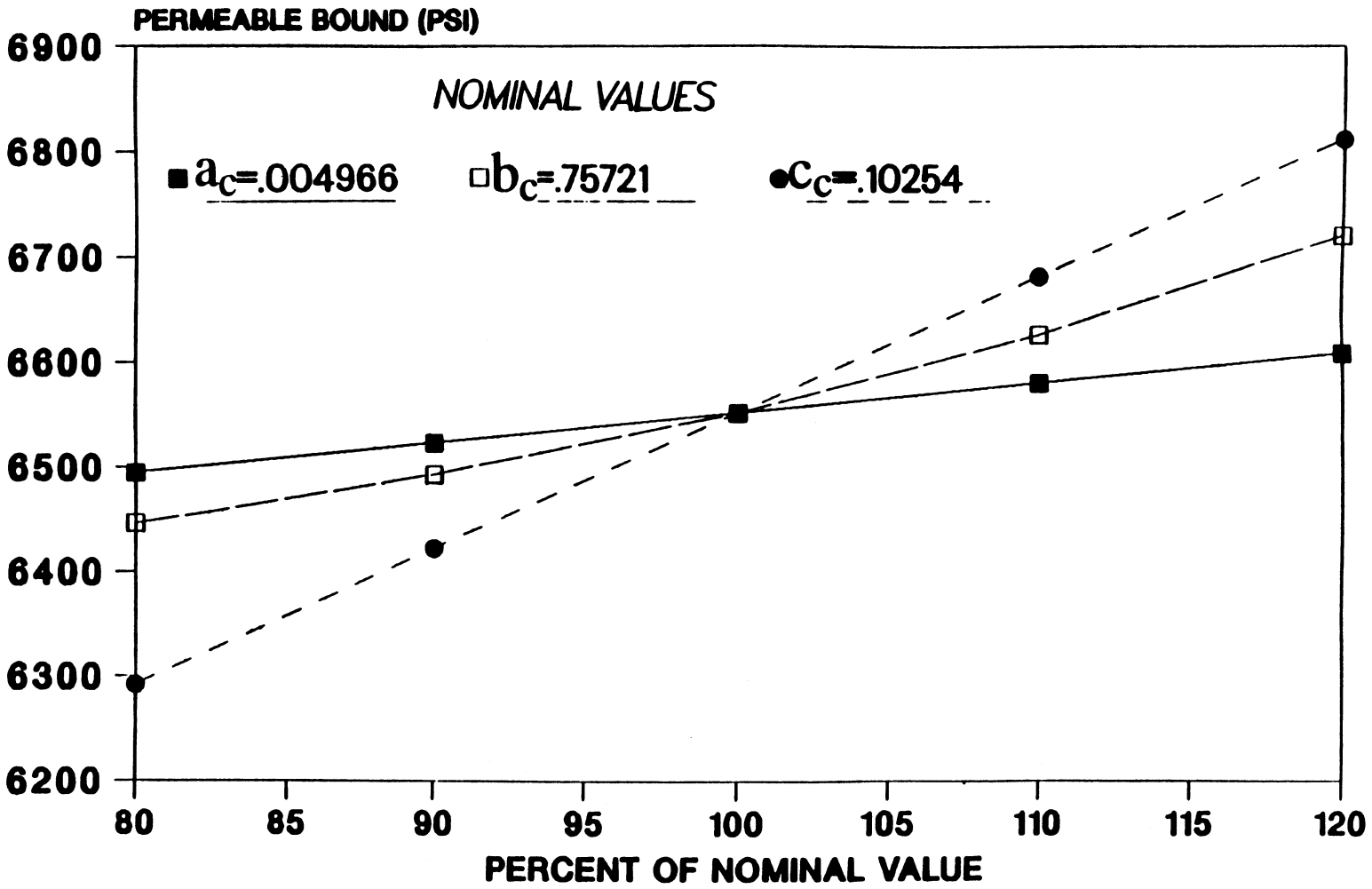

Figure 123. Sensitivity to Chip Hold-Down Coefficients of Permeable Upper In-Situ Stress Bound for a 737 IADC Bit

VITA

Geir Hareland

Candidate for the Degree of

Doctor of Philosophy

Thesis: USE OF DRILLING PARAMETERS TO PREDICT IN-SITU STRESS BOUNDS

Major Field: Mechanical Engineering

Biographical:

Personal Data: Born in Porsgrunn, Norway, October 22, 1959, the son of Arne P. and Solveig Hareland.

Education: Graduated fron Ullern High School, Oslo, Norway, in 1978; received Bachelor of Science Degree in Mechanical Engineering from University of Minnesota in May, 1981; received Master of Sience in Petroleum Engineering from University of Tulsa in August, 1985; completed requirements for Doctor of Philosophy degree in Mechanical Engineering at Oklahoma State University in December, 1991.

Professional Experience: Research Engineer at Amoco Production Company Research Center in Tulsa, August 1985 to December, 1988; Research Engineer, Department of Mechanical Engineering, Oklahoma State University, January, 1989, to December, 1991.